

Electronic Thesis and Dissertation Repository

10-17-2022 3:15 PM

Numerical Investigations of the Fluid Flow and Heat Transfer and Construction of Control System for the Canadian Supercritical Water-Cooled Reactor Power Plant

Huirui Han, *The University of Western Ontario*

Supervisor: Zhang, Chao, *The University of Western Ontario*

A thesis submitted in partial fulfillment of the requirements for the Doctor of Philosophy degree in Mechanical and Materials Engineering

© Huirui Han 2022

Follow this and additional works at: <https://ir.lib.uwo.ca/etd>



Part of the [Nuclear Engineering Commons](#), and the [Power and Energy Commons](#)

Recommended Citation

Han, Huirui, "Numerical Investigations of the Fluid Flow and Heat Transfer and Construction of Control System for the Canadian Supercritical Water-Cooled Reactor Power Plant" (2022). *Electronic Thesis and Dissertation Repository*. 8908.

<https://ir.lib.uwo.ca/etd/8908>

This Dissertation/Thesis is brought to you for free and open access by Scholarship@Western. It has been accepted for inclusion in Electronic Thesis and Dissertation Repository by an authorized administrator of Scholarship@Western. For more information, please contact wlsadmin@uwo.ca.

Abstract

Canada participated in the Generation IV nuclear reactors with the Supercritical Water-Cooled Reactor (SCWR) concept. This work focuses on the numerical studies of the fluid flow and heat transfer of the supercritical water in the nuclear reactor fuel bundle, and the construction of the linear dynamic model and the design of the control system for the Canadian SCWR power plant.

Firstly, the fluid flow and heat transfer of the supercritical water in the vertical tube and the rod bundle is numerically investigated to evaluate whether the existing turbulent models could successfully capture the wall temperature variations at supercritical conditions by comparing the numerical results with the experimental data. The turbulent models that have better performance are modified using a variable turbulent Prandtl number model. The application of the proposed turbulence model shows a great improvement in the prediction of the wall temperatures under supercritical conditions. Accordingly, the full-scale simulation of the fluid flow and heat transfer of the supercritical water flow in the reactor fuel rod bundle was performed by the proposed turbulent model. The results show that the circumferential cladding surface temperature distribution is extremely non-uniform and the maximum cladding surface temperature for each fuel rod also shows large differences. In addition, the effects of operating conditions on the heat transfer of upward supercritical water flow in the reactor fuel bundle are studied numerically. The wall temperatures generally increase with the increase in the inlet temperature, heat flux, or the decrease in the mass flux. Buoyancy-affected zones mainly exist at the region around the pseudocritical temperature.

In this work, the design of the feedback control system for the SCWR is also carried out. The dynamic relationships between inputs and outputs of the reactor are obtained through transient computational fluid dynamics (CFD) simulations. The designed feedback control system can regulate the reactor back to the design point timely. Finally, a linear dynamic model for the entire SCWR power plant is developed, which includes the reactor, feedwater pump, outlet plenum, main steam line, turbine, and condenser. The dynamic characteristics

of the system and the steady-state interaction between different inputs and outputs of the system are analyzed. The control system for the SCWR power plant is constructed and the performance of the control system is satisfactory.

Keywords: SCWR, Prandtl number, numerical simulation, wall temperature, heat transfer, feedback control, control system

Summary for Lay Audience

As the growth of earth's population and the adverse impacts from global climate change, the demand for energy is increasing. Nuclear energy is prominent among all energy supplies with the advantages of clean, safe and cost-effective under appropriate use. The Supercritical Water-Cooled Reactor (SCWR) concept is one of six Generation IV nuclear reactors, which uses supercritical water as the coolant. In the reactor core, the heat produced by the nuclear fission process is absorbed by coolant. Given the peculiarity of thermophysical properties of supercritical water and the geometry of the flow channel, the heat transfer phenomenon in the supercritical water rod bundle is still not well-understood.

Firstly, the heat transfer of supercritical water in different vertical channels is numerically investigated by the existing turbulent models. Considering operating conditions and variations of thermophysical properties, a new variable turbulent Prandtl number model is developed to describe the heat transfer characteristics. Next, the numerical simulation of the upward supercritical water flow in the reactor rod bundle is performed to investigate the fluid flow and variations of wall temperatures. The gradient of the cladding surface temperature along the circumference is found large. Furthermore, influences of operating pressure, inlet temperature, heat flux, and mass flux on the heat transfer in the reactor fuel bundle are studied. The findings of this study show that wall temperature generally increases as the increase in the inlet temperature, heat flux, or the decrease in the mass flux. On the other hand, buoyancy-affected zones mainly exist at the region where thermophysical properties of supercritical water exhibit sharp changes. In addition, the buoyancy-affected zone is reduced with the increase in the inlet temperature, heat flux, and mass flux. This work also presents the design of a feedback control system for the SCWR. It is found that the designed control system can regulate the reactor to the original operating point timely when the reactor is subjected to disturbances. Finally, the control system for the entire SCWR power plant is also constructed. The performance of the control system is evaluated and it is satisfactory.

Co-Authorship Statement

This doctoral thesis is prepared as an integrated-article thesis according to the regulations stipulated by the School of Graduate and Postdoctoral Studies (SGPS) at the University of Western Ontario. Chapters 3 - 7 are papers written by Huirui Han and edited by Chao Zhang. Chapter 3 & 5 has been published in peer-review journal. Chapters 4, 6, 7 has been submitted to peer-review journals for review.

Chapter 3: H. Han, C. Zhang, “A Modified Turbulent Model for the Supercritical Water Flows in the Vertical Upward Channels,” *J. Supercrit. Fluids*, vol. 187, p. 105632, Aug. 2022.

Chapter 4: H. Han, C. Zhang, “Numerical Simulation of the fluid flow and heat transfer of the supercritical water in the 64-element Canadian SCWR fuel bundle,” *J. Nucl. Sci. Technol.* Under Review.

Chapter 5: H. Han, C. Zhang, “Numerical investigations of the effect of operation conditions on the heat transfer of the supercritical water in the Canadian SCWR fuel bundle,” *J. Supercrit. Fluids*. vol. 191, p. 105760, Dec. 2022.

Chapter 6: H. Han, C. Zhang, “Construction of a feedback control system based on CFD simulations for the 64-element Canadian SCWR,” *Prog. Nucl. Energy*. Under Review.

Chapter 7: H. Han, C. Zhang, “Construction of the dynamic model and control system for the Canadian SCWR power plant,” *Ann. Nucl. Energy*. Under Review.

Acknowledgments

It is great honor for me to have the opportunity to conduct my Ph.D. study at Western University. I would like to first thank my supervisor gratefully, Dr. Chao Zhang, for her support, patience and guidance throughout the whole process. The encouragement and invaluable advice from her motivate me to be a better researcher during the study. I also want to truly appreciate all insightful suggestions on my research from my advisory committee members, Dr. Christopher Thomas DeGroot and Dr. Eric Savory.

I would like to thank all my former and present colleagues, Xuelian Xing, Zeneng Sun, Hao Luo, Yunfeng Liu for both our academic discussion in the lab and happy days we spent together in the spare time.

Finally, I would also like to thank my family. My parents, Mr. Jinfeng Han and Mrs. Hongmei Sun. I'm so grateful for your unconditional love and belief to support each decision I made. My sister Mrs. Huijing Han and brother-in-law Mr. Yu Liu, I'm blessed with your encouragement and understanding in my graduate study. My little nephew, Hanyue Liu, we have known each other for more than 4 years and it is fantastic to witness your growth.

The completion of the Ph.D. thesis was not only challenging, but a rewarding experience for me. I appreciate all the gain and loss in the past few years, which made me who I am today.

Table of Contents

Abstract	i
Summary for Lay Audience	iii
Co-Authorship Statement	iv
Acknowledgments	v
Glossary	ix
List of Tables	x
List of Figures	xi
1. Introduction	1
1.1. Nuclear reactors.....	1
1.2. Supercritical fluids	2
1.3. Supercritical Water-Cooled Reactor	4
2. Literature Review	7
2.1. General theory	7
2.2. Heat transfer of supercritical fluids in channels.....	7
2.2.1. Heat transfer in tubes	9
2.2.2. Heat transfer in channels with multiple fuel rods	13
2.3. Control systems for SCWR	16
2.4. Motivations and Objectives.....	18
2.5. Outline of the thesis.....	19
3. A Modified Turbulent Model for the Supercritical Water Flows in the Vertical Upward Channels†	32
3.1. Introduction	34
3.2. Numerical modeling.....	36
3.2.1. Configuration of the flow channels.....	36
3.2.2. Numerical model and governing equations	38
3.3. Evaluation of standard turbulent models.....	40
3.3.1. Flows in the upward circular tube.....	40
3.3.2. Flows in upward 2×2 fuel rod channel	44
3.4. Modified turbulent models	48
3.4.1. Turbulent Prandtl number	48
3.4.2. Results and discussions.....	51

3.5. Conclusions	57
4. Numerical Simulation of the Fluid Flow and Heat Transfer of the Supercritical Water in the 64-element Canadian SCWR Fuel Bundle.....	65
4.1. Introduction	67
4.2. Numerical Procedure.....	69
4.2.1. Configurations of the Canadian SCWR.....	69
4.2.2. Computational domain and mesh generation.....	70
4.2.3. Numerical model and governing equations	73
4.3. Results and Discussions	75
4.3.1. Velocity profiles.....	75
4.3.2. Reynolds stresses	77
4.3.3. Secondary flow	85
4.3.4. Bulk temperature & wall temperatures	86
4.4. Conclusions	94
5. Numerical Investigations of the Effect of Operation Conditions on the Heat Transfer of the Supercritical Water in the Canadian SCWR Fuel Bundle	100
5.1. Introduction	102
5.2. Numerical model	107
5.2.1. Physical model and boundary conditions	107
5.2.2. Governing equations and turbulent models	108
5.3. Results and discussions	114
5.3.1. Bulk fluid temperature distributions under different operating conditions	114
5.3.2. Effects of operation conditions on the heat transfer	116
5.3.3. Effects of buoyancy on the heat transfer at different operating conditions	133
5.4. Conclusions	142
6. Construction of a Feedback Control System Based on CFD Simulations for the 64-element Canadian SCWR	150
6.1. Introduction	153
6.2. Reactor and its mathematical models.....	155
6.2.1. Configurations of 64-element fuel bundle of the Canadian SCWR	155
6.2.2. Mathematical models used in CFD simulations	156
6.3. Construction of the linear dynamic models	158

6.3.1.	Time independent tests	158
6.3.2.	Construction of transfer functions	160
6.3.3.	Validation of transfer functions	162
6.4.	Design of the feedback control system	167
6.5.	Evaluation of the performance of the feedback control system	169
6.6.	Conclusion.....	175
7.	Construction of the Dynamic Model and Control System for the Canadian SCWR Power Plant.....	179
7.1.	Introduction	182
7.2.	Configuration of the Canadian SCWR power plant.....	184
7.3.	Construction of the dynamic model for the Canadian SCWR power plant	185
7.3.1.	Linear dynamic models for each component	185
7.3.2.	Linear dynamic model for the SCWR power plant	188
7.4.	Evaluation of the dynamic model for Canadian SCWR power plant	189
7.4.1.	Dynamic characteristics of the open-loop system	189
7.4.2.	Cross-couple of inputs and outputs.....	192
7.5.	Design and performance evaluation of the feedback control system.....	193
7.5.1.	Design of the feedback control system	193
7.5.2.	Performance evaluation of the control system.....	194
7.6.	Conclusion.....	197
8.	Summary.....	200
8.1.	Summary and contributions	200
8.2.	Recommendations for future work.....	202
	Curriculum Vitae.....	204

Glossary[†]

- **Critical point:** the point in which the distinction between the liquid and vapor phases disappears, i.e. both phases have the same temperature, pressure, and specific volume or density. The critical point is characterized with the phase-state parameters: T_{cr} , P_{cr} and v_{cr} , which have unique values for each pure substance.
- **Supercritical fluid:** is the fluid at pressures and temperatures that are higher than the critical pressure and critical temperature. However, the term of supercritical fluid usually refers to the fluid when the pressure is higher than the critical pressure, but the temperature could be lower than the critical temperature.
- **Supercritical steam:** refers to water when both the pressure and temperature are higher than the critical values.
- **Normal heat transfer (NHT):** can be characterized in general with a heat transfer coefficient (HTC) similar to those of subcritical convective heat transfer far from the critical or pseudocritical regions, when they are calculated according to the conventional single-phase Dittus-Boelter-type correlations: $Nu = 0.0243 Re^{0.8} Pr^{0.4}$.
- **Enhanced heat transfer (EHT):** is characterized with higher HTC compared to those for NHT. Hence, wall temperatures are lower within some part of a heated channel or within the entire heated length. The EHT regime includes peaks or “humps” in the HTC profiles near the critical or pseudocritical points.
- **Deteriorated heat transfer (DHT):** is characterized with lower HTC compared to those for normal heat transfer (NHT). So, wall temperatures are higher within some part of a heated channel or within the entire heated length.
- **Pseudocritical point:** is the point at a pressure above the critical pressure and at a temperature ($T_{pc} > T_{cr}$) corresponding to the maximum specific heat at this particular pressure.
- **Pseudocritical line:** is the line, which consists of pseudocritical points.

[†] I. L. Pioro, "Supercritical-Fluids Thermophysical Properties and Heat Transfer in Power-Engineering Applications", in *Advanced Supercritical Fluids Technologies*. London, United Kingdom: IntechOpen, 2020 [Online]. Available: <https://www.intechopen.com/chapters/71403> doi: 10.5772/intechopen.91474.

List of Tables

Table 3.1 Geometrical and operating conditions of difference cases used in the simulations	37
Table 3.2 Relative errors between the numerical and experimental results for the wall temperature	47
Table 3.3 Relative errors between the numerical and experimental results for the wall temperatures	57
Table 4.1 Geometry specifications of the computational domain	72
Table 4.2 Mesh characteristics and the comparison results	74
Table 5.1 Pseudocritical temperatures and corresponding peak values of the specific heat at different pressures [6]	104
Table 5.2 Operating parameters for different cases	113
Table 6.1 Specifications of the 64-element Canadian SCWR	156
Table 6.2 Disturbances added for time independent tests.....	158
Table 6.3 Specifications of controllers	168
Table 7.1 Specifications of the Canadian SCWR	185
Table 7.2 Parameters and specifications of controllers	193

List of Figures

Figure 1.1: Timeline of the development of nuclear reactors [1]	2
Figure 1.2: Pressure-Temperature diagrams	3
Figure 1.3: Thermophysical properties of water at P = 25 MPa.....	4
Figure 1.4: An example of SCWR system [1]	5
Figure 3.1: Variations of thermophysical properties of water at P = 25 MPa	36
Figure 3.2: Experimental flow channels used in the study	37
Figure 3.3: Comparison of the predicted wall temperatures by different turbulence models with the experimental data for Case 1.....	42
Figure 3.4: Comparison of the predicted wall temperatures by different turbulence models with the experimental data for Case 2.....	43
Figure 3.5: Comparison of the predicted wall temperatures by different turbulence models with the experimental data for Case 3.....	44
Figure 3.6: Comparison of the predicted wall temperatures by different turbulence models with the experimental data for Case 4.....	46
Figure 3.7: Comparison of the predicted wall temperatures by different turbulence models with the experimental data for Case 5.....	47
Figure 3.8: Comparison the predicted wall temperatures using the proposed model with the results using Kong’s model [31] and the experimental data [39]	51
Figure 3.9: Comparison of the predicted wall temperatures by the original and modified turbulence models with the experimental data for Case 1	52
Figure 3.10: Comparison of the predicted wall temperatures by the original and modified turbulence models with the experimental data for Case 2	53
Figure 3.11: Comparison of the predicted wall temperatures by the original and modified turbulence models with the experimental data for Case 3	54
Figure 3.12: Comparison of the predicted wall temperatures by the original and modified turbulence models with the experimental data for Case 4	55
Figure 3.13: Comparison of the predicted wall temperatures by the original and modified turbulence models with the experimental data for Case 5	56
Figure 4.1: Canadian SCWR Core Concept [36].....	70
Figure 4.2: Cross-section view of the 64-element fuel assembly	70
Figure 4.3: Computational domain and mesh of the fuel bundle.....	71
Figure 4.4: Central subchannel and edge subchannel.....	72
Figure 4.5: Distributions of the streamwise velocity at the outlet (m/s).....	75
Figure 4.6: Lines used for analysis	76
Figure 4.7: Plots of the streamwise velocity along lines (m/s).....	77
Figure 4.8: Distributions of the normal Reynolds stresses at the outlet (m ² /s ²)	78
Figure 4.9: Plots of Reynolds normal stresses for lines 1 - 3 (m ² /s ²)	81
Figure 4.10: Plots of Reynolds normal stresses for lines 4 – 6 (m ² /s ²).....	84
Figure 4.11: Streamline of flow at the outlet	86
Figure 4.12: Bulk temperature along axial direction	86

Figure 4.13: Cladding surface temperature distributions in the fuel bundle.....	87
Figure 4.14: Maximum and Minimum cladding surface temperatures along the circumference of the fuel rods at $z = 2.5$ m ($^{\circ}$ C).....	88
Figure 4.15: Maximum and Minimum cladding surface temperatures along the circumference of the fuel rods at $z = 3.75$ m ($^{\circ}$ C).....	89
Figure 4.16: Maximum and Minimum cladding surface temperatures along the circumference of the fuel rods at $z = 4.8$ m ($^{\circ}$ C).....	90
Figure 4.17: Axial cladding surface temperature distributions.....	93
Figure 4.18: Circumferential cladding surface temperature distribution at $z = 4.8$ m for rod 7.....	93
Figure 5.1: Thermophysical properties of water at supercritical pressures [6].....	103
Figure 5.2: Cross- section view of the fuel bundle	108
Figure 5.3: Near wall mesh.....	110
Figure 5.4: Comparison between the simulation results and experimental data for the supercritical water flow in a bare tube.....	111
Figure 5.5: Comparison between the simulation results and experimental data for the supercritical water flow in a rod bundle	112
Figure 5.6: Comparisons of the bulk temperature distributions along the axial direction at different operating conditions.....	116
Figure 5.7: Circumferential wall temperature distributions at $z = 4.8$ m under different operating pressures.....	118
Figure 5.8: Wall temperature distributions along the axial direction under different operating pressures.....	120
Figure 5.9: Circumferential wall temperature distributions at $z = 4.8$ m under different inlet temperatures.....	122
Figure 5.10: Wall temperature distributions along the axial direction under different inlet temperatures.....	124
Figure 5.11: Circumferential wall temperature distributions under different heat fluxes.....	126
Figure 5.12: Wall temperature distributions along the axial direction under different heat fluxes.....	128
Figure 5.13: Circumferential wall temperature distributions under different mass flow rates.....	131
Figure 5.14: Wall temperature distributions along the axial direction under different mass flow rates.....	133
Figure 5.15: Effect of the gravity on the wall temperature of rod # 1 at the design operating condition	135
Figure 5.16: Variations of Gr/Re^2 , $Gr/Re^{2.7}$ and Bo^* along the axial direction at different pressures.....	137
Figure 5.17: Variations of Gr/Re^2 , $Gr/Re^{2.7}$ and Bo^* along the axial direction at different inlet temperatures.....	139
Figure 5.18: Variations of Gr/Re^2 , $Gr/Re^{2.7}$ and Bo^* along the axial direction at different heat fluxes	140

Figure 5.19: Variations of Gr/Re^2 , $Gr/Re^{2.7}$ and Bo^* along the axial direction at different mass flow rates.....	142
Figure 6.1: Configuration of the 64-element fuel bundle	155
Figure 6.2: Outputs with perturbations added using different time step sizes.....	160
Figure 6.3: Block representation of the dynamic model of the fuel bundle	161
Figure 6.4: Comparison of responses obtained by CFD simulations and linear dynamic model with a perturbation in the inlet mass flow rate.....	164
Figure 6.5: Comparison of responses obtained by CFD simulations and linear dynamic model with a perturbation in the inlet temperature.....	165
Figure 6.6: Comparison of responses obtained by CFD simulations and linear dynamic model with a perturbation in the heat flux introduced.....	167
Figure 6.7: Block representation of the feedback control system.....	169
Figure 6.8: Flowchart of embedding controllers in the CFD simulations	170
Figure 6.9: Output responses by CFD simulations when the system is subjected to the perturbation in the inlet mass flow rate.....	172
Figure 6.10: Output responses by CFD simulations when the system is subjected to the perturbation in the inlet temperature.....	173
Figure 6.11: Output responses by CFD simulations when the system is subjected to the perturbation in the heat flux on the fuel rod	175
Figure 7.1: Diagram of the Canadian SCWR power plant	184
Figure 7.2: Block diagram of the linear dynamic model for the Canadian SCWR power plant.....	188
Figure 7.3: Responses of the temperature of the outlet plenum to step variations of different inputs.....	191
Figure 7.4: Responses of the maximum wall temperature of fuel rods to step variations of different inputs	191
Figure 7.5: Responses of the pressure of the main steam line to step variations of different inputs.....	192
Figure 7.6: Response of the temperature of the outlet plenum using the feedback control after the step perturbation introduced	194
Figure 7.7: Response of the maximum wall temperature of fuel rods using the feedback control after the step perturbation introduce.....	195
Figure 7.8: Response of the pressure of the main steam using the feedback control after the step perturbation introduced	196

1. Introduction

1.1. Nuclear reactors

Traditional power generation includes fossil fuel power generation and hydroelectric generation. Because of the limited fossil fuel resources and the problem of global warming, many countries are reducing the percentage of the traditional power generation methods. Nuclear power, wind power, solar power, geothermal power are vigorously developed in recent years to meet the increasing energy needs. The nuclear power accounts for a significant portion of these energy resources.

The first nuclear power plants commenced operations in the 1950s and the design of the reactors has gone through several developmental stages. The thermal cycle in the nuclear power plant is similar to that in a fossil power plant, while the main heat source is the nuclear fission in the reactor. In the nuclear fission process, the nucleus of an atom splits into two or more smaller nuclei and release huge energy. The heat released by the nuclear fission can convert the coolant into steam. The steam then drives the turbine to produce electricity by the generator. Fig. 1.1 shows the general timeline of the existing four generations of the nuclear reactors. Generation I reactors (1950 - 1965) are basically prototypes. The commercial reactors were built later since the 1970s, which stands for Generation II (1965 - 1995), such as boiling water reactors (BWR), pressurized water reactors (PWR), Canada Deuterium Uranium (CANDU) reactors. Generation III (1995 - 2010) are the nuclear reactors in operation nowadays and the thermal efficiency of the water-cooled plants is 30% - 36%. Generation III+ (2010 - 2025) are the reactors with improved parameters with evolutionary design improvements. The thermal efficiency could be up to 38%. Generation IV was proposed in 2002 and planned to be in operation after 2025, aiming to achieve the goals of highly economical, enhanced safety and minimal waste. Generation IV International Forum (GIF) determined six promising reactor concepts: Gas-Cooled Fast Reactor (GFR), Lead-Cooled Fast Reactor (LFR), Molten Salt Reactor (MSR), Sodium-Cooled Fast Reactor (SFR), Supercritical Water-Cooled Reactor (SCWR), Very-High-Temperature Reactor (VHTR) [1].

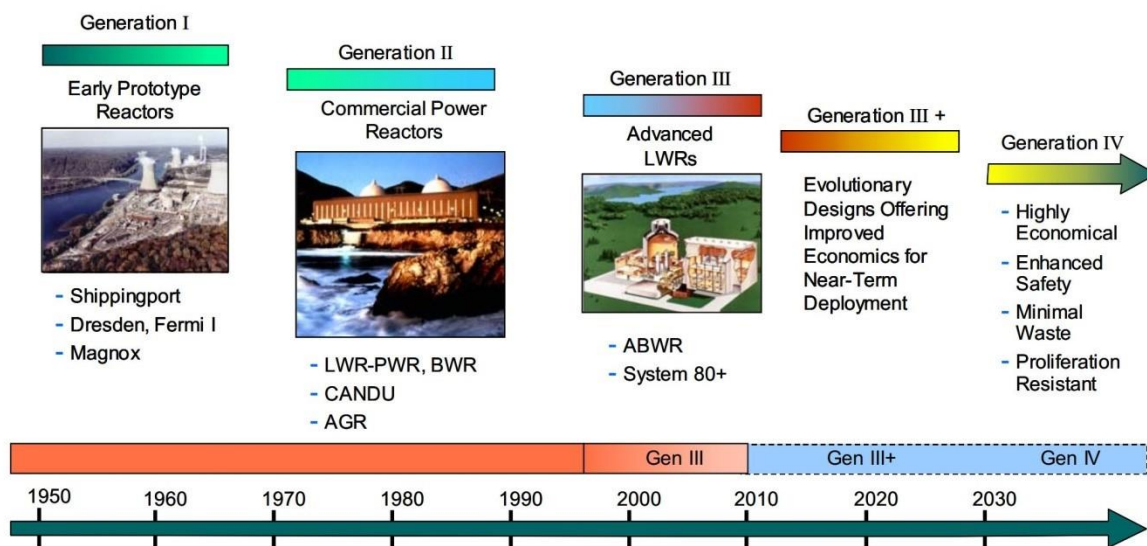


Figure 1.1: Timeline of the development of nuclear reactors [1]

1.2. Supercritical fluids

The application of supercritical fluids in different processes has been developed for more than 60 years. Initially, scientists used the hydrothermal processing of supercritical fluids for creating various crystals, and now it has been widely used in the industrial production of single crystals [2]. The application of supercritical fluids then was extended to thermodynamic processes. In the 1950s, supercritical fluids were used in fossil power plants to increase their thermal efficiency. The thermal efficiency of power plants with the combination of Brayton gas-turbine cycle and subcritical-pressure Rankine steam-turbine cycle can be up to 62%. With the supercritical steam at a pressure between 23.5 MPa and 38 MPa and the turbine inlet temperature of 540 - 625°C, the thermal efficiency can be up to 55% [3]. In addition, supercritical fluids can be used in the heat pump systems, as a fuel in nuclear rockets and supersonic transport, a refrigerant in refrigerating systems, as a coolant of superconducting electronics and power transmission equipment, and for the transformation of geothermal energy into electricity.

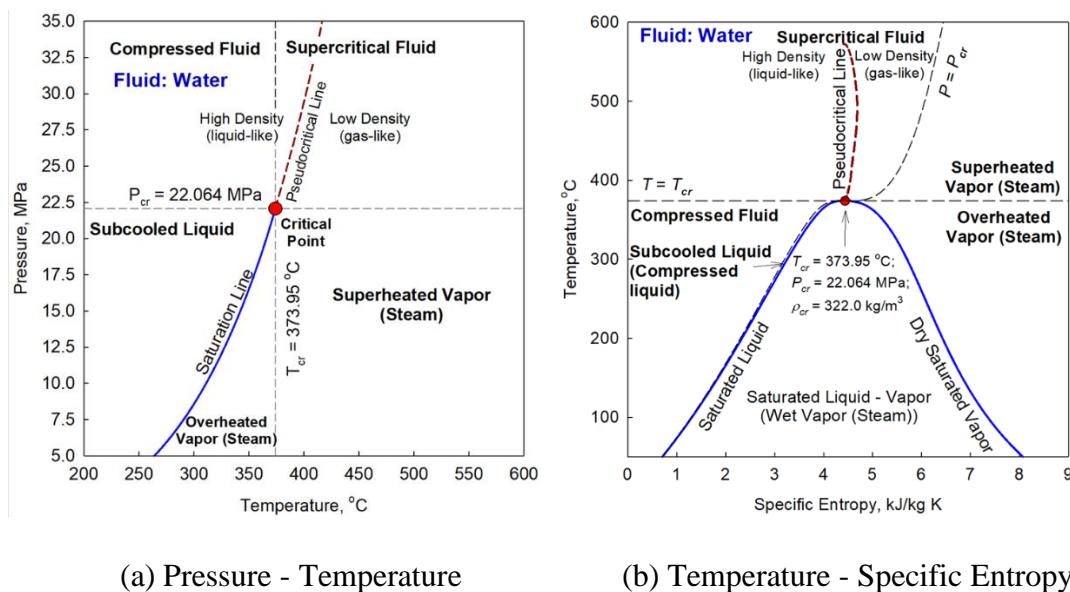


Figure 1.2: Pressure - Temperature - Specific Entropy diagrams for water

Supercritical fluid is a fluid at a temperature and pressure above its critical point. The P-T-S diagrams of a fluid and water are shown in Fig. 1.2 (Courtesy of Dr. I. Piore). For the water, the critical temperature is 374°C and the critical pressure is 22.1 MPa. The term, supercritical water used in the present study, includes both the supercritical water and the compressed water. Despite the supercritical fluids do not undergo phase change, all thermophysical properties of the supercritical fluids experience drastic changes in a narrow band of temperature. This can lead to high complexity in the fluid flow and heat transfer characteristics. The variations of the thermophysical properties of water at $P = 25$ MPa are depicted in Fig. 1.3. The specific heat reaches the maximum value at a point for a given pressure. This point is defined as the pseudo-critical point. Carbon dioxide, water, helium, and refrigerants are the most extensively used supercritical fluids in the industries and labs [4]. Compared with water, the critical temperatures and pressures of carbon dioxide and refrigerants are much lower. Thus, they are usually used in experiments, which could reduce the costs of experiments. In order to safely and efficiently use the supercritical water in nuclear power plants, it is necessary to understand the specific physics of the supercritical water flow and heat transfer mechanism.

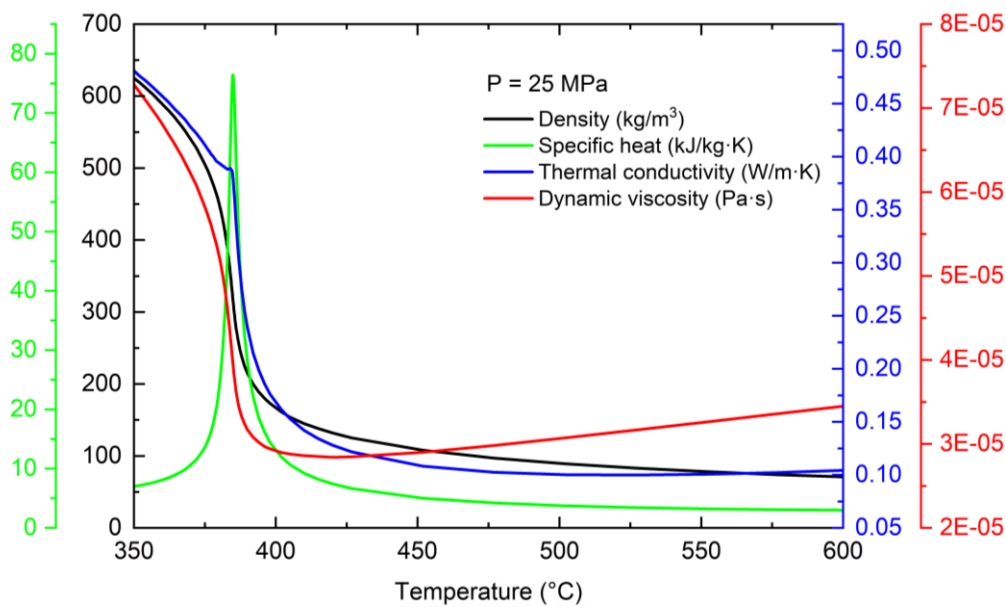


Figure 1.3: Thermophysical properties of water at $P = 25 \text{ MPa}$

1.3. Supercritical Water-Cooled Reactor

The studies of the possibility that supercritical water could be used in nuclear reactors began in the late 1950s and early 60s [4]. Although some design concepts were proposed, the relevant studies were terminated with the development of PWRs and BWRs. In a PWR, a steam generator and a pressurizer are needed. While in a BWR, the steam separation and recirculation system is used. With the development of the technology of Light Water Reactors (LWR), the application of supercritical water in nuclear reactors is starting to draw attention again. SCWRs are light-water-cooled reactors that operate above the critical point of water. The reactor core can have either thermal or fast-neutron spectrum. A typical SCWR system is presented in Fig. 1.4, which is a once through direct steam cycle, i.e. the superheated steam exiting the reactor flows to the turbine directly. Consequently, steam generators and separators, as well as recirculation pumps are not needed. Four Generation IV International Forum members are signatories for the SCWR reactor: Japan, the European Union, Russia, and Canada. Among them, Japan [5] and the European Union [6] adopted pressure-vessel-type, while Canada proposed pressure-tube-type [7]. In addition, China is also developing and constructing its own SCWRs.

Compared with existing water-cooled reactors, the design of SCWRs has some advantages. The construction costs are reduced because of less components. The coolant in SCWRs undergoes higher increase of enthalpy in the reactor core. To produce the same thermal power, the core mass flow in SCWRs is significantly decreased. In addition, the thermal efficiency of SCWRs can achieve 44% or more, which is higher than the existing water-cooled reactors (34 - 36%) [1]. However, the design concept also brings some requirements that need to be met to ensure safety of the nuclear reactors at supercritical conditions, such as the limitation on cladding temperatures, the transient heat transfer behaviors in the reactor, and the reliability of the control system.

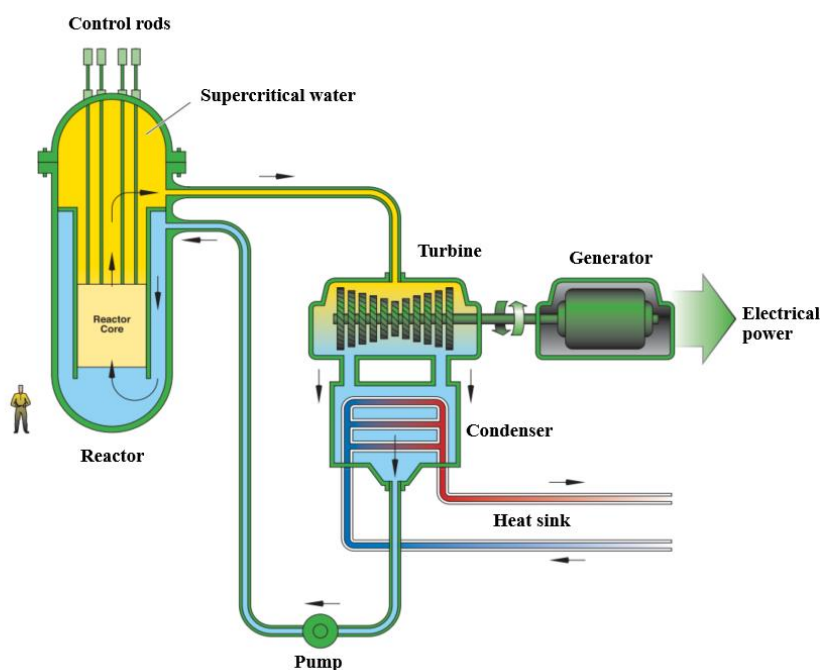


Figure 1.4: An example of SCWR system [1]

References

- [1] US DOE, NERAC, and GIF, "A Technology Roadmap for Generation IV Nuclear Energy Systems," 2002.
- [2] I. Piore and S. Mokry, "Thermophysical Properties at Critical and Supercritical Pressures," in *Heat Transfer - Theoretical Analysis, Experimental Investigations*

and Industrial Systems, 2011, pp. 573–592.

- [3] I. Pioro, R. B. Duffey, P. L. Kirillov, and R. Pioro, “Pros and Cons of Commercial Reactor Designs Part 1: Current Status of Electricity Generation in the World and Selected Countries,” in *Encyclopedia of Nuclear Energy*, E. B. T.-E. of N. E. Greenspan, Ed. Oxford: Elsevier, 2021, pp. 263–287.
- [4] I. L. Pioro and R. B. Duffey, *Heat Transfer and Hydraulic Resistance at Supercritical Pressures in Power Engineering Applications*. New York, NY, USA: ASME Press, 2007.
- [5] Y. OKA and S. KOSHIZUKA, “Supercritical-pressure, Once-through Cycle Light Water Cooled Reactor Concept,” *J. Nucl. Sci. Technol.*, vol. 38, no. 12, pp. 1081–1089, Dec. 2001.
- [6] T. Schulenberg, J. Starflinger, P. Marsault, D. Bittermann, C. Maráczy, E. Laurien, J.A. Lycklama à Nijeholt, H. Anglart, M. Andreani, M. Ruzickova, A. Toivonen, “European supercritical water cooled reactor,” *Nucl. Eng. Des.*, vol. 241, no. 9, pp. 3505–3513, Sep. 2011.
- [7] M. Yetisir, H. Hamilton, R. Xu, M. Gaudet, D. Rhodes, M. King, K. Andrew, B. Benson, “Fuel assembly concept of the canadian supercritical water-cooled reactor,” *J. Nucl. Eng. Radiat. Sci.*, vol. 4, no. 1, pp. 1–7, 2018.

2. Literature Review

2.1. General theory

The increased interest in SCWRs has motivated research in the study of heat transfer behavior of supercritical fluid flows in channels. Strong variations of thermophysical properties of supercritical fluids bring strong coupling between the flow and temperature. Within the narrow band of temperature around the pseudocritical point, the thermal conductivity and density falls quickly with the increase in the temperature. The significant density variation results in the intensive buoyancy effect and flow acceleration. This would consequently suppress turbulent diffusion and could lead to heat transfer deterioration. Meanwhile conversely, the fall-off of the viscosity could contribute to the increase of velocity and Reynolds number, consequently boosting the flow and heat transfer. As described in the last chapter, the specific heat has the maximum value at the pseudocritical point, which implies that the heat absorption at the pseudocritical temperature is stronger than other temperatures. Either normal heat transfer, heat transfer deterioration or heat transfer enhancement could appear because of the non-monotonic effects of different thermophysical properties. This result in the heat transfer behaviors of the supercritical fluids more complicated than those of ordinary fluids. Therefore, it is essential to understand and accurately predict the heat transfer mechanism of supercritical fluids before the applications of supercritical fluids in thermohydraulic designs.

2.2. Heat transfer of supercritical fluids in channels

Heated flows in channels are frequently encountered in practical systems and at the same time used in research purpose to understand the flow physics. Many dimensionless parameters are used to evaluate the heat transfer characteristics of supercritical water in channels. Some of them are described here.

Reynolds number (Re) is used to predict the flow regime. It is the ratios of inertial forces to viscous forces within a fluid, thus it quantifies the relative importance of these two types of forces in specific flow situations. Re is defined as [1]:

$$\text{Re} = \frac{\rho UL}{\mu} = \frac{GL}{\mu} \quad (2.1)$$

where ρ is density, kg/m^3 , U is the flow speed, m/s, L is the characteristic length, m, which is the hydraulic diameter in pipe flows, μ is the dynamic viscosity of the fluid, $\text{kg/m}\cdot\text{s}$ or $\text{Pa}\cdot\text{s}$, and G represents the mass flux, $\text{kg/m}^2\cdot\text{s}$.

Prandtl number (Pr) is used to measure the relative effectiveness of momentum and energy transport by diffusion in the velocity and thermal boundary layers. It is defined as the ratio of momentum diffusivity to thermal diffusivity as shown in the following [1]:

$$\text{Pr} = \frac{\nu}{\alpha} = \frac{\mu/\rho}{k/(c_p\rho)} = \frac{c_p\mu}{k} \quad (2.2)$$

where ν is the kinematic viscosity of the fluid, $\text{m}^2\cdot\text{s}$, α is the thermal diffusivity, $\text{m}^2\cdot\text{s}$, k is thermal conductivity, $\text{W/m}\cdot\text{K}$, and c_p is specific heat capacity, $\text{J/kg}\cdot\text{K}$.

Nusselt number (Nu) is defined as the ratio of convective to conductive heat transfer at a boundary in a fluid. It can be described as [1]:

$$\text{Nu} = \frac{h}{k/L} = \frac{hL}{k} \quad (2.3)$$

where h is convective heat transfer coefficient (HTC), $\text{W/m}^2\cdot\text{K}$. Nu = 1 denotes pure conduction heat transfer and larger Nu represents more convection heat transfer. One well-known empirical correlation for calculating Nu is the Dittus-Boelter equation [2].

2.2.1. Heat transfer in tubes

2.2.1.1. Experimental studies

The experimental studies on supercritical fluids were mainly focused on two aspects: finding the heat transfer mechanism at supercritical conditions and develop heat transfer correlations for supercritical fluids. Earliest experimental research on the heat transfer of supercritical fluids can be found in the 1950s and 1960s [3–6]. This was motivated by the idea of supercritical fossil-fueled power plants. Researchers used carbon dioxide or water to conduct the experiments. They investigated the flow in vertical heated tubes at supercritical conditions in order to obtain the wall temperature and heat transfer coefficient. The comparisons for upward and downward flows at the same operating conditions indicated the effect of buoyancy on the heat transfer characteristics of supercritical fluids [6, 7]. An interesting heat transfer phenomenon found by Yamagata et al. [8] was that the heat transfer coefficient increases rapidly in the pseudocritical region. It reaches the peak value at the pseudocritical point at low heat flux conditions in both vertical and horizontal tubes. The magnitude of the peak value decreases with the increase in the heat flux and pressure. However, at high heat flux conditions, the heat transfer coefficient shows a lower value in the pseudocritical region when the flow rate is low. Based on the experimental data, different heat transfer characteristics for supercritical water were defined [9]. In the normal heat transfer condition, the temperature difference between the wall and the bulk fluid generally shows no great change with the increase of enthalpy. Consequently, the heat transfer coefficients do not vary too much at a fixed heat flux. Heat transfer enhancement in one area is characterized by moderately increased wall temperatures and the condition that the temperature difference between wall and the bulk fluid gets smaller and then reaches a minimum value. Hence, the heat transfer coefficient goes up with the increase in the bulk enthalpy and reaches a maximum value. Heat transfer deterioration condition refers to the condition that the wall temperatures increase significantly and the temperature differences between wall and bulk fluid arise with the increase of bulk fluid enthalpy, meanwhile the heat transfer coefficient plunges. Wang et al. [9] also found that heat transfer deterioration occurs at higher heat fluxes based on their experimental study. This supports the phenomenon observed by Yamagata et al. [8]. Hall and Jackson [10] proposed that the

heat transfer deterioration is a result of the modification of the shear stress distribution near the wall in the pipe. Tanaka et al. [7] considered both the buoyancy force and acceleration effect for a fluid forced through a vertical tube in their study. It was observed that the effects of the buoyancy force and acceleration on the turbulent forced convective heat transfer in vertical tubes are similar, which results in a sharp decrease of the shear stress, even to a negative value near the wall. Consequently, the velocity profile shows M shape which indicates that peaks are in the near wall region. The results from a later experimental study by Kurganov et al. [11] also proved such velocity profiles.

Although the heat transfer deterioration mainly caused by a strong buoyancy force, it can also occur in the forced convection condition when the buoyancy effect is negligible, such as high heat to mass flux condition [12]. Under this type of heat transfer deterioration condition, the fluid temperature is not in the pseudocritical region. Therefore, the flow direction does not matter too much. But, in the mixed convection with strong buoyancy effect, whether the flow direction is downward or upward is important. It was found that the heat transfer deterioration is found only in upward flows. In the downward flows, the buoyancy effect typically enhances the heat transfer. The flow acceleration effect contributing to heat transfer deterioration was discovered in both upward and downward flows. Researchers found that the buoyancy effect caused by the radial gradients of density and the axial gradients of density leads to the acceleration effect for vertical flows [13, 14].

Since 1970s, the experimental studies of supercritical fluids in the tubes were conducted mainly in vertical direction flows, and some in horizontal direction flows under different operating conditions, such as operating pressure, inlet temperature, heat flux, and mass flux [8], [15–29]. In these studies, the velocity and temperature profiles were investigated and compared. Based on the experimental data, researchers attempted to propose heat transfer correlations for supercritical fluids for decades. The most widely used correlation at subcritical pressures for forced convection is the Dittus-Boelter correlation. This correlation is intended for smooth tubes with small temperature differences between wall and the bulk fluid, and it is sensitive to the variations of thermophysical properties. It might

predict unrealistic results at some supercritical flow conditions, especially near the pseudocritical points, based on the studies by Mokry and Piro [30, 31]. Numerous heat transfer correlations were developed for supercritical fluids in heated tubes. Yoo and Piro [32–34] both did extensive and thorough reviews on the correlations developed for the heat transfer of fluids, including water, carbon dioxide, helium in heated tubes at supercritical conditions. However, the applicability of each correlation varies with the operating conditions and it is hard to find one correlation that can successfully predict all heat transfer characteristics, the normal heat transfer, enhanced heat transfer, and deteriorated heat transfer. Further details of the heat transfer correlations are readily available in [32–34].

2.2.1.2. Numerical studies

Experiments at supercritical pressures requires cutting-edge equipment and appropriate measuring techniques, and thus are very expensive. Therefore, the cost-effective Computational Fluid Dynamics (CFD) approach become popular in studying supercritical fluids for decades [35–50, 78]. The objectives of these studies are to provide a detailed fluid flow information and more accurate predictions of heat transfer in supercritical fluids. After validation with the experimental data, CFD can serve as a supplement to the experimental studies. The approaches used to solve the conservation equations which govern the flow field in the CFD simulations can be generally classified as: direct numerical simulations (DNS), large eddy simulations (LES), and the Reynolds-averaged Navier-Stokes simulation (RANS). In the DNS approach, all flow motion scales need to be solved without modeling. Thus, the applicability is limited to relatively small geometries for research use due to the extremely high computational cost. In the LES approach, based on the filtering functions differentiating larger and smaller eddies, larger eddies are solved directly while smaller eddies need to be modelled. Despite LES is more applicable than DNS in the study of supercritical fluids, there are still limitations on Re with less than approximately 20000 for large flow geometries [78]. Thus, the RANS method is the most widely used in the numerical studies of the supercritical fluids.

At the beginning, Bellmore & Reid [35] developed a method of density fluctuations in the equations of turbulent transport in Prandtl's mixing length model for predicting heat transfer of para-hydrogen for upward flows in tubes near critical point. The numerical results showed a good agreement with experimental data over a range of inlet conditions, heat flux, and mass flux. The velocity profiles showed M shapes due to the effect of thermophysical properties near the critical point, as observed in previous experiments [7], [11]. Bellinghausen & Renz [36] conducted the numerical studies including the gravitational effect in the flow in vertical heated tubes filled with supercritical R12 by using the low-Re k - ϵ models developed by Jones & Launder [43, 44] to resolve the flow in the near wall region. The behavior that gravity-driven buoyancy effects tend to relaminarize the flow near the wall in the pseudocritical region could be predicted quite well. Another numerical study was done by Koshizuka et al. [45] using the same models for simulating supercritical water in a vertical tube. The heat transfer coefficient and calculated deteriorated heat flux agreed well with those from the experimental study by Yamagata et al. [8]. He et al. [46] simulated the heat transfer of supercritical carbon dioxide in a vertical mini tube by using several two-equation low-Re k - ϵ models. Compared with respective experimental results, although most of these models can capture the effects of strong influence of buoyancy on heat transfer, the onset of the effect could not be well predicted.

The standard k - ω model [47] is sensitive to free stream conditions. Menter [48] proposed the shear-stress transport (SST) model which combines the advantage of the k - ϵ model in the bulk flow and the low-Re treatment of the boundary layer in the near wall region. This attracts the interest in applying k - ω models in the simulations of the heat transfer in supercritical fluids [37–39], [49, 50]. In these simulations, although the ω type models with automatic wall treatment generally failed to predict the heat transfer coefficients in the near pseudocritical region, they performed better than the low-Re k - ϵ models. In the two-equation models, like k - ϵ and k - ω models, the turbulent viscosity is assumed isotropic indicating that the ratio between Reynolds stress and mean rate of deformation is identical in all directions. This assumption can cause problem in predicting anisotropic behaviors in complicated turbulent flows. The Reynolds stress model (RSM) solves the individual

components of the Reynold stress directly without this assumption, which resulted in increased interest in the use of RSM investigating supercritical fluids in heated tubes [39–42], [50]. Compared with other isotropic models applied in the simulation of heat transfer in supercritical carbon dioxide and supercritical water flows in heated tubes, RSM generally could achieve better agreement with the experimental results [39]. Nevertheless, extensive numerical studies of RSM used in different operating conditions are still needed to assess the applicability conditions.

2.2.2. Heat transfer in channels with multiple fuel rods

2.2.2.1. Experimental work

In the 1990s - 2000s, enthusiasm in new experimental studies were aroused by several reasons [34]: 1) experimental data of supercritical fluids in simple tubes can not represent directly those in rod bundles because of the difference in geometry; 2) experimental technology has been improved; 3) the hydraulic diameters of supercritical fluids in the proposed rod bundle are less than those in tubes/pipes. In recent years, a limited number of experimental studies were devoted to heat transfer of supercritical fluids in annuli and simplified rod bundle simulators [13], [51–64]. The channels were mostly heated with an electrical current. In general, the flow geometries are annulus, 3, 4 and 7 rod bundles. The heat transfer regimes including NHT, EHT, and DHT all could occur, and it varies with operating conditions. In the studies by Razumovskiy et al. [51], [57–59], heat transfer coefficients obtained in the experiments of supercritical water in annulus and 3 rod bundles were compared with those calculated by the Dittus-Boelter correlation for the tube flow. It was found that the difference between the experimental and calculated heat transfer coefficients is not significant, and there is no significant increase in the heat transfer coefficient although multiple rods exist in the flow channel. However, the onset heat fluxes of DHT for annulus, 3 and 7 rod bundles were 1.6 - 1.8 time higher than those in bare tubes with the same operating parameters. Chen et al. [56] studied heat transfer of supercritical water in a 3-rod bundle. The experimental results of wall temperatures showed that there were large gradients in circumferential wall temperature distributions while the gradient

significantly decreased when the bulk fluid temperature approaching the pseudocritical temperature. In addition, the wall temperature is higher in the central subchannel between rods while lower in the corner/edge subchannel region. Richards et al. [62] conducted experiments of supercritical freon R-12 in vertically oriented 7 rod bundle. The bulk fluid temperatures along the axial locations and wall temperatures of the central rod at three circumferential locations for 20 cases were presented. The results proved that all three heat transfer regimes could appear in the rod bundles, which supports the conclusions drawn by Razumovskiy et al. [51], and generally no single correlation could predict HTC profiles within $\pm 50\%$. Experimental studies in [13], [52–56], [63, 64] were for the heat transfer of supercritical water in annuli and rod bundles. It was observed from the experiments in square annular flow geometries [13], [63], that DHT depends on hydraulic diameter and there were wall temperature oscillations when the bulk fluid temperature approaching the pseudocritical point. Square annular rod bundles are not widely seen in the industry applications. On the other hand, experiments were also conducted in circular annular channels by [52], [55], [63, 64]. The results generally showed that the effect of operating pressures on wall temperatures can not be ignored and DHT is more severe in a narrower gap. 2×2 rod geometry were used recently [53, 54] to investigate the heat transfer of supercritical water in rod bundles. It was shown that the wall temperature distributions along fuel rods are not uniform, which could result from the changes of the subchannel flow area around the rods. However, higher wall temperature is in the corner/edge subchannel while lower region is in the central subchannel region between rods. This is opposite to the experimental results from Chen et al. [56]. It can be concluded that the flow geometry strongly affects the heat transfer characteristics of supercritical water in rod bundles.

2.2.2.2. Numerical work

Although the experiments of supercritical fluids could provide the macroscopic data of heat transfer, it is still important to investigate the detailed flow and turbulent behaviors which lead to different heat transfer regimes. Therefore, CFD methods have been widely used to predict the behavior of supercritical water flow and heat transfer in rod bundles. The DNS

method is seldomly used in the investigations of supercritical water in rod bundles. Instead of the DNS methods, the LES method has been used by some researchers. Fischer et al. [65] performed the LES simulations on a single fuel pin through the spectral method. Merzari et al. [66] and Brockmeyer et al. [67] consecutively used Nek500 code to simulate the flow in a 7-pin reactor geometry. Brockmeyer et al. [68] applied STARCCM+ software to perform the simulation using the LES method in a 19-pin flow geometry with a shortened rod length. Recently, Goth et al. [69] employed the same code to investigate the flow behaviors in a 61-pin geometry. Although the LES method is more applicable than the DNS in the study of nuclear reactor, there are still some limitations. The Reynolds number should be less than around 20000 for large flow geometries [78]. In the industrial applications, the Reynolds number of the flow in the reactor usually exceeds this number. Thus, the RANS method is widely used in the numerical study of the high turbulent supercritical water flow in the nuclear reactor.

The numerical studies by RANS simulations for the supercritical flow in rod bundles have been investigated by several researchers [70–75]. Zhao et al. [70] used OpenFOAM to simulate a 7-pin flow geometry with the $k-\omega$ SST turbulence model for different operation conditions. Zhang et al. [71] simulated the heat transfer and flow of supercritical water in a 37-element horizontal arranged SCWR under steady state condition and found that the anisotropic turbulent model, the RSM, behaves much better than the isotropic model in predicting the cladding surface temperature. Furthermore, Han et al. [72] further applied the same model in the vertical channel with multiple fuel rods. Other similar investigations can be found in [73, 74]. The heat transfer characteristics in different type channels were investigated. A recent validation study of the RANS models for different fuel rod assemblies was performed by Dovizio et al. [75]. It was found that the RANS could be a reasonable approach to simulate flows in fuel assemblies. There are also several numerical studies for flows in rod bundles, but the operating conditions are not supercritical conditions [76–78]. Despite the operating conditions are not supercritical, the effects of cross-section geometry and Re on the flow and heat transfer can be investigated. The simulation results from Bovati et al. [78] showed that the axial velocity distribution in the

cross-section of the fuel bundle is more uniform with the increase in Re . In addition, a higher cross-flow was observed at the same time.

2.3. Control systems for SCWR

Based on the experimental and numerical studies in heat transfer of supercritical water, deteriorated heat transfer accompanied with the increase in the wall temperature could threaten the safety of a nuclear reactor. Thus, a reliable control system is necessary to promptly regulate the reactor operating condition at a desired point when there are disturbances. The idea of the supercritical water-cooled reactors (SCWR) is based on established techniques of the boiling water reactors (BWR) and supercritical fossil power plants (SCFPP). The SCWR uses the once-through direct cycle, which is similar to the BWR and supercritical operating pressure, which is similar to the SCFPP. In addition, the high heat to mass flux ratio in the rod bundle and dramatic changes of thermophysical properties at the supercritical conditions bring the complexity for the design of the control system.

The earliest control system designs for reactor operating at supercritical conditions were done by Nakatsuka et al. [79] for the supercritical fast reactor (SCFR) and Ishiwatari et al. [80–81] for the high temperature supercritical pressure light water-cooled thermal reactor (SCLWR-H). The reactor is subjected to disturbances of three inputs: feedwater flow rate, position of control rods, and the turbine control valve opening, respectively. The outputs of the reactor, including operating pressure, main steam temperature, and reactor power were analyzed. According to the responses, the most influenced input and output pairing was identified without considering the cross-couple effects. The structures of controllers were multiple single-input single-output (SISO) feedback control loop designs. With the designed control system, the outputs of reactors were regulated against the disturbances. There are typically two operating modes in nuclear power plants, reactor-following-turbine and turbine-following-reactor. In the reactor-following-turbine mode, the pressure of the main steam in turbine is governed by the reactor power and the output of the electric power

is regulated by the turbine control valves. In this mode, the reactor should respond promptly to load change. In the design of once-through cycle, the strong fluctuations of the steam flow rate and the temperature of the supercritical water in the reactor core could lead to thermal stress on fuel rods and pressure vessel. In contrast, the pressure of the main steam in turbine is controlled by the turbine control valves and the output of the electric power is governed by the reactor power in the turbine-following-reactor mode. Although the reactor is slow to respond to load change in this mode, the operation can be relatively stable. In the case that safety is the main aim of nuclear reactors, the control strategies for reactor operating at supercritical conditions mainly adopted the turbine-following-reactor operation mode [80–83]. Sun & Jiang [82] used one-dimensional thermal hydraulic model to simulate the transient response of outputs for the Canadian SCWR. A least-square system identification method is used to construct a dynamic model representing the dynamic behaviors of inputs and outputs of the reactor. For a multiple-input multiple-output (MIMO) reactor system, the cross-coupling relationship among inputs and outputs at the steady state is first determined by the relative gain array (RGA) [84]. RGA is the normalized form of steady state gain matrix of a MIMO system which measures the effects of the specific input on an output with respect to its effect on other outputs. The most interacted input & output of the system is chosen according to the RGA results. Based on this method, Sun et al. [83] adopted the direct Nyquist array method to decouple the system, so that the dynamic relationship of inputs and outputs of the reactor is in a diagonally dominant form. The work by Sun et al. [83] was based on one-dimensional thermal hydraulic model of the reactor, which cannot represent the full-scale flow and heat transfer behavior of the supercritical water in a reactor. Maitri et al. [85] implemented the same control methodology as that by Sun et al. [83] while used the simulation results by CFD to obtain the dynamic relationship between inputs and outputs of the reactor. Despite the flow was simplified from rod bundle flow to tube flow, the study identified that CFD simulations could be adopted to obtain the linear dynamic models for Canadian SCWR. Decoupling the MIMO system to a diagonally dominant form could reduce the interaction between outputs and inputs, however, the effects of cross-coupling were not obvious except for the control on the outlet steam temperature of the reactor [86]. In addition, decoupling methodology is very sensitive to the accuracy of the linear dynamic model of the system

which make it not commonly utilized in industrial control system. Han et al. [87] used the same CFD assisted control system design approach that used by Maitri et al. [85] for heated channels in a 37-element Canadian SCWR. The construction of dynamic models was based on the results from a full-scale CFD simulation. The performance of design control system was evaluated by combining the control system into CFD simulation process to form the closed loop control. The results showed that the deigned control system could adjust the system to the desired operating point in time.

2.4. Motivations and Objectives

In all of the CFD studies discussed up to this point, different turbulent models have been assessed against the available experimental data. It has been assumed that the turbulent Prandtl number is a constant. The performance of the turbulent models varies case-by-case, which mainly depends on the operating conditions, such as types of supercritical fluids, heat to mass flux ratio, the geometry of the flow channel, and the flow direction. The strong buoyancy and thermal acceleration effects caused by the strong variations of the thermal physical properties of the supercritical water near the pseudo-critical point should be considered in the CFD simulations. Besides, the Reynolds analogy assumption used in the above numerical studies is doubtful since the molecular Prandtl number changes sharply at supercritical conditions [88–95]. It is also worth to point out that the flow channel in the actual nuclear reactor includes multiple heated fuel rods, which leads to a complicated heat transfer phenomenon. The turbulent Prandtl number (Pr_t) is crucial for predicting the heat transfer phenomenon in the channel at the supercritical condition. Thus, it is necessary to include all the relevant parameters to construct a new variable Pr_t model for the supercritical water, which is complemented in this study.

Canadian SCWR has not been built yet, but the fuel assembly concept has been determined. The fuel bundle of the Canadian SCWR consists of 64-element two-ring fuel rods. For each ring, 32 fuel elements are distributed circumferentially around the insulated central flow tube [96]. There is still lack of the investigation of the thermo-hydraulic behaviors of the

supercritical water in the 64-element fuel bundle. In this work, the flow and heat transfer of the supercritical water in the 64-element fuel bundle is investigated numerically by the RANS approach and the detailed fluid flow and heat transfer phenomenon for the supercritical water in the fuel rod channels are presented.

As discussed before, even in rod bundles, the heat transfer regime could be different based on the flow geometry. There are many operating parameters that could influence the flow and heat transfer of the supercritical water in the 64-element Canadian SCWR rod bundle. Effects of different operating pressures, inlet temperatures, heat fluxes, and inlet mass flow rates on the heat transfer regime are investigated in this work.

There has not been a control system design focusing on the heat transfer characteristics in the rod bundle for the 64-element Canadian SCWR now. Based on the CFD simulations, the dynamic relationship between inputs and outputs of reactors will be established in this work. The maximum cladding surface temperature, which is an important parameter for the safety operation of the reactor, is chosen as one of the outputs. A feedback control system will be constructed for the 64-element Canadian SCWR and its performance for the reactor subjected to disturbances of outputs will be evaluated.

In this study, the dynamic model for the entire Canadian SCWR power plant will be constructed, which includes the feedwater pump, reactor, turbine and condenser. The dynamic models of subcomponents in the cycle [84], i.e. the outlet plenum, main steam line, turbine control valve, are also included in the proposed control system.

2.5. Outline of the thesis

The remaining chapters of this thesis will be presented as follows:

- *Chapter 3:* A modified turbulent model for the supercritical water flows in the vertical upward channels is presented. The key contributions in this chapter are the extensive evaluations of the existed conventional turbulent models and the development of a new variable turbulent Prandtl number model.
- *Chapter 4:* The numerical simulation of fluid flow and heat transfer of supercritical water in the 64-element Canadian SCWR fuel bundle by the modified turbulent model is presented. The key outcome of this chapter is filling the gaps of the investigation of the thermo-hydraulic behaviors of the supercritical water in the 64-element fuel bundle.
- *Chapter 5:* Parametric studies on heat transfer of supercritical water flows in the 64-element Canadian SCWR fuel bundle are presented. The results of this chapter could help understand the heat transfer regimes of supercritical water in the rod bundles at various operating conditions.
- *Chapter 6:* A design of the feedback control system for the 64-element Canadian SCWR assisted with CFD simulations is presented. The key contributions of this chapter are filling the gaps of control system design for the 64-element Canadian SCWR and it is the first time the important parameter, the maximum cladding surface temperature is chosen as one of the outputs.
- *Chapter 7:* The control system for the entire SCWR power plant is constructed in this chapter. The key outcome of this chapter is to provide a substantial control strategy for the SCWR power plant under full load operating condition.
- *Chapter 8:* A summary of the contributions of the present study and directions for the future work.

References

- [1] F. P. Incropera, *Fundamentals of heat and mass transfer*, 6th ed. Hoboken, NJ: John Wiley, 2007.
- [2] F. W. Dittus and L. M. K. Boelter, “Heat transfer in automobile radiators of the tubular type,” *Int. Commun. Heat Mass Transf.*, vol. 12, no. 1, pp. 3–22, Jan. 1985.
- [3] M. Shitsman, “Impairment of the heat transmission at supercritical pressures,” *High Temp.*, vol. 1, pp. 237–244, 1963.
- [4] H. S. Swenson, J. . Carver, and C. R. Kakarala, “Heat transfer to supercritical water in smooth-bore tubes,” *J. Heat Transfer*, vol. 87, no. 4, pp. 477–483, 1965.
- [5] E. N. Dubrovina and V. P. Skripov, “Convection and heat transfer near the critical point of carbon dioxide,” *J. Appl. Mech. Tech. Phys.*, vol. 6, no. 1, pp. 107–111, 1966.
- [6] B. Shiralkar and P. Griffith, “Deterioration in heat transfer to fluids at supercritical pressure and high heat fluxes,” *J. Heat Transfer*, vol. 91, no. 1, pp. 27–36, 1969.
- [7] T. Hiroaki, T. Ayao, H. Masaru, and N. Nuchi, “Effects of buoyancy and of acceleration owing to thermal expansion on forced turbulent convection in vertical circular tubes—criteria of the effects, velocity and temperature profiles, and reverse transition from turbulent to laminar flow,” *Int. J. Heat Mass Transf.*, vol. 16, no. 6, pp. 1267–1288, Jun. 1973.
- [8] K. Yamagata, K. Nishikawa, S. Hasegawa, T. Fujii, and S. Yoshida, “Forced convective heat transfer to supercritical water flowing in tubes,” *Int. J. Heat Mass Transf.*, vol. 15, no. 12, pp. 2575–2593, Dec. 1972.
- [9] J. Wang, H. Li, S. Yu, and T. Chen, “Investigation on the characteristics and mechanisms of unusual heat transfer of supercritical pressure water in vertically-upward tubes,” *Int. J. Heat Mass Transf.*, vol. 54, no. 9–10, pp. 1950–1958, Apr. 2011.
- [10] W. B. Hall and J. D. Jackson, “Laminarization of a turbulent pipe flow by buoyancy

- forces,” in *11 th ASME-AIChE National Heat Transfer Conference*, 1969, p. 8.
- [11] V. A. Kurganov and A. G. Kaptil’ny, “Velocity and enthalpy fields and eddy diffusivities in a heated supercritical fluid flow,” *Exp. Therm. Fluid Sci.*, vol. 5, no. 4, pp. 465–478, Jul. 1992.
- [12] B. Shiralkar and P. Griffith, “The Effect of Swirl, Inlet Conditions, Flow Direction, and Tube Diameter on the Heat Transfer to Fluids at Supercritical Pressure,” *J. Heat Transfer*, vol. 92, no. 3, pp. 465–471, Aug. 1970.
- [13] H. Li *et al.*, “Experimental investigation on heat transfer from a heated rod with a helically wrapped wire inside a square vertical channel to water at supercritical pressures,” *Nucl. Eng. Des.*, vol. 239, no. 10, pp. 2004–2012, Oct. 2009.
- [14] J. H. Bae, J. Y. Yoo, and D. M. McEligot, “Direct numerical simulation of heated CO₂ flows at supercritical pressure in a vertical annulus at Re=8900,” *Phys. Fluids*, vol. 20, no. 5, 2008.
- [15] A. P. Ornatskij, L. F. Glushchenko, and S. I. Kalachev, “Heat transfer with rising and falling flows of water in tubes of small diameter at supercritical pressures,” *Thermal Engineering*, vol. 18, no. 5. pp. 137–141, 1971.
- [16] A. Shehata and D. McEligot, “Mean structure in the viscous layer of strongly-heated internal gas flows measurement,” *Int. J. Heat Mass Transf.*, vol. 41, no. 24, pp. 4297–4313, 1998.
- [17] K. Tanimizu and R. Sadr, “Experimental investigation of buoyancy effects on convection heat transfer of supercritical CO₂ flow in a horizontal tube,” *Heat Mass Transf. und Stoffuebertragung*, vol. 52, no. 4, pp. 713–726, 2016.
- [18] R. N. Xu, F. Luo, and P. X. Jiang, “Buoyancy effects on turbulent heat transfer of supercritical CO₂ in a vertical mini-tube based on continuous wall temperature measurements,” *Int. J. Heat Mass Transf.*, vol. 110, pp. 576–586, 2017.
- [19] X. Lei, H. Li, N. Dinh, and W. Zhang, “A study of heat transfer scaling of supercritical pressure water in horizontal tubes,” *Int. J. Heat Mass Transf.*, vol. 114, pp. 923–933, 2017.

- [20] M. Qu, D. Yang, Z. Liang, L. Wan, and D. Liu, "Experimental and numerical investigation on heat transfer of ultra-supercritical water in vertical upward tube under uniform and non-uniform heating," *Int. J. Heat Mass Transf.*, vol. 127, pp. 769–783, Dec. 2018.
- [21] S. Zhang, X. Xu, C. Liu, X. Liu, and C. Dang, "Experimental investigation on the heat transfer characteristics of supercritical CO₂ at various mass flow rates in heated vertical-flow tube," *Appl. Therm. Eng.*, vol. 157, p. 113687, Jul. 2019.
- [22] S. Mokry, I. Pioro, A. Farah, K. King, S. Gupta, W. Peiman, and P. Kirillov, "Development of supercritical water heat-transfer correlation for vertical bare tubes," *Nucl. Eng. Des.*, vol. 241, no. 4, pp. 1126–1136, 2011.
- [23] S. Kang, B. Patil, J. A. Zarate, and R. P. Roy, "Isothermal and heated turbulent upflow in a vertical annular channel – Part I. Experimental measurements," *Int. J. Heat Mass Transf.*, vol. 44, no. 6, pp. 1171–1184, Mar. 2001.
- [24] J. Licht, M. Anderson, and M. Corradini, "Heat Transfer and Fluid Flow Characteristics in Supercritical Pressure Water," *J. Heat Transfer*, vol. 131, no. 7, pp. 72502–72514, Jul. 2009.
- [25] A. Bruch, A. Bontemps, and S. Colasson, "Experimental investigation of heat transfer of supercritical carbon dioxide flowing in a cooled vertical tube," *Int. J. Heat Mass Transf.*, vol. 52, no. 11–12, pp. 2589–2598, May 2009.
- [26] S. J. Mokry, P. L. Kirillov, I. L. Pioro, and Y. K. Gospodinov, "Supercritical Water Heat Transfer in a Vertical Bare Tube: Normal, Improved, and Deteriorated Regimes," *Nucl. Technol.*, vol. 172, no. 1, pp. 60–70, 2010.
- [27] S. Yu, H. Li, X. Lei, Y. Feng, Y. Zhang, H. He, and T. Wang, "Experimental investigation on heat transfer characteristics of supercritical pressure water in a horizontal tube," *Exp. Therm. Fluid Sci.*, vol. 50, pp. 213–221, 2013.
- [28] S. Zhang, H. Gu, X. Cheng, and Z. Xiong, "Experimental study on heat transfer of supercritical Freon flowing upward in a circular tube," *Nucl. Eng. Des.*, vol. 280, pp. 305–315, Dec. 2014.

- [29] H. Y. Gu, M. Zhao, and X. Cheng, “Experimental studies on heat transfer to supercritical water in circular tubes at high heat fluxes,” *Exp. Therm. Fluid Sci.*, 2015.
- [30] S. J. Mokry and I. L. Pioro, “Heat transfer correlation for supercritical carbon dioxide flowing upward in a vertical bare tube,” in *Supercritical CO₂ Power Cycle Symposium*, 2011, pp. 1–10.
- [31] P. Surendran, S. Gupta, T. Preda, and I. Pioro, “Comparison of Existing Supercritical Carbon Dioxide Heat Transfer Correlations for Horizontal and Vertical Bare Tubes,” in *Volume 5: Fusion Engineering; Student Paper Competition; Design Basis and Beyond Design Basis Events; Simple and Combined Cycles*, 2012, pp. 335–342.
- [32] J. Y. Yoo, “The turbulent flows of supercritical fluids with heat transfer,” *Annu. Rev. Fluid Mech.*, vol. 45, pp. 495–525, 2013.
- [33] I. L. Pioro, H. F. Khartabil, and R. B. Duffey, “Heat transfer to supercritical fluids flowing in channels—empirical correlations (survey),” *Nucl. Eng. Des.*, vol. 230, no. 1–3, pp. 69–91, May 2004.
- [34] I. L. Pioro, “Current status of research on heat transfer in forced convection of fluids at supercritical pressures,” *Nucl. Eng. Des.*, vol. 354, no. June, p. 110207, 2019.
- [35] C. P. Bellmore and R. L. Reid, “Numerical Prediction of Wall Temperatures for Near-Critical Para-Hydrogen in Turbulent Upflow Inside Vertical Tubes,” *J. Heat Transfer*, vol. 105, no. 3, pp. 536–541, Aug. 1983.
- [36] R. Bellinghausen and U. Renz, “Pseudocritical heat transfer inside vertical tubes,” *Chem. Eng. Process. Process Intensif.*, vol. 28, no. 3, pp. 183–186, Dec. 1990.
- [37] J. Yang, Y. Oka, Y. Ishiwatari, J. Liu, and J. Yoo, “Numerical investigation of heat transfer in upward flows of supercritical water in circular tubes and tight fuel rod bundles,” *Nucl. Eng. Des.*, vol. 237, no. 4, pp. 420–430, 2007.
- [38] Q. L. Wen and H. Y. Gu, “Numerical simulation of heat transfer deterioration phenomenon in supercritical water through vertical tube,” *Ann. Nucl. Energy*, vol.

- 37, no. 10, pp. 1272–1280, 2010.
- [39] G. Dutta, R. Maitri, C. Zhang, and J. Jiang, “Numerical models to predict steady and unsteady thermal-hydraulic behaviour of supercritical water flow in circular tubes,” *Nucl. Eng. Des.*, vol. 289, pp. 155–165, 2015.
- [40] M. T. Kao, M. Lee, Y. M. Ferng, and C. C. Chieng, “Heat transfer deterioration in a supercritical water channel,” *Nucl. Eng. Des.*, vol. 240, no. 10, pp. 3321–3328, 2010.
- [41] Y. Zhang, C. Zhang, and J. Jiang, “Numerical Simulation of Heat Transfer of Supercritical Fluids in Circular Tubes Using Different Turbulence Models,” *J. Nucl. Sci. Technol.*, vol. 48, no. 3, pp. 366–373, 2011.
- [42] R. Maitri, H. Han, C. Zhang, and J. Jiang, “Numerical Investigation of the Deteriorated Heat Transfer Phenomenon for Supercritical Water Flows in Vertical Circular Tubes,” in *Complementary Resources for Tomorrow*, A. Vassel-Be-Hagh and D. S.-K. Ting, Eds. Cham: Springer International Publishing, 2020, pp. 235–248.
- [43] W. P. Jones and B. E. Launder, “The prediction of laminarization with a two-equation model of turbulence,” *Int. J. Heat Mass Transf.*, vol. 15, no. 2, pp. 301–314, 1972.
- [44] B. E. Launder and B. I. Sharma, “Application of the energy-dissipation model of turbulence to the calculation of flow near a spinning disc,” *Lett. Heat Mass Transf.*, vol. 1, no. 2, pp. 131–137, Nov. 1974.
- [45] S. Koshizuka, N. Takano, and Y. Oka, “Numerical analysis of deterioration phenomena in heat transfer to supercritical water,” *Int. J. Heat Mass Transf.*, vol. 38, no. 16, pp. 3077–3084, Nov. 1995.
- [46] S. He, P. X. Jiang, Y. J. Xu, R. F. Shi, W. S. Kim, and J. D. Jackson, “A computational study of convection heat transfer to CO₂ at supercritical pressures in a vertical mini tube,” *Int. J. Therm. Sci.*, vol. 44, no. 6, pp. 521–530, Jun. 2005.
- [47] D. C. Wilcox, “Reassessment of the scale-determining equation for advanced

- turbulence models,” *AIAA J.*, vol. 26, no. 11, pp. 1299–1310, Nov. 1988.
- [48] F. Menter, “Zonal two equation k-turbulence models for aerodynamic flows,” in *In 24th AIAA Fluid Dynamics Conference*, 1993, pp. 1–21.
- [49] S. He, W. S. Kim, P. X. Jiang, and J. D. Jackson, “Simulation of mixed convection heat transfer to carbon dioxide at supercritical pressure,” *Proc. Inst. Mech. Eng. Part C J. Mech. Eng. Sci.*, vol. 218, no. 11, pp. 1281–1296, Nov. 2004.
- [50] X. Cheng, B. Kuang, and Y. H. Yang, “Numerical analysis of heat transfer in supercritical water cooled flow channels,” *Nucl. Eng. Des.*, vol. 237, no. 3, pp. 240–252, Feb. 2007.
- [51] V. G. Razumovskiy, E. M. Mayevskiy, A. E. Koloskov, E. N. Pis’mennyi, and I. L. Pioro, “Heat Transfer to Water at Supercritical Parameters in Vertical Tubes, Annular Channels, 3- and 7-Rod Bundles,” in *Volume 4: Thermal Hydraulics*, 2013, pp. 1–8.
- [52] Z. Yang, Q. Bi, H. Wang, G. Wu, and R. Hu, “Experiment of heat transfer to supercritical water flowing in vertical annular channels,” *J. Heat Transfer*, vol. 135, no. 4, pp. 1–9, 2013.
- [53] H. Wang, Q. Bi, L. Wang, H. Lv, and L. K. H. Leung, “Experimental investigation of heat transfer from a 2×2 rod bundle to supercritical pressure water,” *Nucl. Eng. Des.*, vol. 275, pp. 205–218, Aug. 2014.
- [54] H. Y. Gu, H. B. Li, Z. X. Hu, D. Liu, and M. Zhao, “Heat transfer to supercritical water in a 2×2 rod bundle,” *Ann. Nucl. Energy*, vol. 83, pp. 114–124, 2015.
- [55] M. Zhao, H. Y. Gu, H. B. Li, and X. Cheng, “Heat transfer of water flowing upward in vertical annuli with spacers at high pressure conditions,” *Ann. Nucl. Energy*, vol. 87, pp. 209–216, 2016.
- [56] S. Chen, H. Gu, M. Liu, Y. Xiao, and D. Cui, “Experimental investigation on heat transfer to supercritical water in a three-rod bundle with spacer grids,” *Appl. Therm. Eng.*, vol. 164, p. 114466, Jan. 2020.

- [57] V. G. Razumovskiy, E. N. Pis'mennyi, K. Sidawi, I. L. Pioro, and A. E. Koloskov, "Experimental heat transfer in an annular channel and 3-rod bundle cooled with upward flow of supercritical water," *J. Nucl. Eng. Radiat. Sci.*, vol. 2, no. 1, pp. 1–8, 2016.
- [58] V. G. Razumovskiy, E. N. Pis'mennyi, A. E. Koloskov, and I. L. Pioro, "Heat Transfer to Supercritical Water in Vertical Annular Channel and 3-Rod Bundle," in *Volume 3: Thermal Hydraulics; Current Advanced Reactors: Plant Design, Construction, Workforce and Public Acceptance*, 2009, vol. 3, pp. 233–238.
- [59] V. G. Razumovskiy, E. N. Pis'mennyi, A. E. Koloskov, and I. L. Pioro, "Heat Transfer to Supercritical Water in Vertical 7-Rod Bundle," in *Volume 3: Thermal Hydraulics; Instrumentation and Controls*, 2008, vol. 3, pp. 963–969.
- [60] I. L. Pioro and R. B. Duffey, *Heat Transfer & Hydraulic Resistance at Supercritical Pressures in Power Engineering Applications*. New York, NY, USA: ASME Press, 2007.
- [61] K. Sidawi, I. Pioro, V. G. Razumovskiy, E. N. Pis'mennyi, and A. E. Koloskov, "HTC CORRELATION APPLICATIONS TO SUPERCRITICAL WATER FLOWING UPWARD IN A VERTICAL ANNULAR CHANNEL AND 3-ROD BUNDLE," in *The Proceedings of the International Conference on Nuclear Engineering (ICONE)*, 2015, vol. 2015.23, p. _ICONE23-1-_ICONE23-1.
- [62] G. Richards, G. D. Harvel, I. L. Pioro, A. S. Shelegov, and P. L. Kirillov, "Heat transfer profiles of a vertical, bare, 7-element bundle cooled with supercritical freon R-12," *Nucl. Eng. Des.*, vol. 264, pp. 246–256, 2013.
- [63] J. Licht, M. Anderson, and M. Corradini, "Heat transfer to water at supercritical pressures in a circular and square annular flow geometry," *Int. J. Heat Fluid Flow*, vol. 29, no. 1, pp. 156–166, 2008.
- [64] W. Gang, Q. Bi, Z. Yang, H. Wang, X. Zhu, H. Hao, and L.K.H. Leung, "Experimental investigation of heat transfer for supercritical pressure water flowing in vertical annular channels," *Nucl. Eng. Des.*, vol. 241, no. 9, pp. 4045–4054, 2011.

- [65] P. Fischer, J. Lottes, A. Siegel, and G. Palmiotti, “Large eddy simulation of wire-wrapped fuel pins i: Hydrodynamics in a periodic array,” in *Joint International Topical Meeting on Mathematics & Computation and Supercomputing in Nuclear Applications, Monterey, CA, USA, 2007*.
- [66] E. Merzari, P. Fischer, H. Yuan, K. Van Tichelen, S. Keijers, J. De Ridder, J. Degroote, J. Vierendeels, H. Doolaard, V. R. Gopala, and F. Roelofs, “Benchmark exercise for fluid flow simulations in a liquid metal fast reactor fuel assembly,” *Nucl. Eng. Des.*, vol. 298, pp. 218–228, Mar. 2016.
- [67] L. Brockmeyer, E. Merzari, J. Solberg, and Y. Hassan, “One-way coupled simulation of FIV in a 7-pin wire-wrapped fuel pin bundle,” *Nucl. Eng. Des.*, vol. 356, p. 110367, Jan. 2020.
- [68] L. Brockmeyer, L. B. Carasik, E. Merzari, and Y. Hassan, “Numerical simulations for determination of minimum representative bundle size in wire wrapped tube bundles,” *Nucl. Eng. Des.*, vol. 322, pp. 577–590, Oct. 2017.
- [69] N. Goth, P. Jones, D. T. Nguyen, R. Vaghetto, Y. A. Hassan, A. Obabko, E. Merzari, and P. F. Fischer, “Comparison of experimental and simulation results on interior subchannels of a 61-pin wire-wrapped hexagonal fuel bundle,” *Nucl. Eng. Des.*, vol. 338, pp. 130–136, Nov. 2018.
- [70] P. Zhao, J. Liu, Z. Ge, X. Wang, and X. Cheng, “CFD analysis of transverse flow in a wire-wrapped hexagonal seven-pin bundle,” *Nucl. Eng. Des.*, vol. 317, pp. 146–157, Jun. 2017.
- [71] Y. Zhang, C. Zhang, and J. Jiang, “Numerical Simulation of Fluid Flow and Heat Transfer of Supercritical Fluids in Fuel Bundles,” *J. Nucl. Sci. Technol.*, vol. 48, no. 6, pp. 929–935, 2011.
- [72] H. Han and C. Zhang, “Numerical Simulation of Fluid Flow and Heat Transfer of the Supercritical Water in Different Fuel Rod Channels,” in *Progress in Canadian Mechanical Engineering*, 2018.
- [73] X. Yang, G. H. Su, W. Tian, J. Wang, and S. Qiu, “Numerical study on flow and

heat transfer characteristics in the rod bundle channels under super critical pressure condition,” *Ann. Nucl. Energy*, vol. 37, no. 12, pp. 1723–1734, 2010.

- [74] K. Podila and Y. Rao, “CFD modelling of supercritical water flow and heat transfer in a 2×2 fuel rod bundle,” *Nucl. Eng. Des.*, vol. 301, pp. 279–289, May 2016.
- [75] D. Dovizio, B. Mikuž, A. Shams, and F. Roelofs, “Validating RANS to predict the flow behavior in wire-wrapped fuel assemblies,” *Nucl. Eng. Des.*, vol. 356, p. 110376, Jan. 2020.
- [76] M. Bruschi, M. H. A. Piro, C. Tropea, and S. Grundmann, “Fluid flow in a diametrically expanded CANDU fuel channel – Part 1: Experimental study,” *Nucl. Eng. Des.*, vol. 357, p. 110371, Feb. 2020.
- [77] M. H. A. Piro, M. Christon, B. Tensuda, M. Poschmann, M. Bruschi, S. Grundmann, and C. Tropea, “Fluid flow in a diametrically expanded CANDU fuel channel – Part 2: Computational study,” *Nucl. Eng. Des.*, vol. 357, p. 110372, Feb. 2020.
- [78] O. Bovati, M. A. Yildiz, Y. Hassan, and R. Vaghetto, “RANS simulations for transition and turbulent flow regimes in wire-wrapped rod bundles,” *Int. J. Heat Fluid Flow*, vol. 90, no. June, p. 108838, Aug. 2021.
- [79] T. Nakatsuka, Y. Oka, and S. Koshizuka, “Control of a Fast Reactor Cooled by Supercritical Light Water,” *Nucl. Technol.*, vol. 121, no. 1, pp. 81–92, Jan. 1998.
- [80] Y. ISHIWATARI, Y. OKA, and S. KOSHIZUKA, “Control of a High Temperature Supercritical Pressure Light Water Cooled and Moderated Reactor with Water Rods,” *J. Nucl. Sci. Technol.*, vol. 40, no. 5, pp. 298–306, May 2003.
- [81] Y. ISHIWATARI, C. PENG, S. IKEJIRI, and Y. OKA, “Improvements of Feedwater Controller for the Super Fast Reactor,” *J. Nucl. Sci. Technol.*, vol. 47, no. 12, pp. 1155–1164, 2010.
- [82] P. Sun and J. Jiang, “Construction and Analysis of a Dynamic Model for a Canadian Direct-Cycle SCWR for Control System Studies,” *Nucl. Technol.*, vol. 180, no. 3, pp. 399–421, Dec. 2012.

- [83] P. Sun, J. Jiang, and K. Wang, “Decoupling Control of Canadian Supercritical Water-Cooled Reactors,” *Nucl. Technol.*, vol. 185, no. 3, pp. 239–258, 2014.
- [84] E. Bristol, “On a new measure of interaction for multivariable process control,” *IEEE Trans. Automat. Contr.*, vol. 11, no. 1, pp. 133–134, Jan. 1966.
- [85] R. V. Maitri, C. Zhang, and J. Jiang, “Computational fluid dynamic assisted control system design methodology using system identification technique for CANDU supercritical water cooled reactor (SCWR),” *Appl. Therm. Eng.*, vol. 118, pp. 17–22, 2017.
- [86] P. Sun, B. Wang, J. Zhang, and G. Su, “Control of Canadian once-through direct cycle supercritical water-cooled reactors,” *Ann. Nucl. Energy*, vol. 81, pp. 6–17, Jul. 2015.
- [87] H. Han, C. Zhang, and J. Jiang, “Dynamic models and control system design for heated channels in a Canadian SCWR,” *Ann. Nucl. Energy*, vol. 151, p. 107973, Feb. 2021.
- [88] X. Chai, X. Liu, J. Xiong, and X. Cheng, “Numerical Investigation of Turbulent Heat Transfer Properties at Low Prandtl Number,” vol. 8, no. July, pp. 1–11, 2020.
- [89] H. K. MYONG, N. KASAGI, and M. HIRATA, “Numerical Prediction of Turbulent Pipe Flow Heat Transfe for Various Prandtl Number Fluids with the Improved k - ϵ Turbulence Model,” *JSME Int. journal. Ser. 2, Fluids Eng. heat Transf. power, Combust. Thermophys. Prop.*, vol. 32, no. 4, pp. 613–622, 1989.
- [90] W. M. Kays, “Turbulent Prandtl Number - Where Are We ?,” no. May, 1994.
- [91] W. M. (William M. Kays, *Convective heat and mass transfer.*, 4th ed. /. Boston ; McGraw-Hill Higher Education, 2005.
- [92] R. Tian, X. Dai, D. Wang, and L. Shi, “Study of Variable Turbulent Prandtl Number Model for Heat Transfer to Supercritical Fluids in Vertical Tubes,” *J. Therm. Sci.*, vol. 27, no. 3, pp. 213–222, 2018.
- [93] X. Kong, D. Sun, L. Gou, S. Wang, N. Yang, and H. Li, “Numerical Investigation

on Heat Transfer of Supercritical Water With a Variable Turbulent Prandtl Number Model,” *J. Nucl. Eng. Radiat. Sci.*, vol. 6, no. 3, pp. 1–10, Jul. 2020.

- [94] P. X. Jiang, Z. C. Wang, and R. N. Xu, “A modified buoyancy effect correction method on turbulent convection heat transfer of supercritical pressure fluid based on RANS model,” *Int. J. Heat Mass Transf.*, vol. 127, pp. 257–267, Dec. 2018.
- [95] Y. Y. Bae, “A new formulation of variable turbulent Prandtl number for heat transfer to supercritical fluids,” *Int. J. Heat Mass Transf.*, vol. 92, pp. 792–806, Jan. 2016.
- [96] M. Yetisir, H. Hamilton, R. Xu, M. Gaudet, D. Rhodes, M. King, K. Andrew, and B. Benson, “Fuel assembly concept of the canadian supercritical water-cooled reactor,” *J. Nucl. Eng. Radiat. Sci.*, vol. 4, no. 1, pp. 1–7, 2018.
- [97] US DOE, NERAC, and GIF, “A Technology Roadmap for Generation IV Nuclear Energy Systems,” 2002.

3. A Modified Turbulent Model for the Supercritical Water

Flows in the Vertical Upward Channels†

Nomenclature

Symbols

c_p	Specific heat, J/kg·K
D	Diameter of a tube, m
g	Gravitational acceleration, m/s ²
G	Mass flux, kg/m ² s
k	Turbulence kinetic energy, m ² /s ²
L	Length, m
P	Pressure, Pa
Pr	Prandtl number
q	Heat flux, W/m ² , kW/m ²
T	Temperature, °C
u	Velocity, m/s
y	Distance from the wall, m
y^+	Nondimensional distance from the wall, $y^+ = \frac{u_\tau y}{\nu}$
z	Axial location, m

Greek Letters

α	Thermal diffusivity, m ² /s
ε	Turbulence kinetic energy dissipation, m ² /s ³

† A version of this chapter entitled “A Modified Turbulent Model for the Supercritical Water Flows in the Vertical Upward Channels” has been published in J. Supercrit. Fluids, vol. 187, p. 105632, Aug. 2022. <https://doi.org/10.1016/j.supflu.2022.105632>.

μ	Dynamic viscosity, Pa · s
ν	Kinematic viscosity, m ² /s
λ	Thermal conductivity, W/m · K
ρ	Density of a fluid, kg/m ³
σ_k	Turbulent Prandtl number for k
σ_ε	Turbulent Prandtl number for ε
σ_ω	Turbulent Prandtl number for ω
ω	Specific dissipation rate, 1/s

Subscripts

<i>cr</i>	Critical
<i>in</i>	Inlet
<i>m</i>	Mean
<i>pc</i>	Pseudo-critical
<i>t</i>	Turbulent
<i>w</i>	Wall

Acronyms

CFD	Computational Fluid Dynamics
NHT	Normal Heat Transfer
DHT	Deteriorate Heat transfer
MAE	Mean of Absolute Error
RE	Relative Error
RNG	Renormalization Group
RSM	Reynold Stress Model
SCWR	Supercritical Water-Cooled Reactor
SD	Standard Deviation
SST	Shear Stress Transport

3.1.Introduction

The supercritical water-cooled reactor (SCWR) is one of the proposed six Generation IV reactors [1]. The working fluid used as the coolant in the fuel bundle of the Canadian SCWR core is the supercritical water. The thermal physical properties of the supercritical water change dramatically near the pseudo-critical point (as shown in Fig. 3.1) [2]. The abnormal heat transfer phenomenon, either the heat transfer enhancement or the heat transfer deterioration could appear in the upward channels at the supercritical condition [3–6]. When the heat transfer deterioration happens, the heat transfer coefficient is lower, which may lead to higher wall temperatures that might be above the maximum allowable temperature for the cladding surface of the fuel rods. Therefore, an accurate prediction of the wall temperature is very important before the fuel assembly is put into use in the reactor. Thus far, several researchers have made efforts on both the experimental and numerical studies on the fluid flow and heat transfer of the supercritical water in the circular tube [7–17]. The works showed the effects of the buoyancy and the thermal acceleration due to the sharp variations of thermal physical properties of the supercritical water near the pseudo-critical point might be the main reasons of the abnormal heat transfer phenomenon.

Extensive experimental studies using the supercritical water in the vertical upward tube have been made by several researchers, such as the works by Shen et al. and Piro [10], [12, 13]. Most of the studies focused on the investigation of the heat transfer characteristics or developing the heat transfer correlations at the supercritical conditions. However, there were just a few experimental works for the supercritical water in the upward fuel bundle of the reactor [14], [18–21] until now. In addition to the experimental studies, researchers have performed many numerical studies by the CFD simulations of flow and thermal field in the supercritical water channels [7–10], [22–24]. Most of the CFD studies applied the Reynolds-averaged Navier-Stokes approach. Different turbulent models have been assessed against the available experimental data. The performance of the turbulent models varied case-by-case. It mainly depends on the operating conditions, such as the heat to mass flux ratio, the geometry of the flow channel, and the flow direction [14], [25]. Among them, the heat to mass flux ratio plays a dominant role. However, there is no general consensus

on the criterion of the heat to mass flux ratio for the onset of the heat transfer deterioration. Due to the limited experimental data under the supercritical conditions, the turbulent Prandtl number was assumed to be a constant in the previous CFD simulations. The dramatic variations of the thermal physical properties near the pseudo-critical point makes the predictive assessment more difficult. The strong buoyancy and thermal acceleration effect caused by the strong variations of the thermophysical properties of the supercritical water near the pseudo-critical point should be considered in the simulations. Most turbulent models used in CFD simulations were developed for incompressible and constant-property flows. For conventional fluids without large variations of thermal physical properties, Pr_t can be treated as a constant based on the Reynolds analogy assumption, ranging from 0.8–0.9. However, the Pr_t changes sharply at supercritical conditions [26–33]. Therefore, an appropriate treatment of the turbulent Prandtl number at the supercritical condition is needed. There are no available experimental data of Pr_t for the supercritical fluid now. Several Pr_t models have been proposed in literatures. Myong et al. [27] proposed a variable Pr_t model for the heat transfer in a fully developed turbulent pipe flow which was heated by a constant heat flux. The fluid used in the numerical simulations were not mentioned. Two Pr_t models were put developed by Kays and Crawford [28, 29]. The parameters used in the models were derived from the experimental studies on the heat transfer of transformer oil, water, air, but, not under a supercritical condition. Tang et al. [30] introduced a variable Pr_t model for the heat transfer of the supercritical carbon dioxide in the upward tube. Kong et al. [31] then assessed the accuracy of Tang et al.'s model for the heat transfer of the supercritical water in the upward tube. The results showed the prediction is not satisfactory. This seems to signify that the difference of the critical parameters may lead to the variations of the turbulent Prandtl number although the heat transfer characteristics of supercritical fluids are similar. Jiang et al. [32] and Bae [33] developed similar Pr_t models for supercritical carbon dioxide and supercritical water in circular tubes. The models were both functions of non-dimensional distance from the wall (y^+). After investigating the accuracy of the previous turbulent models, Kong et al. [31] introduced a new variable Pr_t model considering the effects of the pressure, turbulent viscosity, and molecular Prandtl number for the heat transfer of the supercritical water in an upward tube. The predictions of the wall temperatures by this model are satisfactory

except for deteriorated heat transfer operating conditions where there are still large discrepancies.

The objectives of the present study are (1) to propose a new variable Pr_t model for supercritical fluid flows, (2) to find the best existing turbulent models for the prediction of the wall temperature in the supercritical flow channels, and (3) to modify the existing turbulent models using the proposed variable Pr_t model.

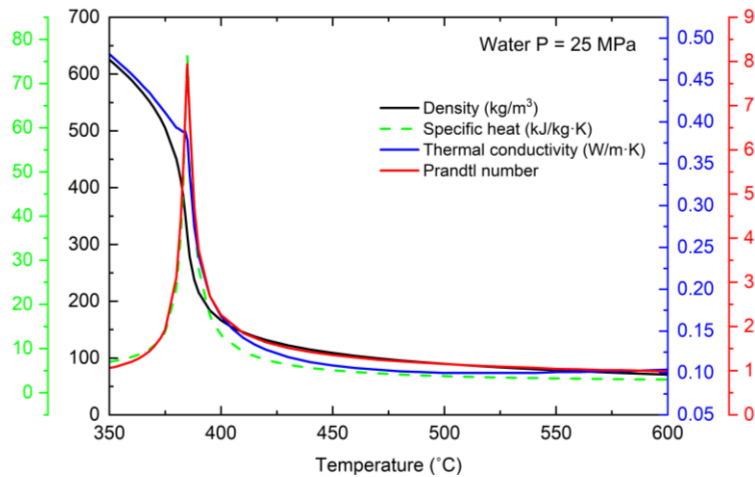
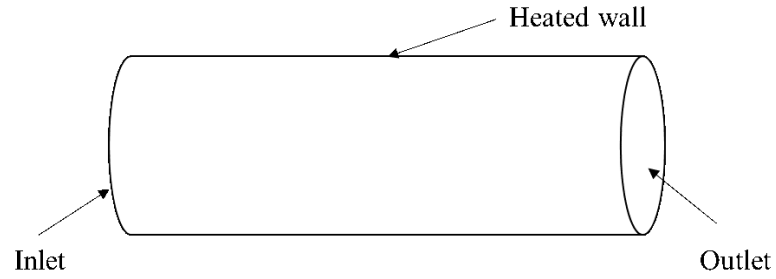


Figure 3.1: Variations of thermophysical properties of water at $P = 25$ MPa

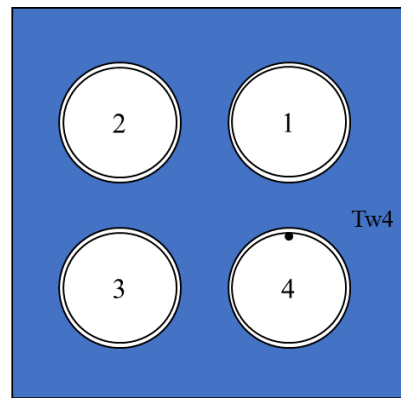
3.2. Numerical modeling

3.2.1. Configuration of the flow channels

In this work, the experimental data used for the assessment of the simulations of the supercritical water in the upward circular tube and the multiple fuel rods channels are from Mokry et al. [34] and Li [14], respectively. The experimental uncertainties of the wall temperatures for Cases 1 - 3 are $\pm 3.0\%$ and Cases 4 - 5 are $\pm 1.5^\circ\text{C}$. The configurations of these two types of channels are shown in Fig. 3.2 and the geometrical and operating parameters used in all simulations are listed in Table 3.1.



(a) Circular tube



(b) Cross-section view of the 2×2 fuel rod channel

Figure 3.2: Experimental flow channels used in the study

Table 3.1 Geometrical and operating conditions of difference cases used in the simulations

Case #	D(mm)	L(m)	P (MPa)	T_{in} (°C)	G (kg/m ² s)	q_w (kW/m ²)	q_w/G (kJ/kg)	Heat transfer condition
1[34]	10	4	24.1	350	1503	590	0.393	NHT
2[34]	10	4	23.9	350	1002	681	0.681	NHT
3[34]	10	4	24.1	350	203	129	0.635	DHT
4[14]	8	1.328	25	339.6	795.1	1007.6	1.267	NHT
5[14]	8	1.328	25	340.1	451.2	551.6	1.223	DHT

3.2.2. Numerical model and governing equations

The numerical simulations are carried out by the commercial software ANSYS FLUENT. The governing equations of the fluid flow and heat transfer of the supercritical water in the channels are the conservation of mass, momentum, and energy. The Reynolds averaged form of the governing equations can be described as [35]:

$$\frac{\partial \rho \bar{u}_i}{\partial x_i} = 0 \quad (3.1)$$

$$\frac{\partial (\rho \bar{u}_i \bar{u}_j)}{\partial x_j} = -\frac{\partial \bar{p}}{\partial x_i} + \frac{\partial}{\partial x_j} \left(\mu \frac{\partial \bar{u}_i}{\partial x_j} - \rho \overline{u_i' u_j'} \right) + \rho g_i \quad (3.2)$$

$$\frac{\partial}{\partial x_i} \left(\bar{u}_i \rho c_p T \right) = \frac{\partial}{\partial x_i} \left[\left(\lambda + \frac{c_p \mu_t}{Pr_t} \right) \frac{\partial T}{\partial x_i} \right] \quad (3.3)$$

where u is the velocity, T is the temperature, μ is the dynamic viscosity, ρ is the density, λ is the thermal conductivity, c_p is the specific heat, μ_t is the turbulent viscosity, Pr_t is the turbulent Prandtl number. Four turbulent models are applied in this study to solve the Reynolds stress term, including the realizable k - ε model [34], the RNG (renormalization group) k - ε model [34], the k - ω SST model [35], and the Reynolds Stress Model [35].

The transport equations for the turbulent kinetic energy (k) and the dissipation rate (ε) in the realizable k - ε model are given as [35]:

$$\frac{\partial}{\partial x_i} (\rho k u_i) = \frac{\partial}{\partial x_j} \left[\left(\mu + \frac{\mu_t}{\sigma_k} \right) \frac{\partial k}{\partial x_j} \right] + G_k + G_b - \rho \varepsilon + S_k \quad (3.4)$$

$$\frac{\partial}{\partial x_i} (\rho \varepsilon u_i) = \frac{\partial}{\partial x_j} \left[\left(\mu + \frac{\mu_t}{\sigma_\varepsilon} \right) \frac{\partial \varepsilon}{\partial x_j} \right] + \rho C_1 S \varepsilon - \rho C_2 \frac{\varepsilon^2}{k + \sqrt{\nu \varepsilon}} + C_{1\varepsilon} \frac{\varepsilon}{k} C_{3\varepsilon} G_b + S_\varepsilon \quad (3.5)$$

where G_k is the generation of the turbulent kinetic energy, G_b is the generation of the turbulent kinetic energy due to buoyancy, S_k and S_ε are user-defined source terms, $C_1 = \max \left[0.43, \frac{\eta}{\eta + 5} \right]$, $\eta = S \frac{k}{\varepsilon}$, $S = \sqrt{2 S_{ij} S_{ij}}$, $S_{ij} = \frac{1}{2} \left(\frac{\partial u_i}{\partial x_j} + \frac{\partial u_j}{\partial x_i} \right)$, C_2 , $C_{1\varepsilon}$, σ_k , and σ_ε are constants.

For the RNG k - ε model, the transport equation for k is the same as that in the realizable k - ε model while the transport equation for the dissipation rate (ε) is different [35]:

$$\frac{\partial}{\partial x_i}(\rho \varepsilon u_i) = \frac{\partial}{\partial x_j} \left(\alpha_\varepsilon \mu_{eff} \frac{\partial \varepsilon}{\partial x_j} \right) + C_{1\varepsilon} \frac{\varepsilon}{k} (G_k + C_{3\varepsilon} G_b) - C_{2\varepsilon} \rho \frac{\varepsilon^2}{k} - R_\varepsilon + S_\varepsilon \quad (3.6)$$

where $R_\varepsilon = \frac{C_\mu \rho \eta^3 (1-\eta/\eta_0) \varepsilon^2}{1+\beta \eta^3} \frac{\varepsilon^2}{k}$, η_0 , β , C_μ and $C_{2\varepsilon}$ are constants.

The transport equations for k and the specific dissipation rate ω , which is the rate at which turbulent kinetic energy is converted into thermal internal energy per unit volume and time, in the k - ω SST model are expressed as [35]:

$$\frac{\partial}{\partial x_i}(\rho k u_i) = \frac{\partial}{\partial x_j} \left(\left(\mu + \frac{\mu_t}{\sigma_k} \right) \frac{\partial k}{\partial x_j} \right) + \widetilde{G}_k - Y_k + S_k \quad (3.7)$$

$$\frac{\partial}{\partial x_i}(\rho \omega u_i) = \frac{\partial}{\partial x_j} \left(\left(\mu + \frac{\mu_t}{\sigma_\omega} \right) \frac{\partial \omega}{\partial x_j} \right) + \widetilde{G}_\omega - Y_\omega + D_\omega + S_\omega \quad (3.8)$$

where \widetilde{G}_k and \widetilde{G}_ω are the generations of k and ω , respectively, Y_k and Y_ω are the dissipations of k & ω due to turbulence, D_ω is the cross-diffusion term.

As for the Reynolds stress model, the transport equation can be written as [34]:

$$\begin{aligned} \underbrace{\frac{\partial}{\partial x_k} \left(\rho u_k \overline{u_i' u_j'} \right)}_{C_{ij} \equiv \text{Convection}} &= - \underbrace{\frac{\partial}{\partial x_k} \left[\rho \overline{u_i' u_j' u_k'} + \overline{p' \left(\delta_{kj} u_i' + \delta_{ik} u_j' \right)} \right]}_{D_{T,ij} \equiv \text{Turbulent Diffusion}} + \\ &\underbrace{\frac{\partial}{\partial x_k} \left[\mu \frac{\partial}{\partial x_k} \left(\overline{u_i' u_j'} \right) \right]}_{D_{L,ij} \equiv \text{Molecular Diffusion}} - \underbrace{\rho \left(\overline{u_i' u_k'} \frac{\partial u_j'}{\partial x_k} + \overline{u_j' u_k'} \frac{\partial u_i'}{\partial x_k} \right)}_{P_{ij} \equiv \text{Stress Production}} - \underbrace{\rho \beta \left(\overline{g_i u_j' \theta} + \overline{g_j u_i' \theta} \right)}_{G_{ij} \equiv \text{Buoyancy Production}} + \\ &\underbrace{\overline{p' \left(\frac{\partial u_i'}{\partial x_j} + \frac{\partial u_j'}{\partial x_i} \right)}}_{\phi_{ij} \equiv \text{Pressure Strain}} - \underbrace{2\mu \frac{\partial u_i'}{\partial x_k} \frac{\partial u_j'}{\partial x_k}}_{\varepsilon_{ij} = \text{Dissipation}} - \underbrace{2\rho \Omega_k \left(\overline{u_j' u_m'} \varepsilon_{ikm} + \overline{u_i' u_m'} \varepsilon_{jkm} \right)}_{F_{ij} \equiv \text{Production by System Rotation}} + \\ &\underbrace{S_{user}}_{\text{User-Defined Source Term}} \end{aligned} \quad (3.9)$$

The modeling of the above terms is explained detail in [35]. In the numerical simulations, the mesh near the wall in the radial direction is refined until $y^+ \approx 1$ at the first node from the wall so that the enhanced wall treatment method can be applied. The thermophysical properties of supercritical water from the NIST standard REFPROP database 9.1 [2] were implemented into Fluent by using piecewise-linear function of temperature. The SIMPLEC solution algorithm is used for the pressure-velocity coupling and the QUICK method is used for the spatial discretization in the simulations. The grid independent tests were also performed for each geometry in the simulations. In all the simulations of the present work, the heat flux applied on the walls are assumed constant and uniform. The thermophysical properties of the supercritical water are from [4].

3.3.Evaluation of standard turbulent models

Five experimental cases are selected in the study to assess the performance of different turbulent models, among them Cases 1- 3 are for the flows in an upward circular tube and Cases 4 -5 are for flows in upward multiple fuel rods channels. Since an accurate wall temperature prediction of the fuel rod in the reactor is significant for the design and safety of the SCWR, the wall temperatures are compared with the experimental data in the present work.

3.3.1. Flows in the upward circular tube

The comparisons of the numerical results for the wall temperatures with different turbulent models and the experimental data as well as the relative errors are presented in Figs. 3.3 - 3.5.

It is obvious that most of the selected turbulent models can predict the wall temperature variations from the entrance to the exit of the circular tube reasonably well in Cases 1 and 2 except that the Realisable $k-\varepsilon$ model overpredicts the wall temperatures in Case 2. In Case 3, the Realisable $k-\varepsilon$ model and $k-\omega$ SST model show a good agreement with the experimental data in the entrance region ($z = 0 - 0.5$ m), while all selected turbulent models

except for the RNG $k-\varepsilon$ model behave well near the exit region ($z = 3 - 4$ m). None of the turbulent models can give good predictions for the wall temperature in the middle region of the tube ($z = 0.5 - 3$ m) where the experimental wall temperature increases along the x direction and reaches a peak value at $z = 2.25$ m, however, all models cannot predict a peak temperature in this region and the predicted wall temperatures are much lower than the experimental data. The RNG $k-\varepsilon$ model predicts the lowest the wall temperature compared with other models. Other three turbulent models could capture the wall temperature variations near the exit ($z = 3$ m - 4 m) quite well. Both the $k-\omega$ SST model and RSM show a drastic wall temperature increase near the inlet, which does not agree with the experimental data. Cases 1 and 3 have the same operating pressure and the inlet temperature, but different heat to mass flux ratios. However, the selected turbulent models at the high heat to mass flux ratio condition (Case 3) cannot predict the wall temperature distribution as well as that at the low heat to mass flux ratio condition (Case 1). For the cases with the same inlet temperature and similar heat to mass flux ratio (Cases 2 and 3), the deviations between the predicted results by different turbulent models and the experimental data become larger at the lower mass flux condition (Case 3) where heat transfer deterioration happens.

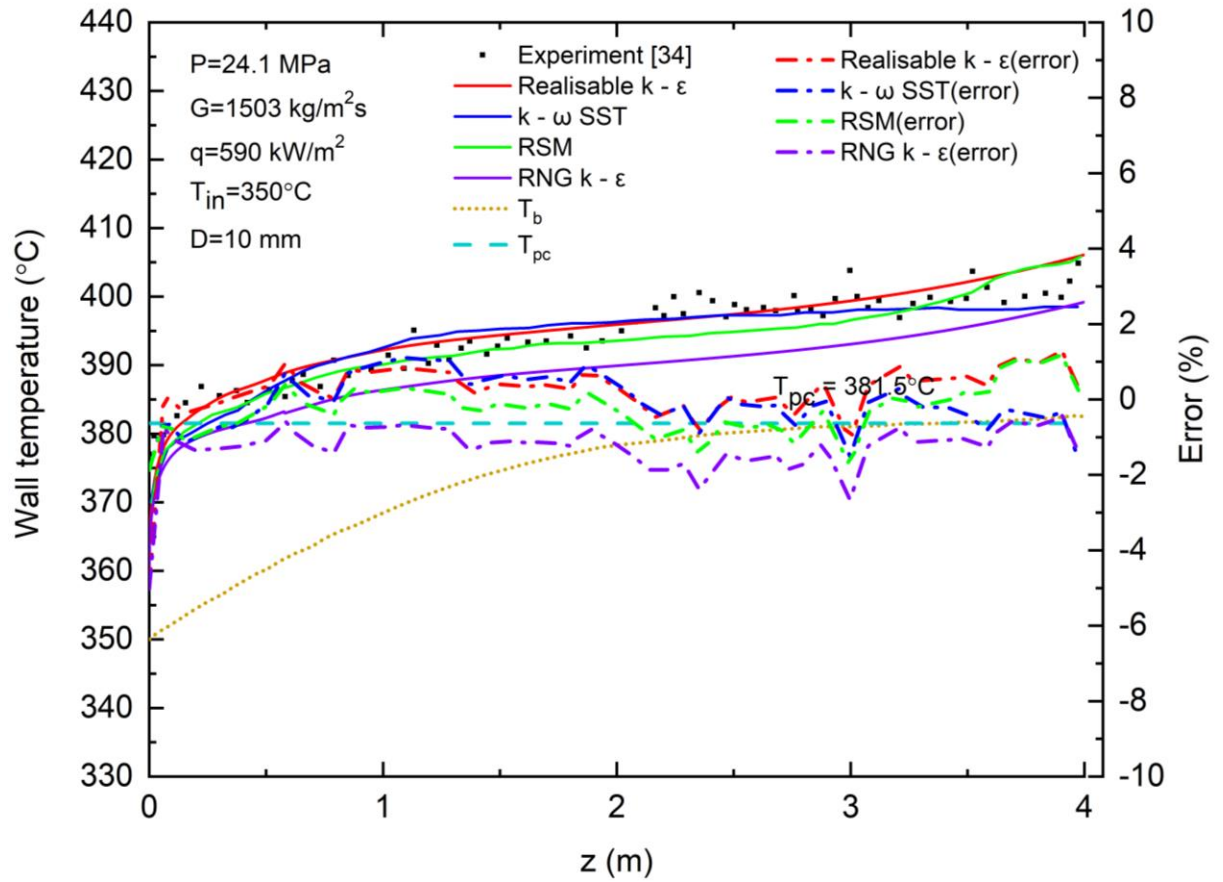


Figure 3.3: Comparison of the predicted wall temperatures by different turbulence models with the experimental data for Case 1

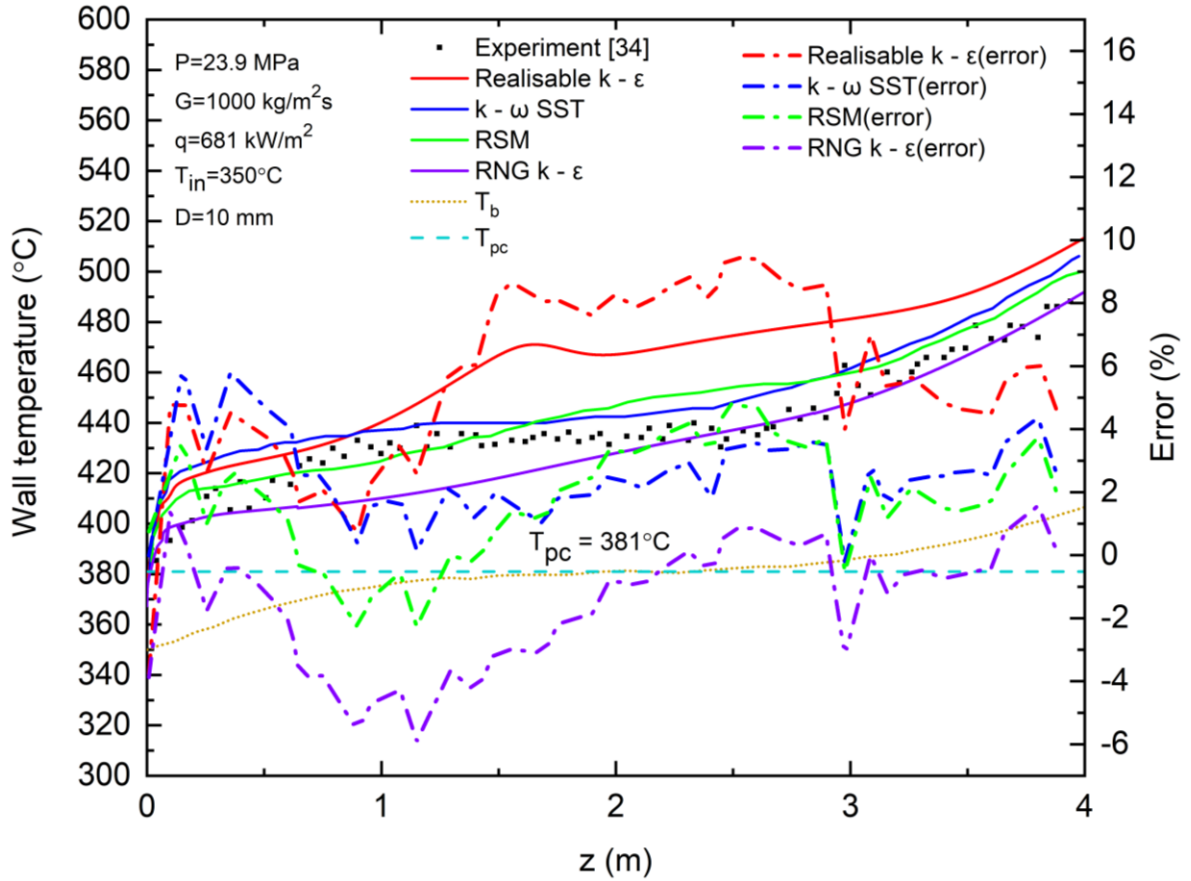


Figure 3.4: Comparison of the predicted wall temperatures by different turbulence models with the experimental data for Case 2

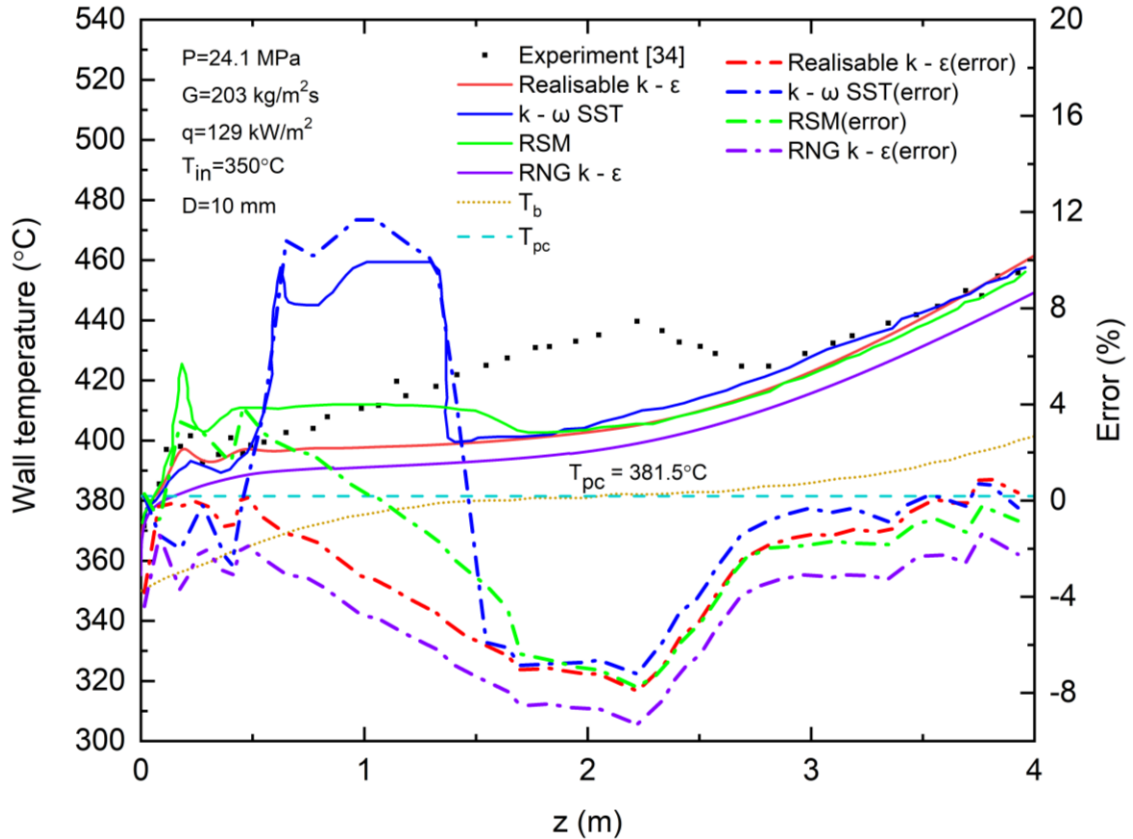


Figure 3.5: Comparison of the predicted wall temperatures by different turbulence models with the experimental data for Case 3

3.3.2. Flows in upward 2×2 fuel rod channel

Figs. 3.6 - 3.7 show the comparison of the predicted wall temperatures using different turbulent models for the 2×2 fuel rod channel with the experimental data. The sudden drop and then sharp increase in the wall temperature near the entrance observed in the experimental data in Case 4 are not predicted by any of the turbulent models as shown in Fig. 3.6. For Case 4, the $k-\omega$ SST model underestimates the wall temperatures in the region $z = 0.6$ m - 0.8 m while other turbulent models overpredict the wall temperatures. In the region $z = 0.8$ m - 1.1 m, all models behave well except the $k-\omega$ SST model gives much higher wall temperature than the experimental data. The Reynolds stress model performs quite well both qualitatively and quantitatively while both the RNG and Realizable $k-\epsilon$ models predict lower wall temperatures than the experimental data in the region $z = 1.1$ m - 1.2 m. For Case 5, the RSM gives much higher wall temperatures than the experimental

data in the region $z = 0.4 \text{ m} - 0.6 \text{ m}$. All other three turbulent models cannot predict the wall temperature drop in the region $z = 0.4 \text{ m} - 0.6 \text{ m}$, which was observed in the experimental data. However, they all can capture the wall temperature distributions well in the region $0.6 \text{ m} - 1.2 \text{ m}$, except for the sudden wall temperature drop at $z = 1.0 \text{ m}$ as shown in the experimental data. In addition, the RSM generally gives a high wall temperature prediction, but it can reproduce the drop and increase trend of the wall temperature near $z = 1.0 \text{ m}$, which was observed in the experimental data.

Table 3.2 shows the relative errors between the numerical and experimental wall temperatures for all the cases mentioned above. It can be seen that the errors of the predicted results for Cases 4 and 5 are higher than Cases 1 - 3. This might attribute the complexity of the flow in a shield side of a tube bundle than the internal flow in a tube. The flows in such tightly packed nuclear reactor rod bundle have unique regimes, which not appear in the tube flow in simple channels [35]. Strong transverse and large-scale motions could be observed in the narrow gaps between the neighbouring fuel rods or between a fuel rod and the surrounding adiabatic walls [8], [20–23]. The heat and turbulence transfer in the near rod region, especially in the boundary layer, may not be accurately predicted by the conventional turbulent models. Among all cases, the average error from the RNG $k-\varepsilon$ model is higher than the other three turbulent models. Therefore, the Realisable $k-\varepsilon$ model, $k-\omega$ SST model and the Reynolds stress model will be modified further to improve the performance.

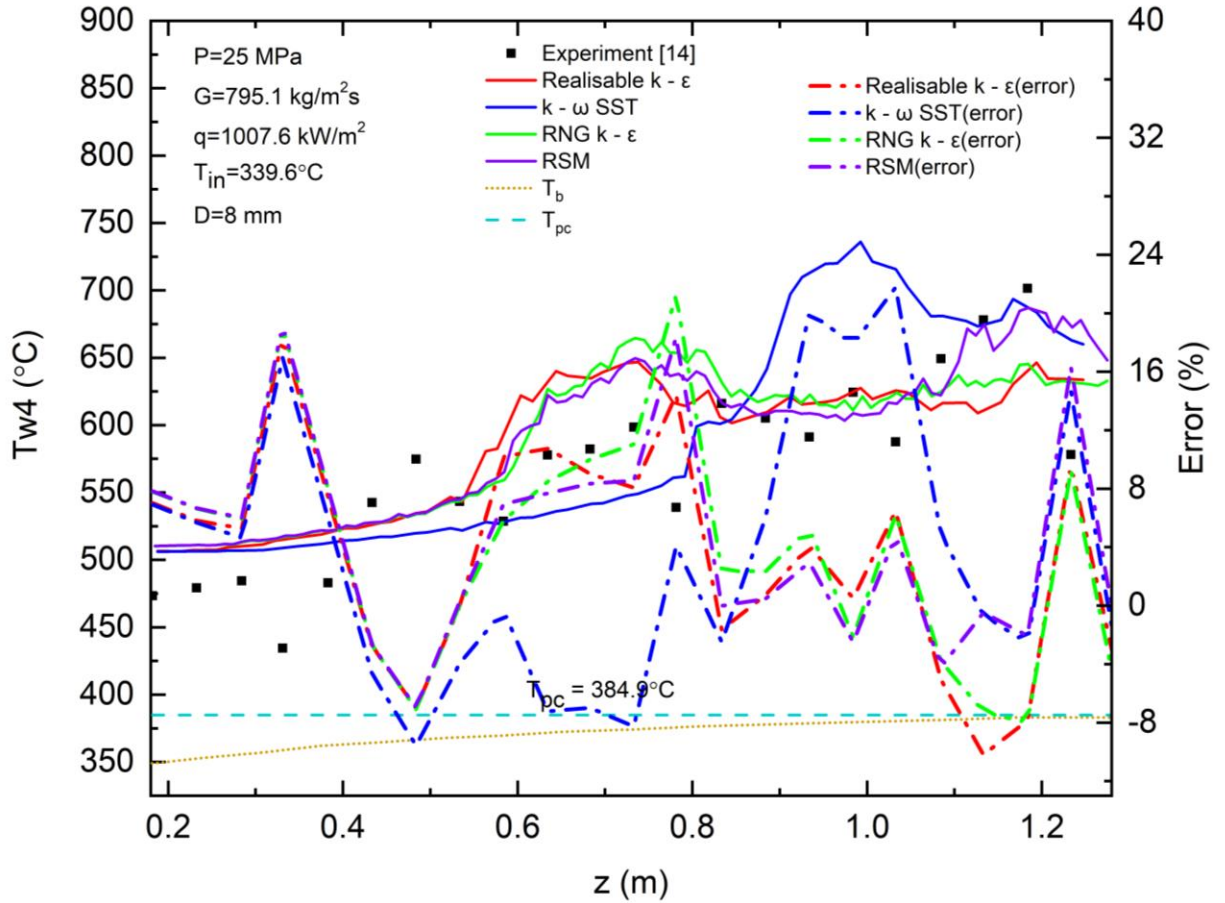


Figure 3.6: Comparison of the predicted wall temperatures by different turbulence models with the experimental data for Case 4

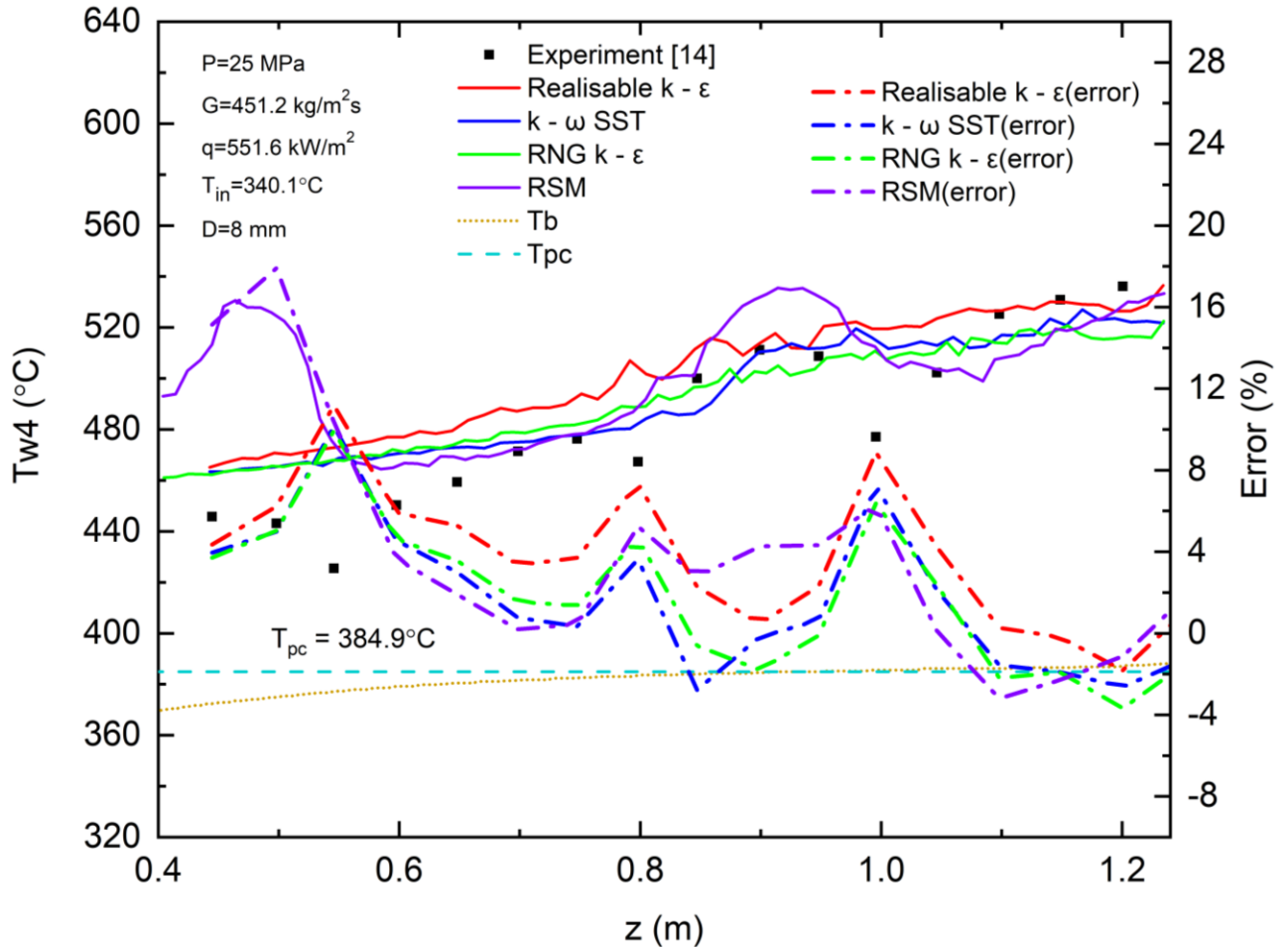


Figure 3.7: Comparison of the predicted wall temperatures by different turbulence models with the experimental data for Case 5

Table 3.2 Relative errors between the numerical and experimental results for the wall temperature

Case#	$RE = \left \frac{T_{w,num} - T_{w,exp}}{T_{w,exp}} \right \times 100\%$									
Model	Realisable $k - \epsilon$		RNG $k - \epsilon$		$k - \omega$ SST		RSM		Average	
Error (%)	MAE	SD	MAE	SD	MAE	SD	MAE	SD	MAE	SD
Single tube										
1	0.55	0.65	1.38	0.66	0.34	0.44	0.35	0.40	0.66	0.54

2	5.44	2.56	1.94	1.63	1.56	0.75	1.22	1.06	2.54	1.5
3	2.80	2.51	4.44	2.43	2.39	3.32	1.70	2.04	2.83	2.58
Average_ Single tube	2.93	1.91	2.59	1.57	1.43	1.50	1.09	1.17	2.01	1.54
Tube bundle										
4	6.34	4.36	9.28	7.25	8.96	5.63	6.57	5.26	7.79	5.63
5	4.01	3.15	3.39	2.47	3.07	2.66	4.75	5.28	3.81	3.39
Average_ Tube bundle	5.18	3.76	6.34	4.86	6.02	4.15	5.66	5.27	5.8	4.51
Average	3.83	2.65	4.09	2.89	3.26	2.56	2.92	2.81	3.53	2.73

MAE - Mean of Absolute Error; SD - Standard Deviation; RE – Relative Error

3.4. Modified turbulent models

3.4.1. Turbulent Prandtl number

The discrepancies between the numerical results and the experimental data for supercritical fluid flow and heat transfer can be due to the improper treatment of the momentum and heat eddy diffusivity at the supercritical conditions. The turbulent Prandtl number used in the governing equations is a non-dimensional parameter which measures the relationship of the momentum eddy diffusivity and the heat transfer eddy diffusivity. It can be defined as:

$$Pr_t = \frac{v_t}{\alpha_t} = \frac{\mu_t/\rho}{\lambda_t/(\rho c_p)} = \frac{\mu_t c_p}{\lambda_t} \quad (3.10)$$

In the energy equation, Eq. (3.3), the diffusion can be rearranged as:

$$\frac{\partial}{\partial x_i} \left[\left(\lambda + \frac{c_p \mu_t}{Pr_t} \right) \frac{\partial T}{\partial x_i} \right] = \frac{\partial}{\partial x_i} \left[\left(\frac{\lambda}{c_p} + \frac{\lambda_t}{c_p} \right) \frac{\partial h}{\partial x_i} \right] = \frac{\partial}{\partial x_i} \left[\mu \left(\frac{1}{Pr} + \frac{\mu_t/\mu}{Pr_t} \right) \frac{\partial h}{\partial x_i} \right] \quad (3.11)$$

Thus, the heat transfer is influenced by both Pr and Pr_t . The term $\frac{1}{Pr}$ stands for the heat transfer contributed by the molecular conduction and the term $\frac{\mu_t/\mu}{Pr_t}$ represents the heat transfer contributed by the turbulent mixing. Thus, it can be concluded that the heat transfer contributed by the turbulent mixing will increase if the turbulent Prandtl number decreases.

For the flow in the near wall region, especially in the viscous sublayer, it is known that $\mu_t/\mu \ll 1$. The molecular conduction plays a dominant role in the heat transfer [38]. Similarly, the heat transfer contributed by the turbulent mixing dominates in the high Reynolds number core flow region since $\mu_t/\mu \gg 1$. However, in the buffer layer near the wall region, where $\mu_t/\mu \approx 1$, the heat transfer contributions by the molecular conduction and turbulent mixing are in the same magnitude. Thus, it is necessary to determine the Pr_t realistically, so that the heat transfer contributions can be accurately predicted.

Pr_t is commonly assumed as a constant, 0.85 or 0.9 in the existing turbulent models, whose value was based on the experimental or direct numerical simulations for common fluids. This is generally accurate for fully developed turbulent flow. However, the thermal physical properties of the supercritical fluid vary sharply near the pseudo-critical region. It is irrational to still assume Pr_t as a constant under the supercritical condition, especially if the fluid undergoes the dramatic variations of properties in the buffer layer. There is no experimental data of Pr_t for the supercritical water to date. Most of the proposed Pr_t models for the supercritical fluids in the previous studies [30–33] are for the supercritical carbon dioxide in the tube flow. The Pr_t model proposed by Kong et al. [31] was for the supercritical water flow and heat transfer inside a tube. They assessed the existing turbulent Prandtl models in their study and then compared the performance of their proposed model with the existing models. Generally, the Pr_t model proposed by Kong et al. achieved better prediction accuracy than the existing models. Thus, Kong et al.'s Pr_t model is selected here to be modified further for the supercritical water flow and heat transfer in rod bundles. The Kong et al.'s model is given as:

$$Pr_t = \begin{cases} 0.4 & \mu_t/\mu < 0.2 \\ 0.3 + 0.03 \times (P/P_{cr}) \times Pr \times (\mu_t/\mu) & 0.2 \leq \mu_t/\mu \leq 10 \\ 0.85 & \mu_t/\mu > 10 \end{cases} \quad (3.12)$$

Number of researchers pointed out that the heat to mass flux ratio may be the key factor that affects the heat transfer phenomenon [7–8, 10–11,15–19]. Thus, a new variable Pr_t model based on Kong et al.'s model is developed in this study as below:

$$Pr_t = \begin{cases} 0.4 & \mu_t/\mu < 0.2 \\ 0.3 + 0.03 \times (P/P_{cr}) \times Pr \times (\mu_t/\mu) \times (q/G) & 0.2 \leq \mu_t/\mu \leq 10 \\ 0.85 & \mu_t/\mu > 10 \end{cases} \quad (3.13)$$

where q is in kW/m^2 and G is in $\text{kg/m}^2\text{s}$. The proposed turbulent model with the variable Pr_t model given in Eq. (13) will be assessed first by comparing the predictions of the wall temperatures with the experimental data for the case with a heat transfer deterioration in a tube flow [39], which was used in the study by Kong et al [31], as well as the numerical results from Kong et al [31]. Since $k-\omega$ SST model was used in the work by Kong et al [31], it is also used here for the comparison purpose. Fig. 3. 8 presents the comparison of the predicted wall temperature distributions using the proposed variable Pr_t model with the experimental data [39] and the numerical results from Kong et al [31]. It can be seen that the numerical results using the proposed Pr_t model gives much better prediction than the results from the Pr_t model by Kong et al.'s [31] compared with the experimental data as shown in Fig. 3.8. However, this is just for one low heat flux and low mass flux tube flow case ($q_w/G = 0.784$). Therefore, the performance of the proposed variable Pr_t model will also be assessed under different operating conditions of tube flows and the fuel rod channel flows as well as for other turbulent models. Thus, the proposed variable Pr_t model is used with the Realisable $k-\varepsilon$ model, the $k-\omega$ SST model and the Reynolds Stress model to simulate the fluid flow and heat transfer of the supercritical water in both the upward flows in tubes and the channel with multiple fuel rods.

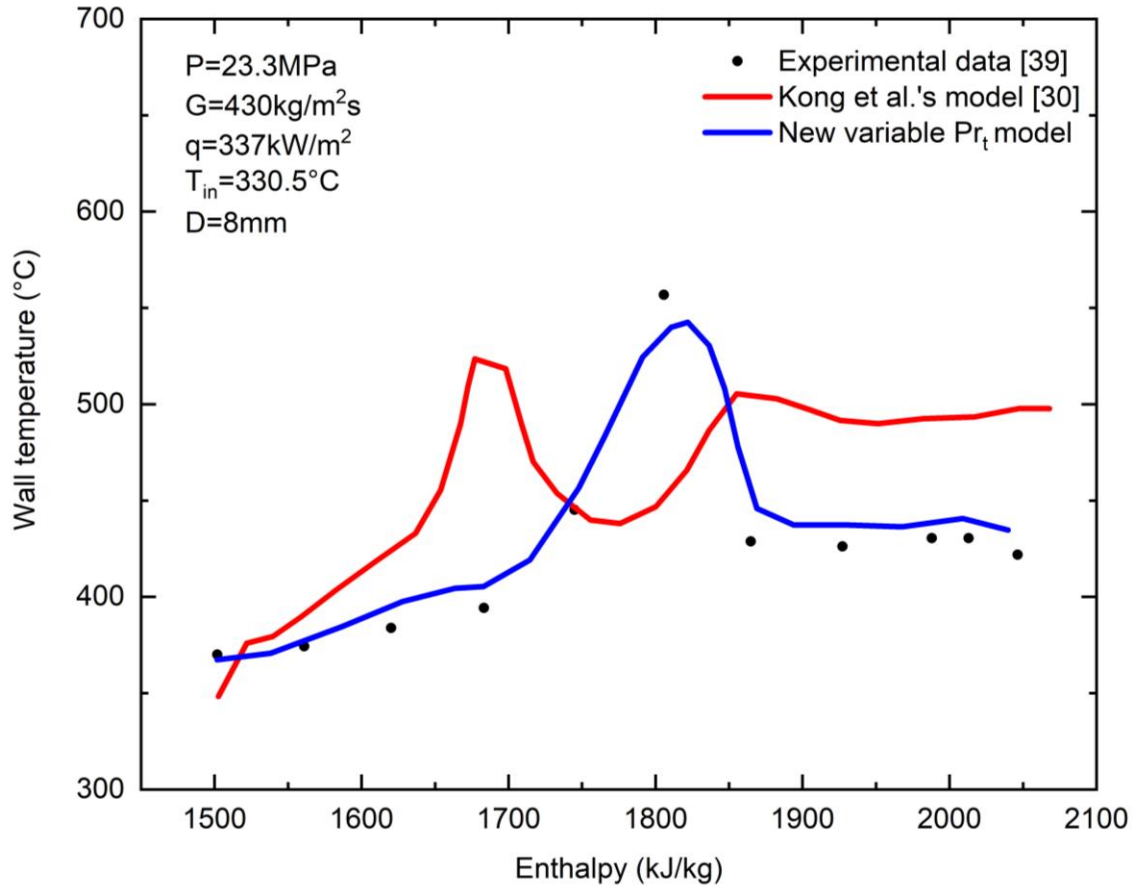


Figure 3.8: Comparison the predicted wall temperatures using the proposed model with the results using Kong's model [31] and the experimental data [39]

3.4.2. Results and discussions

The five cases listed in Table 3.1 are applied here to evaluate the performance of the modified turbulent models. Figs. 3.9 - 3.11 are the comparisons between the numerical results by the original and modified turbulent models and the experimental results for the upward circular tube (Cases 1 - 3). Figs. 3.12 - 3.13 are the comparisons for the upward 2×2 fuel rod channel (Cases 4 - 5). The relative errors between the numerical and experimental results are presented in Table 3.3.

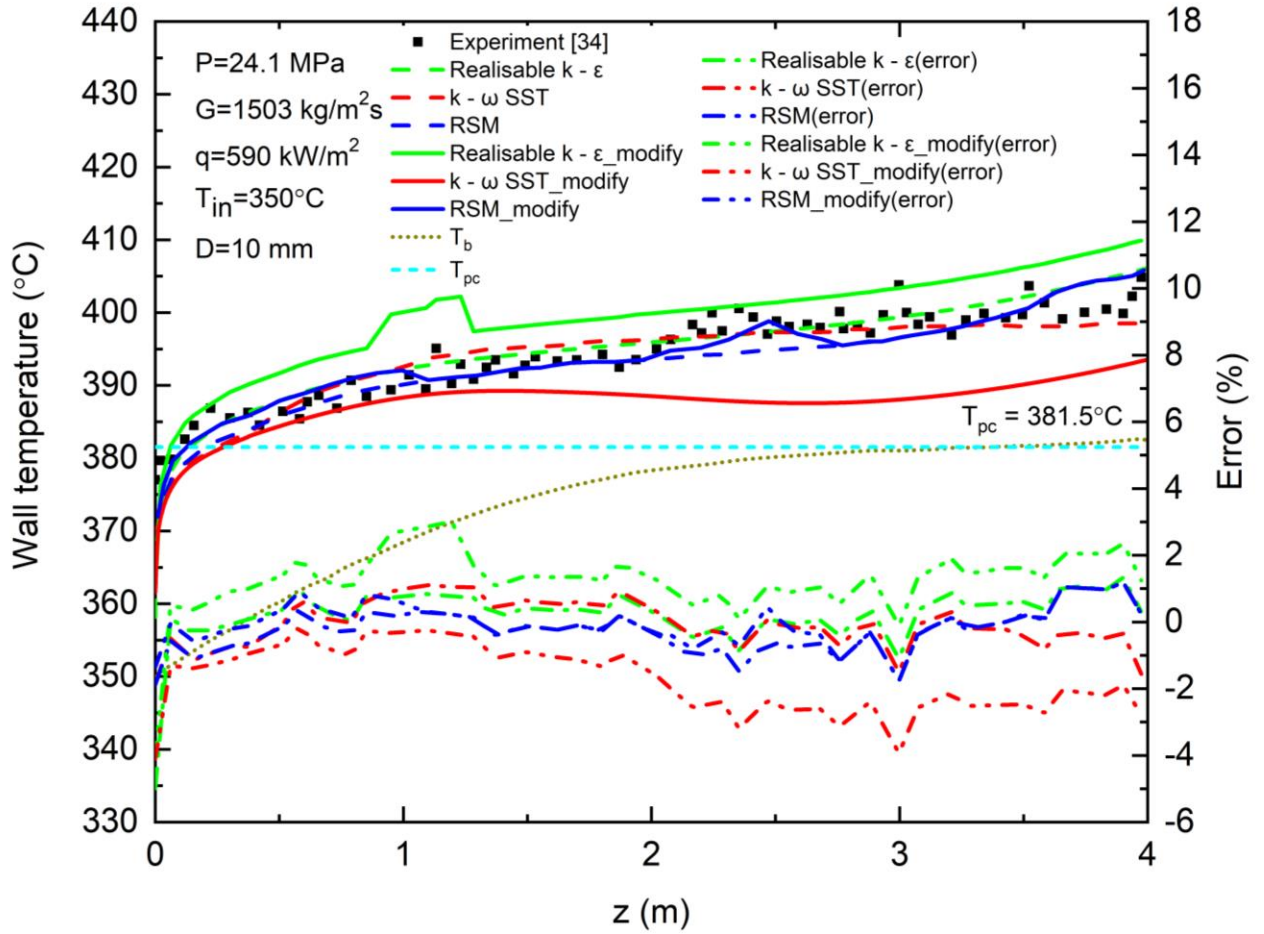


Figure 3.9: Comparison of the predicted wall temperatures by the original and modified turbulence models with the experimental data for Case 1

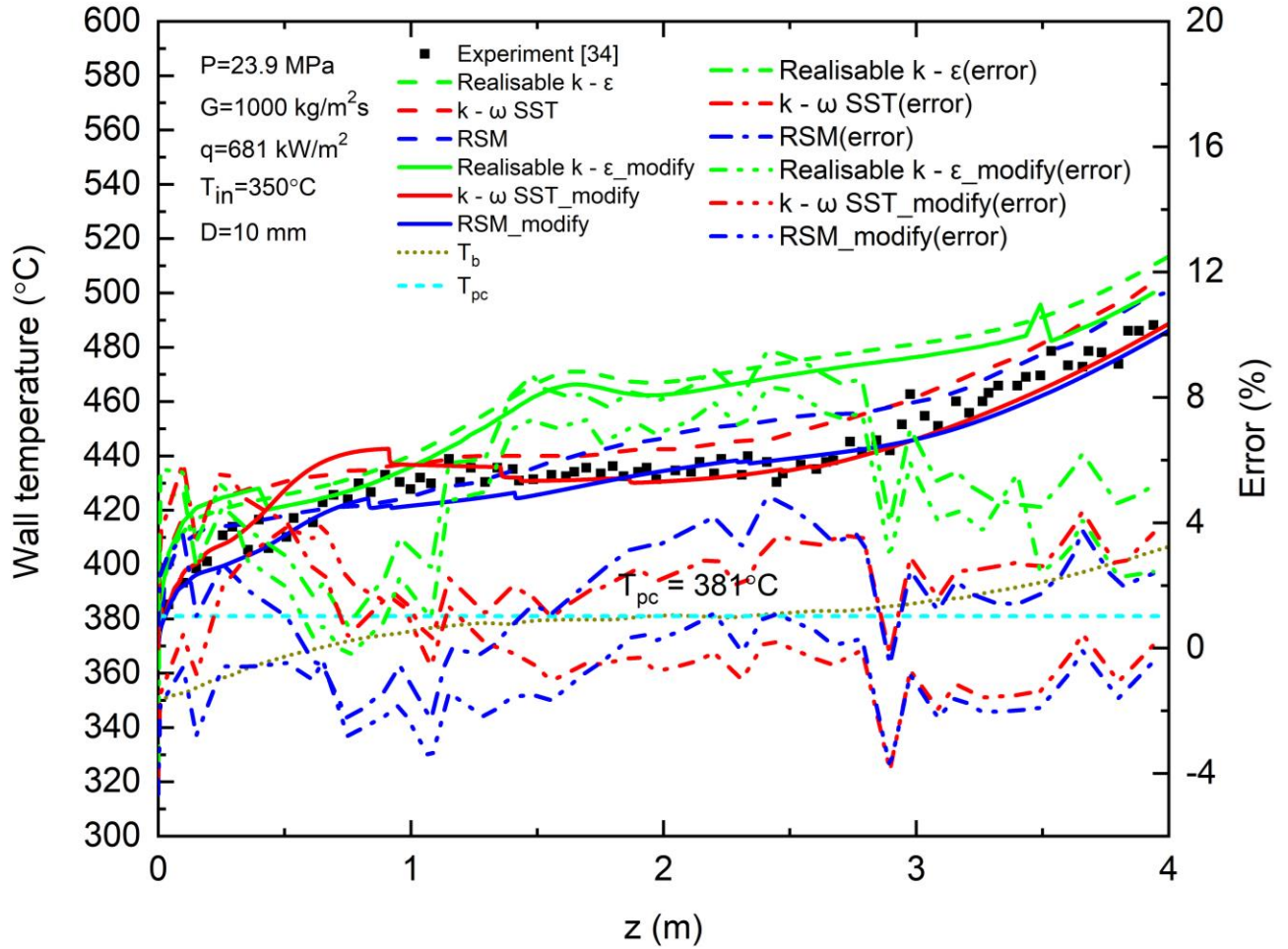


Figure 3.10: Comparison of the predicted wall temperatures by the original and modified turbulence models with the experimental data for Case 2

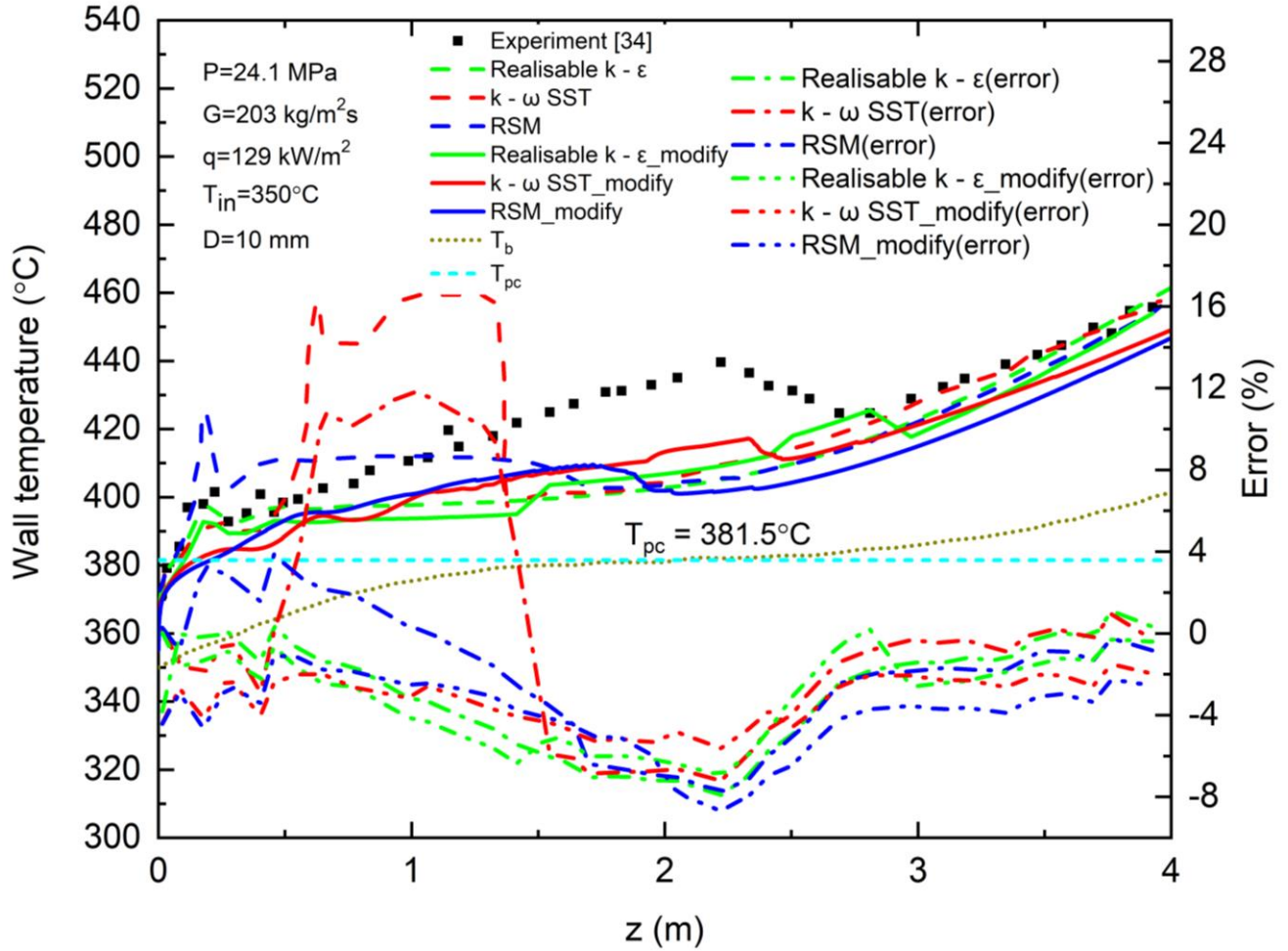


Figure 3.11: Comparison of the predicted wall temperatures by the original and modified turbulence models with the experimental data for Case 3

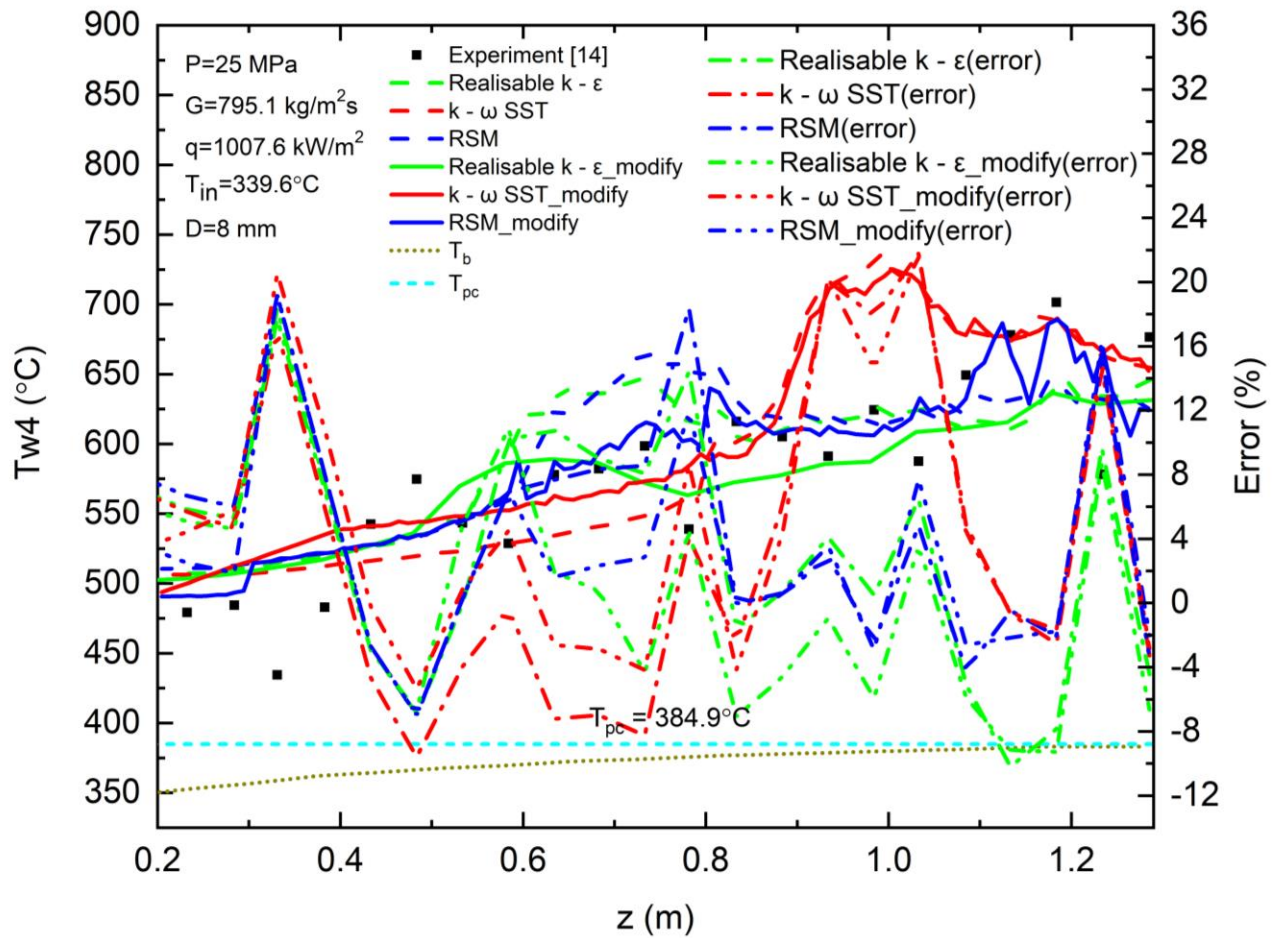


Figure 3.12: Comparison of the predicted wall temperatures by the original and modified turbulence models with the experimental data for Case 4

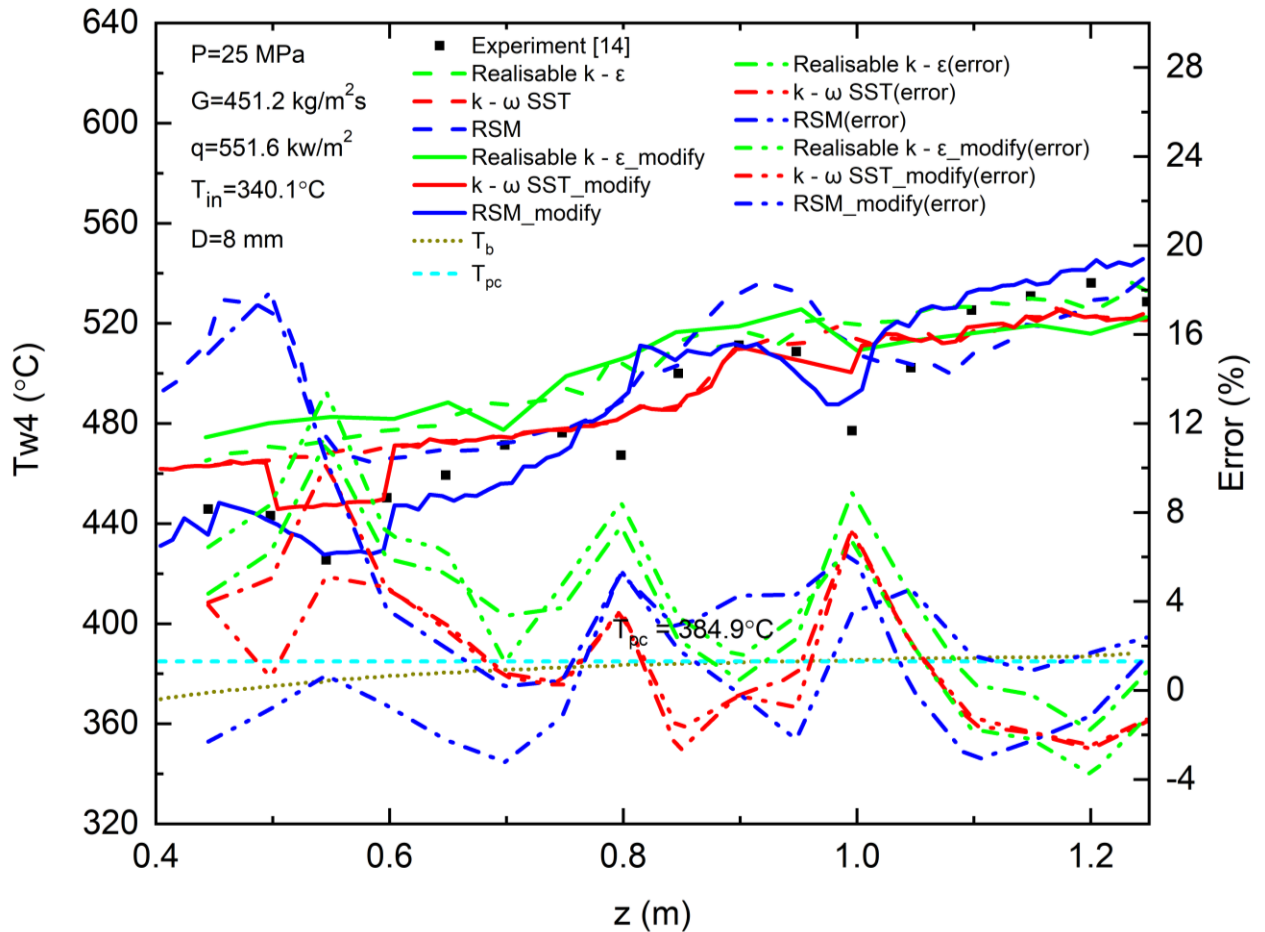


Figure 3.13: Comparison of the predicted wall temperatures by the original and modified turbulence models with the experimental data for Case 5

It is obvious that the modified Reynolds stress model shows a great improvement on the predictions of the wall temperature and could predict the general trend of the wall temperatures well in all cases. However, it should be noted that all the modified turbulent models still underpredict the wall temperature at the center region in Case 3. For the multiple fuel rods channel, although the modified RSM can predict the wall temperature reasonably well, there are some fluctuations in the wall temperatures at the exit region in Case 4. The modified RSM gives the best agreement with the experimental data compared with other turbulent models.

Table 3.3 Relative errors between the numerical and experimental results for the wall temperatures

Case#	$RE = \left(\frac{T_{w,num} - T_{w,exp}}{T_{w,exp}} \right) \times 100\%$							
Model	Realisable _modified		SST_ modified		RSM_ modified		Average	
Error (%)	MAE	SD	MAE	SD	MAE	SD	MAE	SD
Single tube								
1	1.33	0.72	1.79	0.99	0.31	0.28	1.14	0.66
2	4.54	2.45	1.25	1.11	1.27	0.85	2.35	1.47
3	3.01	2.10	3.09	1.26	3.62	1.93	3.24	1.76
Average_ Single tube	2.96	1.76	2.04	1.12	1.73	1.02	2.24	1.30
Tube bundle								
4	6.05	3.62	7.17	6.60	4.60	5.04	5.94	5.09
5	4.81	3.34	1.95	1.59	1.88	1.24	2.88	2.06
Average_ Tube bundle	5.43	3.48	4.56	4.10	3.24	3.14	4.41	3.58
Average	3.95	2.45	3.05	2.31	2.34	1.87	3.11	2.21

3.5. Conclusions

In this study, a correlation for the variable Pr_t is developed. The realisable $k-\varepsilon$ model, $k-\omega$ SST model and RSM are modified by using the variable Pr_t instead of constant Pr_t , to improve the performance of the numerical models for supercritical fluid flow and heat transfer. The assessment of the proposed turbulent models is carried out for the supercritical water flows in both the upward circular tube and the upward channel with

multiple fuel rods. The wall temperatures predicted by the modified Realisable $k-\varepsilon$ model, the $k-\omega$ SST model and the RSM with the new variable Pr_t are strongly improved compared with the standard Realisable $k-\varepsilon$ model, the $k-\omega$ SST model and the RSM. The modified RSM gives the best agreement with the experimental data than other modified turbulent models. The future work will focus on improving the modified RSM quantitatively through the calibrations of the constants used in the model with more experimental data at various operating conditions when they are available.

References

- [1] GIF, “GIF R&D Outlook for Generation IV Nuclear Energy Systems 2018 Update,” *Nuclear Energy*, 2018.
- [2] Lemmon E., Huber M., McLinden M., NIST reference fluid thermodynamic and transport properties-RFFPROP, version 9.1. National Institute of Standard Technology. 2013.
- [3] I. L. Pioro, Ed., *Handbook of Generation IV Nuclear Reactors*, 1st ed. Duxford, UK: Elsevier— Woodhead Publishing, 2016.
- [4] I. Pioro and S. Mokry, “Thermophysical Properties at Critical and Supercritical Pressures,” in *Heat Transfer - Theoretical Analysis, Experimental Investigations and Industrial Systems*, 2011, pp. 573–592.
- [5] I. Pioro, S. Mokry, and S. Draper, “Specifics of thermophysical properties and forced-convective heat transfer at critical and supercritical pressures,” *Reviews in Chemical Engineering*, 2011.
- [6] S. J. Mokry, P. L. Kirillov, I. L. Pioro, and Y. K. Gospodinov, “Supercritical Water Heat Transfer in a Vertical Bare Tube: Normal, Improved, and Deteriorated Regimes,” *Nuclear Technology*, vol. 172, no. 1, pp. 60–70, 2010.
- [7] S. Koshizuka, N. Takano, and Y. Oka, “Numerical analysis of deterioration phenomena in heat transfer to supercritical water,” *International Journal of Heat and Mass Transfer*, vol. 38, no. 16, pp. 3077–3084, 1995.

- [8] B. Zhang, J. Shan, and J. Jiang, "Numerical analysis of supercritical water heat transfer in horizontal circular tube," *Progress in Nuclear Energy*, vol. 52, no. 7, pp. 678–684, 2010.
- [9] X. Cheng, B. Kuang, and Y. H. Yang, "Numerical analysis of heat transfer in supercritical water-cooled flow channels," *Nuclear Engineering and Design*, vol. 237, no. 3, pp. 240–252, 2007.
- [10] Z. Shen, D. Yang, S. Wang, W. Wang, and Y. Li, "Experimental and numerical analysis of heat transfer to water at supercritical pressures," *International Journal of Heat and Mass Transfer*, vol. 108, pp. 1676–1688, 2017.
- [11] Q. L. Wen and H. Y. Gu, "Numerical simulation of heat transfer deterioration phenomenon in supercritical water through vertical tube," *Annals of Nuclear Energy*, vol. 37, no. 10, pp. 1272–1280, 2010.
- [12] G. Zhang, H. Zhang, H. Gu, Y. Yang, and X. Cheng, "Experimental and numerical investigation of turbulent convective heat transfer deterioration of supercritical water in vertical tube," *Nuclear Engineering and Design*, vol. 248, pp. 226–237, Jul. 2012.
- [13] I. L. Piro and R. B. Duffey, "Experimental heat transfer in supercritical water flowing inside channels (survey)," *Nuclear Engineering and Design*, vol. 235, no. 22, pp. 2407–2430, 2005.
- [14] H. Li, M. Zhao, Z. Hu, Y. Zhang, and F. Wang, "Experimental study of supercritical water heat transfer deteriorations in different channels," *Annals of Nuclear Energy*, vol. 119, pp. 240–256, 2018.

- [15] S. Q. Yu, H. X. Li, X. L. Lei, Y. C. Feng, Y. F. Zhang, H. He, and T. Wang, “Experimental investigation on heat transfer characteristics of supercritical pressure water in a horizontal tube,” *Experimental Thermal and Fluid Science*, vol. 50, pp. 213–221, 2013.
- [16] H. Y. Gu, M. Zhao, and X. Cheng, “Experimental studies on heat transfer to supercritical water in circular tubes at high heat fluxes,” *Experimental Thermal and Fluid Science*, 2015.
- [17] K. Yamagata, K. Nishikawa, S. Hasegawa, T. Fujii, and S. Yoshida, “Forced convective heat transfer to supercritical water flowing in tubes,” *International Journal of Heat and Mass Transfer*, vol. 15, pp. 2575–2593, 1972.
- [18] M. Zhao and H. Y. Gu, “Experimental and numerical investigation on heat transfer of supercritical water flowing upward in 2×2 rod bundles,” *Nucl. Eng. Des.*, vol. 370, no. October, 2020.
- [19] X. Feng, T. Zhou, J. L. Zhang, B. Y. Zhang, and D. L. Ma, “Research on heat transfer coefficient of supercritical water based on factorial and correspondence analysis,” *Nucl. Eng. Technol.*, vol. 52, no. 7, pp. 1409–1416, Jul. 2020.
- [20] F. Bertocchi, M. Rohde, D. De Santis, A. Shams, H. Dolfen, J. Degroote, and J. Vierendeels, “Fluid-structure interaction of a 7-rods bundle: Benchmarking numerical simulations with experimental data,” *Nucl. Eng. Des.*, vol. 356, p. 110394, Jan. 2020.

- [21] M. Bruschewski, M. H. A. Piro, C. Tropea, and S. Grundmann, “Fluid flow in a diametrically expanded CANDU fuel channel – Part 1: Experimental study,” *Nucl. Eng. Des.*, no. September, p. 110371, 2019.
- [22] Z. Shang and S. Lo, “Numerical investigation of supercritical water-cooled nuclear reactor in horizontal rod bundles,” *Nuclear Engineering and Design*, vol. 240, no. 4, pp. 776–782, 2010.
- [23] Z. Shen, D. Yang, S. Wang, W. Wang, and Y. Li, “Experimental and numerical analysis of heat transfer to water at supercritical pressures,” *International Journal of Heat and Mass Transfer*, vol. 108, 2017.
- [24] Y. ZHANG, C. ZHANG, and J. JIANG, “Numerical Simulation of Fluid Flow and Heat Transfer of Supercritical Fluids in Fuel Bundles,” *Journal of Nuclear Science and Technology*, vol. 48, no. 6, pp. 929–935, 2011.
- [25] X. Lei, H. Li, W. Zhang, N. T. Dinh, Y. Guo, and S. Yu, “Experimental study on the difference of heat transfer characteristics between vertical and horizontal flows of supercritical pressure water,” *Applied Thermal Engineering*, vol. 113, pp. 609–620, 2017.
- [26] X. Chai, X. Liu, J. Xiong, and X. Cheng, “Numerical Investigation of Turbulent Heat Transfer Properties at Low Prandtl Number,” vol. 8, no. July, pp. 1–11, 2020,
- [27] H. K. MYONG, N. KASAGI, and M. HIRATA, “Numerical Prediction of Turbulent Pipe Flow Heat Transfer for Various Prandtl Number Fluids with the Improved k-epsilon Turbulence Model,” *JSME Int. journal. Ser. 2, Fluids Eng. heat Transf. power, Combust. Thermophys. Prop.*, vol. 32, no. 4, pp. 613–622, 1989.

- [28] W. M. Kays, "Turbulent Prandtl Number - Where Are We?," . May, 1994.
- [29] W. M. Kays, *Convective heat and mass transfer.*, 4th ed. /. Boston ; McGraw-Hill Higher Education, 2005.
- [30] R. Tian, X. Dai, D. Wang, and L. Shi, "Study of Variable Turbulent Prandtl Number Model for Heat Transfer to Supercritical Fluids in Vertical Tubes," *Journal of Thermal Science*, vol. 27, no. 3, pp. 213–222, 2018.
- [31] X. F. Kong, D. Sun, L. Gou, S. Wang, and N. Yang, "Numerical investigation on heat transfer of supercritical water with a variable turbulent prandtl number model," *Journal of Nuclear Engineering and Radiation Science*, vol. 6, no. 3, pp. 1–10, 2020.
- [32] P. X. Jiang, Z. C. Wang, and R. N. Xu, "A modified buoyancy effect correction method on turbulent convection heat transfer of supercritical pressure fluid based on RANS model," *International Journal of Heat and Mass Transfer*, vol. 127, pp. 257–267, Dec. 2018. <https://doi.org/>
- [33] Y. Y. Bae, "A new formulation of variable turbulent Prandtl number for heat transfer to supercritical fluids," *International Journal of Heat and Mass Transfer*, vol. 92, pp. 792–806, Jan. 2016.
- [34] S. Mokry, I. Pioro, A. Farah, K. King, S. Gupta, W. Peiman, and P. Kirillov, "Development of supercritical water heat-transfer correlation for vertical bare tubes," *Nuclear Engineering and Design*, vol. 241, no. 4, pp. 1126–1136, 2011.
- [35] Ansys. Inc, "14.0 ANSYS FLUENT Theory Guide," 2011.

- [36] S. Tavoularis, “Rod bundle vortex networks, gap vortex streets, and gap instability: A nomenclature and some comments on available methodologies,” *Nucl. Eng. Des.*, vol. 241, no. 7, pp. 2624–2626, Jul. 2011.
- [37] A. Kraus, E. Merzari, T. Norddine, O. Marin, and S. Benhamadouche, “Direct numerical simulation of fluid flow in a 5x5 square rod bundle,” *Int. J. Heat Fluid Flow*, vol. 90, p. 108833, Aug. 2021.
- [38] H. Schlichting and K. Gersten, *Boundary-Layer Theory*, 9th ed. 20. Berlin, Heidelberg: Springer Berlin / Heidelberg, 2016.
- [39] M. E. Shitsman. Impairment of the heat transmission at supercritical pressures(heat transfer process examined during forced motion of water at supercritical pressures). *High Temperature Science*, 1:237–244, 1963.

4. Numerical Simulation of the Fluid Flow and Heat Transfer of the Supercritical Water in the 64-element Canadian SCWR

Fuel Bundle

Nomenclature

Symbols

c_p	Specific heat, J/kg·K
g	Gravitational acceleration, m/s ²
k	Turbulence kinetic energy, m ² /s ²
P	Pressure, Pa
Pr	Prandtl number
T	Temperature, °C
u	Velocity, m/s
y^+	Nondimensional distance from the wall, $y^+ = \frac{u_\tau y}{\nu}$ (y: distance from the wall,m)
z	Axial location, m

Greek Letters

ε	Turbulence kinetic energy dissipation, m ² /s ³
μ	Dynamic viscosity, Pa · s
λ	Thermal conductivity, W/m · K
ρ	Density of a fluid, kg/m ³

δ_{ij}	Kronecker delta tensor, $\delta_{ij} = 1$ if $i = j$, $\delta_{ij} = 0$ if $i \neq j$
ω	Specific dissipation rate, 1/s

Subscripts

<i>cr</i>	Critical
<i>t</i>	Turbulent

Acronyms

3D	Three-dimensional
CFD	Computational Fluid Dynamics
DNS	Direct Numerical Simulation
RNG	Renormalization Group
RSM	Reynold Stress Model
SCWR	Supercritical Water-Cooled Reactor
SST	Shear Stress Transport
LES	Large Eddy Simulation
RANS	Reynolds-Averaged Navier-Stokes simulation
RSM	Reynolds Stress Model

4.1. Introduction

Supercritical Water-Cooled Reactors (SCWRs) were proposed as one of the six Generation IV nuclear reactors [1–2]. The Canadian SCWR core concept is based on the pressure tube reactor design. A potentially improved thermal efficiency at a reduced price and lower maintenance are the motivation of the investigations on the heat transfer mechanism. During the past few years, several researchers have conducted experimental studies on the supercritical water flows in the circular tubes [3–10]. The heat transfer mechanism varies with operating conditions and there is no common consensus on the experimental results for the criteria of the heat transfer deterioration. Recently, limited experimental studies were conducted for the supercritical water flow in a channel with fuel rods [11–13]. The experimental data for the supercritical water flows in the fuel rod channels in the open literature are quite limited. Because of the cost of producing more detailed velocity and heat transfer data inside the rod bundle, the computational fluid dynamics (CFD) method has been used for investigating the fluid flow and heat transfer phenomenon in the supercritical water channels for many years [14–18].

Several approaches can be used to solve the conservation equations which govern the flow field in the CFD simulations, including the direct numerical simulations (DNS), the large eddy simulations (LES), and the Reynolds-averaged Navier-Stokes simulation (RANS). Since the DNS needs to solve all flow motion scales, the applicability of the DNS is restricted to relatively small geometries due to the high computational cost. Thus, DNS is not commonly used in the study for nuclear reactors. Some researchers conducted the LES simulations for nuclear reactors. Fischer et al. [19] performed the LES simulations on a single fuel pin through the spectral method. Merzari et al. [20] and Brockmeyer et al. [21] consecutively using Nek500 code to simulate the flow in a 7-pin reactor geometry. Brockmeyer et al. [22] applied STARCCM+ software to perform the LES in a 19-pin flow geometry with a shortened rod length. Recently, Goth et al. [23] employed the same code to investigate the flow behaviors in a 61-pin geometry. Although the LES is more applicable than the DNS in the study of nuclear reactors. There are still some limitations. The Reynolds number should be less than around 20000 for large flow geometries. In

practical applications, the Reynolds number of the flow in the reactor usually exceeds this number. Thus, the RANS method is widely used in the numerical study of the high turbulent supercritical water flow in nuclear reactors. Several turbulent models can be used in the simulation of supercritical fluid flows. Jones and Launder [24] first proposed the standard k - ε turbulence model for the condition of the fully developed turbulent flows where the influence of the molecular viscosity is not considered. To be applicable in a wider class of flows than the standard model, the renormalization group theory (RNG) k - ε model using a mathematical technique was developed [25]. Subsequently, the realizable k - ε model was developed [26], which differs from the standard one in satisfying certain mathematical constraints on the Reynolds stress in order to be consistent with the physics of the turbulent flow. It shows better performance for the flows involving rotation and the boundary layers under strong adverse pressure gradients. Wilcox [26] presented the standard k - ω model. This model shows an improved performance for the boundary layer under strong adverse pressure gradients. Later, the k - ω shear stress transport (SST) model was proposed by Menter [27]. The modification is that the linear constitutive equation of the standard k - ω allows the k - ω model used in the boundary layer region while the k - ε model used for the free stream region. Kim et al. [28] investigated the vertical upward supercritical water flow in a heated tube by selected turbulent models: standard, RNG, and realizable k - ε models, standard k - ω and k - ω SST models. The numerical results were compared with the experimental data from Yamagata et al. [29]. Although the RNG k - ε model with the enhanced wall treatment showed the best performance, the predictions of the wall temperatures are not satisfactory. The above two-equation turbulent models are based on the assumption of the isotropic eddy-viscosity. The Reynolds stress model (RSM) closes the Reynolds-averaged Navier-Stokes equations by solving transport equations for the Reynolds stresses directly and together with an equation for the dissipation rate without the isotropic hypothesis.

The numerical studies by RANS simulations for the supercritical flow in rod bundles have been investigated by several researchers recently. Zhao et al. [30] used OpenFOAM to simulate a 7-pin flow geometry with the k - ω SST turbulence model for different operation

conditions. Zhang et al. [31] simulated the heat transfer and flow of the supercritical water in a 37-element horizontal arranged SCWR under steady state condition and found that the anisotropic turbulent model, the Reynolds stress model, behaves much better than the isotropic model in predicting the cladding surface temperature. Furthermore, Han et al. [32] further applied the same turbulence model for the simulation in the vertical channel with multiple fuel rods. Similar investigations can also be found in [33, 34]. The heat transfer characteristics in different type channels were investigated. A recent validation study of the RANS models for different fuel rod assemblies was performed by Dovizio et al. [35]. It was found that the RANS could be a reasonable approach to study this kind of fuel assemblies.

However, there is still lack of the investigation of the thermo-hydraulic behaviors of the supercritical water in the 64-element fuel bundle. Since the Canadian SCWR is still not put into use, there is no experimental data in the literature now. In this work, the supercritical water flow in the 64-element fuel bundle is investigated numerically by the RANS approach and the detailed fluid flow and heat transfer phenomenon for the supercritical water flow in the fuel rod channels are presented. The CFD simulations are carried out by the commercial software ANSYS FLUENT.

4.2. Numerical Procedure

4.2.1. Configurations of the Canadian SCWR

The Canadian SCWR core is proposed as shown in Fig. 4.1. There are 336 fuel channels in the Canadian SCWR core and generate a total 2540 MW thermal power. The fuel bundle of the Canadian SCWR consists of 64-element two-ring fuel rods. For each ring, 32 fuel elements are distributed circumferentially around the insulated central flow tube. The cross-section view of the fuel bundle is presented schematically in Fig. 4.2. The coolant supercritical water flow absorbs the heat produced by the fuel rods in the fuel bundle. The operating pressure is 25 MPa.

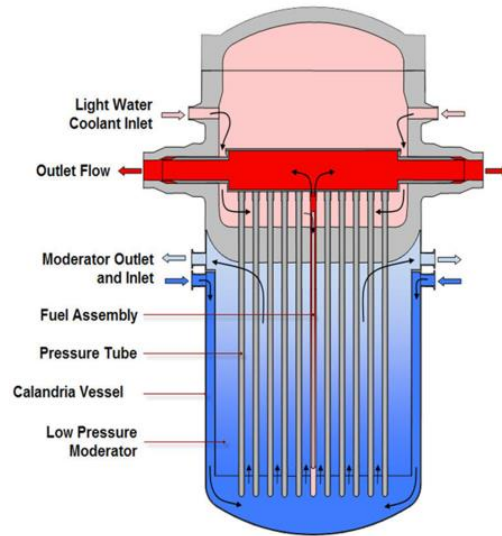


Figure 4.1: Canadian SCWR Core Concept [36]

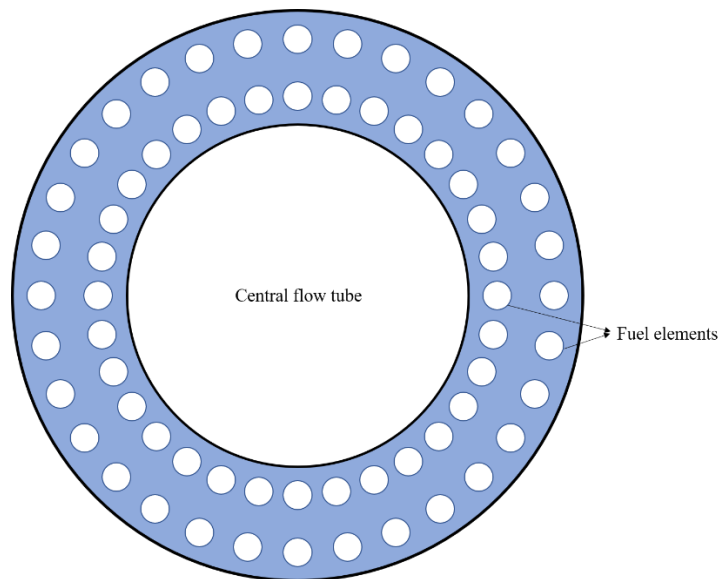
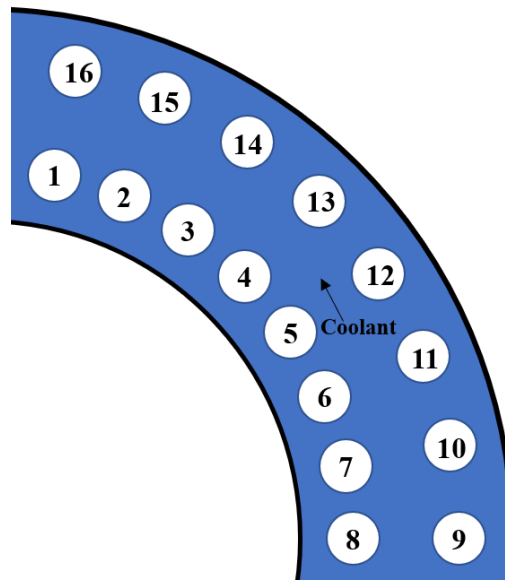


Figure 4.2: Cross-section view of the 64-element fuel assembly

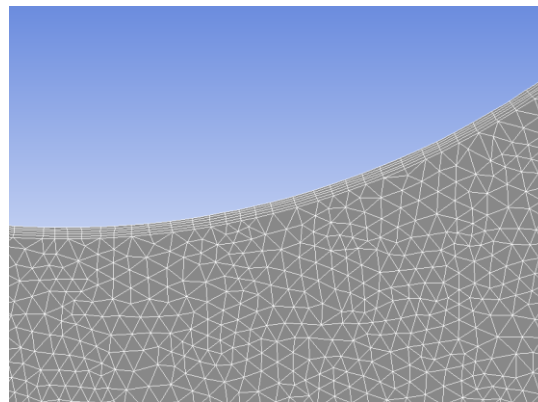
4.2.2. Computational domain and mesh generation

The flow in the fuel rods region is upward. In this study, only quarter of the region with fuel rods in the fuel bundle is considered because of the symmetry to reduce the

computational time. The computational domain and the mesh generated are shown in Fig. 4.3. The geometry specifications are shown Table 4.1. The thermal physical properties of the supercritical water were calculated by the physical property software (National Institute of Standards and Technology, NIST) and added to the ANSYS fluent using piecewise linear fitting method. Fig. 4.4 shows the two types of subchannels in the flow channel, the inner central subchannels between fuel rods and the edge subchannels.

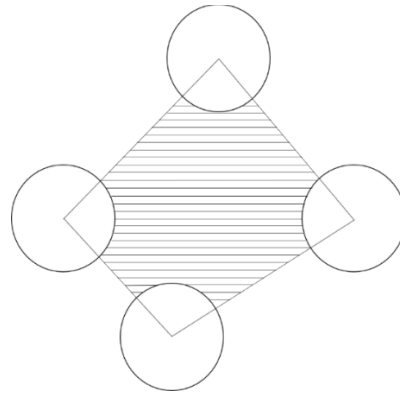


(a) Computational domain

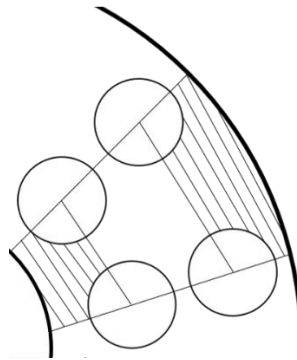


(b) Mesh

Figure 4.3: Computational domain and mesh of the fuel bundle



(a) central subchannel



(b) edge subchannel

Figure 4.4: Central subchannel and edge subchannel

Table 4.1 Geometry specifications of the computational domain

Parameter	Dimension (mm)
Inner fuel rod diameter	9.5
Outer fuel rod diameter	10
Heated length	5000

4.2.3. Numerical model and governing equations

The governing equations for this three-dimensional steady state flow and heat transfer are conservations of mass, momentum and energy, which are shown in the Reynolds averaged form as follows [37]:

$$\frac{\partial \rho \bar{u}_i}{\partial x_i} = 0 \quad (4.1)$$

$$\frac{\partial (\rho \bar{u}_i \bar{u}_j)}{\partial x_j} = -\frac{\partial \bar{p}}{\partial x_i} + \frac{\partial}{\partial x_j} \left(\mu \frac{\partial \bar{u}_i}{\partial x_j} - \rho \overline{u'_i u'_j} \right) + \rho g_i \quad (4.2)$$

$$\frac{\partial}{\partial x_i} \left(\bar{u}_i \rho c_p T \right) = \frac{\partial}{\partial x_i} \left[\left(\lambda + \frac{c_p \mu_t}{Pr_t} \right) \frac{\partial T}{\partial x_i} \right] \quad (4.3)$$

The modified Reynolds stress model with the variable Pr_t for supercritical fluid flows proposed in a previous study [38] is used in the simulations of the supercritical water flow in the 64-element fuel bundle. The Reynolds stresses, $-\rho \overline{u'_i u'_j}$, are solved by the Reynolds stress model to close the momentum equation. The transport equations for the Reynolds stress model can be described as:

$$\begin{aligned} \underbrace{\frac{\partial}{\partial x_k} (\rho u_k \overline{u'_i u'_j})}_{C_{ij} \equiv \text{Convection}} &= - \underbrace{\frac{\partial}{\partial x_k} \left[\rho \overline{u'_i u'_j u'_k} + p' (\delta_{kj} u'_i + \delta_{ik} u'_j) \right]}_{D_{T,ij} \equiv \text{Turbulent Diffusion}} \\ &+ \underbrace{\frac{\partial}{\partial x_k} \left[\mu \frac{\partial}{\partial x_k} (\overline{u'_i u'_j}) \right]}_{D_{L,ij} \equiv \text{Molecular Diffusion}} - \underbrace{\rho \left(\overline{u'_i u'_k} \frac{\partial u_j}{\partial x_k} + \overline{u'_j u'_k} \frac{\partial u_i}{\partial x_k} \right)}_{P_{ij} \equiv \text{Stress Production}} - \underbrace{\rho \beta (g_i \overline{u'_j \theta} + g_j \overline{u'_i \theta})}_{G_{ij} \equiv \text{Buoyancy Production}} \\ &+ \underbrace{p' \left(\frac{\partial u'_i}{\partial x_j} + \frac{\partial u'_j}{\partial x_i} \right)}_{\phi_{ij} \equiv \text{Pressure Strain}} - \underbrace{2\mu \frac{\partial u'_i}{\partial x_k} \frac{\partial u'_j}{\partial x_k}}_{\varepsilon_{ij} = \text{Dissipation}} - \underbrace{2\rho \Omega_k (\overline{u'_j u'_m} \varepsilon_{ikm} + \overline{u'_i u'_m} \varepsilon_{jkm})}_{F_{ij} \equiv \text{Production by System Rotation}} \\ &+ \underbrace{S_{user}}_{\text{User-Defined Source Term}} \end{aligned} \quad (4.4)$$

Because of the drastic changes of the thermal physical properties of the supercritical water, the turbulent Prandtl number is not a constant value [38, 39], which is expressed as a piecewise function:

$$Pr_t = \begin{cases} 0.4 & \mu_t/\mu < 0.2 \\ 0.3 + 0.03 \times \frac{P}{P_{cr}} \times P_r \times (\mu_t/\mu) \times (q/G) & 0.2 \leq \mu_t/\mu \leq 10 \\ 0.85 & \mu_t/\mu > 10 \end{cases} \quad (4.5)$$

where q is in kW/m^2 and G is in $\text{kg/m}^2\text{s}$. The enhanced wall treatment is selected for the near wall treatment with the RSM and mesh is fine enough to ensure $y^+ \approx 1$ near the wall. ANSYS Fluent software is applied in this study to perform the computational fluid dynamics simulations. The reference pressure is 25 MPa. The inlet velocity is 1.05 m/s and the inlet temperature are 350°C , respectively. The heat flux on the fuel rod is assumed uniform and the wall surfaces are set as no-slip boundary condition. A mesh sensitivity study is conducted. The simulations using three different meshes with increasing the number of cells are executed. Table 4.2 presents the characteristics of the meshes and the comparison of the respective simulation results. It can be seen that the relative differences of the simulations results are small and decreases with the mesh becoming finer. Considering the accuracy of the simulation results and the cost of the computation, mesh 2 is employed in this simulation to investigate the flow physics in the rod channel.

Table 4.2 Mesh characteristics and the comparison results

Mesh ID	Cells	Maximum wall temperature ($^\circ\text{C}$) at $z = 4.8$ m	Relative difference between consecutive meshes (%)	Outlet velocity magnitude (m/s)	Relative difference between consecutive meshes (%)
1	6139234	808.77		12.05	
2	11419161	813.41	0.574	11.67	3.154

3	19578137	814.09	0.0836	11.73	0.514
---	----------	--------	--------	-------	-------

4.3. Results and Discussions

4.3.1. Velocity profiles

The streamwise velocity profile in the cross-section at the outlet is provided in Fig. 4.5, which demonstrates the primary feature of the flow field. It is found that the distribution of the streamwise velocity component is similar along the circumferential direction and the streamwise velocities at the inner subchannels are higher than those at edge subchannels.

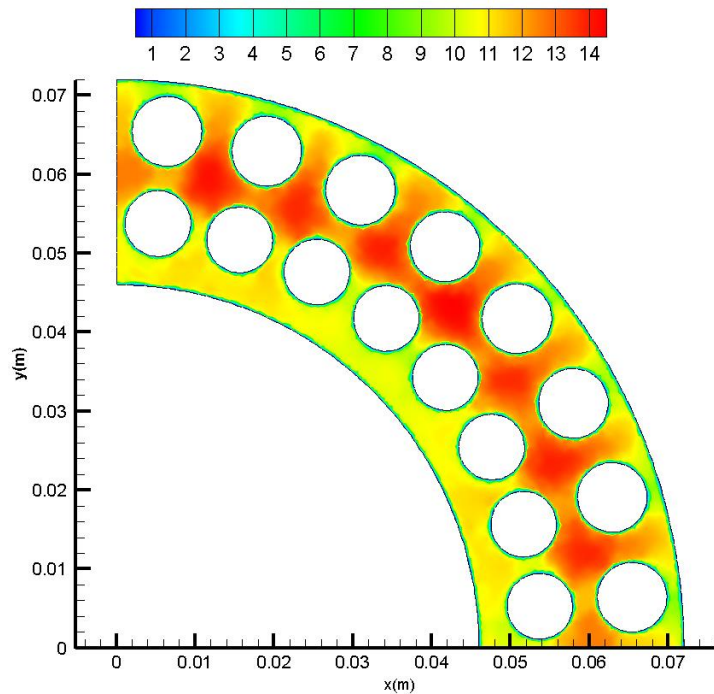


Figure 4.5: Distributions of the streamwise velocity at the outlet (m/s)

Fig. 4.6 displays 6 lines (Lines 1 to 6) along the radial direction, which are used for quantitative comparisons in subsequent plots. These lines span the gaps between the inner wall and rod, between the rods, and between the rod and outer wall from the inner wall to the outer wall. The radial distribution of the streamwise velocity profiles along these six

lines are provided in Fig. 4.7. As expected, the velocities are higher in the region away from the walls and decrease sharply toward the near wall region. And the gradient of the velocity decrease along the radial direction at edge subchannels (lines 1, 3, 4, 6) are smaller than those at central subchannels (lines 2, 5). The dramatic decrease in the velocity near the wall could deteriorate the heat transfer from the wall to the free stream and consequently cause higher wall temperatures.

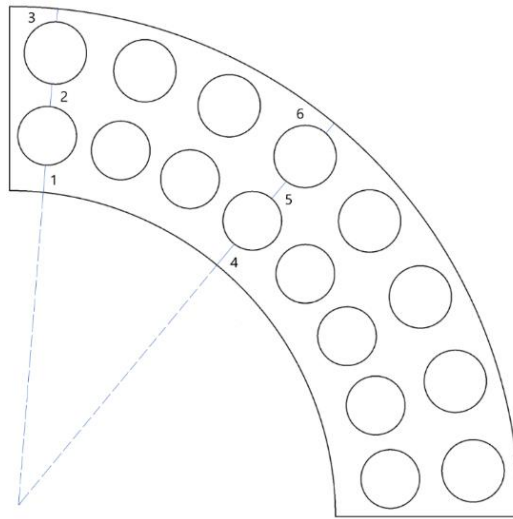
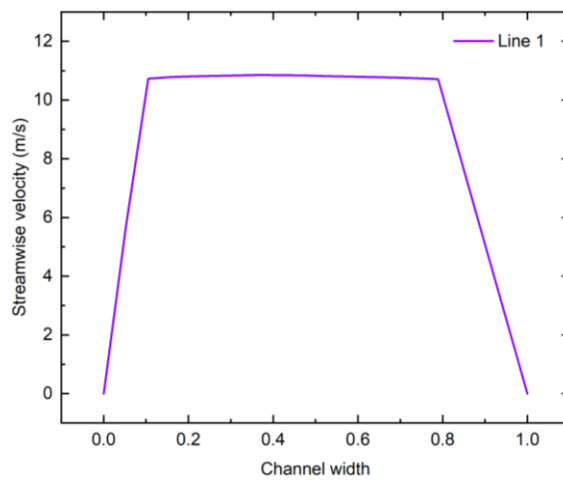
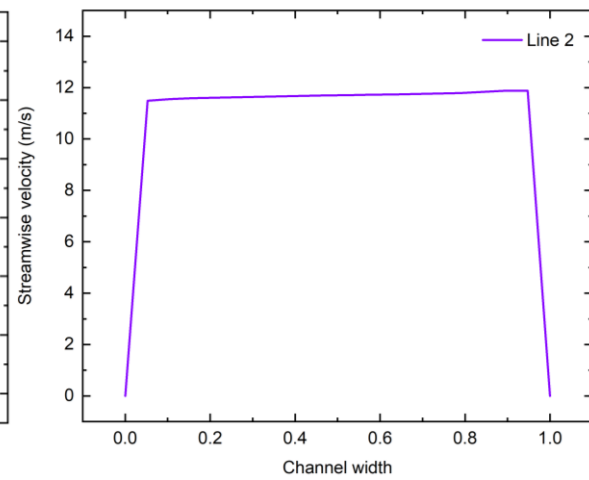


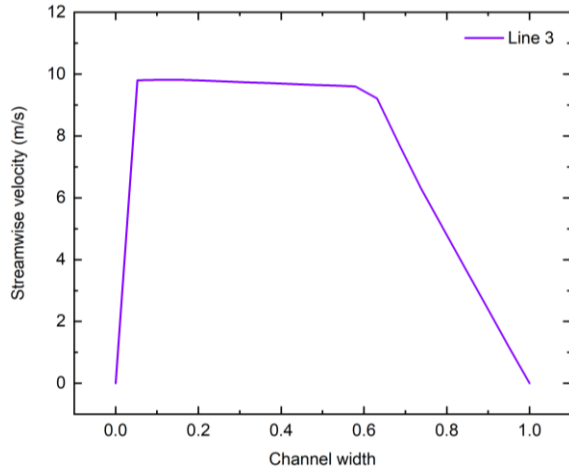
Figure 4.6: Lines used for analysis



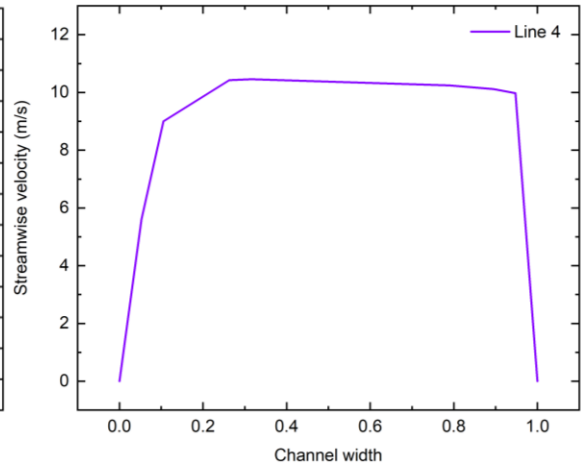
(a) Line 1



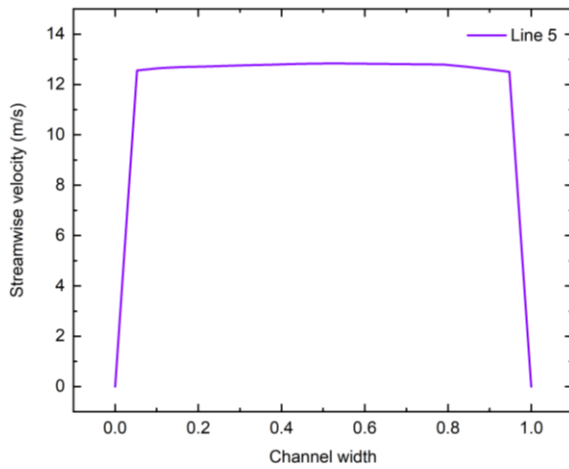
(b) Line 2



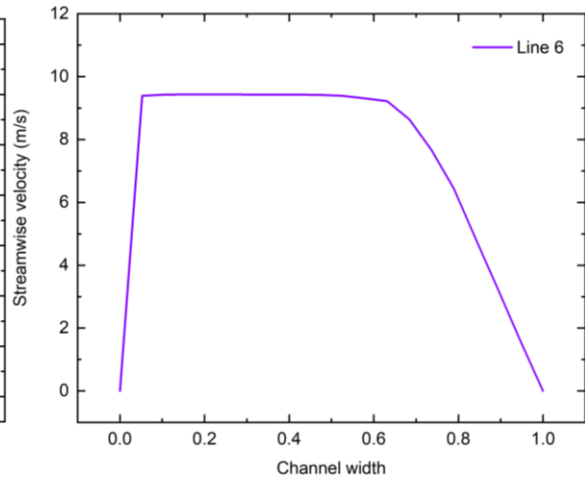
(c) Line 3



(d) Line 4



(e) Line 5



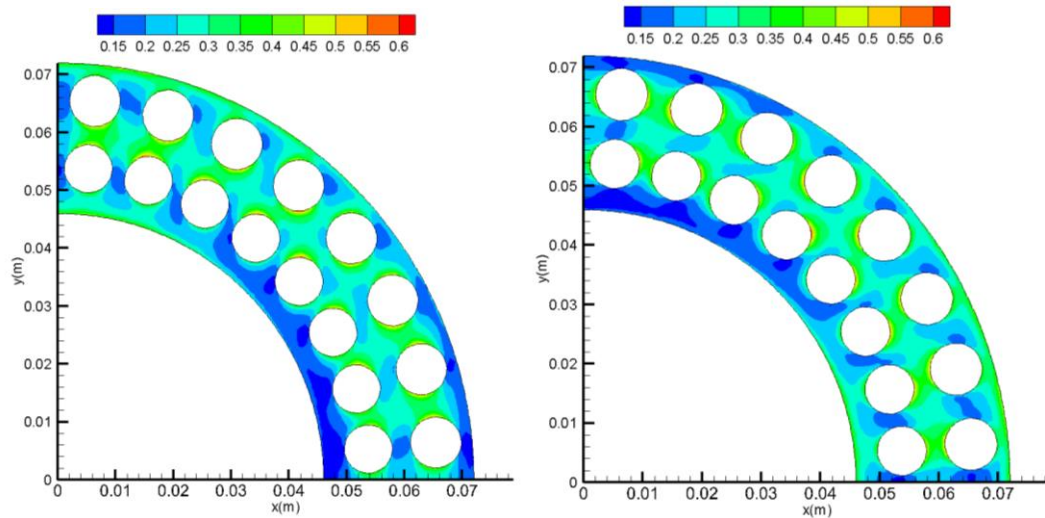
(f) Line 6

Figure 4.7: Plots of the streamwise velocity along lines (m/s)

4.3.2. Reynolds stresses

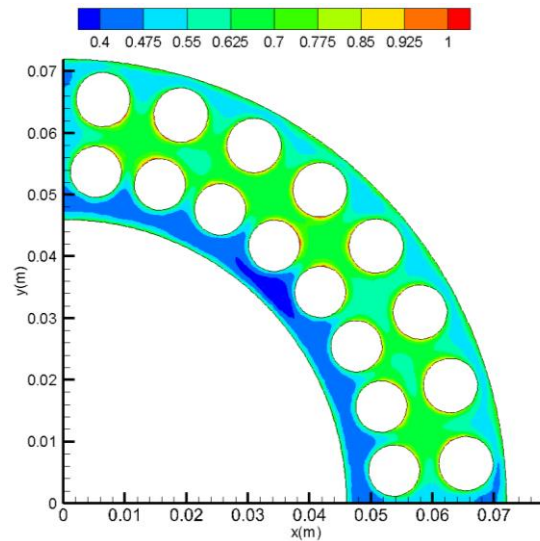
Reynolds stresses were also extracted from the domain. Fig. 4.8 provides the distributions of the normal Reynolds stresses at the outlet and the normal Reynolds stresses along each line are provided in Figs. 4.9 - 4.10. As expected in wall-bounded shear flows, the streamwise normal Reynolds stress is the dominant component throughout most of the domain. It shows that the normal Reynolds stresses are generally larger in the central

subchannels than those in the edge subchannels, and the streamwise Reynolds stresses have dual peaks at the same magnitude near the rods in the central subchannels. While in the edge subchannels, the peak value exists near the edge, except for the distributions along line 3, the peak value is near the rod. The lateral stresses follow a similar pattern but with reduced peaks due to less production from the mean shear.



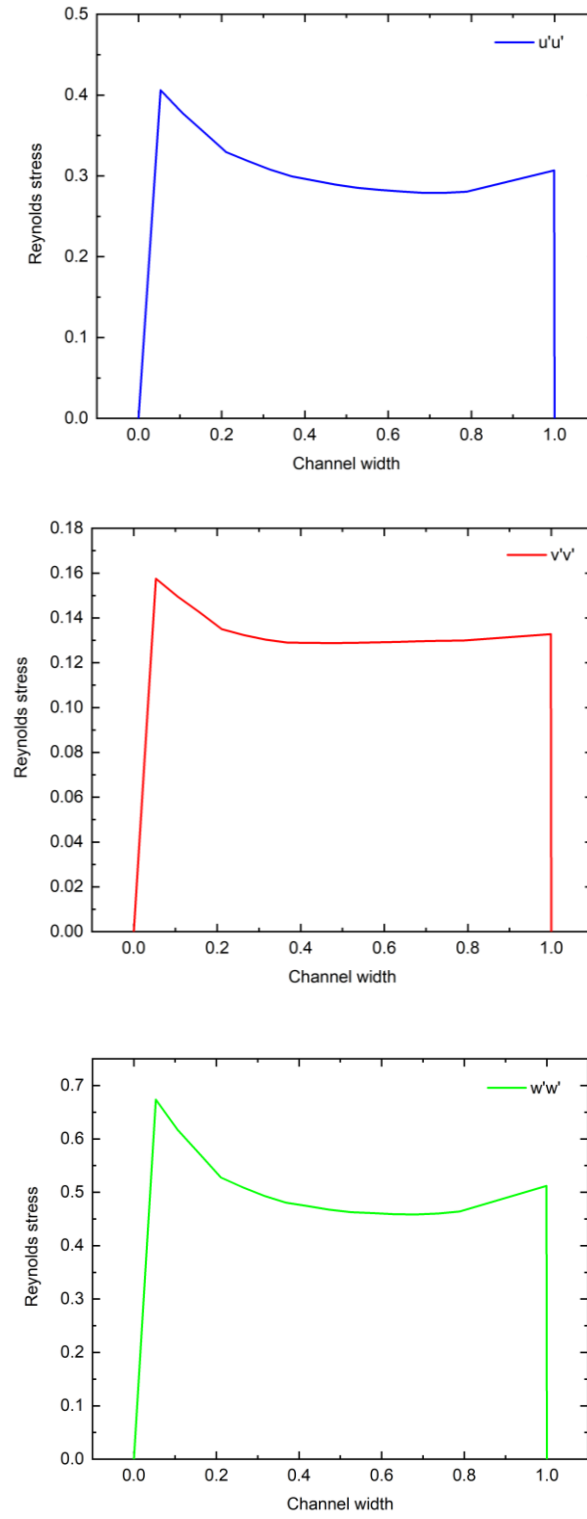
(a) Reynolds stress - $\overline{u'u'}$ profile

(b) Reynolds stress - $\overline{v'v'}$ profile

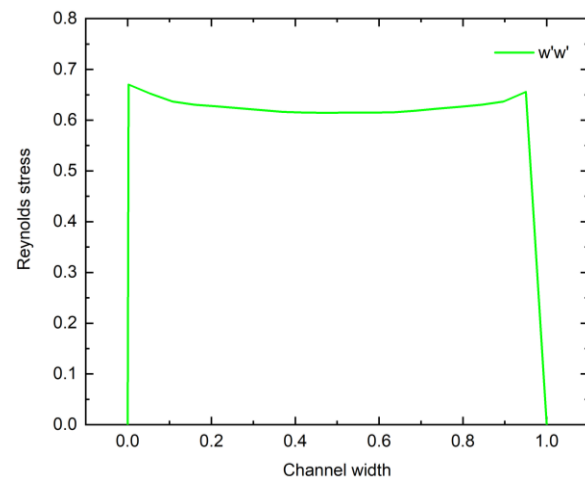
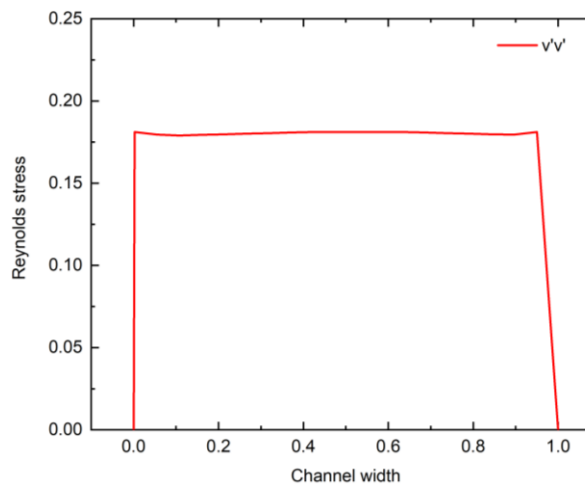
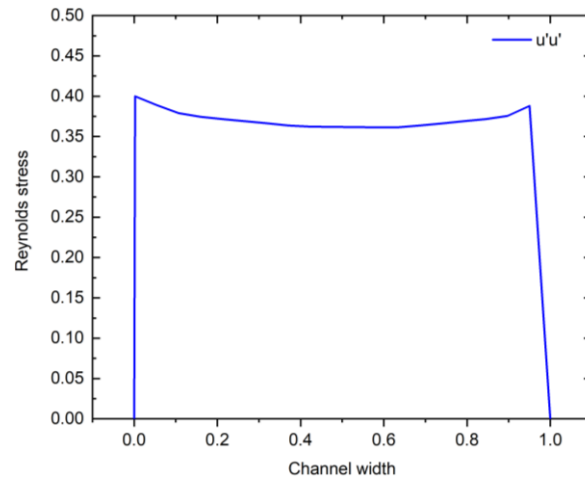


(c) Reynolds stress - $\overline{w'w'}$ profile

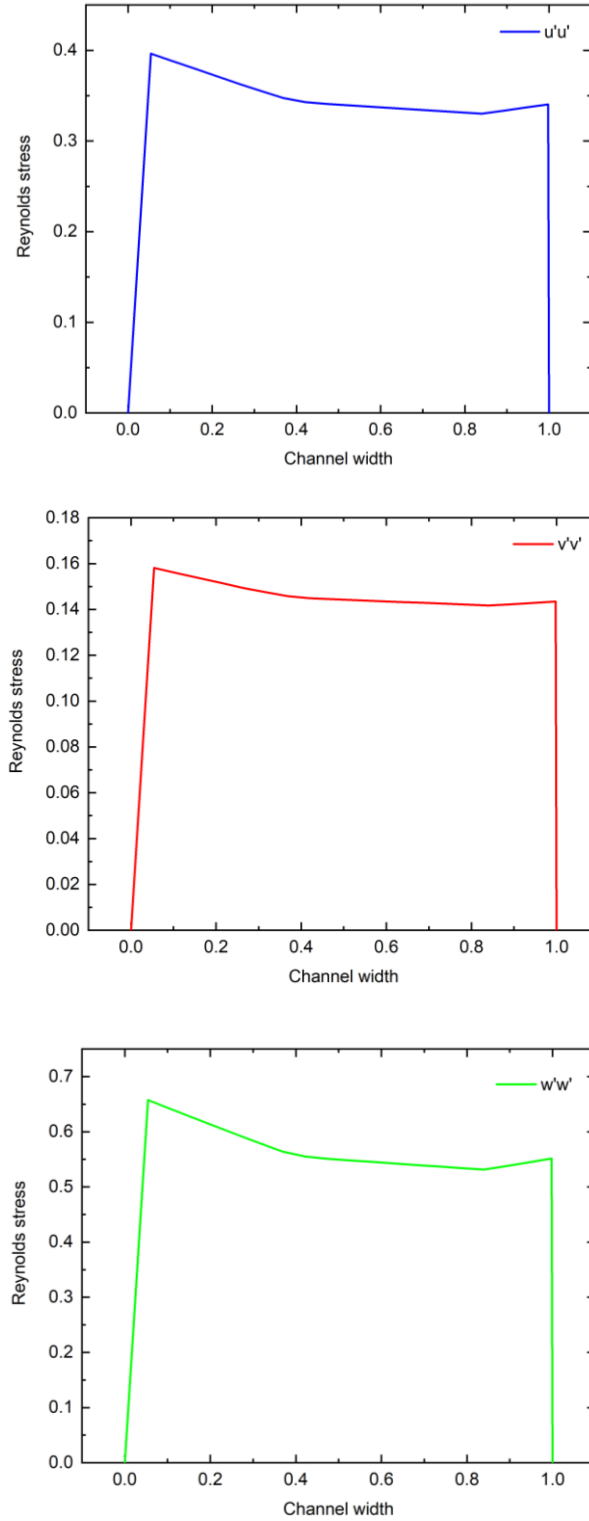
Figure 4.8: Distributions of the normal Reynolds stresses at the outlet (m^2/s^2)



(a) Line 1

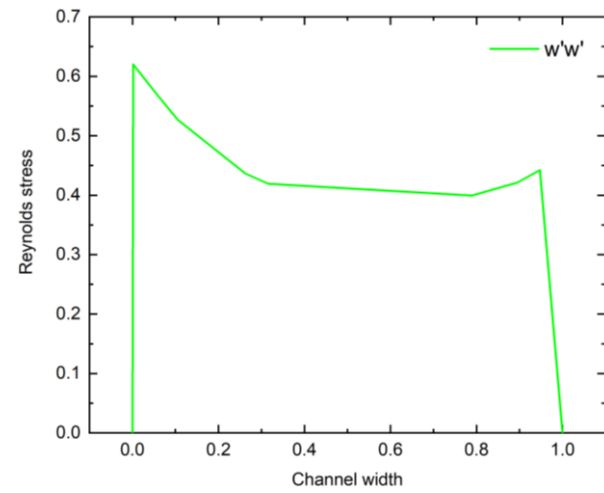
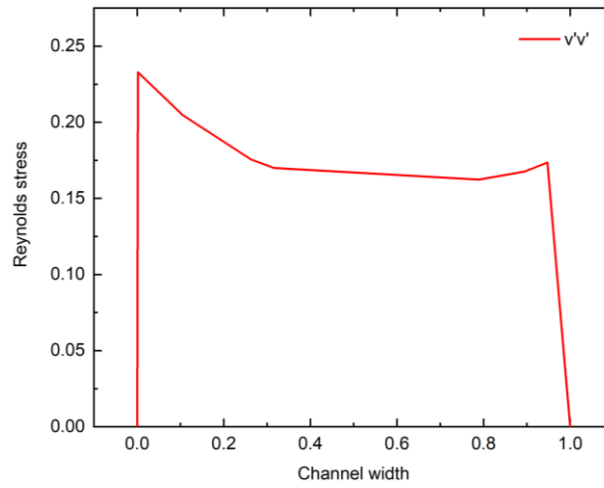
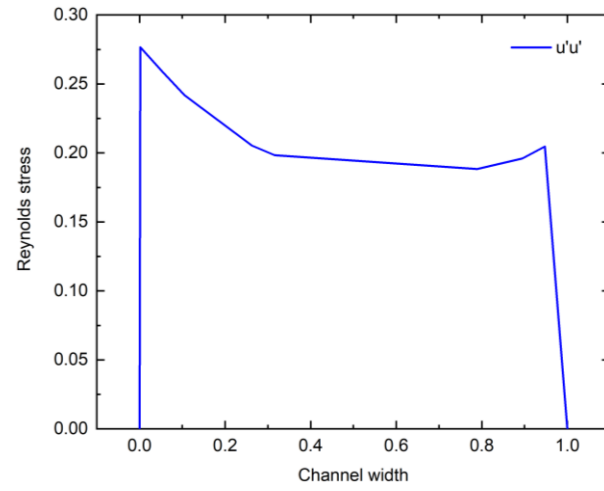


(b) Line 2

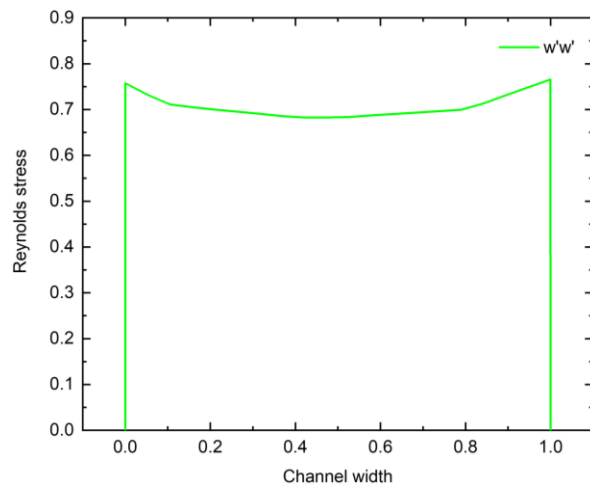
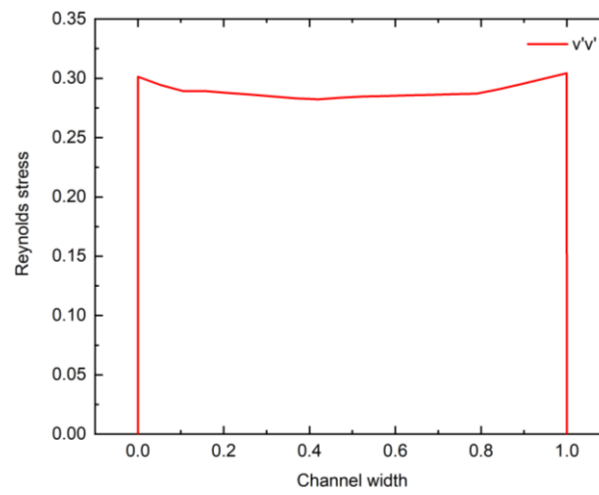
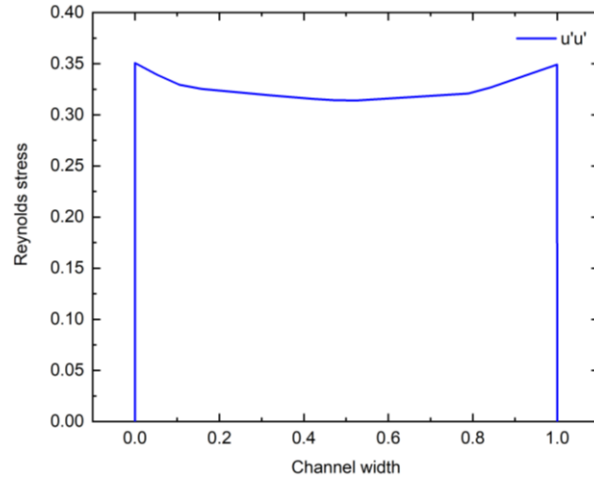


(c) Line 3

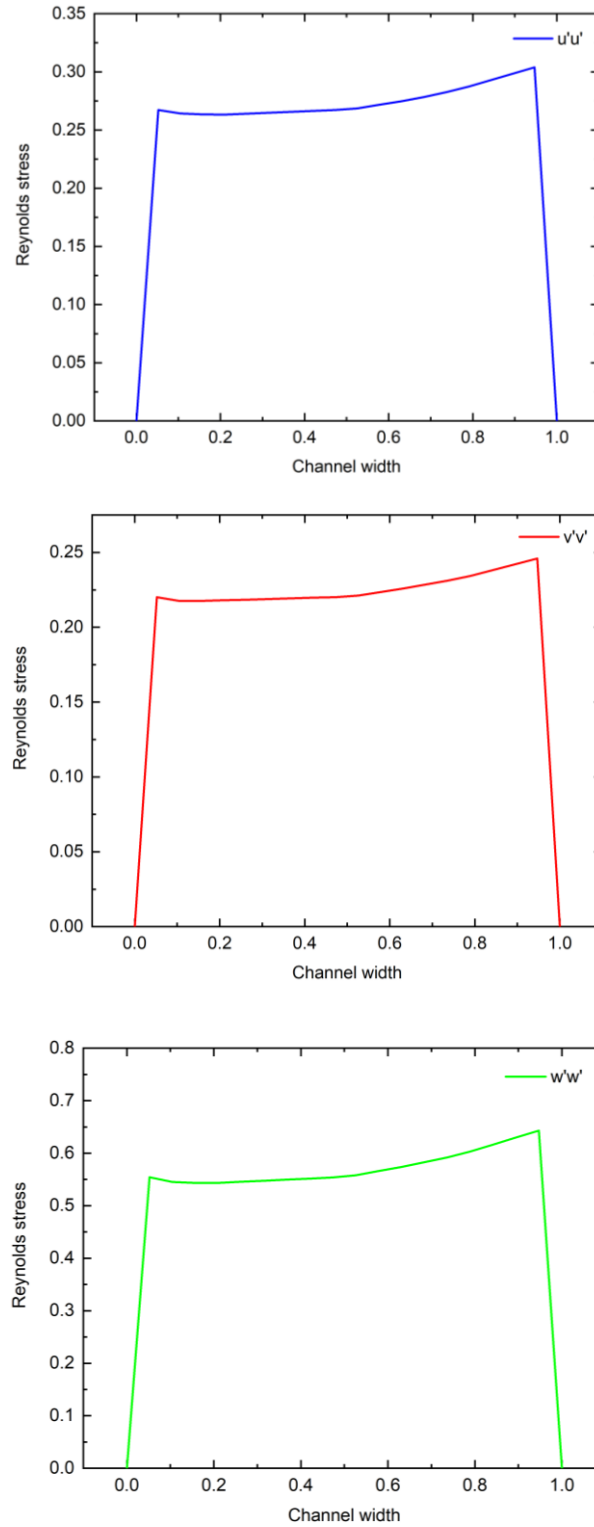
Figure 4.9: Plots of Reynolds normal stresses for lines 1 - 3 (m^2/s^2)



(a) Line 4



(b) Line 5

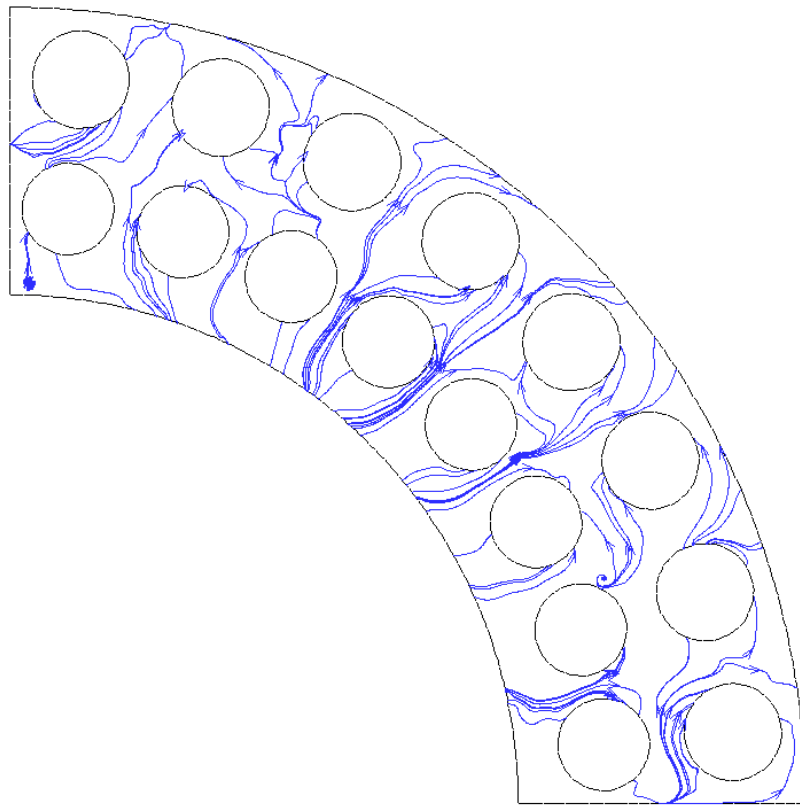


(c) Line 6

Figure 4.10: Plots of Reynolds normal stresses for lines 4 – 6 (m^2/s^2)

4.3.3. Secondary flow

The lateral secondary flows in rod bundles are important for inter-channel mixing and heat transfer, and the results of the simulation confirm that there is non-organized lateral motion in the flow at the outlet, presented in Fig. 4.11. The cross flows show that in the edge subchannel, such as near rod #1, the flow is moving towards the rod, whereas in the center subchannel, such as near rod #7, the flow is moving toward the center of the subchannel, which provides further evidence of the existence of gap vortex in the subchannels [40–41].



(a) Streamline

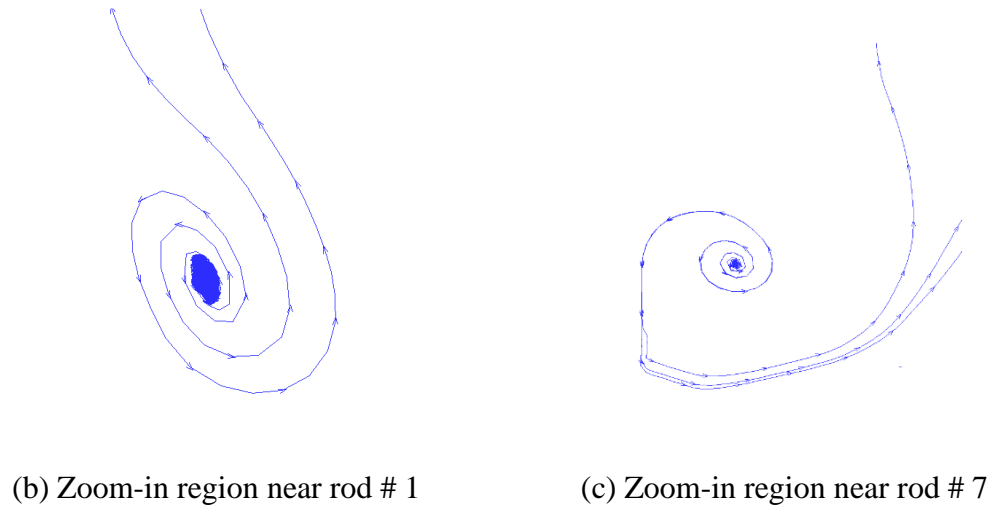


Figure 4.11: Streamline of flow at the outlet

4.3.4. Bulk temperature & wall temperatures

The bulk temperature of the supercritical water at the cross section along the axial direction is shown in Fig. 4.12. The fluid temperature increases along the upward flow direction. Fig. 4.13 depicts the distribution of the cladding surface temperatures on the fuel rods in the entire domain.

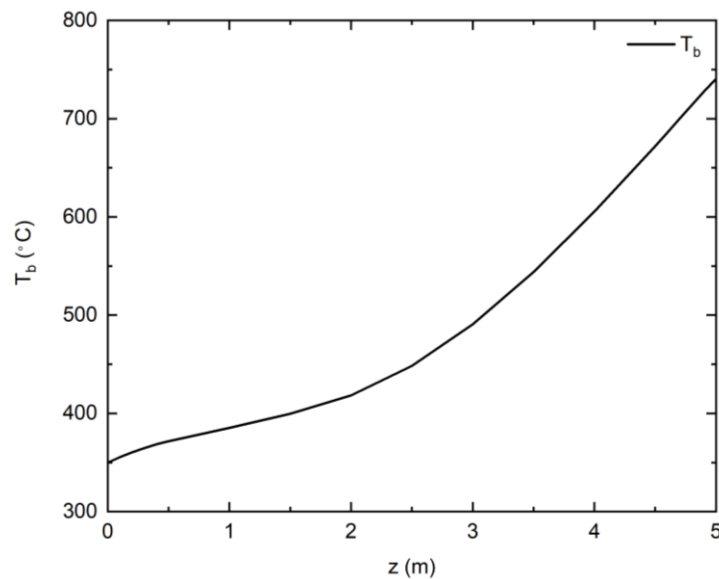


Figure 4.12: Bulk temperature along axial direction

The maximum and minimum cladding surface temperatures along the circumference of the fuel rods at $z = 2.5$ m, $z = 3.75$ m, and $z = 4.8$ m are also shown in Figs 4.14 - 4.16. The bulk fluid temperatures at these three planes are 448.4°C , 573.9°C , and 713.3°C , respectively. It is found that the maximum cladding surface temperatures at $z = 2.5$ m, $z = 3.75$ m, and $z = 4.8$ m occur at fuel rods #4, #4, and #12, respectively, while the minimum cladding surface temperatures appear at fuel rods # 1, #4, and # 4, respectively. The results show that the largest circumferential cladding surface temperature difference is 166.5°C at $z = 4.8$ m of fuel rod #7.

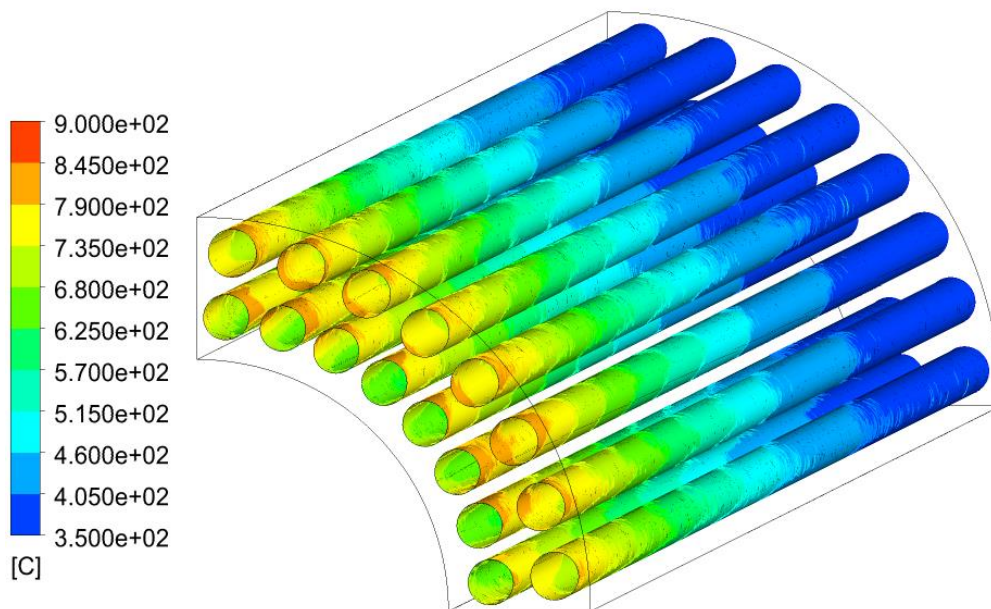
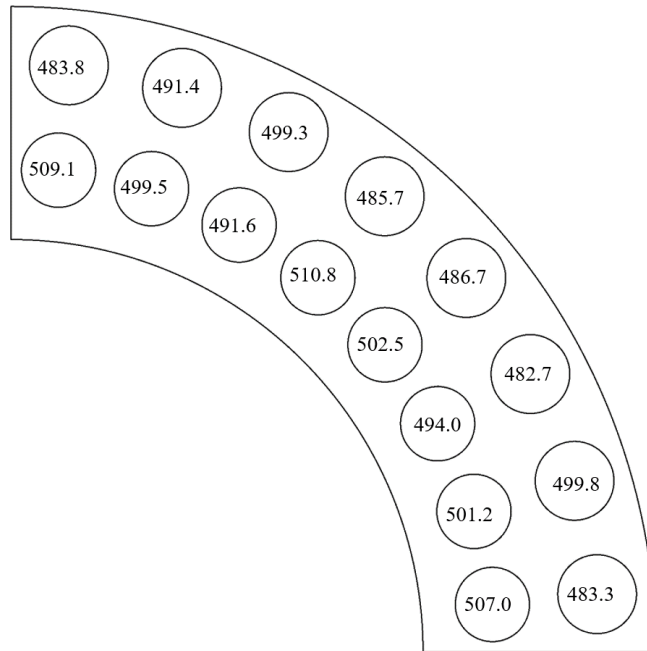
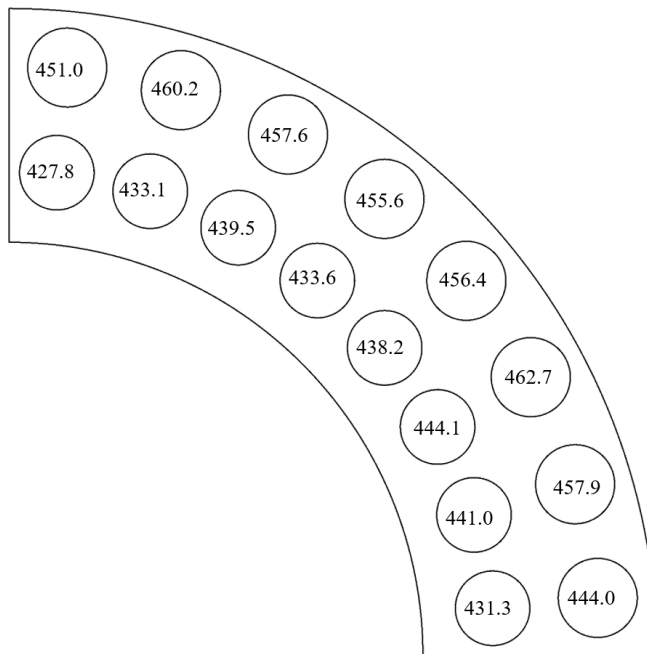


Figure 4.13: Cladding surface temperature distributions in the fuel bundle

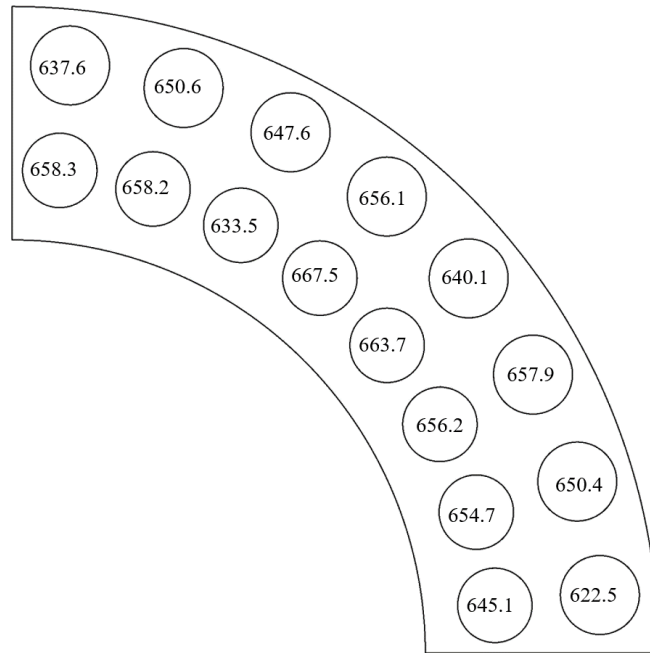


(a) Maximum

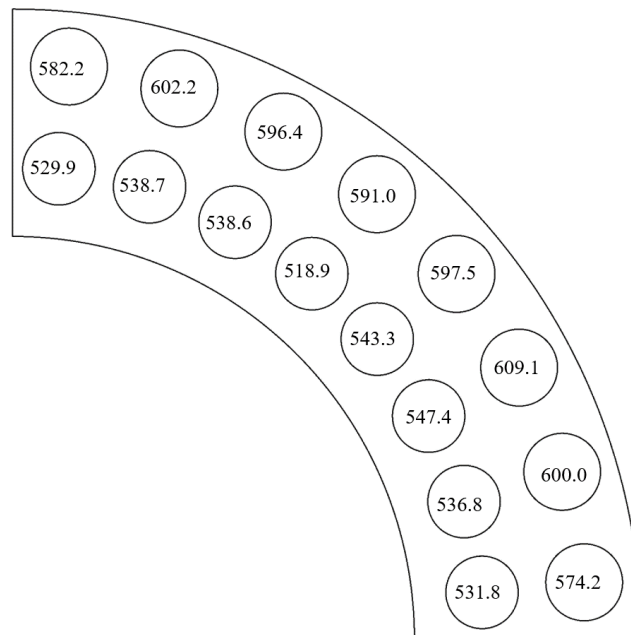


(b) Minimum

Figure 4.14: Maximum and Minimum cladding surface temperatures along the circumference of the fuel rods at $z = 2.5\text{m}$ ($^{\circ}\text{C}$)

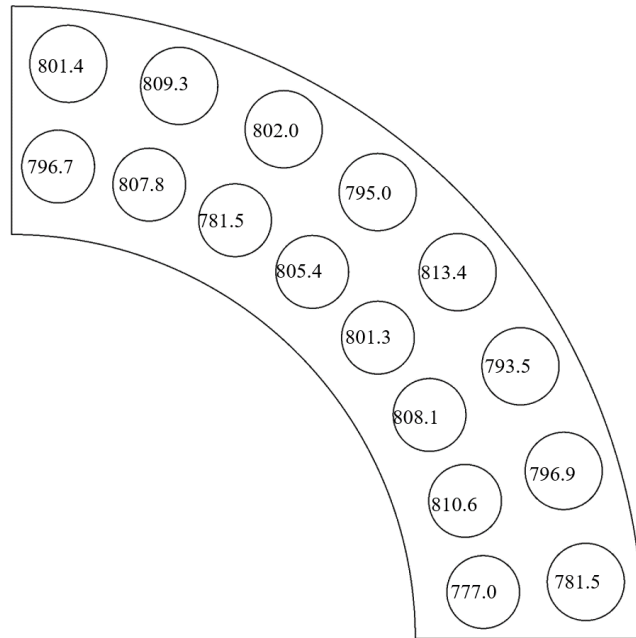


(a) Maximum

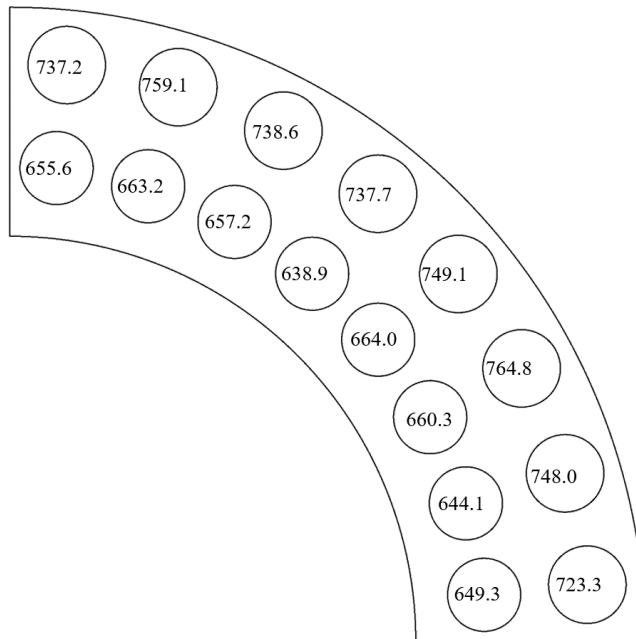


(b) Minimum

Figure 4.15: Maximum and Minimum cladding surface temperatures along the circumference of the fuel rods at $z = 3.75$ m (°C)



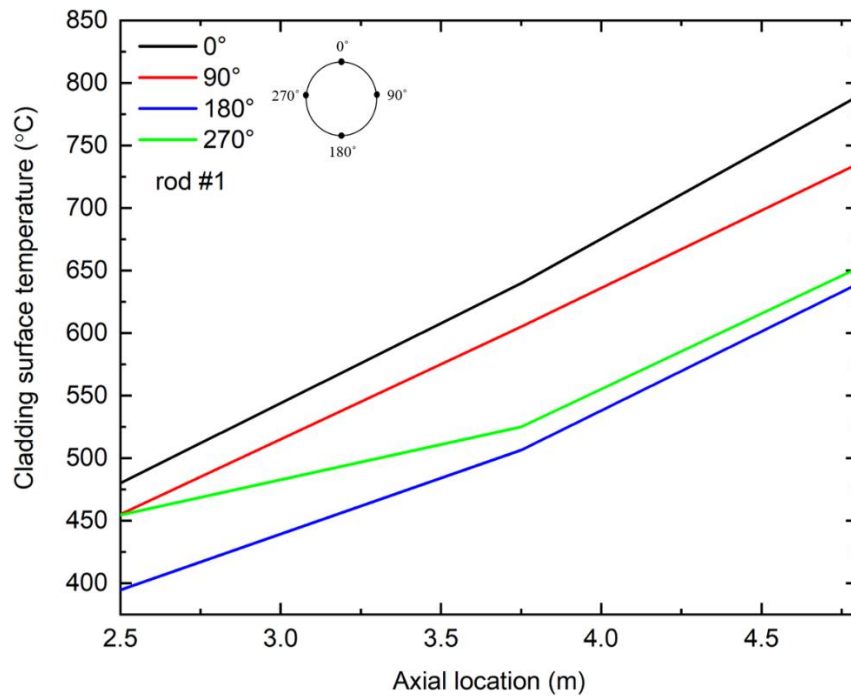
(a) Maximum



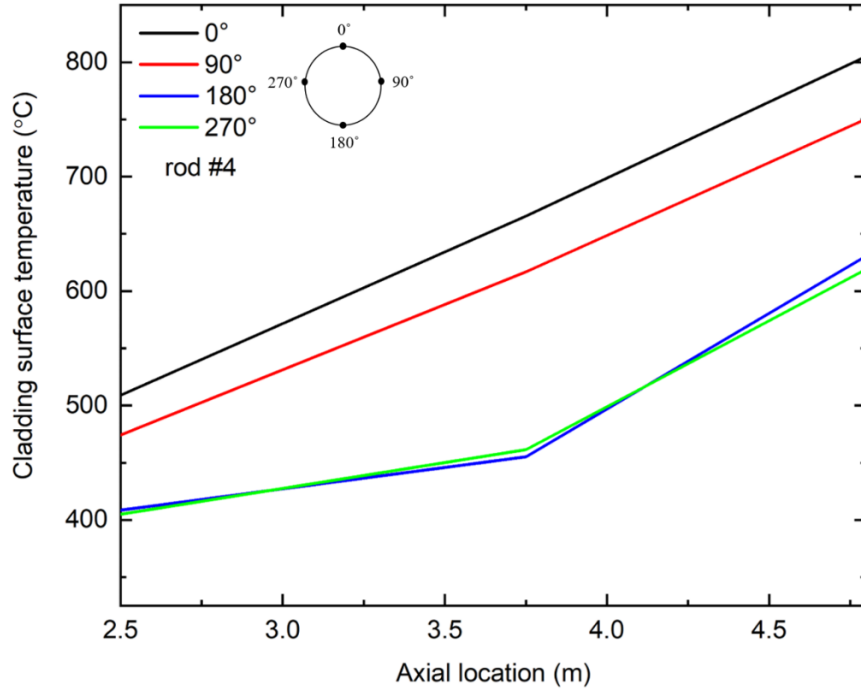
(b) Minimum

Figure 4.16: Maximum and Minimum cladding surface temperatures along the circumference of the fuel rods at $z = 4.8$ m ($^{\circ}\text{C}$)

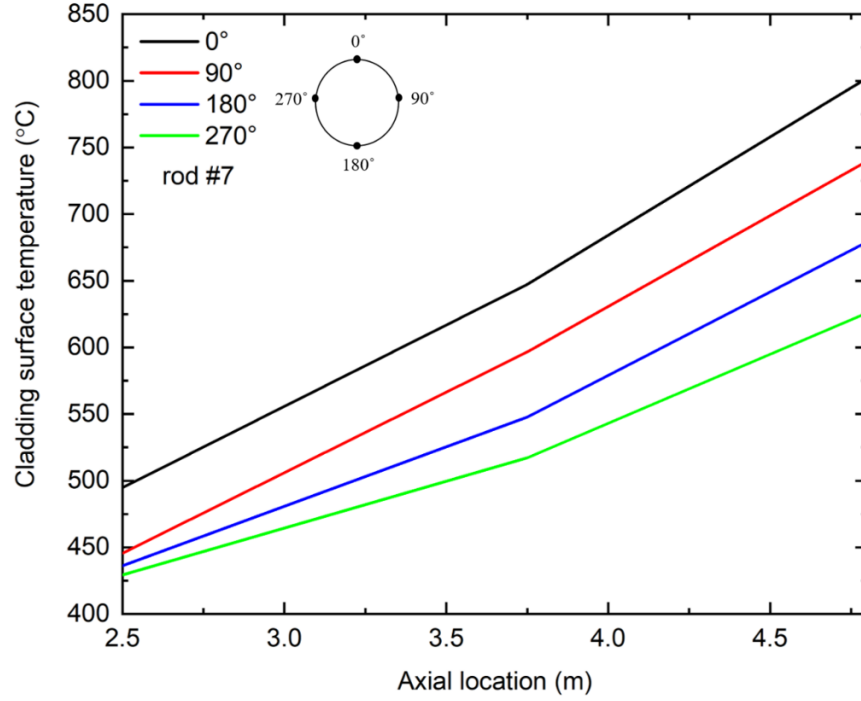
The axial cladding surface temperature distribution at the fuel rods #1, #4, #7 & #12 are shown in Fig. 4.17. The circumferential cladding surface temperature difference at x-y plane increases along the axial location. Fig. 4.18 presents the cladding surface temperature distribution along the circumference for fuel rod #7 at $z = 4.8$ m. It can be concluded that the higher wall temperatures always exist at the center subchannel fluid region. Although the maximum cladding surface temperature at the selected axial locations is below the recommended value (850°C), the maximum wall temperature for each fuel rod is quite different and the temperature of the circumferential direction is very non-uniform.



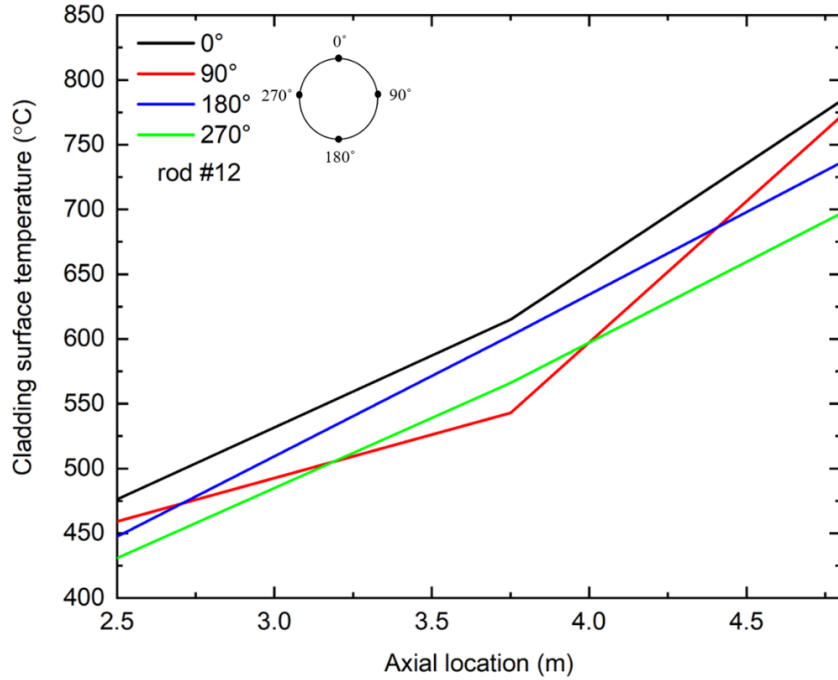
(a) rod # 1



(b) rod # 4

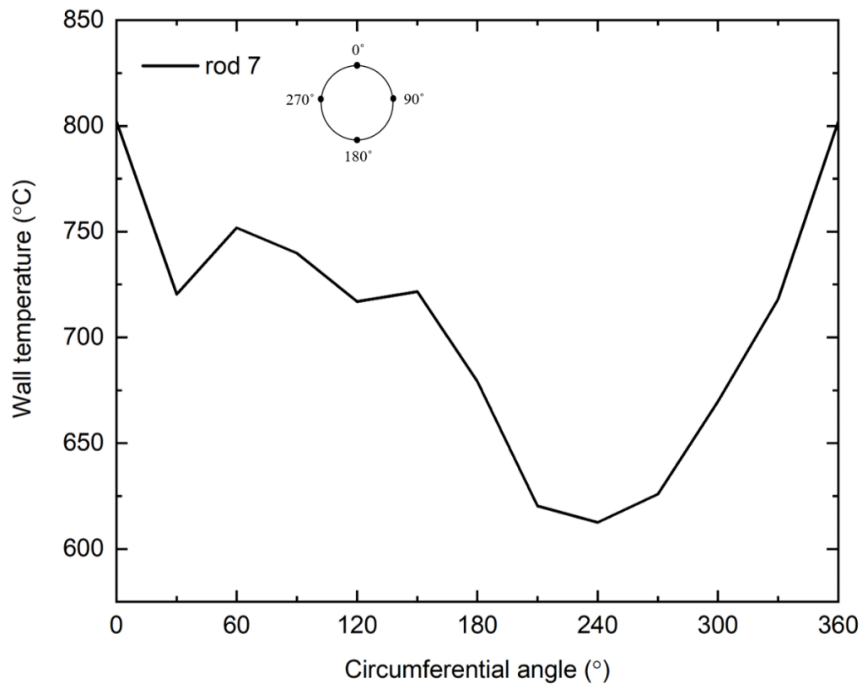


(c) rod # 7



(d) rod # 12

Figure 4.17: Axial cladding surface temperature distributions

Figure 4.18: Circumferential cladding surface temperature distribution at $z = 4.8$ m for rod 7

4.4. Conclusions

In this study, CFD studies were performed using turbulent model with a modified turbulent Prandtl number to simulate the full-scale 3D flow and heat transfer of the supercritical water in the bundles with fuel rods. The fluid flow and heat transfer phenomena in the rod bundle have been clarified, especially the possibility of the existence of the gap vortex in the edge subchannels. This phenomenon might be due to the intrinsic aspects of the turbulence and geometry of the flow subchannels. The fluid bulk temperature and the wall temperatures of the fuel rods generally increase along the axial flow direction. It is observed that the circumferential wall temperature distribution around the fuel rod surface is extremely non-uniform and the maximum cladding surface temperature for each fuel rod is also different. The maximum cladding temperature and the circumferential distributions are significant for the safety design of the assembly of the nuclear reactor, notably when there are accidental disturbances. Thus, a more appropriate thermal power distribution for each fuel rod based on the present work is needed. In addition, the respective experimental work is needed in the future to validate the numerical results.

References

- [1] GIF (Generation IV International Forum), “Technology Roadmap Update for Generation IV Nuclear Energy Systems,” 2014.
- [2] GIF, “GIF R&D Outlook for Generation IV Nuclear Energy Systems 2018 Update,” *Nuclear Energy*, 2018.
- [3] M. Qu, D. Yang, Z. Liang, L. Wan, and D. Liu, “Experimental and numerical investigation on heat transfer of ultra-supercritical water in vertical upward tube under uniform and non-uniform heating,” *International Journal of Heat and Mass Transfer*, vol. 127, pp. 769–783, Dec. 2018.
- [4] X. Lei, H. Li, N. Dinh, and W. Zhang, “A study of heat transfer scaling of supercritical pressure water in horizontal tubes,” *International Journal of Heat and Mass Transfer*, vol. 114, pp. 923–933, 2017.

- [5] Z. Shen, D. Yang, S. Wang, W. Wang, and Y. Li, “Experimental and numerical analysis of heat transfer to water at supercritical pressures,” *International Journal of Heat and Mass Transfer*, vol. 108, pp. 1676–1688, 2017.
- [6] H. Y. Gu, M. Zhao, and X. Cheng, “Experimental studies on heat transfer to supercritical water in circular tubes at high heat fluxes,” *Experimental Thermal and Fluid Science*, 2015.
- [7] S. Yu, H. Li, X. Lei, Y. Feng, Y. Zhang, H. He, and T. Wang, “Experimental investigation on heat transfer characteristics of supercritical pressure water in a horizontal tube,” *Experimental Thermal and Fluid Science*, vol. 50, pp. 213–221, Oct. 2013.
- [8] G. Zhang, H. Zhang, H. Gu, Y. Yang, and X. Cheng, “Experimental and numerical investigation of turbulent convective heat transfer deterioration of supercritical water in vertical tube,” *Nuclear Engineering and Design*, vol. 248, pp. 226–237, Jul. 2012.
- [9] S. J. Mokry, P. L. Kirillov, I. L. Pioro, and Y. K. Gospodinov, “Supercritical Water Heat Transfer in a Vertical Bare Tube: Normal, Improved, and Deteriorated Regimes,” *Nuclear Technology*, vol. 172, no. 1, pp. 60–70, 2010.
- [10] K. Yamagata, K. Nishikawa, S. Hasegawa, T. Fujii, and S. Yoshida, “Forced convective heat transfer to supercritical water flowing in tubes,” *International Journal of Heat and Mass Transfer*, vol. 15, pp. 2575–2593, 1972.
- [11] H. Wang, Q. Bi, L. Wang, H. Lv, and L. K. H. Leung, “Experimental investigation of heat transfer from a 2×2 rod bundle to supercritical pressure water,” *Nuclear Engineering and Design*, vol. 275, pp. 205–218, Aug. 2014.
- [12] H. Y. Gu, H. B. Li, Z. X. Hu, D. Liu, and M. Zhao, “Heat transfer to supercritical water in a 2×2 rod bundle,” *Annals of Nuclear Energy*, vol. 83, pp. 114–124, 2015.
- [13] M. Zhao and H. Y. Gu, “Experimental and numerical investigation on heat transfer of supercritical water flowing upward in 2×2 rod bundles,” *Nuclear Engineering and Design*, vol. 370, no. October, 2020.

- [14] B. Zhang, J. Shan, and J. Jiang, "Numerical analysis of supercritical water heat transfer in horizontal circular tube," *Progress in Nuclear Energy*, vol. 52, no. 7, pp. 678–684, 2010.
- [15] J. Xiong and X. Cheng, "Turbulence modelling for supercritical pressure heat transfer in upward tube flow," *Nuclear Engineering and Design*, vol. 270, pp. 249–258, Apr. 2014.
- [16] B. Zhang, J. Q. Shan, and J. Jiang, "Simulation of heat transfer of supercritical water in obstacle-bearing vertical tube," *Nuclear Science and Techniques*, vol. 21, no. 4, pp. 241–245, 2010.
- [17] Q. L. Wen and H. Y. Gu, "Numerical simulation of heat transfer deterioration phenomenon in supercritical water through vertical tube," *Annals of Nuclear Energy*, vol. 37, no. 10, pp. 1272–1280, 2010.
- [18] Y. Zhang, C. Zhang, and J. Jiang, "Numerical Simulation of Heat Transfer of Supercritical Fluids in Circular Tubes Using Different Turbulence Models," *Journal of Nuclear Science and Technology*, vol. 48, no. 3, pp. 366–373, 2011.
- [19] P. Fischer, J. Lottes, A. Siegel, and G. Palmiotti, "Large eddy simulation of wire-wrapped fuel pins i: Hydrodynamics in a periodic array," in *Joint International Topical Meeting on Mathematics & Computation and Supercomputing in Nuclear Applications*, Monterey, CA, USA, 2007.
- [20] E. Merzari, P. Fischer, H. Yuan, K. Van Tichelen, S. Keijers, J. De Ridder, J. Degroote, J. Vierendeels, H. Doolaard, V. R. Gopala, and F. Roelofs, "Benchmark exercise for fluid flow simulations in a liquid metal fast reactor fuel assembly," *Nucl. Eng. Des.*, vol. 298, pp. 218–228, Mar. 2016.
- [21] L. Brockmeyer, E. Merzari, J. Solberg, and Y. Hassan, "One-way coupled simulation of FIV in a 7-pin wire-wrapped fuel pin bundle," *Nucl. Eng. Des.*, vol. 356, p. 110367, Jan. 2020.

- [22] L. Brockmeyer, L. B. Carasik, E. Merzari, and Y. Hassan, “Numerical simulations for determination of minimum representative bundle size in wire wrapped tube bundles,” *Nucl. Eng. Des.*, vol. 322, pp. 577–590, Oct. 2017.
- [23] N. Goth, P. Jones, D. T. Nguyen, R. Vaghetto, Y. A. Hassan, A. Obabko, E. Merzari, and P. F. Fischer, “Comparison of experimental and simulation results on interior subchannels of a 61-pin wire-wrapped hexagonal fuel bundle,” *Nucl. Eng. Des.*, vol. 338, pp. 130–136, Nov. 2018.
- [24] W. P. Jones and B. E. Launder, “The prediction of laminarization with a two-equation model of turbulence,” *Int. J. Heat Mass Transf.*, vol. 15, no. 2, pp. 301–314, 1972.
- [25] S. A. Orszag, V. Yakhot, W. Flannery, F. Boysan, D. Choudhury, J. Maruzewski, and B. Patel, “Renormalization group modeling and turbulence simulations,” *Int. Conf. Near-Wall Turbul. Flows*, pp. 1031–1046, 1993.
- [26] D. C. Wilcox and others, *Turbulence modeling for CFD*, vol. 2. DCW industries La Canada, CA, 1998.
- [27] F. R. Menter, “Two-equation eddy-viscosity turbulence models for engineering applications,” *AIAA J.*, vol. 32, no. 8, pp. 1598–1605, 1994.
- [28] S. H. Kim, Y. I. Kim, Y. Y. Bae, and B. H. Cho, “Numerical simulation of the vertical upward flow of water in a heated tube at supercritical pressure,” *Proc. 2004 Int. Congr. Adv. Nucl. Power Plants, ICAPP’04*, pp. 1527–1534, 2004.
- [29] K. Yamagata, K. Nishikawa, S. Hasegawa, T. Fujii, and S. Yoshida, “Forced convective heat transfer to supercritical water flowing in tubes,” *Int. J. Heat Mass Transf.*, vol. 15, pp. 2575–2593, 1972.
- [30] P. Zhao, J. Liu, Z. Ge, X. Wang, and X. Cheng, “CFD analysis of transverse flow in a wire-wrapped hexagonal seven-pin bundle,” *Nucl. Eng. Des.*, vol. 317, pp. 146–157, Jun. 2017.

- [31] Y. Zhang, C. Zhang, and J. Jiang, “Numerical Simulation of Fluid Flow and Heat Transfer of Supercritical Fluids in Fuel Bundles,” *Journal of Nuclear Science and Technology*, vol. 48, no. 6, pp. 929–935, 2011.
- [32] H. Han and C. Zhang, “Numerical Simulation of Fluid Flow and Heat Transfer of the Supercritical Water in Different Fuel Rod Channels,” *Proceedings of The Canadian Society for Mechanical Engineering International Congress*, 2018.
- [33] X. Yang, G. H. Su, W. Tian, J. Wang, and S. Qiu, “Numerical study on flow and heat transfer characteristics in the rod bundle channels under super critical pressure condition,” *Annals of Nuclear Energy*, vol. 37, no. 12, pp. 1723–1734, 2010.
- [34] K. Podila and Y. Rao, “CFD modelling of supercritical water flow and heat transfer in a 2×2 fuel rod bundle,” *Nucl. Eng. Des.*, vol. 301, pp. 279–289, May 2016.
- [35] D. Dovizio, B. Mikuž, A. Shams, and F. Roelofs, “Validating RANS to predict the flow behavior in wire-wrapped fuel assemblies,” *Nucl. Eng. Des.*, vol. 356, p. 110376, Jan. 2020.
- [36] M. Yetisir, H. Hamilton, R. Xu, M. Gaudet, D. Rhodes, M. King, K. Andrew, B. Benson, “Fuel assembly concept of the canadian supercritical water-cooled reactor,” *Journal of Nuclear Engineering and Radiation Science*, vol. 4, no. 1, pp. 1–7, 2018.
- [37] Ansys. Inc, “14.0 ANSYS FLUENT Theory Guide,” 2011.
- [38] H. Han and C. Zhang, “A Modified Turbulent Model for the Supercritical Water Flows in the Vertical Upward Channels,” *J. Supercrit. Fluids*, vol. 187, p. 105632, Aug. 2022.
- [39] X. Kong, D. Sun, L. Gou, S. Wang, and N. Yang, “Numerical investigation on heat transfer of supercritical water with a variable turbulent Prandtl number model,” *Journal of Nuclear Engineering and Radiation Science*, vol. 6, no. 3, pp. 1–10, 2020.
- [40] S. Tavoularis, “Rod bundle vortex networks, gap vortex streets, and gap instability: A nomenclature and some comments on available methodologies,” *Nucl. Eng. Des.*, vol. 241, no. 7, pp. 2624–2626, Jul. 2011.

- [41] E. Merzari and H. Ninokata, "Anisotropic turbulence and coherent structures in eccentric annular channels," *Flow, Turbul. Combust.*, vol. 82, no. 1, pp. 93–120, 2009.

5. Numerical Investigations of the Effect of Operation Conditions on the Heat Transfer of the Supercritical Water in the Canadian SCWR Fuel Bundle

Nomenclature

Symbols

Bo^*	Dimensionless parameter, $Bo^* = Gr / (Re^{3.425} Pr^{0.8})$
c_p	Specific heat, J/kg·K
D	Diameter of the tube, mm
g	Gravitational acceleration, m/s ²
G	Mass flux, kg/m ² ·s
Gr	Grashof number
\dot{m}	Mass flow rate, kg/s
P	Pressure, Pa
Pr	Prandtl number
q	Heat flux, W/m ²
Re	Reynolds number
T	Temperature, °C
u	Velocity, m/s
x_i	Position vector
y^+	Nondimensional distance from the wall, $y^+ = \frac{u_\tau y}{\nu}$
z	Axial location, m

Greek letters

θ	Circumferential degree
μ	Dynamic viscosity, Pa·s
δ_{ij}	Kronecker delta tensor, $\delta_{ij} = 1$ if $i = j$, $\delta_{ij} = 0$ if $i \neq j$
λ	Thermal conductivity, W/m·K
ρ	Density of a fluid, kg/m ³

Subscripts

<i>b</i>	Bulk
<i>in</i>	Inlet
<i>pc</i>	Pseudocritical
<i>t</i>	Turbulent
<i>w</i>	Wall

Acronyms

DHT	Deteriorated Heat Transfer
NIST	National Institute of Standards and Technology
RSM	Reynold Stress Model
SCWR	Supercritical Water-Cooled Reactor
SIMPLEC	Semi-Implicit Pressure-Linked Equations-Consistent

5.1. Introduction

Supercritical water was first considered as the working fluid in the concept of the supercritical fossil-fueled power plants in the 1950s. Later in the 1960s-1970s, some early studies were conducted to find the possibility of the supercritical water used in nuclear reactors [1–5]. The thermophysical properties of the supercritical water undergo significant changes within around $\pm 25^\circ\text{C}$ in the vicinity of the pseudocritical temperature. Fig. 5.1 shows the variations of thermophysical properties of the supercritical water versus temperatures at different pressures [6]. The specific heat increases first and then decreases with the increase in the temperature. The temperature corresponding to the peak value of the specific heat is the pseudocritical temperature. The pseudocritical temperatures and corresponding peak values of the specific heat at different pressures are presented in Table 5.1. At a given temperature, the fluid with a higher specific heat absorbs more heat. It is found that the pseudocritical temperature increases with the pressure while the maximum value of the specific heat decreases with the increase of the pressure. Similar variations of density and thermal conductivity are observed. The density and thermal conductivity decrease with the increase of the temperature and the gradient of the reduction is relatively large near the pseudocritical temperature. The density decrease could increase the effects of the buoyancy force and the flow acceleration. In addition, the reduction of the thermal conductivity would also impair the heat transfer. Generally, the density and thermal conductivity increase with the pressure. However, there is a peak in the thermal conductivity near the pseudocritical temperature when the pressure, $P = 23 \text{ MPa}$, which is similar to the peak in the specific heat at the same pressure. But there are no peaks in the thermal conductivity at other pressures. The dynamic viscosity decreases with the increase in the temperature when the temperature is less than $400 - 410^\circ\text{C}$. Near the pseudocritical point, the dramatic decrease of the viscosity could lead to a significant increase in the velocity of the fluid and the Reynolds number. It is also shown that the dynamic viscosity slightly increases with the increase in the temperature before the pseudocritical points. When the temperature is higher than the pseudocritical temperatures, the viscosities at different pressures gradually increase and become almost the same after 500°C . All of the

variations of the thermophysical properties listed above results in different heat transfer characteristics of supercritical water at various operating conditions.

The supercritical water-cooled reactors (SCWRs) were proposed as one of the six Generation IV nuclear reactors since 2002 [7], which have regained researchers' interest in the heat transfer characteristics of the water at supercritical pressures. Many experimental and numerical studies have been devoted to the heat transfer of supercritical

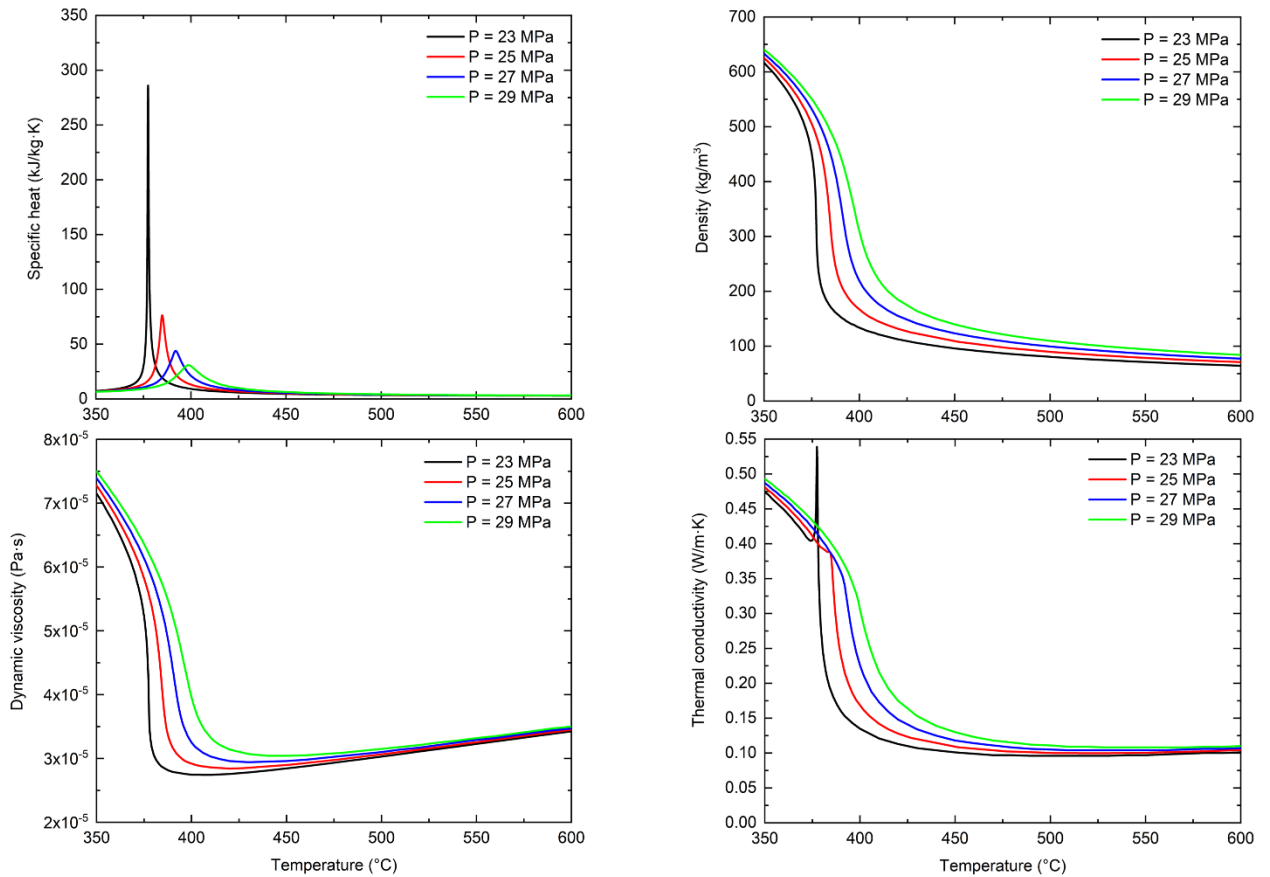


Figure 5.1: Thermophysical properties of water at supercritical pressures [6]

Table 5.1 Pseudocritical temperatures and corresponding peak values of the specific heat at different pressures [6]

Pressure (MPa)	Pseudocritical temperature (°C)	Peak value of specific heat (kJ/kg·K)
23	377.5	284.3
25	384.9	76.4
27	392.0	43.9
29	398.7	30.9

water in different flow channels, including horizontal and vertical tubes, and rod bundles. Three types of heat transfer regimes could occur: normal heat transfer, deteriorated heat transfer, and enhanced heat transfer [6], [8–11]. According to these studies, several operating parameters are found influencing the heat transfer of the supercritical water in channels, such as operating pressure, inlet temperature, heat flux and mass flux, heat to mass flux ratio. The heat transfer deterioration mostly exists at high heat fluxes or low mass fluxes conditions. In the existing studies of the supercritical water in the horizontal tubes [5], [12–14], the results generally showed that there are large differences between the top and bottom wall temperatures. This can be explained by the buoyancy effect due to the significant decrease of the density in the near wall region. In the present study, the investigations of heat transfer of the supercritical water in vertical channels will be carried out.

At a supercritical pressure, the dynamic viscosity and thermal conductivity are higher at higher operating pressures. The experiment results [15–17] indicated that the heat transfer coefficient generally increases with the decrease in the pressure when other operating parameters are kept constant. However, contrary results were also observed by Gang et al.

[18]. Their results showed that the heat transfer coefficient increased with the increase in the pressure when the mass flux, $G = 350 \text{ kg/m}^2\cdot\text{s}$ while decreased with the increase in the pressure when $G = 1000 \text{ kg/m}^2\cdot\text{s}$. This opposite trend was assumed due to the heat transfer deterioration occurring at $G = 350 \text{ kg/m}^2\cdot\text{s}$ when the operating pressure, $P = 23 \text{ MPa}$. Some researchers [18–20] claimed that the heat transfer coefficient would increase with the pressure when the heat to mass flux ratio is relatively high. In such condition, the heat transfer deterioration due to the buoyancy effect prevails over the heat transfer enhancement by the pressure changes. There are limited studies on the effects of the inlet temperature on the heat transfer of supercritical fluids in channels [21, 22]. The investigations on the heat transfer phenomenon of supercritical water in the rod bundles conducted by Podila et al. [21] indicated that the increase of the inlet temperature could effectively restrain the occurrence of the heat transfer deterioration.

The effects of heat flux on the heat transfer of the supercritical water in channels were investigated by several researchers [5], [12], [15], [18–19], [23–25]. In these studies, the influence of the heat flux on the heat transfer was investigated at different bulk fluid temperatures and the wall temperatures. When the heat flux rises, both the fluid temperature and wall temperature would go up accordingly. When the fluid temperature is near the pseudocritical temperature, the sharp increase of the specific heat and decrease of viscosity could enhance the heat transfer. On the other hand, when the wall temperature is higher than the pseudocritical temperature, the density, thermal conductivity, and specific heat of the fluid near the wall could be much lower, which in turn deteriorate the heat transfer between the wall and the fluid. With a relatively lower heat flux, the enhanced effect on the heat transfer contributed from the fluid temperature overwhelms the deteriorated effect on the heat transfer caused by the wall temperature when the fluid temperature is near the pseudocritical temperature and wall temperature is slightly high than the pseudocritical temperature. Conversely, at relatively high heat flux condition, the deteriorated effect on the heat transfer due to the wall temperature prevails over the enhanced effect on the heat transfer caused by the fluid temperature when the fluid temperature is near or slightly higher than the pseudocritical temperature and wall

temperature is appreciably higher than the pseudocritical temperature. In addition, the effects of buoyancy and flow acceleration due to the significant density drop are more obvious at a higher heat flux. This further makes the effects of heat flux on the heat transfer of the supercritical water in channels more complicated.

The effects of the mass flux on the heat transfer of the supercritical water in channels were investigated by several researchers [14], [25–28], [30], [31–33]. Generally, under a relatively high mass flux condition, the heat transfer is improved with the increase in the mass flux. However, under a low mass flux condition, the heat transfer is found impaired with the increase in the mass flux. In the investigations on the heat transfer of the supercritical water in an inclined upward tube by Yin et al. [34], they found that the wall temperature at the top of the cross section decreased with the increase in the mass flux. However, the wall temperature at the bottom of the cross section increased with the increase in the mass flux ($G = 600 - 900 \text{ kg/m}^2 \cdot \text{s}$) at first and then decreased with further increase in the mass flux ($G = 1200 \text{ kg/m}^2 \cdot \text{s}$). Therefore, the effect of the mass flux on the heat transfer of the supercritical water in channels is different for high and low heat flux. Many efforts were made to use the heat to mass flux ratio (q/G) to determine the criterion for the prediction of the onset of the heat transfer deterioration [24], [29], [31], [35, 36]. Some researchers proposed the occurrence of the heat transfer deterioration when the heat flux to the mass flux ratio, $q/G > 0.6 - 0.9 \text{ kJ/kg}$ within the range of $G = 310 - 1830 \text{ kg/m}^2 \cdot \text{s}$ and $P = 22.5 - 29.4 \text{ MPa}$ and others proposed $q/G > 0.81 - 1.21 \text{ kJ/kg}$ at $P = 22.5 - 29.4 \text{ MPa}$ for the onset of the heat transfer deterioration. There are obvious differences in the proposed heat to mass flux ratio for the heat transfer deterioration in the literature. Therefore, a simple heat to mass flux ratio might not be able to exactly represent the onset of the heat transfer deterioration since the complicated heat transfer of the supercritical water in channels under different operating conditions.

Existing studies on the effects of different operating parameters on the heat transfer of the supercritical water in channels mainly focus on the tube flows. One study was for a 2×2

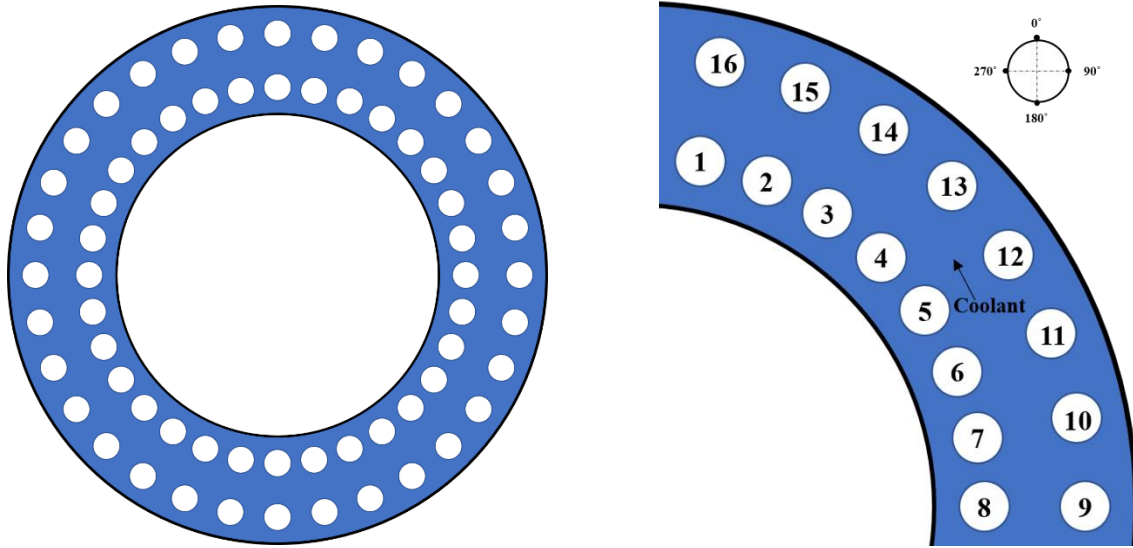
rod bundle [27]. Because of the difference of the geometry in heated surface, the results from existing studies on the heat transfer of the supercritical water in simple channels cannot be regarded directly applicable in the fuel bundle in engineering applications. In this study, the investigations of the effects of various operating parameters, including the operating pressure, inlet temperature, heat flux, and mass flux on the heat transfer of the supercritical water in the 64-element fuel bundle in the Canadian SCWR were conducted. In addition, the buoyancy effect on the heat transfer at under different operating conditions was also evaluated.

5.2.Numerical model

5.2.1. Physical model and boundary conditions

To investigate the heat transfer characteristics of the supercritical water in the fuel bundle, numerical simulations are conducted in the present study. The cross-section views of the physical model of the fuel bundle and the computational domain used in the simulation are shown in Fig. 5.2. The rod bundle design used in this work consists of 64 fuel rods, which are arranged in a two-ring configuration with 32 elements circumferentially distributed in each ring [37] as shown in Fig. 5.2 (a). The diameters of the inner and outer fuel rods are 9.5 mm and 10 mm, respectively. The supercritical water flows vertical upward in the channel. The length of the channel is 5 m. Due to the symmetry of the fuel bundle, the computational domain is reduced to a quarter of the fuel bundle to reduce the computational time, which is presented in Fig. 5.2(b).

The boundary conditions of the simulations are summarized here. The inlet mass flow rate and the inlet temperatures are specified as inlet boundary conditions. The outflow are used for the outlet boundary condition. At the wall, no slip and the uniform heat fluxes are specified.



(a) Physical model of the fuel bundle

(b) Computational domain

Figure 5.2: Cross- section view of the fuel bundle

5.2.2. Governing equations and turbulent models

The convective heat transfer of the supercritical water in the fuel bundle is considered as a steady state in this study. The governing equations for the three-dimensional steady state flow and heat transfer are conservations of mass, momentum and energy. They are presented as follows in the Reynolds averaged form [38]:

$$\frac{\partial \rho \bar{u}_i}{\partial x_i} = 0 \quad (5.1)$$

$$\frac{\partial (\rho \bar{u}_i \bar{u}_j)}{\partial x_j} = -\frac{\partial \bar{p}}{\partial x_i} + \frac{\partial}{\partial x_j} \left(\mu \frac{\partial \bar{u}_i}{\partial x_j} - \rho \overline{u'_i u'_j} \right) + \rho g_i \quad (5.2)$$

$$\frac{\partial}{\partial x_i} \left(\bar{u}_i \rho c_p T \right) = \frac{\partial}{\partial x_i} \left[\left(\lambda + \frac{c_p \mu_t}{Pr_t} \right) \frac{\partial T}{\partial x_i} \right] \quad (5.3)$$

The Reynolds stress model (RSM) with the variable turbulent Prandtl number (Pr_t) proposed in the previous study [39] is used in the present work to simulate the heat transfer of the supercritical water.

The transport equations for the RSM can be described as [38]:

$$\begin{aligned}
 \underbrace{\frac{\partial}{\partial x_k} (\rho u_k \overline{u'_i u'_j})}_{C_{ij} \equiv \text{Convection}} = & \underbrace{-\frac{\partial}{\partial x_k} \left[\rho \overline{u'_i u'_j u'_k} + p' (\delta_{kj} u'_i + \delta_{ik} u'_j) \right]}_{D_{T,ij} \equiv \text{Turbulent Diffusion}} + \\
 & \underbrace{\frac{\partial}{\partial x_k} \left[\mu \frac{\partial}{\partial x_k} (\overline{u'_i u'_j}) \right]}_{D_{L,ij} \equiv \text{Molecular Diffusion}} - \underbrace{\rho \left(\overline{u'_i u'_k} \frac{\partial u_j}{\partial x_k} + \overline{u'_j u'_k} \frac{\partial u_i}{\partial x_k} \right)}_{P_{ij} \equiv \text{Stress Production}} - \underbrace{\rho \beta (g_i \overline{u'_j \theta} + g_j \overline{u'_i \theta})}_{G_{ij} \equiv \text{Buoyancy Production}} + \\
 & \underbrace{p' \left(\frac{\partial u'_i}{\partial x_j} + \frac{\partial u'_j}{\partial x_i} \right)}_{\phi_{ij} \equiv \text{Pressure Strain}} - \\
 & \underbrace{2\mu \frac{\partial u'_i}{\partial x_k} \frac{\partial u'_j}{\partial x_k}}_{\varepsilon_{ij} = \text{Dissipation}} - \underbrace{2\rho \Omega_k (\overline{u'_j u'_m} \varepsilon_{ikm} + \overline{u'_i u'_m} \varepsilon_{jkm})}_{F_{ij} \equiv \text{Production by System Rotation}} + \\
 & \underbrace{S_{user}}_{\text{User-Defined Source Term}}
 \end{aligned} \tag{5.4}$$

And Pr_t is treated as a variable and calculated as:

$$Pr_t = \begin{cases} 0.4 & \mu_t/\mu < 0.2 \\ 0.3 + 0.03 \times \frac{P}{P_{cr}} \times P_r \times (q/G) \times (\mu_t/\mu) & 0.2 \leq \mu_t/\mu \leq 10 \\ 0.85 & \mu_t/\mu > 10 \end{cases} \tag{5.5}$$

The enhanced wall treatment is used to model the near wall region and the mesh near the wall is refined to allow y^+ around 1, as shown in Fig. 5.3. All the simulations use the mesh with 13,463,031 cells, which gives grid independent results based on previous work [40]. The finite volume method is used to solve the governing equations. The Fluent software from ANSYS is used for the simulations. The thermophysical properties of the supercritical water from the NIST standard database 9.1 [41] were implemented into the Fluent solver by using a piecewise-linear function of the temperature. The SIMPLEC scheme is used for the pressure-velocity coupling and the QUICK method is used for the discretization of the convection terms. The convergence criteria of the residuals are set to 10^{-6} to ensure sufficient accuracy. Table 5.2 illustrates the operating parameters of all cases for the 64-element Canadian SCWR fuel bundle in this work. The heat flux is assumed uniform for the fuel rods.

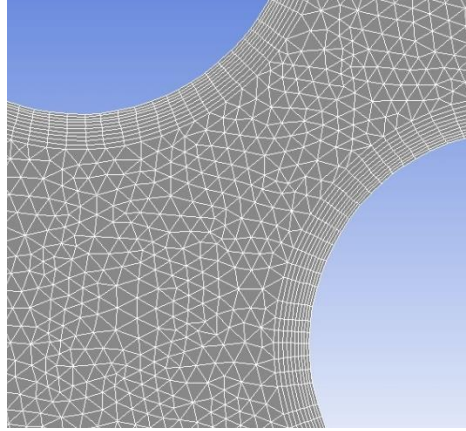
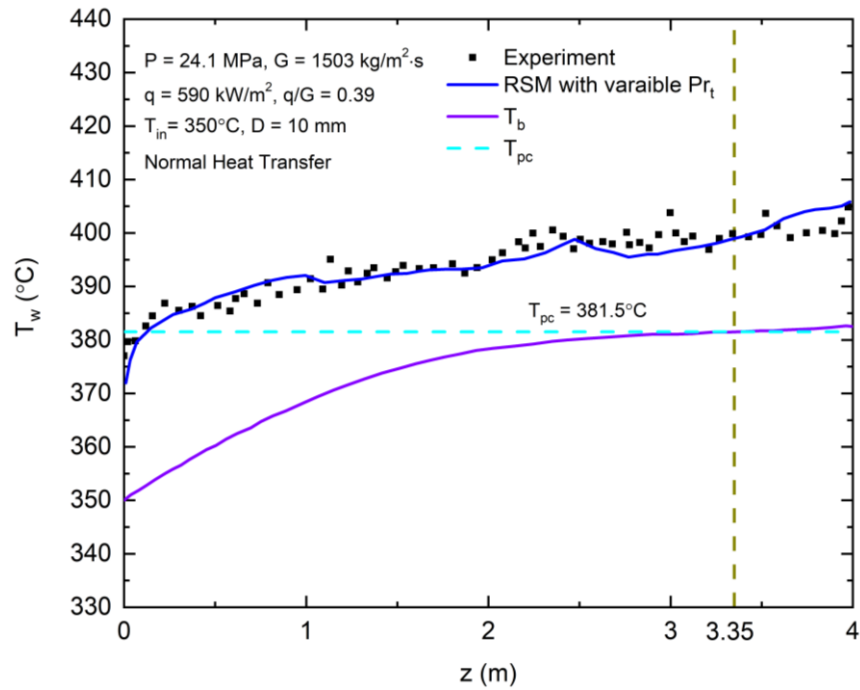
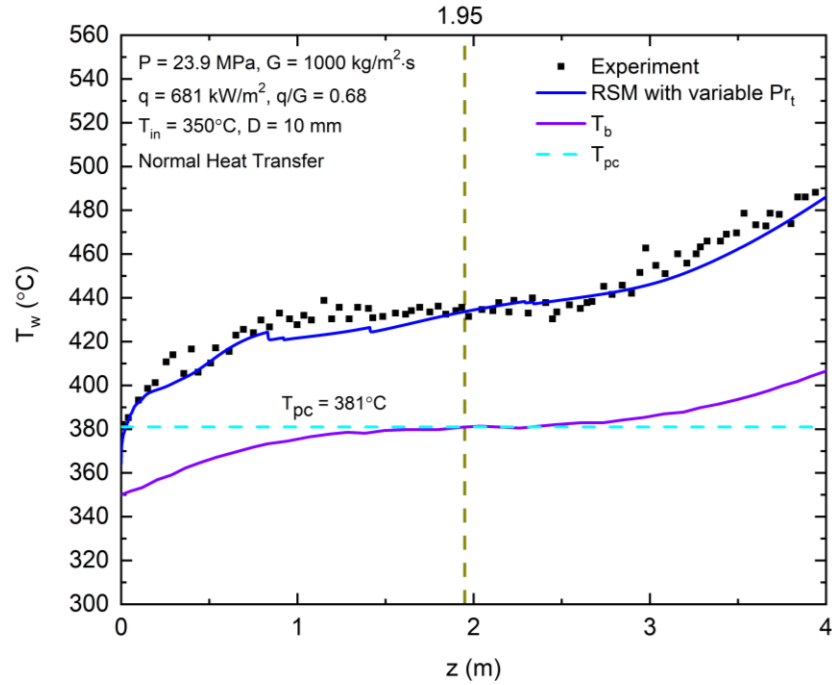


Figure 5.3: Near wall mesh

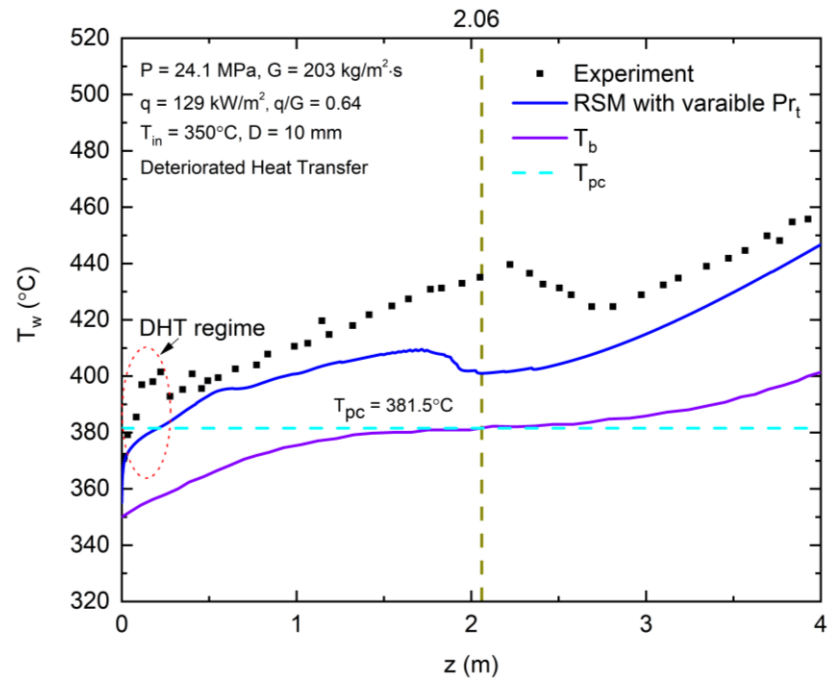
The comparison of the wall temperatures between the simulation results and experimental data by the RSM with the variable Pr_t turbulence model for the upward supercritical water flows in a bare tube (Cases # a - c) is shown in Fig. 5.4 and in a rod bundle (Cases # d - e) is shown in Fig. 5.5 [39]. The comparisons show that this turbulence model can give reasonable simulation results. Therefore, it is used in this study.



(a)

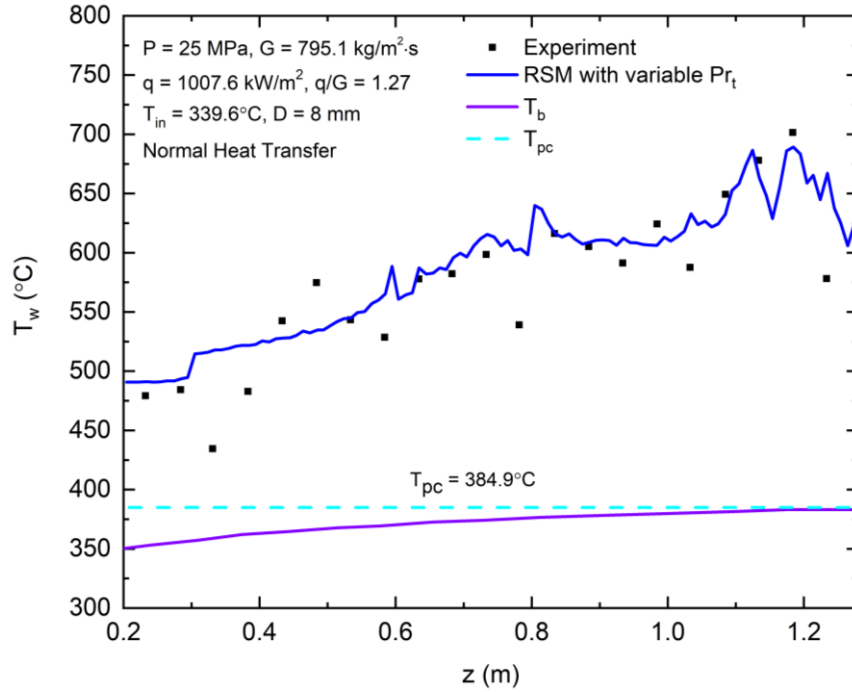


(b)

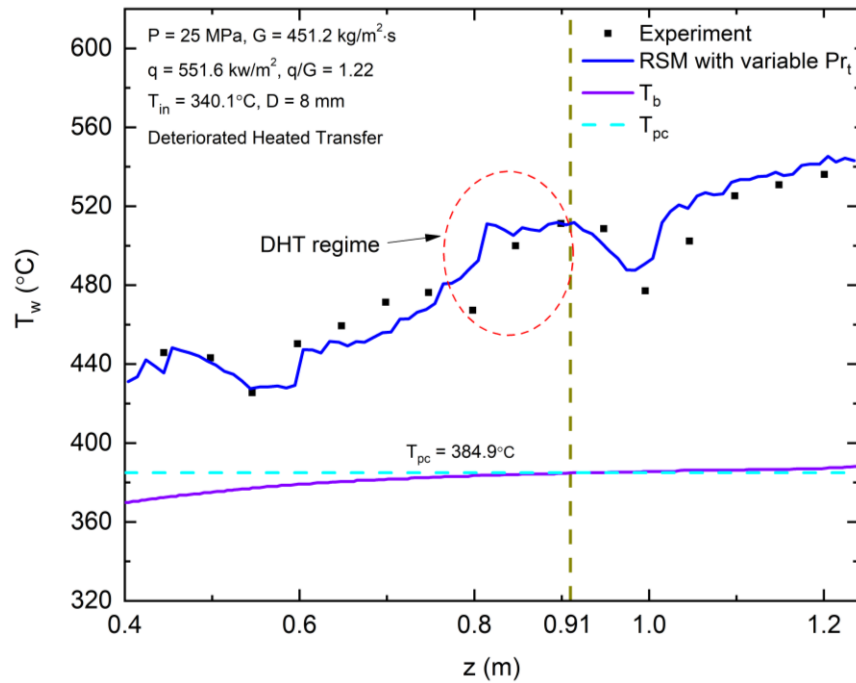


(c)

Figure 5.4: Comparison between the simulation results and experimental data for the supercritical water flow in a bare tube



(d)



(e)

Figure 5.5: Comparison between the simulation results and experimental data for the supercritical water flow in a rod bundle

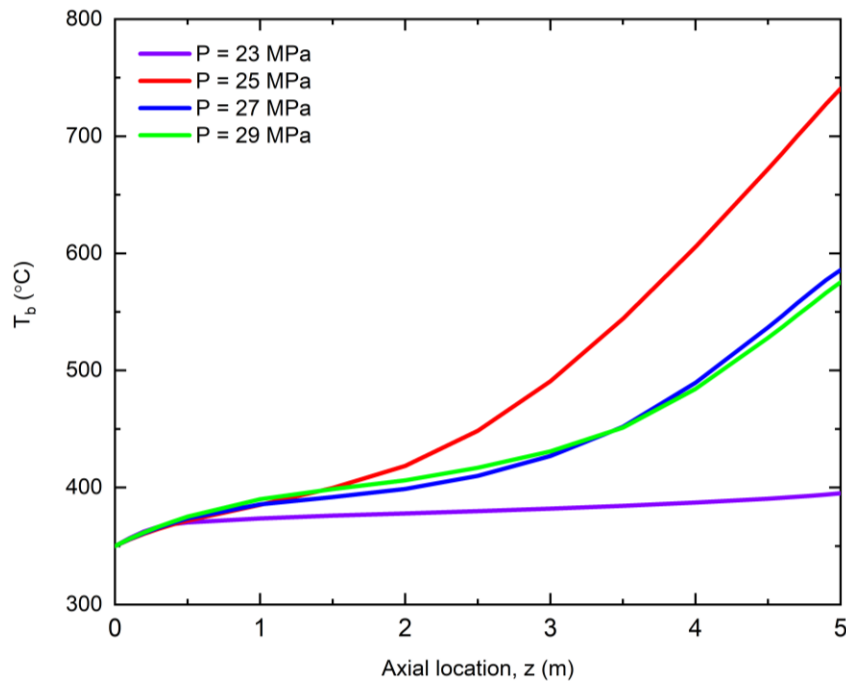
Table 5.2 Operating parameters for different cases

Case #	Pressure (MPa)	Inlet temperature (°C)	Heat flux (kW/m ²)	Mass flow rate (kg/s)	Heat to mass flux ratio
1	25	350	879.93	3.93	1.02
2	23	350	879.93	3.93	
3	27	350	879.93	3.93	
4	29	350	879.93	3.93	
5	25	340	879.93	3.93	
6	25	360	879.93	3.93	
7	25	370	879.93	3.93	
8	25	350	600	3.93	0.70
9	25	350	700	3.93	0.81
10	25	350	800	3.93	0.93
11	25	350	879.93	6	0.67
12	25	350	879.93	8	0.50
13	25	350	879.93	12	0.33
14	25	350	879.93	15.7	0.26
15	25	350	879.93	20	0.20

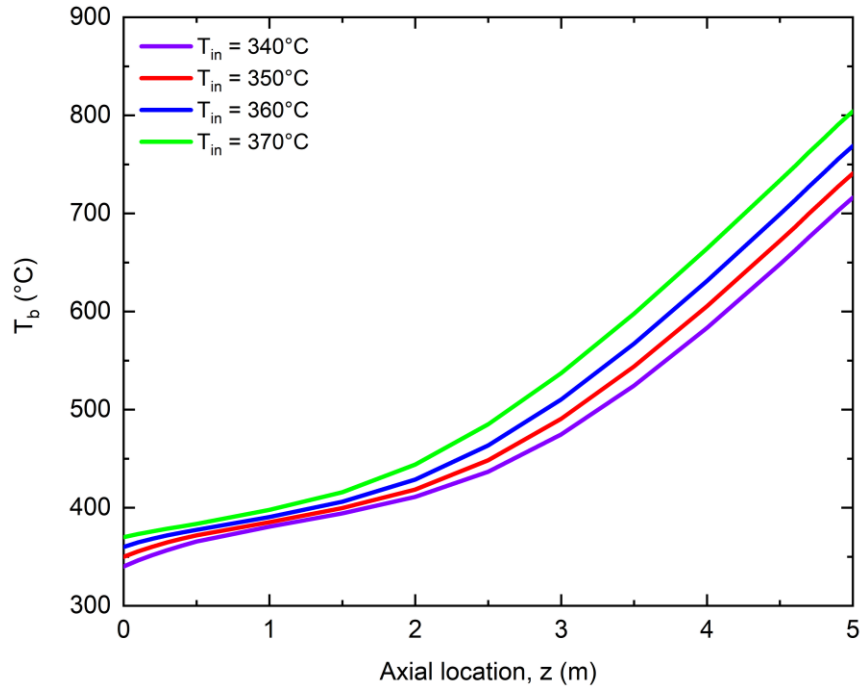
5.3. Results and discussions

5.3.1. Bulk fluid temperature distributions under different operating conditions

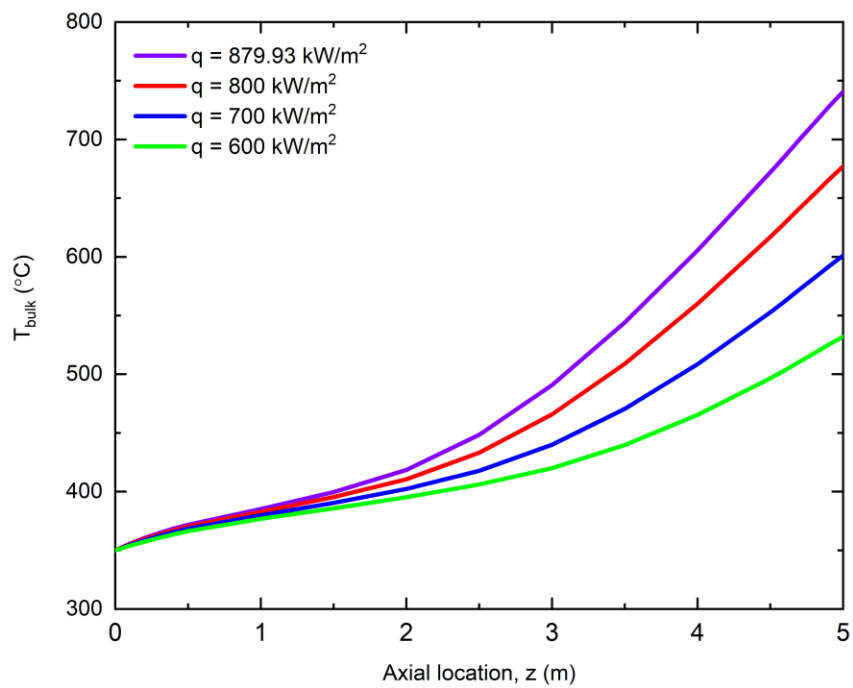
Fig. 5.6 shows the bulk fluid temperature along the axial flow direction in the fuel bundle at different operating conditions. The axial bulk fluid temperature generally increases with the increase of the inlet temperature and the heat flux, while decreases with the increase of the inlet mass flow rate. When it comes to the axial fluid temperature distribution at different operating pressures, the temperature decreases when the operating pressure increases from 25 MPa to 29 MPa, while there is little difference in the fluid temperatures at 27 MPa and 29 MPa as shown in Fig. 5.6(a). At the condition of 23 MPa, the variation of the fluid temperature along the axial location is much less than those at other supercritical pressure conditions. This might be due to the fact that the specific heat at $P = 23$ MPa is more than four times higher than those at other supercritical pressure conditions when the fluid temperature is between 375°C and 380°C as shown in Fig. 5.1.



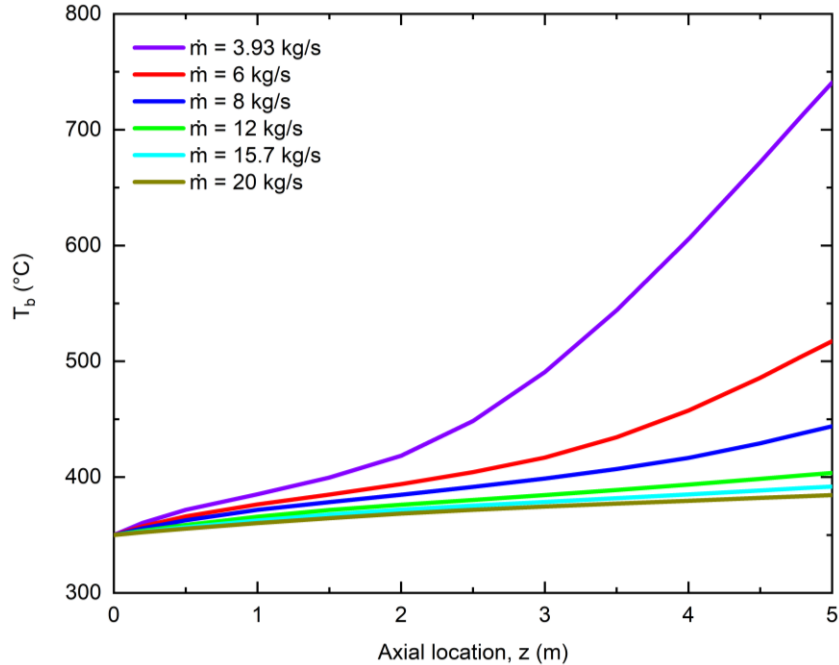
(a) Different operation pressures (Cases#1-4)



(b) Different inlet temperatures (Cases#1, 5-7)



(c) Different heat fluxes (Cases#1, 8-10)



(d) Different mass flow rates (Cases#1, 11-15)

Figure 5.6: Comparisons of the bulk temperature distributions along the axial direction at different operating conditions

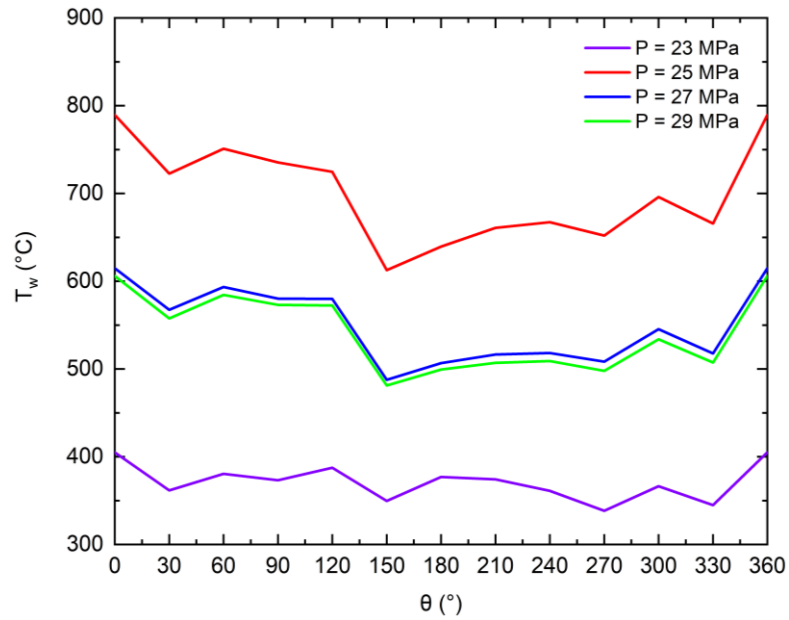
5.3.2. Effects of operation conditions on the heat transfer

To investigate the details of the heat transfer in the fuel bundle, rods #1, #4, #7, and #8 are chosen. The circumferential wall temperatures at the axial location, $z = 4.8$ m and the axial wall temperature distributions are presented to investigate the heat transfer in the fuel bundle.

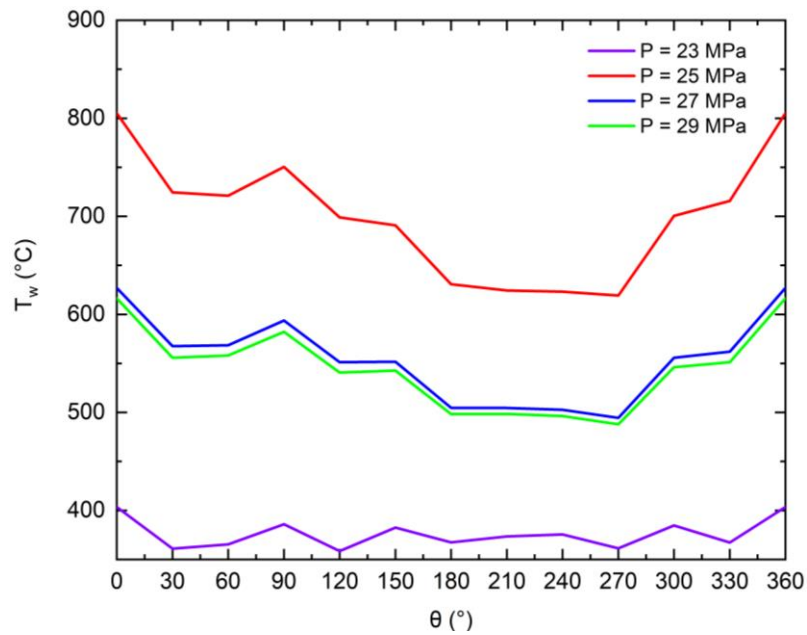
5.3.2.1. Effect of the operating pressure

Figs. 5.7 and 5.8 show the effect of the operating pressure on the cladding surface temperature distributions in the circumferential and axial directions, respectively. It can be seen that the wall temperature increases drastically from 370°C to 740°C at $z = 4.8$ m, when the operating pressure increases from 23 MPa to 25 MPa. However, when the pressure increases from 25 MPa to 27 MPa, the wall temperature decreases from 740°C to 575°C at $z = 4.8$ m. When the pressure increases further from 27 MPa to 29 MPa, the distributions

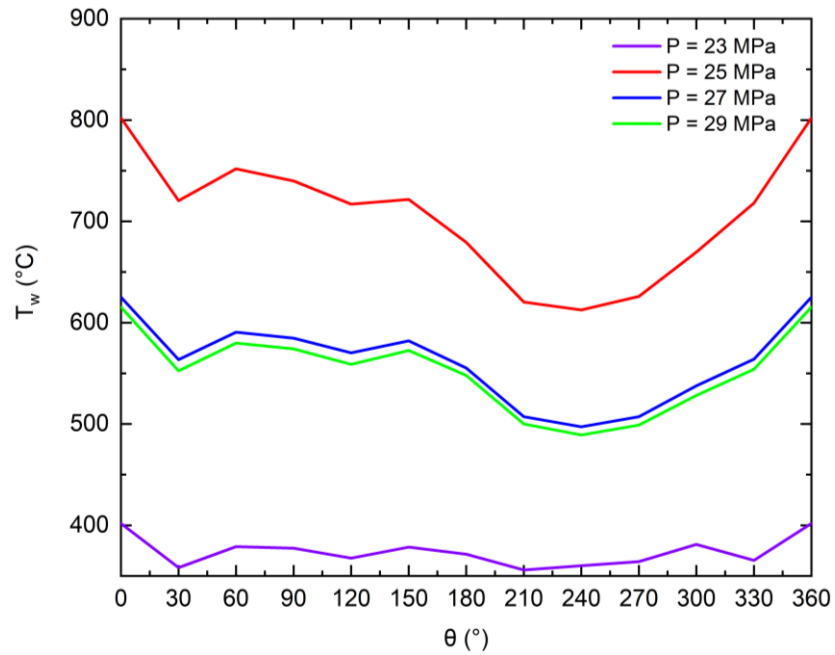
of wall temperature in both circumferential and axial directions are almost the same, which might be due to the fact that the thermophysical properties of the supercritical water do not change much when the pressure is far away from the critical point.



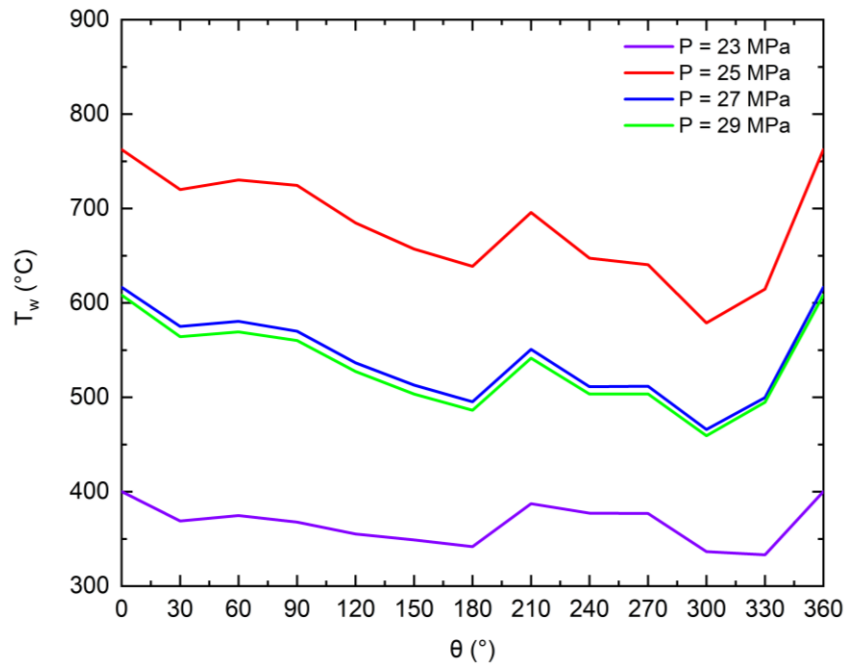
(a) rod 1



(b) rod 4

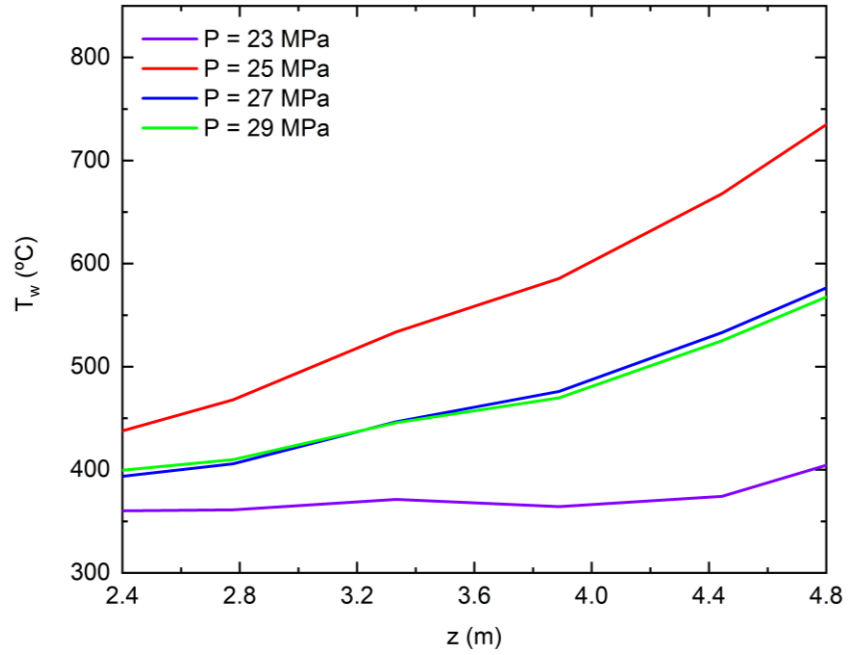


(c) rod 7

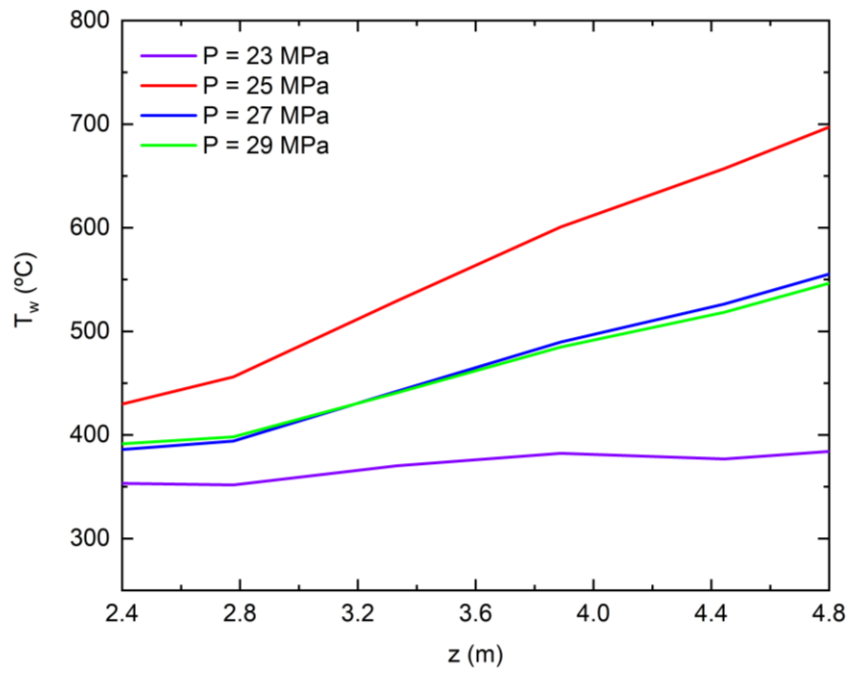


(d) rod 8

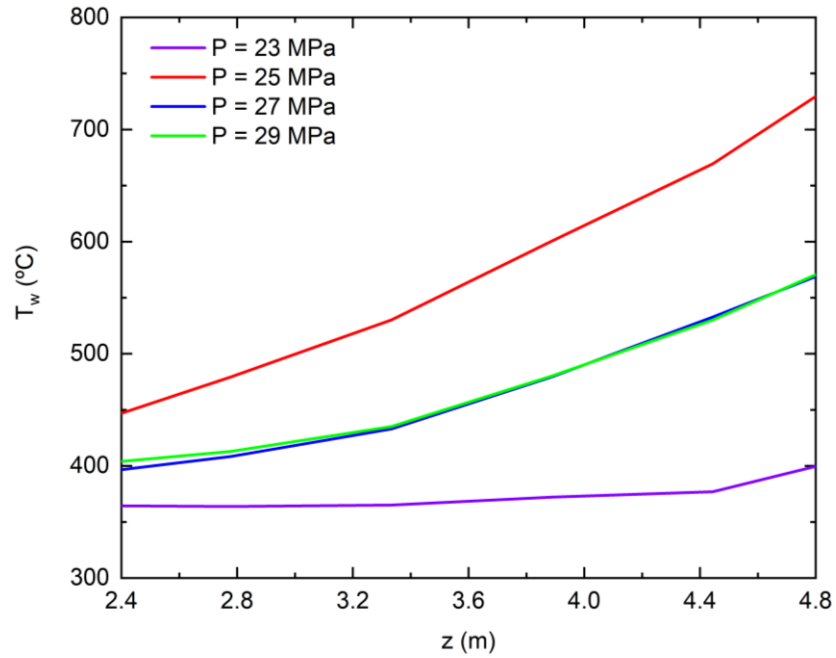
Figure 5.7: Circumferential wall temperature distributions at $z = 4.8$ m under different operating pressures



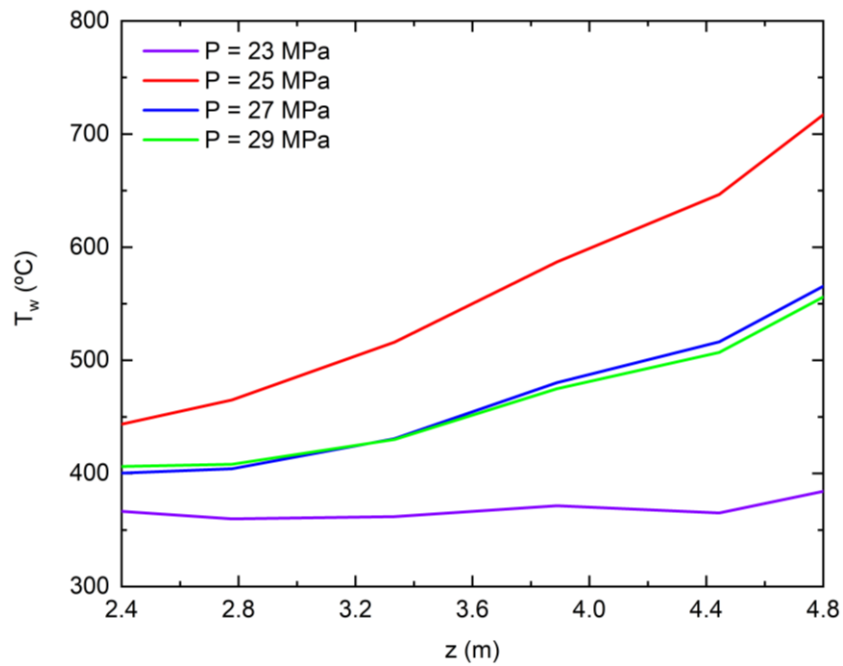
(a) rod 1



(b) rod 4



(c) rod 7

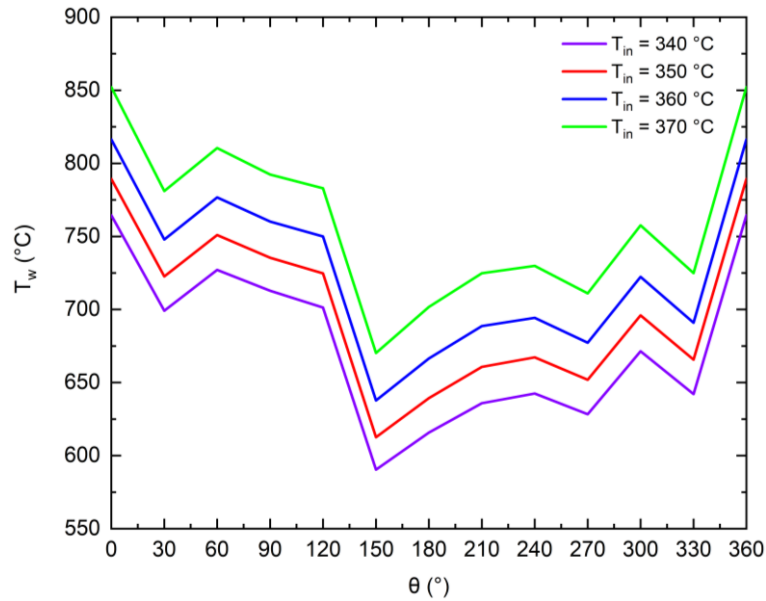


(d) rod 8

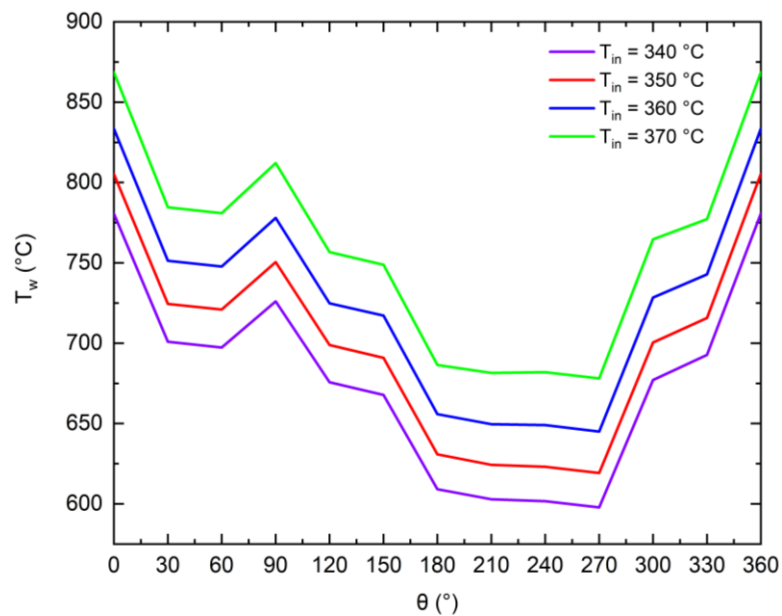
Figure 5.8: Wall temperature distributions along the axial direction under different operating pressures

5.3.2.2. Effect of the inlet temperature

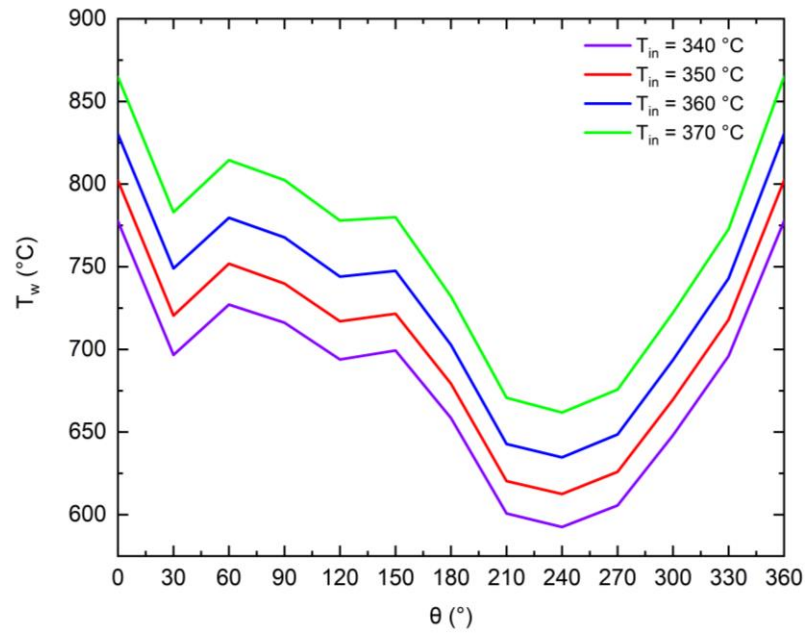
The circumferential cladding surface temperature distributions at $z = 4.8$ m at different inlet temperatures are plotted in Fig. 5.9. The circumferential wall temperatures generally increase with the increase of the inlet temperature as shown in Fig. 5.9, as well as the axial wall temperatures, as shown in Fig. 5.10.



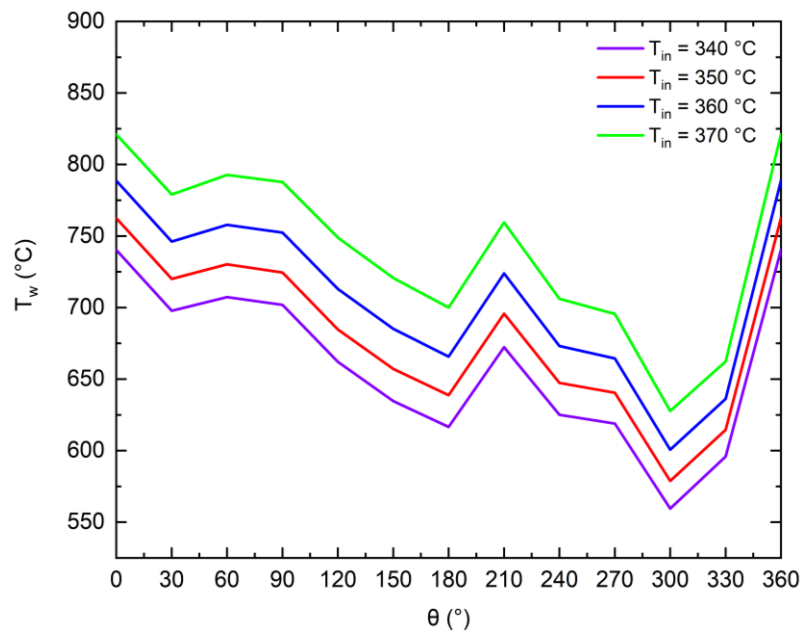
(a) rod 1



(b) rod 4

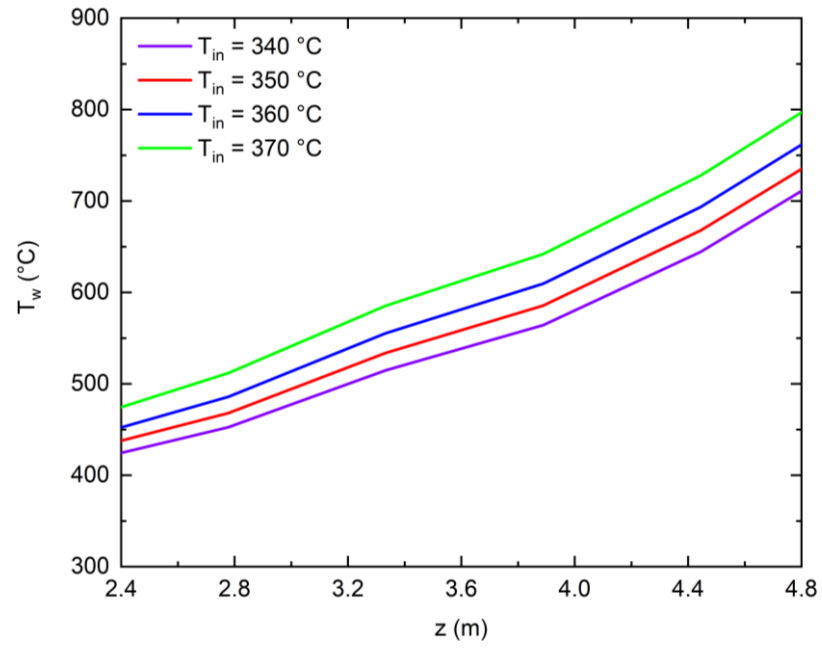


(c) rod 7

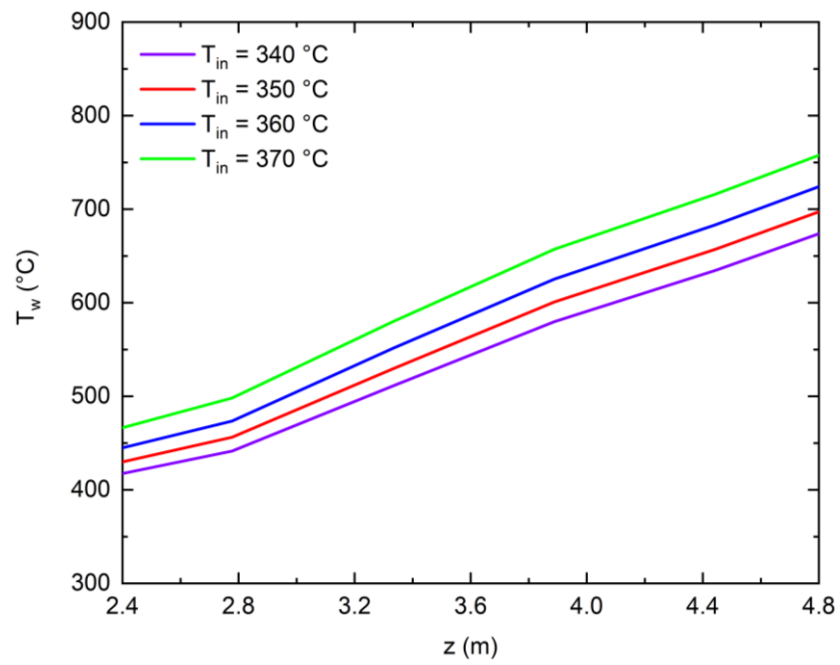


(d) rod 8

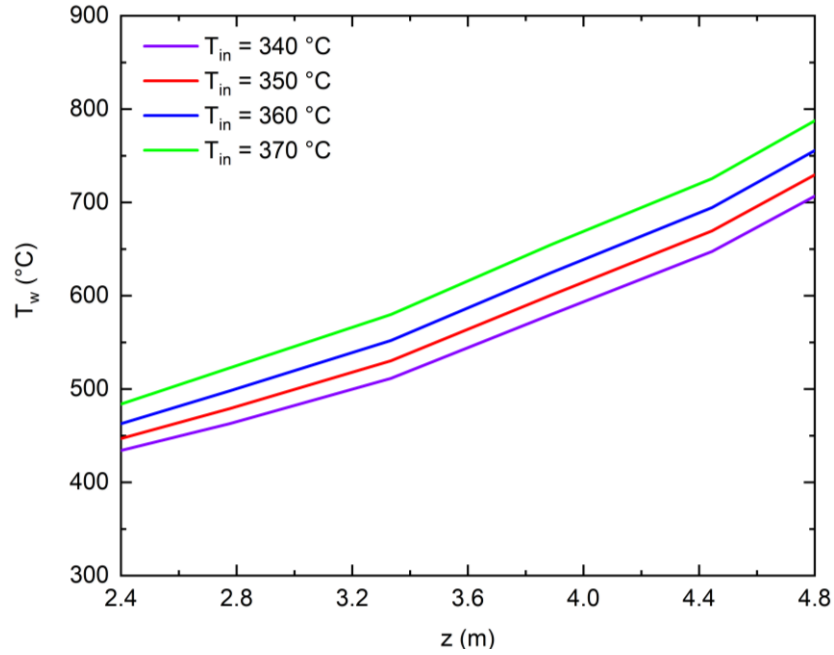
Figure 5.9: Circumferential wall temperature distributions at $z = 4.8$ m under different inlet temperatures



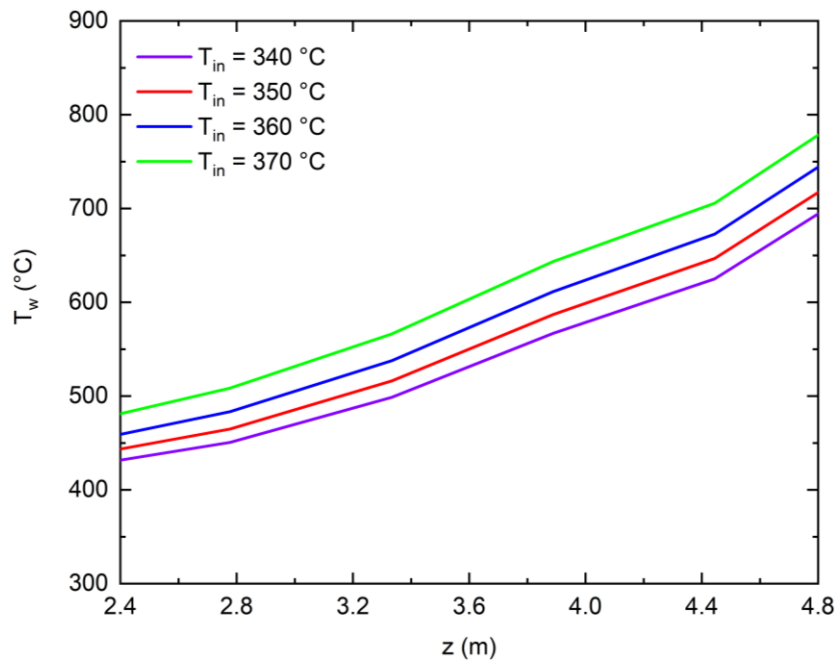
(a) rod 1



(b) rod 4



(c) rod 7

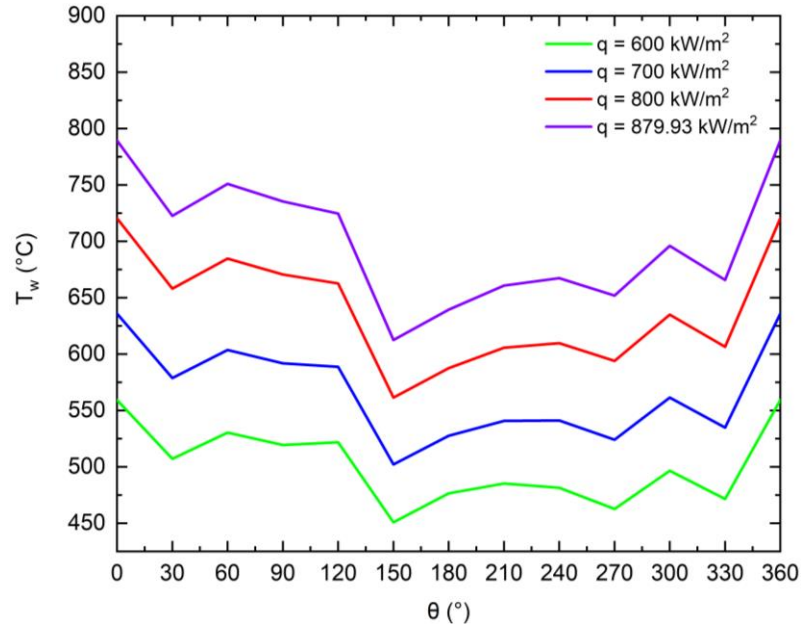


(d) rod 8

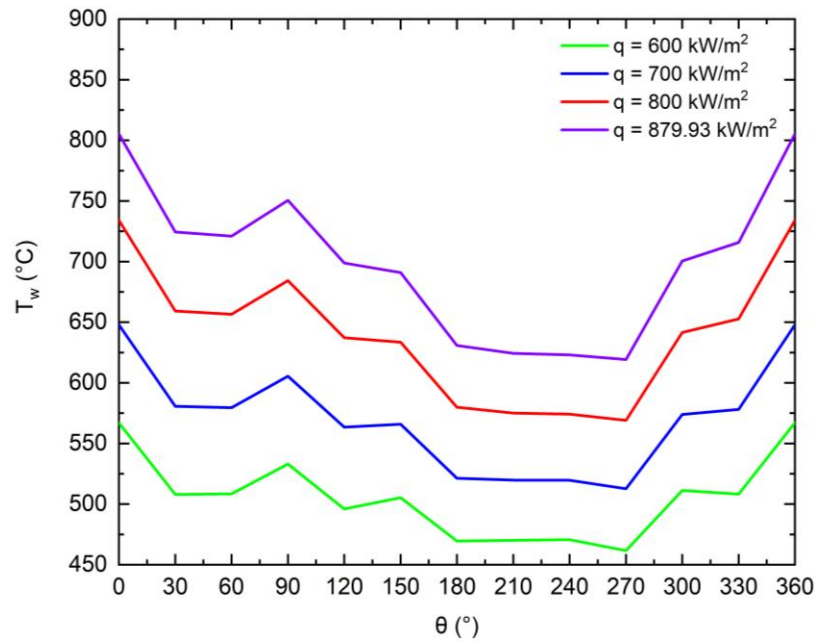
Figure 5.10: Wall temperature distributions along the axial direction under different inlet temperatures

5.3.2.3. Effect of the heat flux

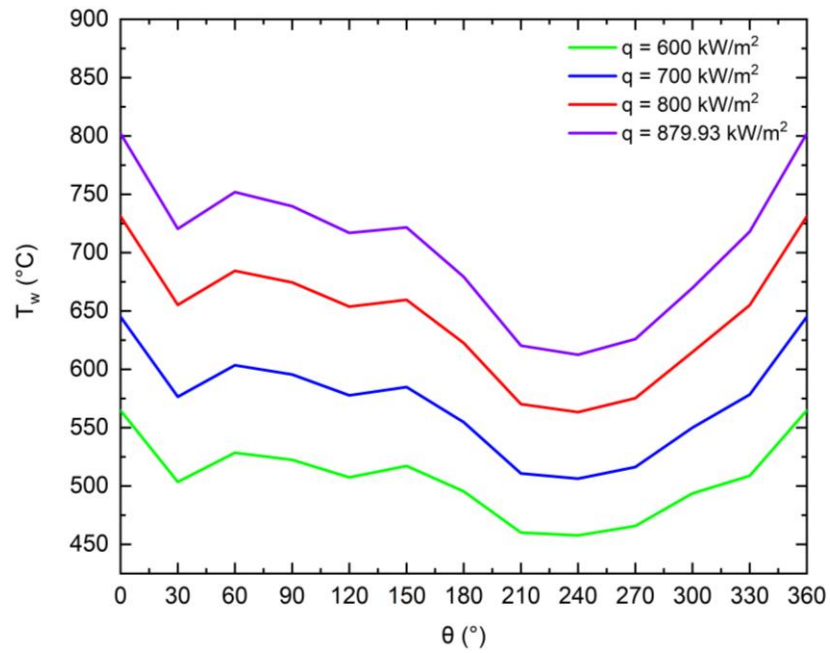
Variations of circumferential wall temperatures and axial wall temperatures at different heat fluxes are presented in Fig. 5.11 and Fig. 5.12, respectively. The wall temperatures increase with the increase of the heat flux.



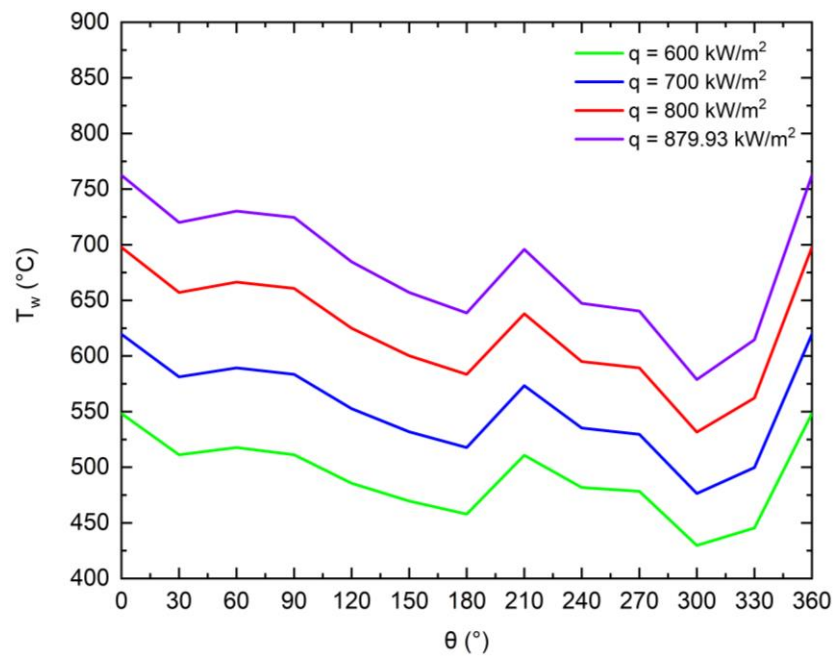
(a) rod 1



(b) rod 4

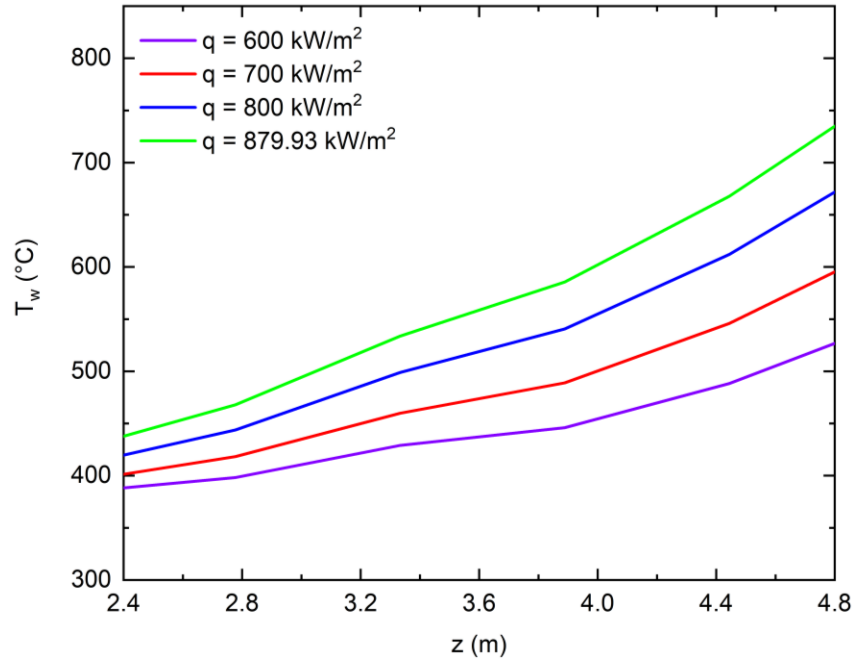


(c) rod 7

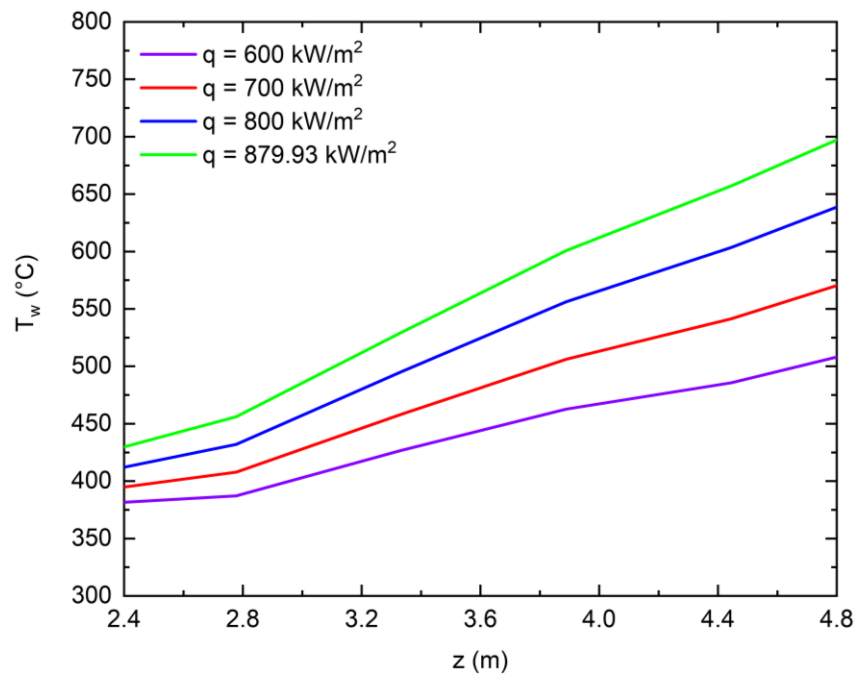


(d) rod 8

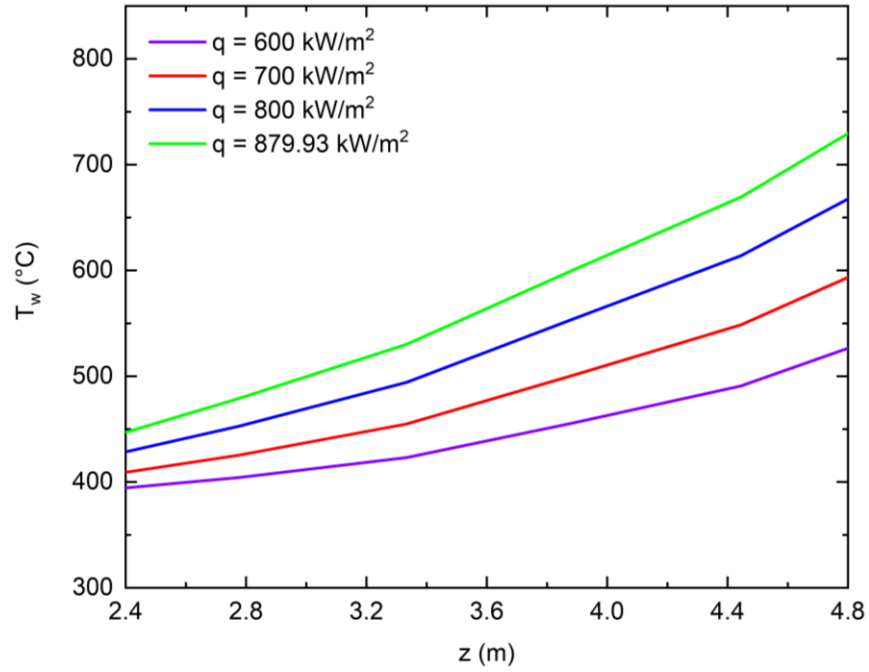
Figure 5.11: Circumferential wall temperature distributions under different heat fluxes



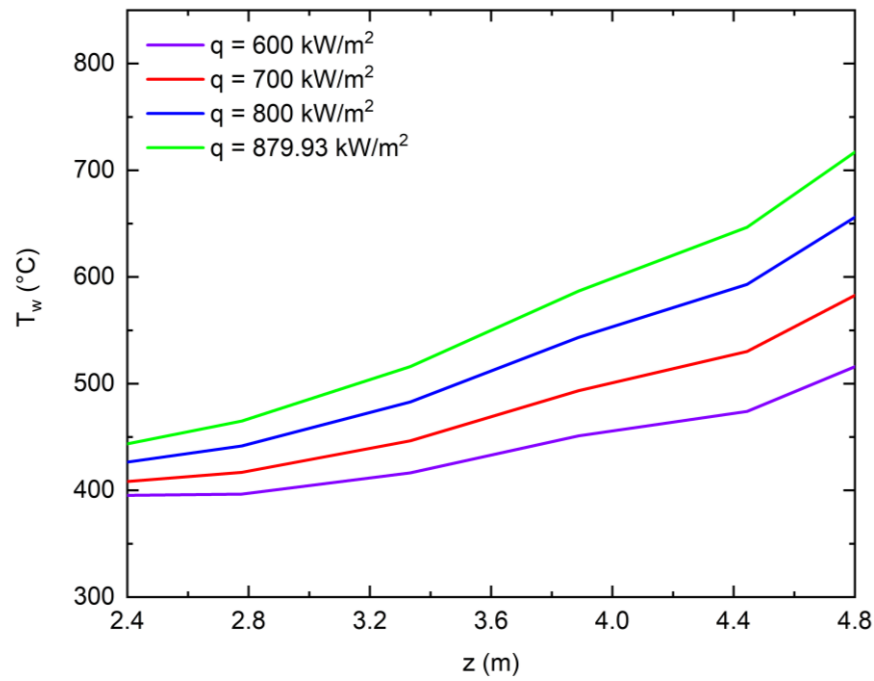
(a) rod 1



(b) rod 4



(c) rod 7

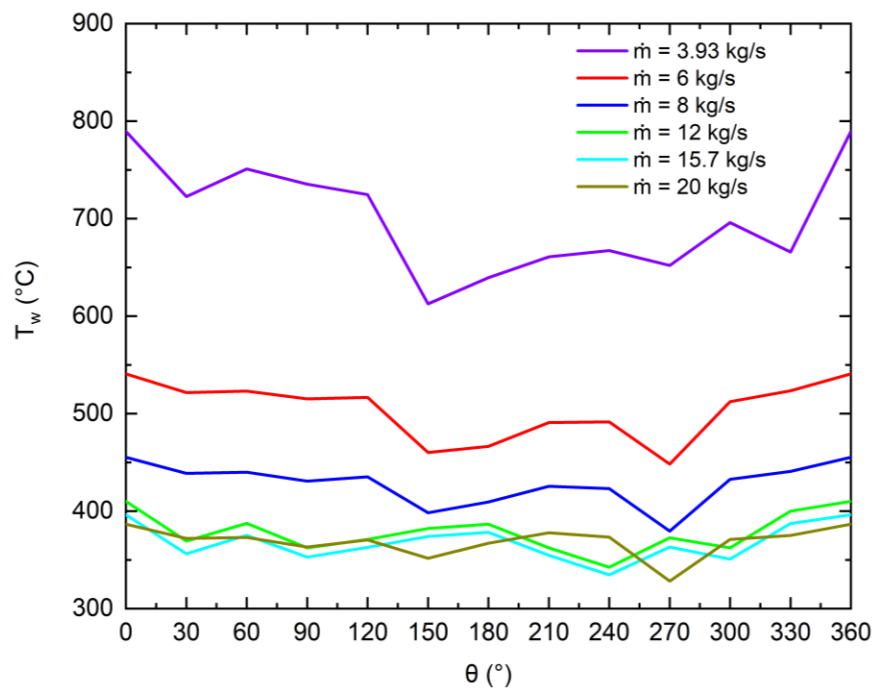


(d) rod 8

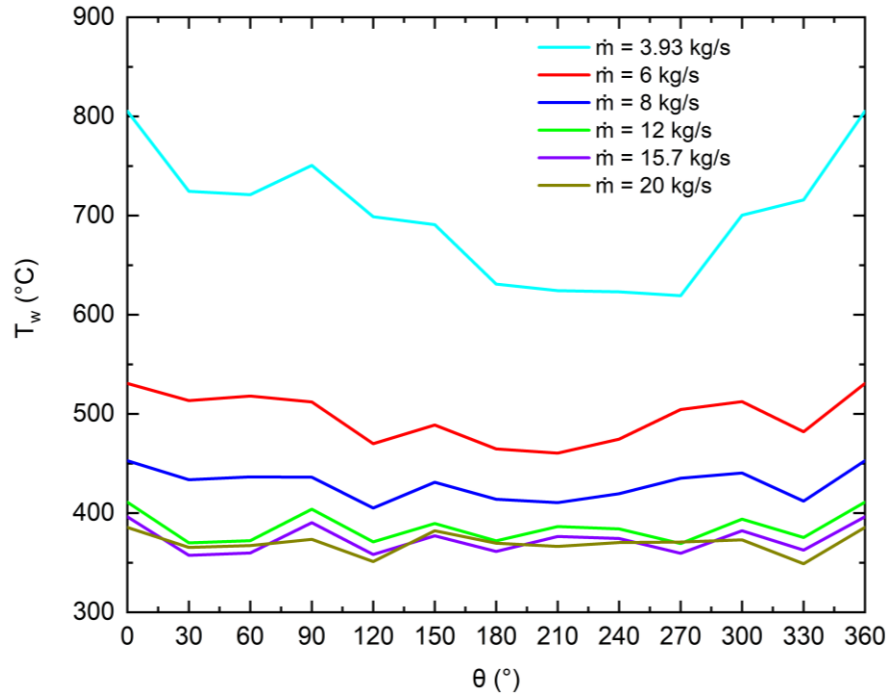
Figure 5.12: Wall temperature distributions along the axial direction under different heat fluxes

5.3.2.4. Effect of the mass flow rate

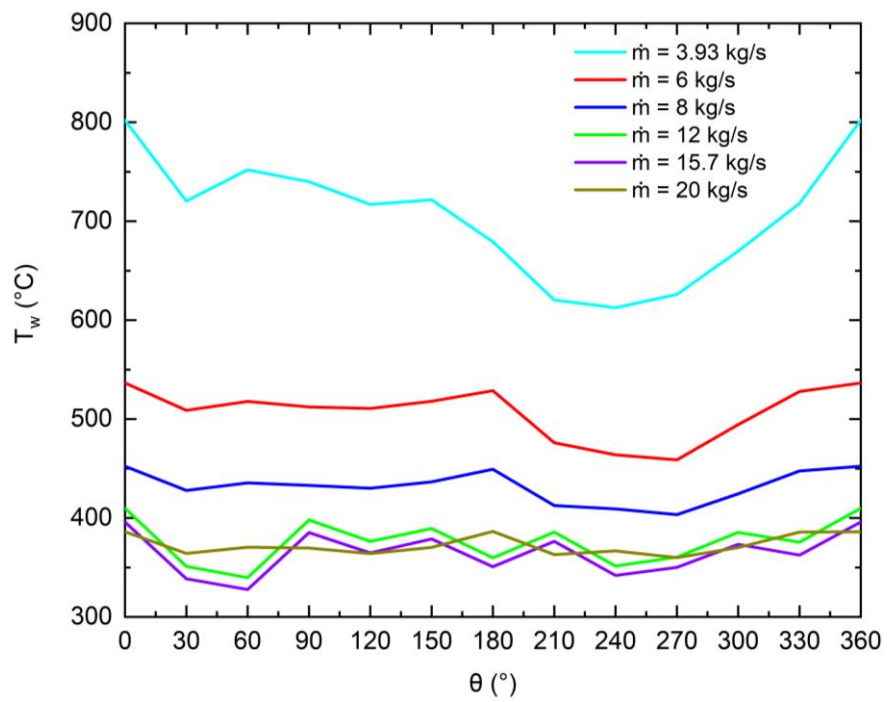
Fig. 5.13 shows the circumferential wall temperature distributions at different mass flow rates. The wall temperature decreases with the increase in the mass flow rate up to 12 kg/s. When the mass flow rate is higher than 12 kg/s, the changes of wall temperatures are much smaller compared with those when the mass flow rate is less than 12 kg/s. Similar trends of variations of wall temperatures are also observed in the axial direction, as presented in Fig. 5.14.



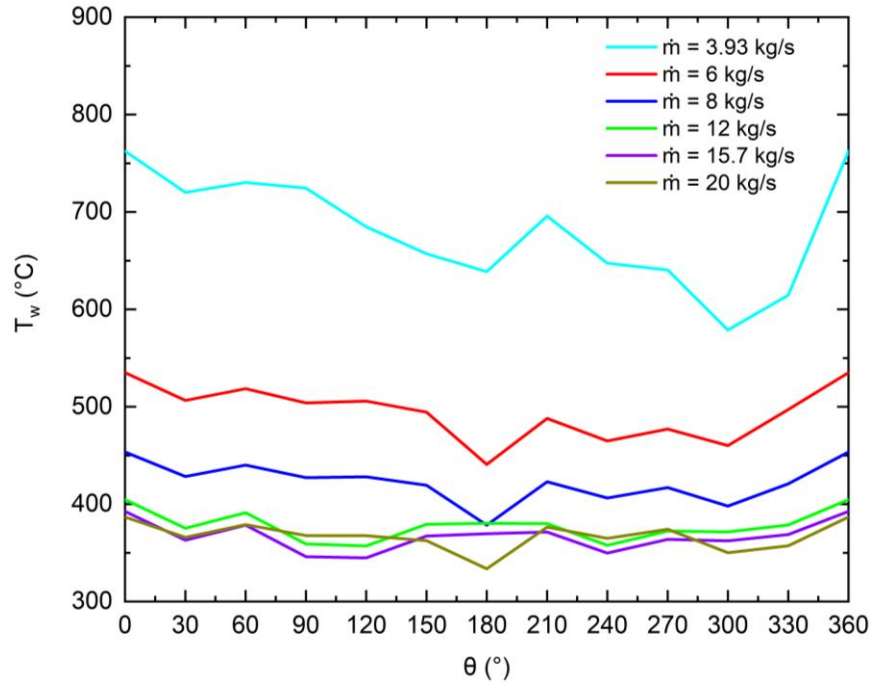
(a) rod 1



(b) rod 4

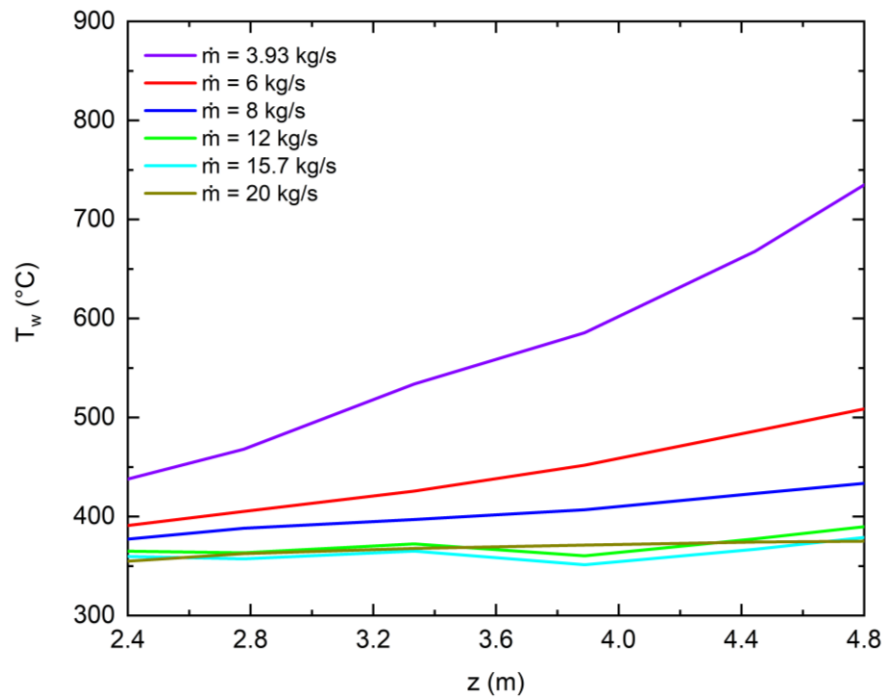


(c) rod 7

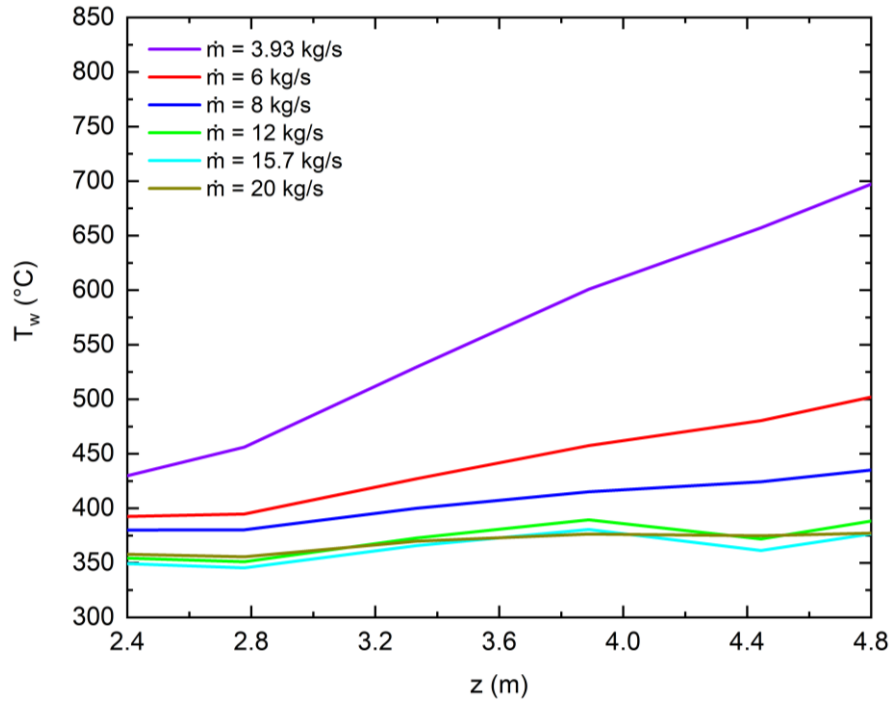


(d) rod 8

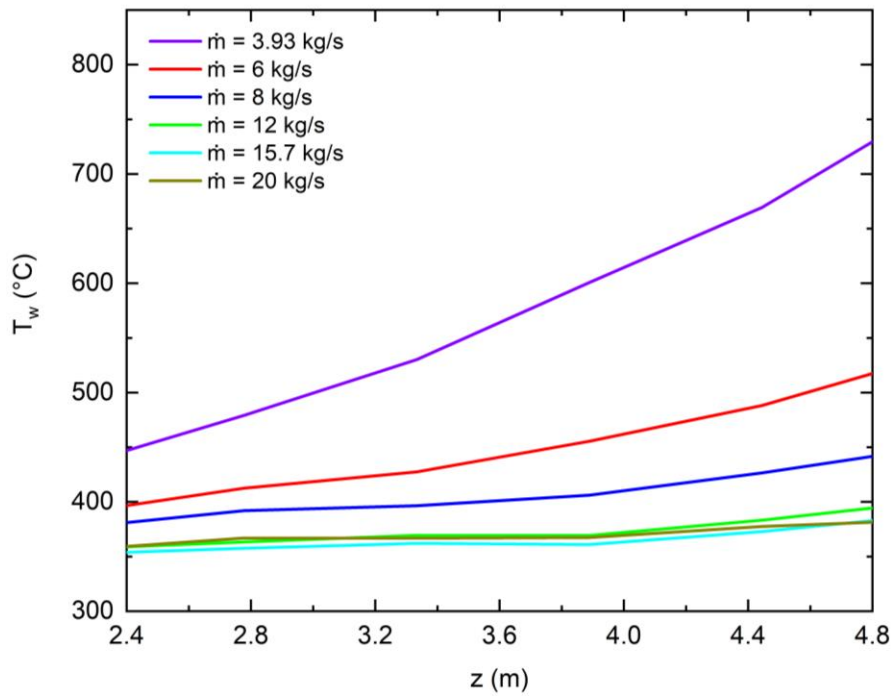
Figure 5.13: Circumferential wall temperature distributions under different mass flow rates



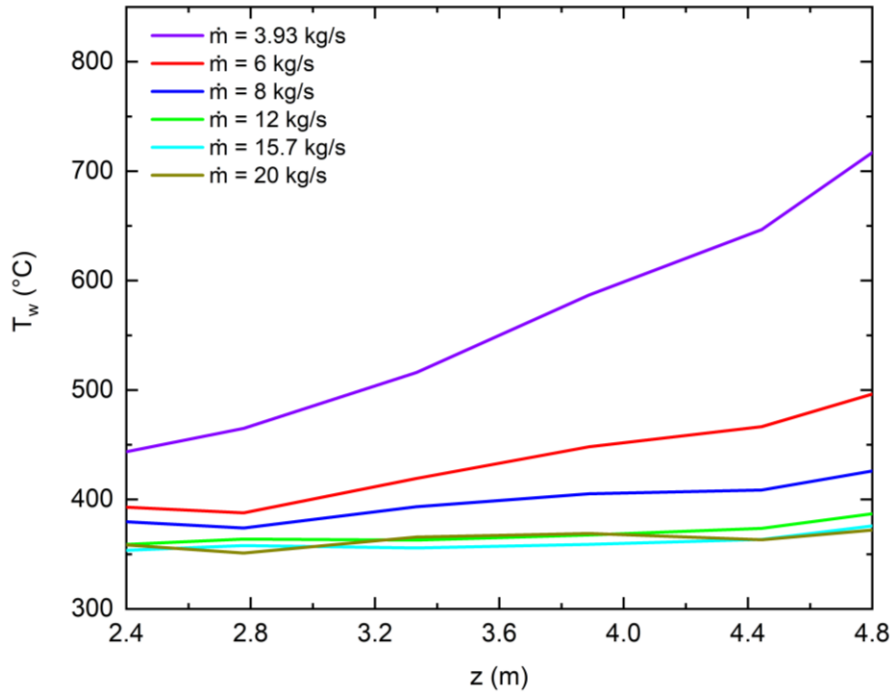
(a) rod 1



(b) rod 4



(c) rod 7



(d) rod 8

Figure 5.14: Wall temperature distributions along the axial direction under different mass flow rates

5.3.3. Effects of buoyancy on the heat transfer at different operating conditions

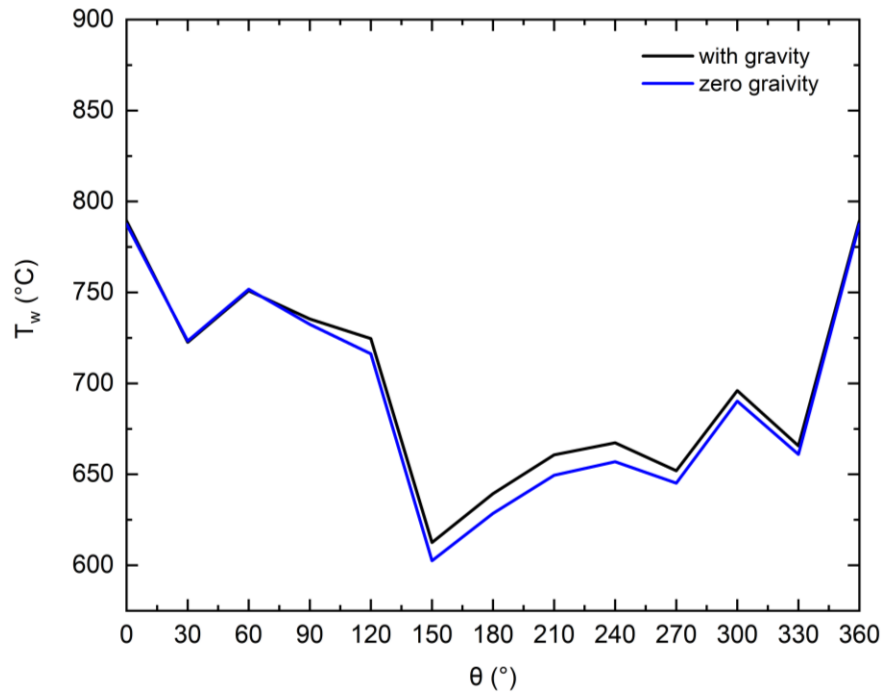
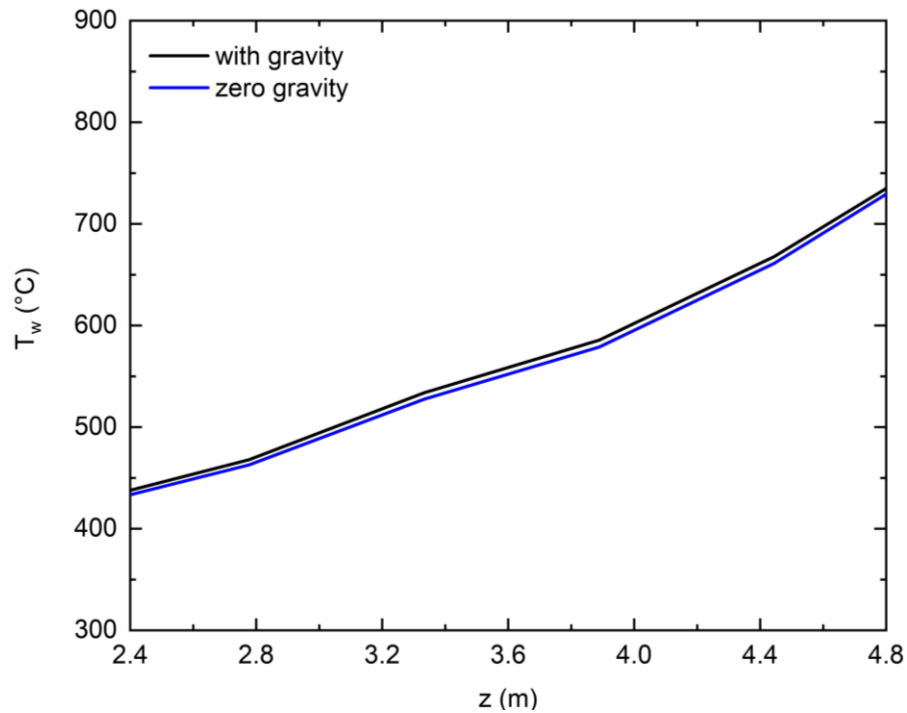
Fig. 5.15 presents the circumferential wall temperature distributions at $z = 4.8$ m and the axial wall temperature distributions of rod #1 at $z = 2.4 - 4.8$ m for Case # 1 ($P = 25$ MPa and $T_{in} = 350^\circ\text{C}$) at the design operating conditions of 64-element Canadian SCWR with and without considering the effect of buoyancy (gravity). It can be seen that the difference between cases with and without gravity is small. This indicates that the effect of buoyancy on the heat transfer for supercritical water in the vertical fuel rod bundle can be ignored at the design operating conditions.

The heat transfer in the fuel bundle flow can be mixed convection, including both natural convection and forced convection. The behavior of a natural convection process depends

on the Grashof number (Gr), which approximates the ratio of the buoyancy force to the viscous force acting on a fluid. In another aspect, the role of the Reynolds number (Re) in the forced convection is the same as the Gr on the natural convection. When analyzing the mixed convection, the effect of the buoyancy force on the mixed convection is approximately characterized by the ratio of Gr and Re. Several criteria have been proposed in previous studies. One criterion is Gr/Re^2 [42]. The effect of the buoyancy force can be ignored when $Gr/Re^2 < 0.1$ [42–45]. Jackson and Hall [45] proposed $Gr/Re^{2.7}$ to evaluate the effect of buoyancy force for the supercritical carbon dioxide in a vertical tube. It will be a buoyancy-free region if $Gr/Re^{2.7} < 10^{-5}$ [46]. This criterion has been verified reliable for the upward supercritical water flow in vertical tubes [44], [45], [47–49]. In addition, the dimensionless parameter, Bo^* is also used to investigate the effect of the buoyancy force on the heat transfer in vertical tubes [48], [50, 51] and it is defined as follows:

$$Bo^* = Gr / (Re^{3.425} Pr^{0.8}) \quad (5.6)$$

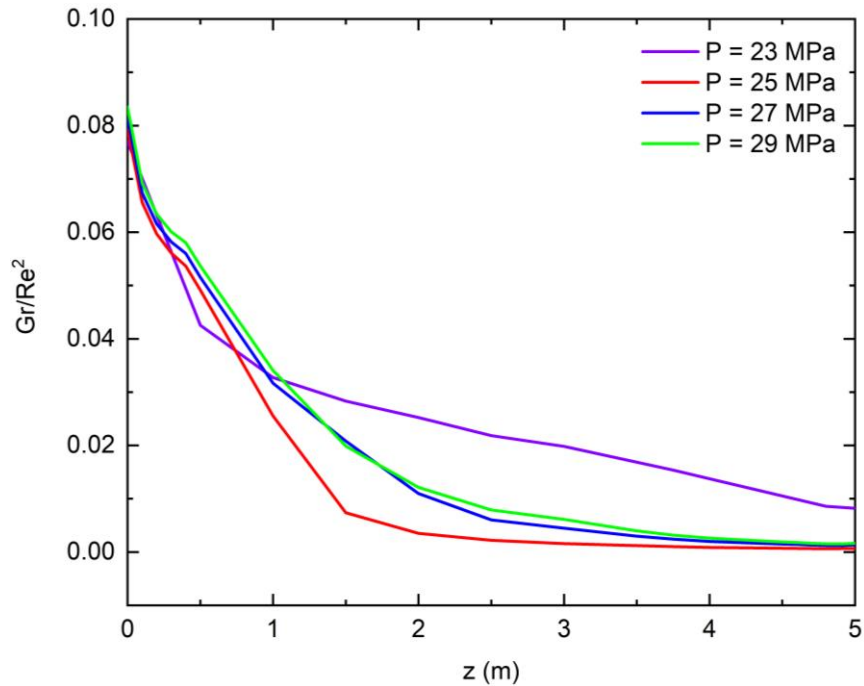
The effect of the buoyancy force on the heat transfer cannot be ignored when $5.67 \times 10^{-7} < Bo^* < 8 \times 10^{-6}$. In the present study, the above-mentioned three dimensionless parameters (Gr/Re^2 , $Gr/Re^{2.7}$ and Bo^*) proposed for pipe flows in the literature are used to evaluate the effect of the buoyancy force on the heat transfer at different operating conditions (Cases #1 - 16). The objectives are to verify whether the criteria work for the heat transfer of the supercritical water in the fuel bundle and further evaluate the effect of the buoyancy force on heat transfer of the supercritical water in the 64-element SCWR fuel bundle under different operation parameters.

(a) Circumferential wall temperature distribution at $z = 4.8$ m

(b) Axial wall temperature distribution

Figure 5.15: Effect of the gravity on the wall temperature of rod # 1 at the design operating condition

Figs. 5.16 - 5.19 present the variations of Gr/Re^2 , $Gr/Re^{2.7}$ and Bo^* , along the axial direction for different cases. Based on the criteria of Gr/Re^2 and Bo^* , the buoyancy force effect is negligible for all cases, while based on the criterion of $Gr/Re^{2.7}$ both buoyancy-affected and buoyancy-free zones exist along the axial direction. The buoyancy-affected zones exist at the entrance region for all operating parameters. As seen from Fig. 5.16b, the buoyancy-affected zone is at around $z = 0 - 1$ m for all pressures (23 MPa - 29 MPa). This is due to the sharp decrease of the density at around $z = 0 - 1$ m, as shown in Fig. 5.1. Figs. 5.17b and 5.18b show that with the increase of the inlet temperature and the heat flux, the buoyancy-affected zone is reduced. It is reasonable because the pseudocritical region where the gradient of density is large is narrowed with the increase of the inlet temperature and heat flux. Results shown in Fig. 19b indicate that the buoyancy effect on the heat transfer of the supercritical water in the fuel bundle can be ignored when the mass flow rate is greater than 6 kg/s.

(a) Gr/Re^2

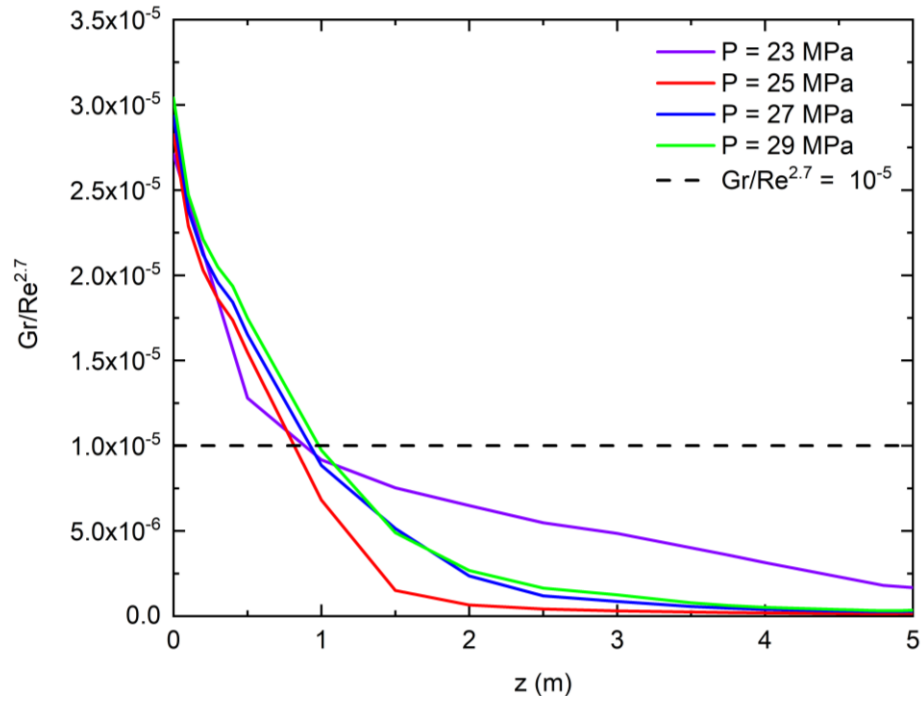
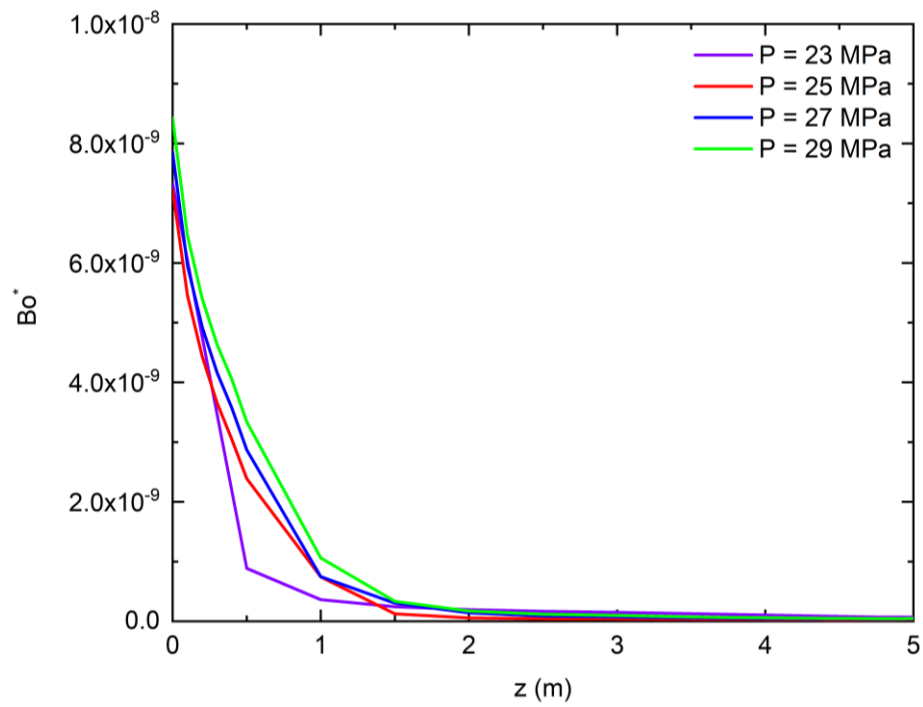
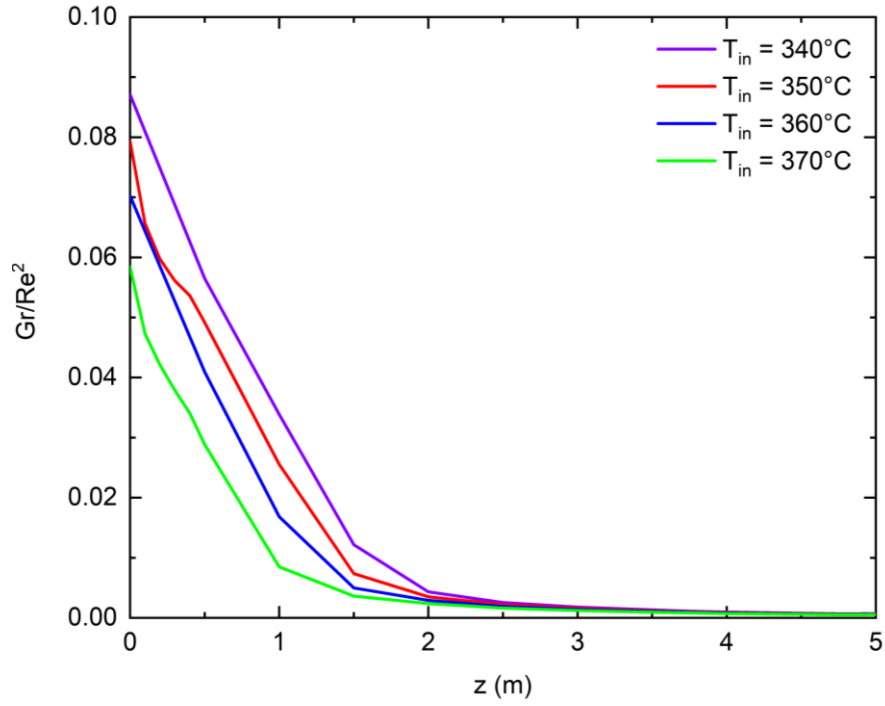
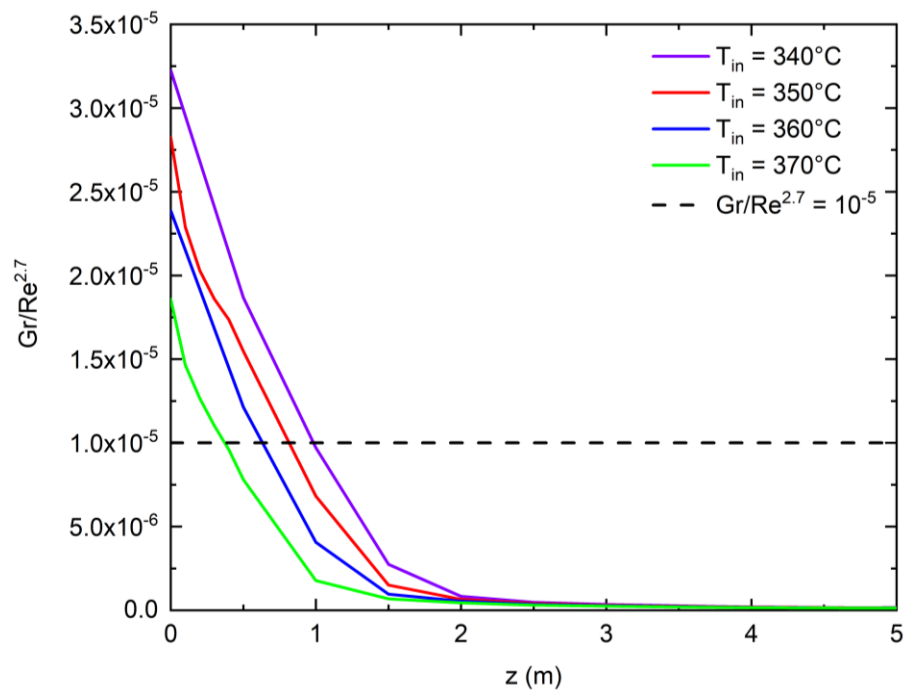
(b) $Gr/Re^{2.7}$ (c) Bo^*

Figure 5.16: Variations of Gr/Re^2 , $Gr/Re^{2.7}$ and Bo^* along the axial direction at different pressures

(a) Gr/Re^2 (b) $Gr/Re^{2.7}$

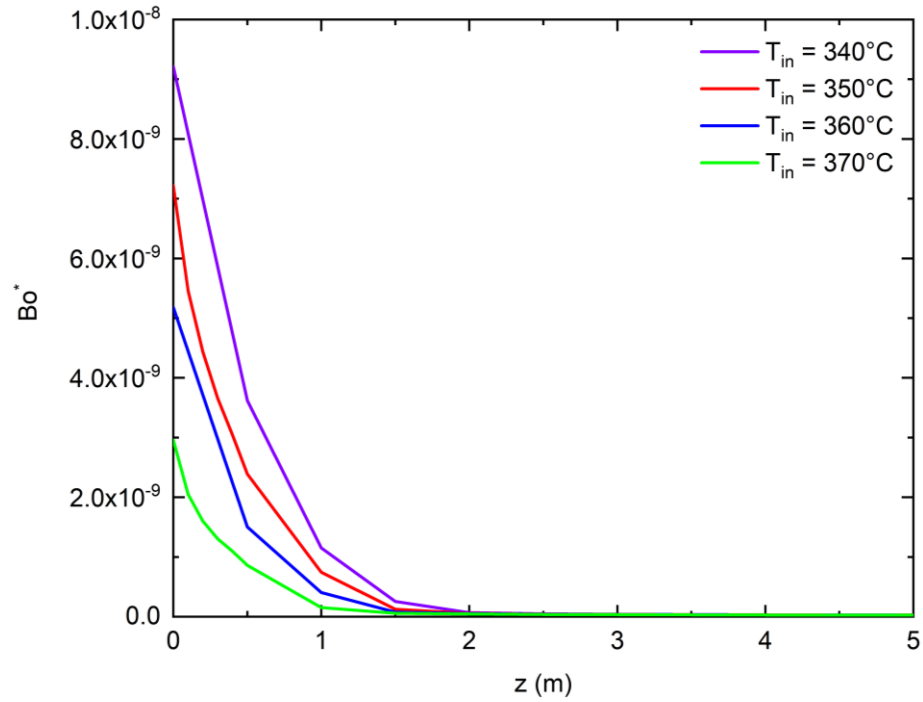
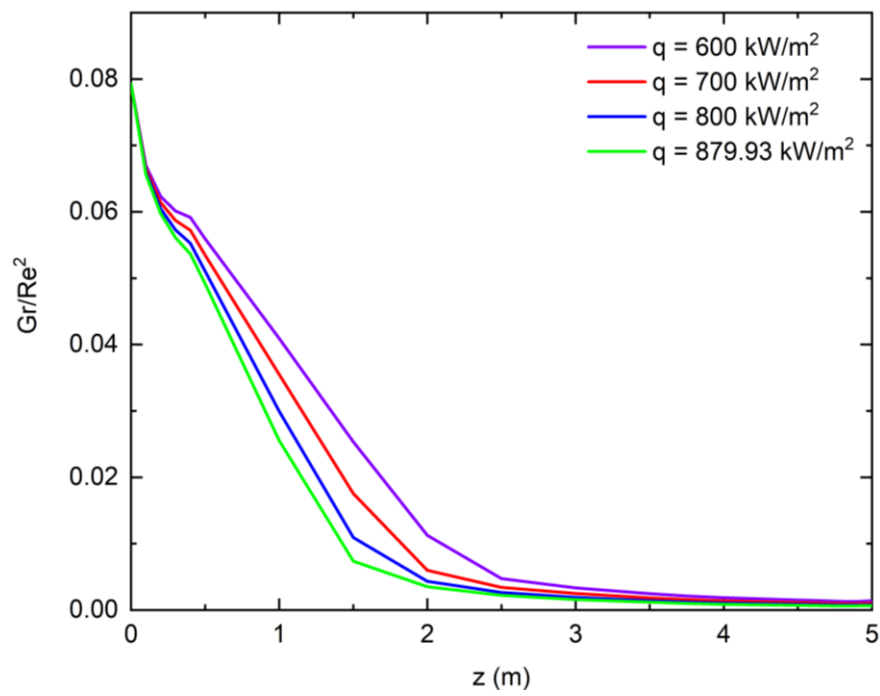
(c) Bo^*

Figure 5.17: Variations of Gr/Re^2 , $Gr/Re^{2.7}$ and Bo^* along the axial direction at different inlet temperatures

(a) Gr/Re^2

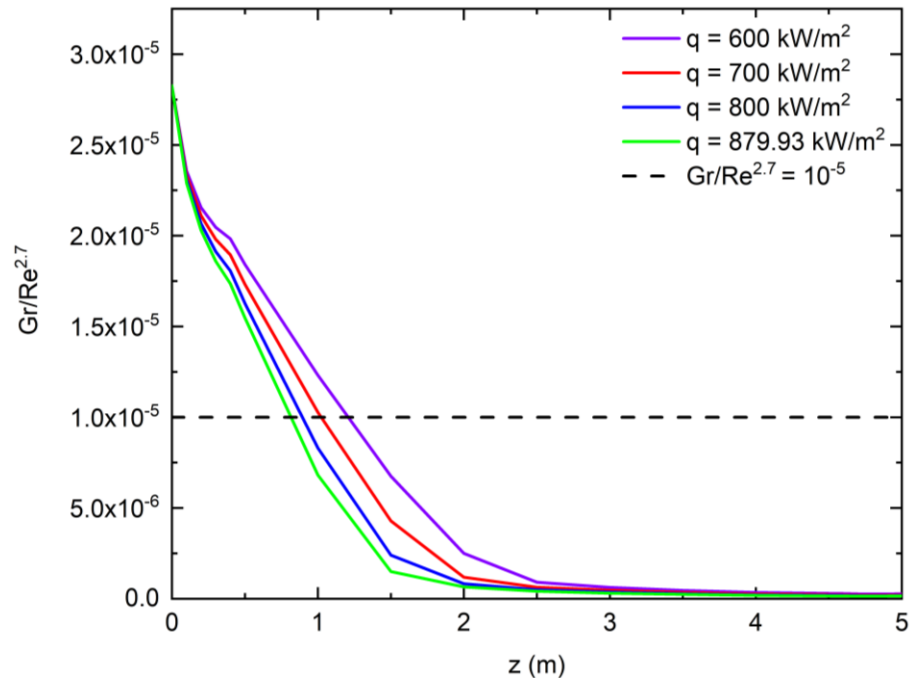
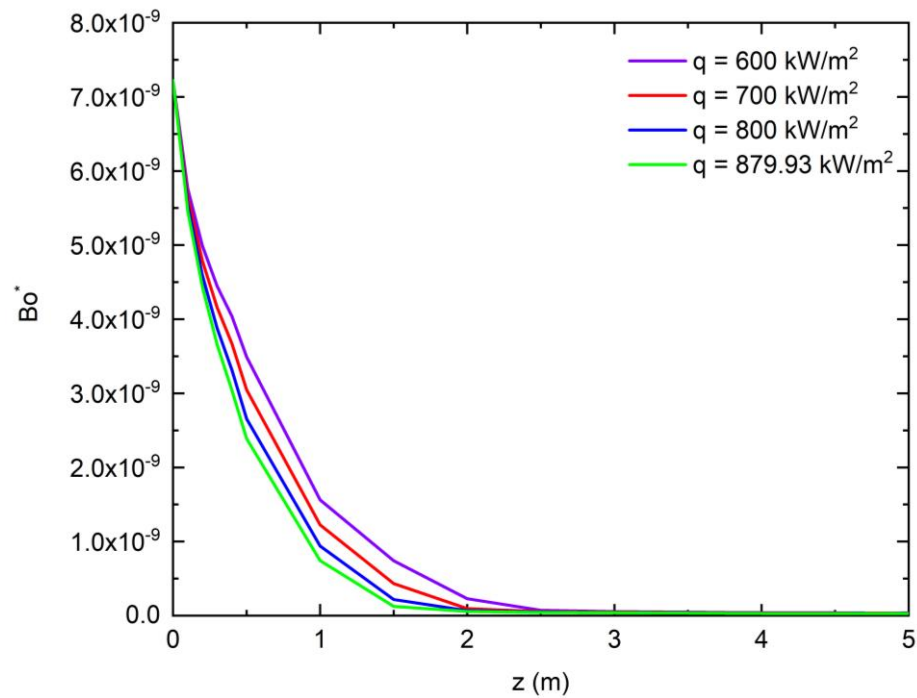
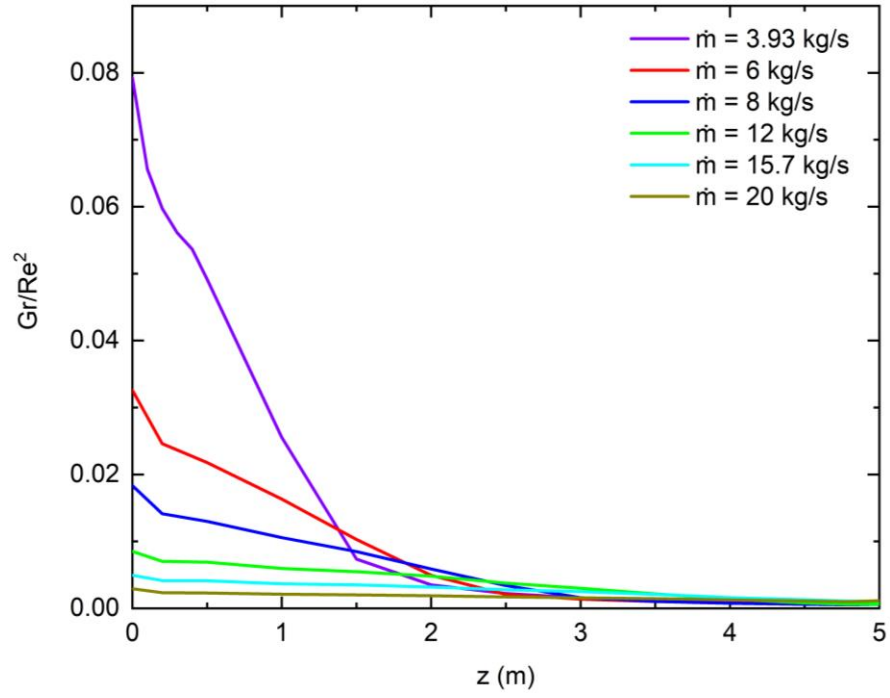
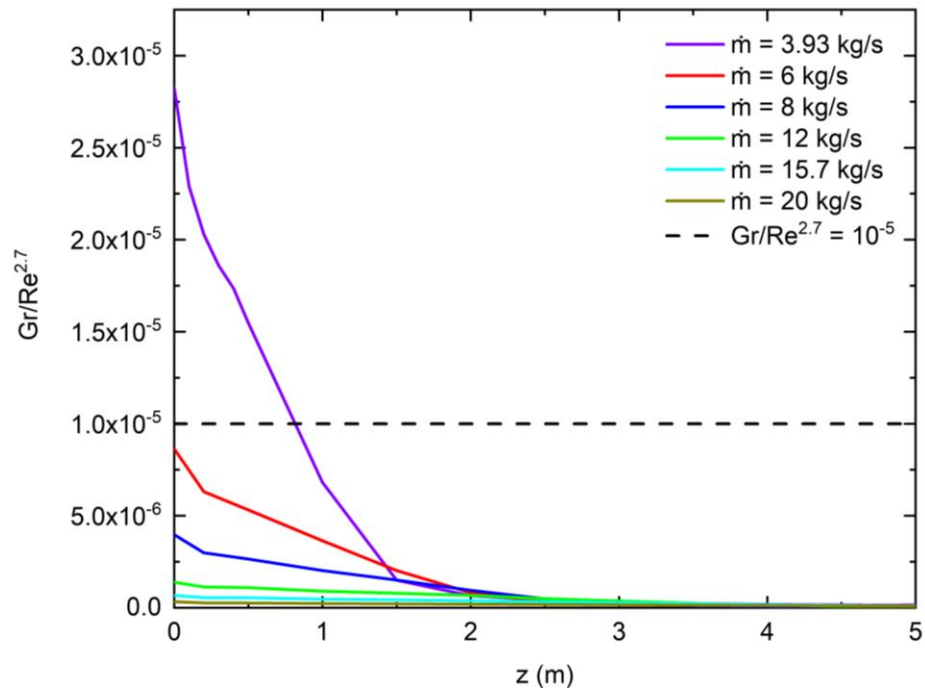
(b) $Gr/Re^{2.7}$ (c) Bo^*

Figure 5.18: Variations of Gr/Re^2 , $Gr/Re^{2.7}$ and Bo^* along the axial direction at different heat fluxes

(a) Gr/Re^2 (b) $Gr/Re^{2.7}$

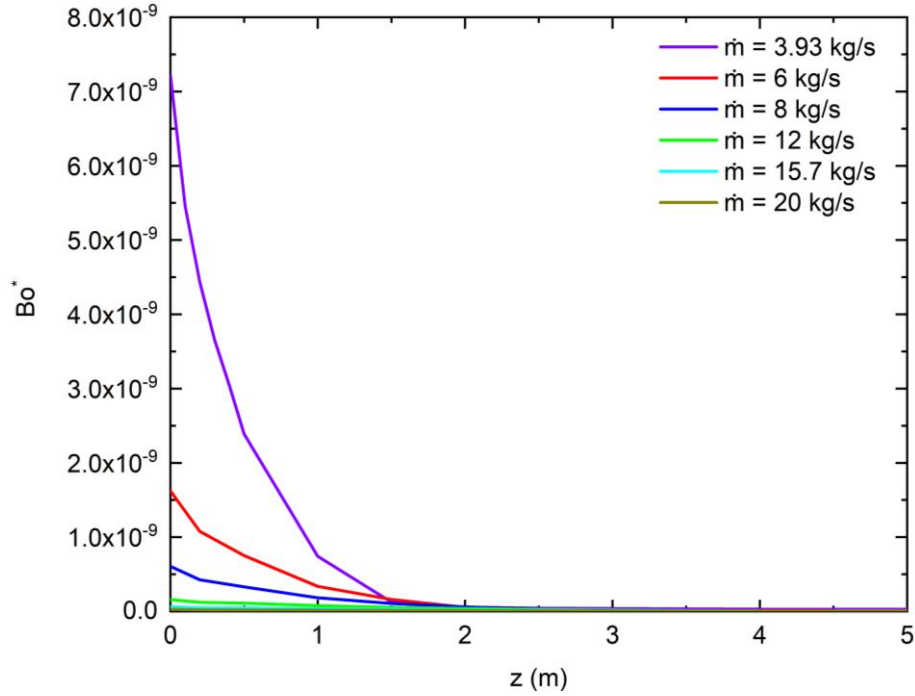
(c) Bo^*

Figure 5.19: Variations of Gr/Re^2 , $Gr/Re^{2.7}$ and Bo^* along the axial direction at different mass flow rates

5.4. Conclusions

The heat transfer of the supercritical water was investigated in the 64-element Canadian SCWR fuel bundle under different operating conditions using previously validated RSM with the variable Pr_t . The effects of the operating pressure, inlet temperature, heat flux, mass flux were analyzed. The wall temperature generally increases with the increase in the inlet temperature, increase in the heat flux, or decrease in the mass flux. When the operating pressure is away from the critical pressure, the wall temperatures does not change much with the change of pressure. Since the buoyancy effect contributes to the heat transfer deterioration, several criteria in the literature for evaluating the buoyancy effects for supercritical water flow in heated tube, Gr/Re^2 , $Gr/Re^{2.7}$, and Bo^* , were also examined in this study. These criteria for the supercritical water in the 64-element SCWR fuel bundle at different operating conditions were compared and discussed. Based on the criteria Gr/Re^2 and Bo^* , there is no buoyancy-affected region under all operating conditions

considered in this study. Based on the criterion $Gr/Re^{2.7}$, the buoyancy-affected zones exist at the entrance region ($z = 0 - 1\text{m}$) where the fluid bulk temperature (T_b) is close to the pseudocritical temperature (T_{pc}) and other regions along the axial direction are buoyancy-free zones where $T_b > T_{pc}$ at all pressures (23 MPa - 29 MPa). With the increase of the inlet temperature and the heat flux, the buoyancy-affected zone is reduced. The results for different mass fluxes indicate that the buoyancy effect on heat transfer of the supercritical water in the fuel bundle is negligible when the mass flow rate is greater than 6 kg/s.

References

- [1] M. Shitsman, “Impairment of the heat transmission at supercritical pressures,” *High Temp.*, vol. 1, pp. 237–244, 1963.
- [2] H. S. Swenson, J. . Carver, and C. R. Kakarala, “Heat transfer to supercritical water in smooth-bore tubes,” *J. Heat Transfer*, vol. 87, no. 4, pp. 477–483, 1965.
- [3] B. Shiralkar and P. Griffith, “Deterioration in heat transfer to fluids at supercritical pressure and high heat fluxes,” *J. Heat Transfer*, vol. 91, no. 1, pp. 27–36, 1969.
- [4] A. P. Ornatskij, L. F. Glushchenko, and S. I. Kalachev, “Heat transfer with rising and falling flows of water in tubes of small diameter at supercritical pressures,” *Thermal Engineering*, vol. 18, no. 5. pp. 137–141, 1971.
- [5] K. Yamagata, K. Nishikawa, S. Hasegawa, T. Fujii, and S. Yoshida, “Forced convective heat transfer to supercritical water flowing in tubes,” *Int. J. Heat Mass Transf.*, vol. 15, no. 12, pp. 2575–2593, Dec. 1972.
- [6] I. Pioro and S. Mokry, “Thermophysical Properties at Critical and Supercritical Pressures,” in *Heat Transfer - Theoretical Analysis, Experimental Investigations and Industrial Systems*, InTech, 2011, pp. 573–592.
- [7] OECD Nuclear Energy Agency, “Technology Roadmap Update for Generation IV Nuclear Energy Systems,” *Gen IV Int. Forum*, pp. 1–66, 2014.
- [8] S. Koshizuka, N. Takano, and Y. Oka, “Numerical analysis of deterioration phenomena in heat transfer to supercritical water,” *Int. J. Heat Mass Transf.*, vol. 38, no. 16, pp. 3077–3084, Nov. 1995.
- [9] S. H. Lee and J. R. Howell, “Turbulent developing convective heat transfer in a tube for fluids near the critical point,” *Int. J. Heat Mass Transf.*, vol. 41, no. 10, pp. 1205–1218, May 1998.
- [10] Y. Zhang, C. Zhang, and J. Jiang, “Numerical simulation of fluid flow and heat transfer of supercritical fluids in fuel bundles,” *J. Nucl. Sci. Technol.*, vol. 48, no. 6, pp. 929–935, 2011.

- [11] H. Wang, S. Wang, and D. Lu, “Large eddy simulation on the heat transfer of supercritical pressure water in a circular pipe,” *Nucl. Eng. Des.*, vol. 377, no. February, p. 111146, 2021.
- [12] S. Yu, H. Li, X. Lei, Y. Feng, Y. Zhang, H. He, T. Wang, “Experimental investigation on heat transfer characteristics of supercritical pressure water in a horizontal tube,” *Exp. Therm. Fluid Sci.*, vol. 50, pp. 213–221, Oct. 2013.
- [13] X. Lei, H. Li, W. Zhang, N. T. Dinh, Y. Guo, and S. Yu, “Experimental study on the difference of heat transfer characteristics between vertical and horizontal flows of supercritical pressure water,” *Appl. Therm. Eng.*, vol. 113, pp. 609–620, 2017.
- [14] X. Lei, H. Li, N. Dinh, and W. Zhang, “A study of heat transfer scaling of supercritical pressure water in horizontal tubes,” *Int. J. Heat Mass Transf.*, vol. 114, pp. 923–933, 2017.
- [15] H. Wang, Q. Bi, L. Wang, H. Lv, and L. K. H. Leung, “Experimental investigation of heat transfer from a 2×2 rod bundle to supercritical pressure water,” *Nucl. Eng. Des.*, vol. 275, pp. 205–218, Aug. 2014.
- [16] V. I. Deev, V. S. Kharitonov, A. M. Baisov, and A. N. Churkin, “Heat transfer in rod bundles cooled by supercritical water – Experimental data and correlations,” *Therm. Sci. Eng. Prog.*, vol. 15, Mar. 2020.
- [17] H. Wang, Q. Bi, and L. K. H. Leung, “Heat transfer from a 2×2 wire-wrapped rod bundle to supercritical pressure water,” *Int. J. Heat Mass Transf.*, vol. 97, pp. 486–501, 2016.
- [18] W. Gang, Q. Bi, Z. Yang, H. Wang, X. Zhu, H. Hao, L. K. H. Leung, “Experimental investigation of heat transfer for supercritical pressure water flowing in vertical annular channels,” *Nucl. Eng. Des.*, vol. 241, no. 9, pp. 4045–4054, 2011.
- [19] J. Wang, H. Li, S. Yu, and T. Chen, “Investigation on the characteristics and mechanisms of unusual heat transfer of supercritical pressure water in vertically-upward tubes,” *Int. J. Heat Mass Transf.*, vol. 54, no. 9–10, pp. 1950–1958, Apr. 2011.

- [20] X. Zhu, Q. Bi, D. Yang, and T. Chen, "An investigation on heat transfer characteristics of different pressure steam-water in vertical upward tube," *Nucl. Eng. Des.*, vol. 239, no. 2, pp. 381–388, Feb. 2009.
- [21] K. Podila and Y. F. Rao, "CFD analysis of flow and heat transfer in Canadian supercritical water reactor bundle," *Ann. Nucl. Energy*, vol. 75, pp. 1–10, 2014.
- [22] I. L. Pioro and R. B. Duffey, *Heat Transfer and Hydraulic Resistance at Supercritical Pressures in Power Engineering Applications*. New York, NY, USA: ASME Press, 2007.
- [23] S. Mokry, I. Pioro, A. Farah, K. King, S. Gupta, W. Peiman, P. Kirillov, "Development of supercritical water heat-transfer correlation for vertical bare tubes," *Nucl. Eng. Des.*, vol. 241, no. 4, pp. 1126–1136, Apr. 2011.
- [24] L. Liu, Z. Xiao, X. Yan, X. Zeng, and Y. Huang, "Heat transfer deterioration to supercritical water in circular tube and annular channel," *Nucl. Eng. Des.*, vol. 255, pp. 97–104, 2013.
- [25] M. Zhao, H. Y. Gu, and X. Cheng, "Experimental study on heat transfer of supercritical water flowing downward in circular tubes," *Ann. Nucl. Energy*, vol. 63, pp. 339–349, Jan. 2014.
- [26] W. Wang, L. Guo, G. Zhu, X. Zhu, and Q. Bi, "Experimental investigation on heat transfer of supercritical water flowing in the subchannel with grid spacer in supercritical water-cooled reactor," *Energies*, vol. 13, no. 5, 2020.
- [27] M. Zhao and H. Y. Gu, "Experimental and numerical investigation on heat transfer of supercritical water flowing upward in 2×2 rod bundles," *Nucl. Eng. Des.*, vol. 370, no. October, p. 110903, Dec. 2020.
- [28] X. Hao, P. Xu, H. Suo, and L. Guo, "Numerical investigation of flow and heat transfer of supercritical water in the water-cooled wall tube," *Int. J. Heat Mass Transf.*, vol. 148, p. 119084, 2020.
- [29] R. Maitri, H. Han, C. Zhang, and J. Jiang, "Numerical Investigation of the Deteriorated Heat Transfer Phenomenon for Supercritical Water Flows in Vertical

- Circular Tubes,” in *Complementary Resources for Tomorrow*, A. Vassel-Be-Hagh and D. S.-K. Ting, Eds. Cham: Springer International Publishing, 2020, pp. 235–248.
- [30] H. Y. Gu, Z. X. Hu, D. Liu, H. B. Li, M. Zhao, and X. Cheng, “Experimental study on heat transfer to supercritical water in 2×2 rod bundle with wire wraps,” *Exp. Therm. Fluid Sci.*, vol. 70, pp. 17–28, 2016.
- [31] W. Zhang, H. Li, Q. Zhang, X. Lei, and Q. Zhang, “Experimental investigation on heat transfer deterioration of supercritical pressure water in vertically-upward internally-ribbed tubes,” *Int. J. Heat Mass Transf.*, vol. 120, pp. 930–943, May 2018.
- [32] H. Han and C. Zhang, “Numerical Simulation of Fluid Flow and Heat Transfer of the Supercritical Water in Different Fuel Rod Channels,” in *Progress in Canadian Mechanical Engineering*, 2018.
- [33] X. Lei, Y. Guo, W. Zhang, H. Li, and L. Li, “Development of Heat Transfer Correlation for Supercritical Water in Vertical Upward Tubes,” *Heat Transf. Eng.*, vol. 40, no. 8, pp. 652–666, May 2019.
- [34] F. Yin, T.-K. Chen, and H.-X. Li, “An Investigation on Heat Transfer to Supercritical Water in Inclined Upward Smooth Tubes,” *Heat Transf. Eng.*, vol. 27, no. 9, pp. 44–52, Oct. 2006.
- [35] V. A. Grabezhnaya and P. L. Kirillov, “Heat transfer under supercritical pressures and heat transfer deterioration boundaries,” *Therm. Eng.*, vol. 53, no. 4, pp. 296–301, Apr. 2006.
- [36] M. T. Kao, M. Lee, Y. M. Ferng, and C. C. Chieng, “Heat transfer deterioration in a supercritical water channel,” *Nucl. Eng. Des.*, vol. 240, no. 10, pp. 3321–3328, 2010.
- [37] M. Yetisir, H. Hamilton, R. Xu, M. Gaudet, D. Rhodes, M. King, K. Andrew, and B. Benson, “Fuel Assembly Concept of the Canadian Supercritical Water- Cooled Reactor,” *J. Nucl. Eng. Radiat. Sci.*, vol. 4, no. 1, pp. 1–7, Jan. 2018.
- [38] ANSYS, “Ansys Fluent Theory Guide,” 2013.

- [39] H. Han and C. Zhang, "A Modified Turbulent Model for the Supercritical Water Flows in the Vertical Upward Channels," *J. Supercrit. Fluids*, p. 105632, May 2022.
- [40] H. Han and C. Zhang, "Numerical simulation of fluid flow and heat transfer of the supercritical water in the 64-element Canadian SCWR fuel bundle,"(submitted).
- [41] Lemmon E., Huber M., McLinden M., 2013. NIST reference fluid thermodynamic and transport properties-RFFPROP, version 9.1. National Institute of Standard Technology. 2013.
- [42] B. Metais and E. R. G. Eckert, "Forced, Mixed, and Free Convection Regimes," *J. Heat Transfer*, vol. 86, no. 2, pp. 295–296, May 1964.
- [43] F. P. Incropera, *Fundamentals of heat and mass transfer*, 6th ed. Hoboken, NJ: John Wiley, 2007.
- [44] B. Zhang, J. Shan, and J. Jiang, "Numerical analysis of supercritical water heat transfer in horizontal circular tube," *Prog. Nucl. Energy*, vol. 52, no. 7, pp. 678–684, 2010.
- [45] Z. Gao and J. Bai, "Numerical analysis on nonuniform heat transfer of supercritical pressure water in horizontal circular tube," *Appl. Therm. Eng.*, vol. 120, pp. 10–18, Jun. 2017.
- [46] J. D. Jackson and W. B. Hall, "Influences of buoyancy on heat transfer to fluids flowing in vertical tubes under turbulent conditions," 1979.
- [47] A. Bruch, A. Bontemps, and S. Colasson, "Experimental investigation of heat transfer of supercritical carbon dioxide flowing in a cooled vertical tube," *Int. J. Heat Mass Transf.*, vol. 52, no. 11–12, pp. 2589–2598, May 2009.
- [48] J. Guo, M. Xiang, H. Zhang, X. Huai, K. Cheng, and X. Cui, "Thermal-hydraulic characteristics of supercritical pressure CO₂ in vertical tubes under cooling and heating conditions," *Energy*, vol. 170, pp. 1067–1081, Mar. 2019.

- [49] R. Peng, X. Lei, Z. Guo, Y. Wang, H. Li, and X. Zhou, "Forced convective heat transfer of supercritical carbon dioxide in mini-channel under low mass fluxes," *Int. J. Heat Mass Transf.*, vol. 182, p. 121919, Jan. 2022.
- [50] J. D. Jackson, M. A. Cotton, and B. P. Axcell, "Studies of mixed convection in vertical tubes," *Int. J. Heat Fluid Flow*, vol. 10, no. 1, pp. 2–15, Mar. 1989.
- [51] D. P. Mikielewicz, A. M. Shehata, J. D. Jackson, and D. M. McEligot, "Temperature, velocity and mean turbulence structure in strongly heated internal gas flows Comparison of numerical predictions with data," *Int. J. Heat Mass Transf.*, vol. 45, no. 21, pp. 4333–4352, Oct. 2002.

6. Construction of a Feedback Control System Based on CFD Simulations for the 64-element Canadian SCWR

Nomenclature

Symbols

g	Gravitational acceleration, m/s^2
G	Mass flux, $\text{kg/m}^2 \cdot \text{s}$
G_{r11}	Transfer function from the outlet mass flow rate to the inlet mass flow rate
G_{r12}	Transfer function from the outlet mass flow rate to the inlet temperature
G_{r13}	Transfer function from the outlet mass flow rate to the heat flux
G_{r21}	Transfer function from the outlet temperature to the inlet mass flow rate
G_{r22}	Transfer function from the outlet temperature to the inlet temperature
G_{r23}	Transfer function from the outlet temperature to the heat flux
G_{r31}	Transfer function from the maximum wall temperature to the inlet mass flow rate
G_{r32}	Transfer function from the maximum wall temperature to the inlet temperature

G_{r33}	Transfer function from the maximum wall temperature to the heat flux
K_D	Derivative gain
K_I	Integral gain
K_P	Proportional gain
P	Pressure, Pa
Pr	Prandtl number
q	Heat flux, W/m^2
s	Complex variable in Laplace transform
t	Time, s
T	Temperature, $^{\circ}\text{C}$
U	Input variables
u	Velocity, m/s
Y	Output variables

Greek Letters

μ	Dynamic viscosity, $\text{Pa} \cdot \text{s}$
ρ	Density of a fluid, kg/m^3

Subscripts

cr	Critical
in	Inlet

<i>out</i>	Outlet
<i>r</i>	Reactor
<i>t</i>	Turbulent
<i>w</i>	Wall
<i>max</i>	Maximum

Acronyms

CANDU	Canada Deuterium Uranium
CFD	Computational Fluid Dynamics
LWR	Light Water-Cooled Reactor
SCFPP	Supercritical Fossil-Fueled Power Plant
SCFR	Supercritical Water-Cooled Fast Reactor
SCWR	Supercritical Water-Cooled Reactor
SISO	Single-Input-Single-Output
RGA	Relative Gain Array
RSM	Reynolds Stress Model

6.1.Introduction

Supercritical water-cooled reactors (SCWRs) are nuclear reactors that operate at pressures and temperatures above the critical point of water (22.1 MPa, 374°C). The SCWR is one of six Generation IV nuclear reactor concepts that is under development in several countries [1]. The concept of the SCWR is proposed based on the mature technologies of existing supercritical fossil-fueled power plants (SCFPP) and light water-cooled reactors (LWRs). Thus, the reactor coolant system in the SCWR is similar to that in the SCFPP, which is a once-through direct cycle. The main advantages of SCWRs are the potential of improved thermal efficiency and relatively simple plant system with fewer major components. The Canadian SCWR is a supercritical light water-cooled pressure-tube type nuclear reactor. The fuel channel of the reactor is vertically placed.

Since the thermophysical properties of the supercritical water vary significantly near the pseudocritical region, the understanding of dynamic characteristics of SCWRs is essential for the design and analysis of the control system. A few studies on the control system design for supercritical water-cooled type reactors have been conducted [2–10]. The earliest study of the control on the SCWR was conducted by Nakatsuka et al. [2] for the supercritical water -cooled fast reactor (SCFR) and then similar design method was applied in the further study [3] for the supercritical high temperature thermal reactor. The stepwise responses of the reactor systems were analyzed with added perturbations. Based on the analysis, the relationship of inputs and outputs of the reactor system was obtained, and the control system was established accordingly. The results showed that the reactor with the control system can operate stably when disturbances were added. Sun [4–6] linearized the dynamic process in the reactor system and proposed a simplified one-dimensional dynamic model for the CANDU SCWR system. The dynamic characteristics of the control system were analyzed and the control relationship were the same as in [2, 3]. Based on these studies, Sun [7, 8] also used different control methods, such as feedback controller, feed-forward controller [7] and linear parameter-varying controller [8] to further improve the performance of the control system. In order to construct a feedback control system, a linear dynamic model is needed. The physical process is normally nonlinear. Therefore, several

approaches can be used to linearize the process depending on the property of the process. If there is analytical solution for describing the physical process, the Taylor series expansion can be used and then only the linear terms are used. If experimental data are available, a linear dynamic model of the process can be obtained by system identification techniques depending on dynamic behaviors of inputs and outputs through introducing small perturbations at the design point. However, when the above two methods are not feasible, full scale computational fluid dynamics (CFD) simulations could be used instead to describe the physical process. Maitri et al. [9] derived the dynamic relationships of inputs and outputs of the reactor by using the numerical results from CFD simulations of supercritical water flow in the heated tube. Perturbations were introduced and linear dynamic models were constructed and validated. Although the flow of the supercritical water in the reactor was simplified as a two-dimensional tube flow, this work proved that CFD simulations could be used as the method to obtain dynamic relationships between inputs and outputs of the supercritical water flow in the reactor. Studies used the similar methodology could be found in [11–13] for other transient physical processes. Han [10] used the full scale three-dimensional CFD simulations of the supercritical water flow in the rod channels instead of the flow in a single tube and implemented a feedback control system. The performance of the control system has been evaluated around the operating point. In order to ensure the safety of a nuclear reactor, the maximum cladding surface temperature is an important parameter. The heat transfer characteristics of the supercritical water in the rod bundle directly influence the cladding temperature. Although the 64-element Canadian SCWR concept was proposed, there is still lack of studies in the design of the control system.

Therefore, in this study, we first obtain the dynamic relationships of inputs and outputs of the heat transfer process in the rod bundle and construct the linear dynamic models accordingly. This is followed by the design of the feedback control system design for the simplified thermal hydraulic models of the 64-element reactor and the performance evaluation of the control system.

6.2. Reactor and its mathematical models

6.2.1. Configurations of 64-element fuel bundle of the Canadian SCWR

The fuel bundle used in the study is the newest proposed vertically oriented 64-element two-ring rod bundle [14] and the cross-section view of the fuel bundle is shown in Fig. 6.1. The fuel rods are symmetrically distributed with 32 rods in each ring. The heated length is 5 m. Operating parameters of the 64-element Canadian SCWR are summarized in Table 6.1 [14, 15]. The main heat transfer process in the reactor mainly occurs in the fuel bundle, which directly influences the safety of the reactor since the temperature in the reactor depends on the heat transfer process. Three controllable inputs of the reactor are the inlet mass flow rate of water, inlet temperature of water, and the heat flux on the fuel rod. The controlled outputs are the outlet mass flow rate, outlet temperature, and the maximum cladding temperature. Before constructing the control system, the relationship between inputs and outputs need to be determined, which is obtained with the help of transient CFD simulations of the fluid flow and heat transfer of the supercritical water in the fuel bundle.

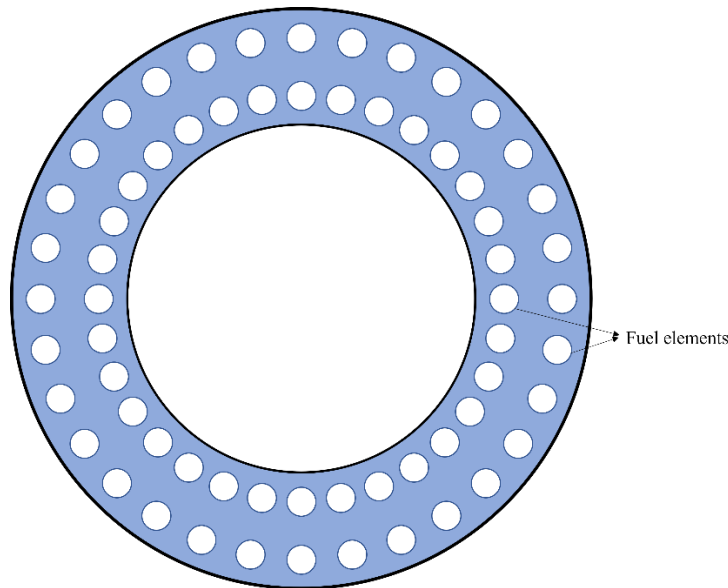


Figure 6.1: Configuration of the 64-element fuel bundle

Table 6.1 Specifications of the 64-element Canadian SCWR

Thermal power	2540 MW
Flow rate	1320 kg/s
Number of channels	336
Inlet temperature	350°C
Operating pressure	25 MPa
Heated length	5 m

6.2.2. Mathematical models used in CFD simulations

6.2.2.1. Governing equation

The fluid flow and heat transfer process in the fuel bundle is governed by the conservation equations of mass, momentum, and energy. The Reynolds averaged form of these equations are given as follows [16]:

$$\frac{\partial \rho}{\partial t} + \frac{\partial \rho \bar{u}_i}{\partial x_i} = 0 \quad (6.1)$$

$$\frac{\partial \rho \bar{u}_i}{\partial t} + \frac{\partial (\rho \bar{u}_i \bar{u}_j)}{\partial x_j} = -\frac{\partial \bar{p}}{\partial x_i} + \frac{\partial}{\partial x_j} \left(\mu \frac{\partial \bar{u}_i}{\partial x_j} - \rho \overline{u'_i u'_j} \right) + \rho g_i \quad (6.2)$$

$$\frac{\partial (\rho c_p T)}{\partial t} + \frac{\partial}{\partial x_i} (\bar{u}_i \rho c_p T) = \frac{\partial}{\partial x_i} \left[\left(\lambda + \frac{c_p \mu_t}{Pr_t} \right) \frac{\partial T}{\partial x_i} \right] \quad (6.3)$$

6.2.2.2. Turbulent models

In order to solve the Reynolds stress term ($\rho \overline{u'_i u'_j}$), which needs an appropriate treatment of the turbulent Prandtl number (Pr_t) for the heat transfer of the supercritical water in the fuel bundle, the previously validated Reynolds stress model (RSM) with a variable Pr_t model is used for the turbulent modeling in this study. The transport equation for the RSM is given as [16]:

$$\begin{aligned}
\underbrace{\frac{\partial}{\partial t}(\rho \overline{u'_i u'_j})}_{\text{Local time derivative}} + \underbrace{\frac{\partial}{\partial x_k}(\rho u_k \overline{u'_i u'_j})}_{C_{ij} \equiv \text{Convection}} &= - \underbrace{\frac{\partial}{\partial x_k} [\rho \overline{u'_i u'_j u'_k} + p'(\delta_{kj} u'_i + \delta_{ik} u'_j)]}_{D_{T,ij} \equiv \text{Turbulent Diffusion}} \\
&+ \underbrace{\frac{\partial}{\partial x_k} \left[\mu \frac{\partial}{\partial x_k} (\overline{u'_i u'_j}) \right]}_{D_{L,ij} \equiv \text{Molecular Diffusion}} - \underbrace{\rho \left(\overline{u'_i u'_k} \frac{\partial u_j}{\partial x_k} + \overline{u'_j u'_k} \frac{\partial u_i}{\partial x_k} \right)}_{P_{ij} \equiv \text{Stress Production}} \\
&\underbrace{- \rho \beta (g_i \overline{u'_j \theta} + g_j \overline{u'_i \theta})}_{G_{ij} \equiv \text{Buoyancy Production}} + \underbrace{p' \left(\frac{\partial u'_i}{\partial x_j} + \frac{\partial u'_j}{\partial x_i} \right)}_{\phi_{ij} \equiv \text{Pressure Strain}} \\
&\underbrace{- 2\mu \frac{\partial u'_i}{\partial x_k} \frac{\partial u'_j}{\partial x_k}}_{\varepsilon_{ij} \equiv \text{Dissipation}} - \underbrace{2\rho \Omega_k (\overline{u'_j u'_m} \varepsilon_{ikm} + \overline{u'_i u'_m} \varepsilon_{jkm})}_{F_{ij} \equiv \text{Production by System Rotation}} \\
&+ \underbrace{S_{user}}_{\text{User-Defined Source Term}} \tag{6.4}
\end{aligned}$$

The variable Pr_t model used in this work [17] is:

$$Pr_t = \begin{cases} 0.4 & \mu_t/\mu < 0.2 \\ 0.3 + 0.03 \times (P/P_{cr}) \times Pr \times (\mu_t/\mu) \times (q/G) & 0.2 \leq \mu_t/\mu \leq 10 \\ 0.85 & \mu_t/\mu > 10 \end{cases} \tag{6.5}$$

The transient CFD simulations of the supercritical water flow in the fuel bundle were conducted by ANSYS FLUENT to capture the dynamic characteristics of inputs and outputs. The control volume method is used to discretize the physical domain and convert the partial differential equations to sets of algebraic equations. Accordingly, algebraic equations are solved iteratively until the convergence criteria are satisfied.

6.3. Construction of the linear dynamic models

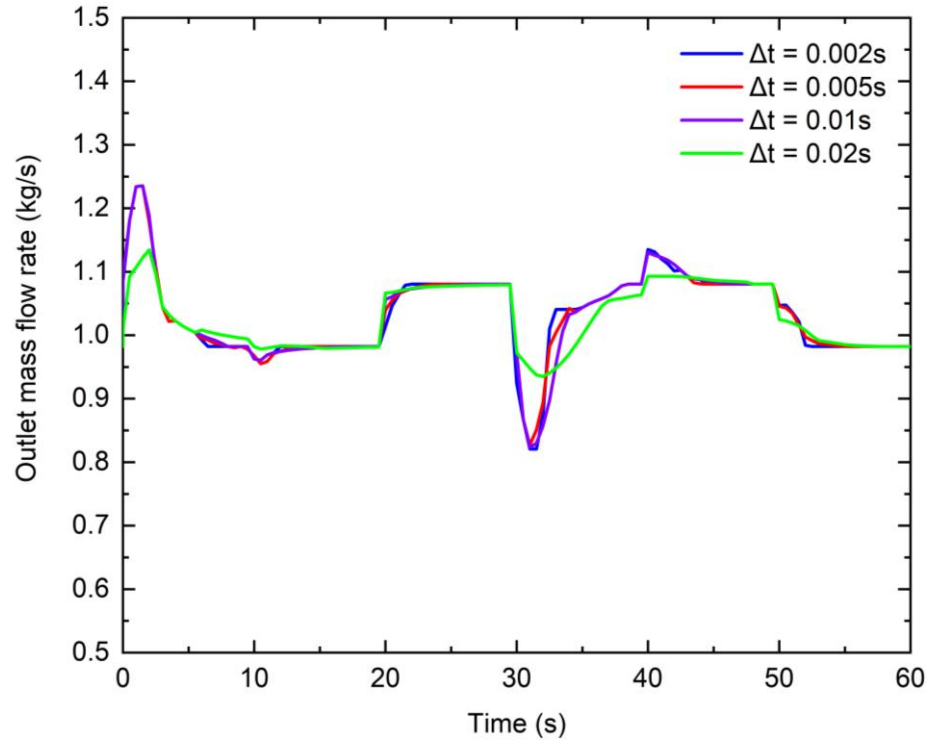
6.3.1. Time independent tests

The dynamic relationship between inputs and outputs are obtained by transient CFD simulations, which is the basis of the construction of dynamic models. Therefore, it is important to determine an appropriate time step size used in transient simulations so that the results from transient simulations are independent of the time step size. In the time independent tests, continuous perturbations of inputs are added at each 10 s and lasts for 20 s starting from the design point (0 s). Table 2 shows the order of added perturbations in 60 s. The respective variations of all outputs captured by transient CFD simulations with various time step sizes are plotted in Fig. 6.2. It is seen that there are small differences between the simulation results when the time step is less than 0.01 s. Therefore, the time step size 0.01s is used in transient CFD simulations to obtain the dynamic relationship between inputs and outputs.

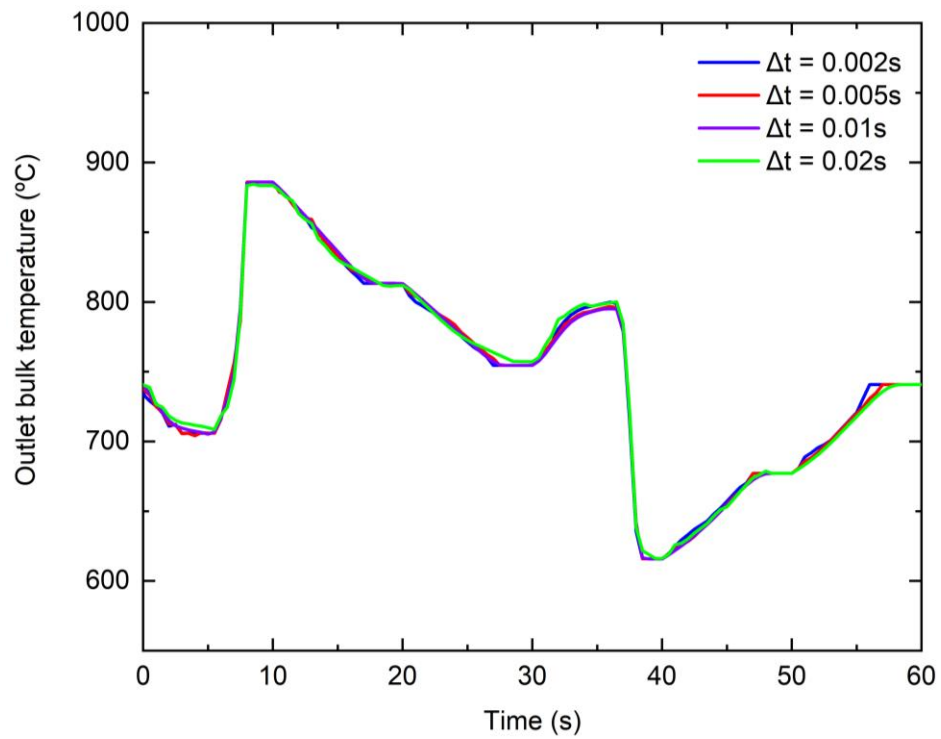
Table 6.2 Disturbances added for time independent tests

Time (s) \ Inputs	0	10	20	30	40	50	60
m_{in}	1	1	+ 10%	+ 10%	+ 10%	1	1
T_{in}	+ 10%	+ 10%	+ 10%	1	1	1	1
q	1	- 10%	- 10%	- 10%	1	1	1

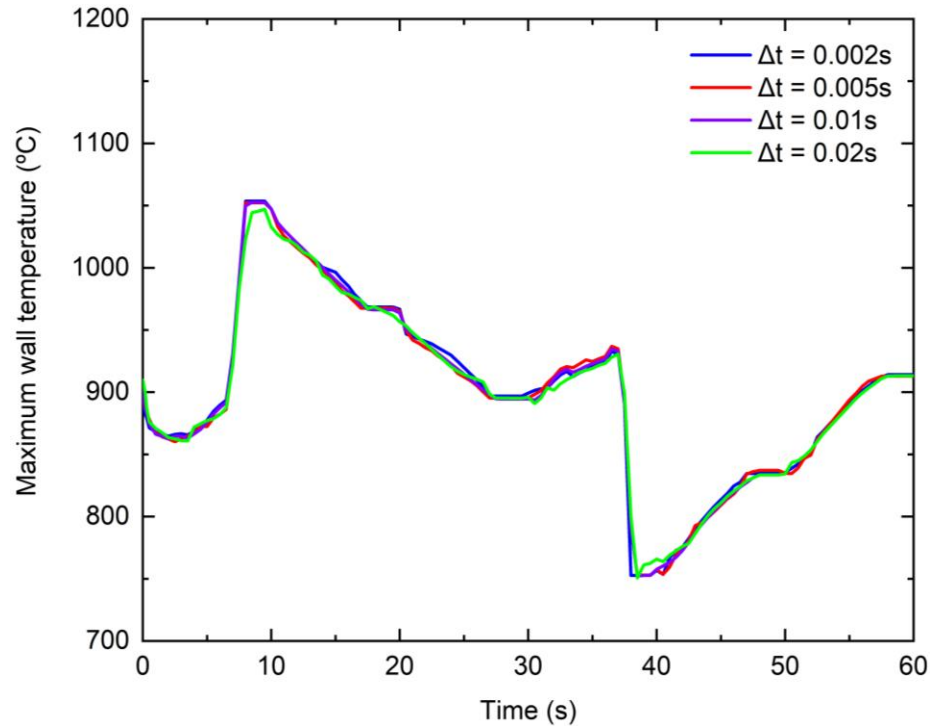
1 means the design point



(a) Change of outlet mass flow rate



(b) Change of outlet temperature



(c) Change of maximum cladding temperature

Figure 6.2: Outputs with perturbations added using different time step sizes

6.3.2. Construction of transfer functions

The dynamic model for the fuel bundle consists of three inputs and three outputs, as illustrated in Fig. 6.3. The governing equations for the fluid flow and heat transfer of the supercritical water are highly nonlinear. It is unrealistic to directly linearize governing equations. Therefore, a linear dynamic model of the fuel bundle is constructed on the basis of dynamic relationship between the changes of the inputs and outputs obtained from transient CFD simulations.

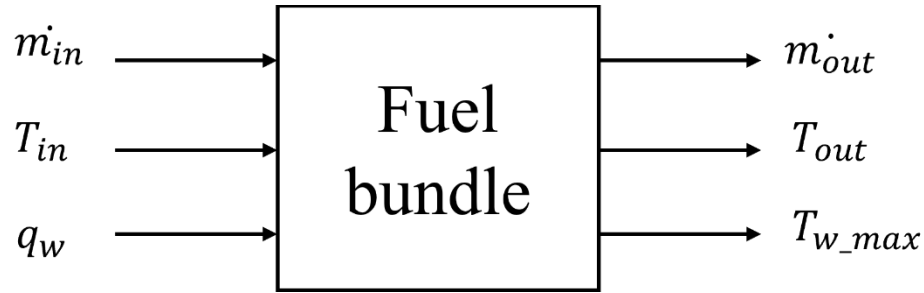


Figure 6.3: Block representation of the dynamic model of the fuel bundle

The methodology to obtain the linear dynamic model of the fuel bundle is described as follows. 10% step perturbation of only one input is added to the steady state at $t = 2$ s and the resulting changes of all three outputs are obtained through transient CFD simulations. This process is repeated for each input variable. Since there are three input variables, the recorded responses would consist of 9 sets of input and output variables. The changes of the flow and heat transfer process in the fuel bundle can be expressed in matrix form of transfer functions:

$$Y_{r(s)} = \begin{bmatrix} Y_{r1(s)} \\ Y_{r2(s)} \\ Y_{r3(s)} \end{bmatrix} = G_{r(s)} U_{r(s)} = \begin{bmatrix} G_{r11}(s) & G_{r12}(s) & G_{r13}(s) \\ G_{r21}(s) & G_{r22}(s) & G_{r23}(s) \\ G_{r31}(s) & G_{r32}(s) & G_{r33}(s) \end{bmatrix} \begin{bmatrix} U_{r1(s)} \\ U_{r2(s)} \\ U_{r3(s)} \end{bmatrix} \quad (6.6)$$

From these data sets, the least square method-based system identification technique is used to choose the best fitting for the dynamic models [18]. The parameters of the dynamic models are regulated to minimize the sum of the squares of differences between the results from CFD simulations and the outputs from the dynamic models. Transfer functions of the linear dynamic models in the Laplace form are shown as follows:

$$G_{r11}(s) = \frac{42.95s^2 + 52.54s + 44.28}{s^3 + 68.48s^2 + 96.16s + 44.29} \quad (6.7)$$

$$G_{r12}(s) = \frac{0.01139s^5 + 0.02959s^4 + 0.1029s^3 + 0.1088s^2 + 0.1427s + 0.03218}{s^5 + 2.707s^4 + 8.535s^3 + 10.62s^2 + 10.94s + 3.182} \quad (6.8)$$

$$G_{r13}(s) = \frac{0.0004862s^8 + 0.002397s^7 + 0.03164s^6 + 0.1042s^5 + 0.5411s^4 + 1.088s^3 + 2.705s^2 + 2.906s + 1.057}{s^9 + 262.7s^8 + 1501s^7 + 1.655 \times 10^4 s^6 + 5.982 \times 10^4 s^5 + 2.491 \times 10^5 s^4 + 4.864 \times 10^5 s^3 + 8.496 \times 10^5 s^2 + 7.166 \times 10^5 s + 2.13 \times 10^5} \quad (6.9)$$

$$G_{r21}(s) = \frac{-35.43s^6 - 50.78s^5 - 797.6s^4 - 170s^3 - 1537s^2 + 5183s + 3600}{s^7 + 4.627s^6 + 30.51s^5 + 92.96s^4 + 175.4s^3 + 202.8s^2 + 53.42s + 22.47} \quad (6.10)$$

$$G_{r22}(s) = \frac{166.2s^{15} + 6078s^{14} + 1.071 \times 10^4 s^{13} + 3.949 \times 10^5 s^{12} + 1.82 \times 10^5 s^{11} + 7.999 \times 10^6 s^{10} + 9.215 \times 10^5 s^9 + 6.96 \times 10^7 s^8 - 1.624 \times 10^6 s^7 + 2.763 \times 10^8 s^6 - 2.191 \times 10^7 s^5 + 4.669 \times 10^8 s^4 - 4.11 \times 10^7 s^3 + 2.655 \times 10^8 s^2 - 1.392 \times 10^7 s + 2.132 \times 10^7}{s^{19} + 13.11s^{18} + 179.1s^{17} + 1429s^{16} + 1.043 \times 10^4 s^{15} + 5.761 \times 10^4 s^{14} + 2.716 \times 10^5 s^{13} + 1.101 \times 10^6 s^{12} + 3.575 \times 10^6 s^{11} + 1.11 \times 10^7 s^{10} + 2.46 \times 10^7 s^9 + 6.09 \times 10^7 s^8 + 8.591 \times 10^7 s^7 + 1.767 \times 10^8 s^6 + 1.376 \times 10^8 s^5 + 2.429 \times 10^8 s^4 + 7.938 \times 10^7 s^3 + 1.215 \times 10^8 s^2 + 6.714 \times 10^6 s + 9.625 \times 10^6} \quad (6.11)$$

$$G_{r23}(s) = \frac{10^{-4}(2.576s^3 + 6.862s^2 + 4.012s + 2.553)}{s^4 + 2.373s^3 + 2.146s^2 + 1.093s + 0.299} \quad (6.12)$$

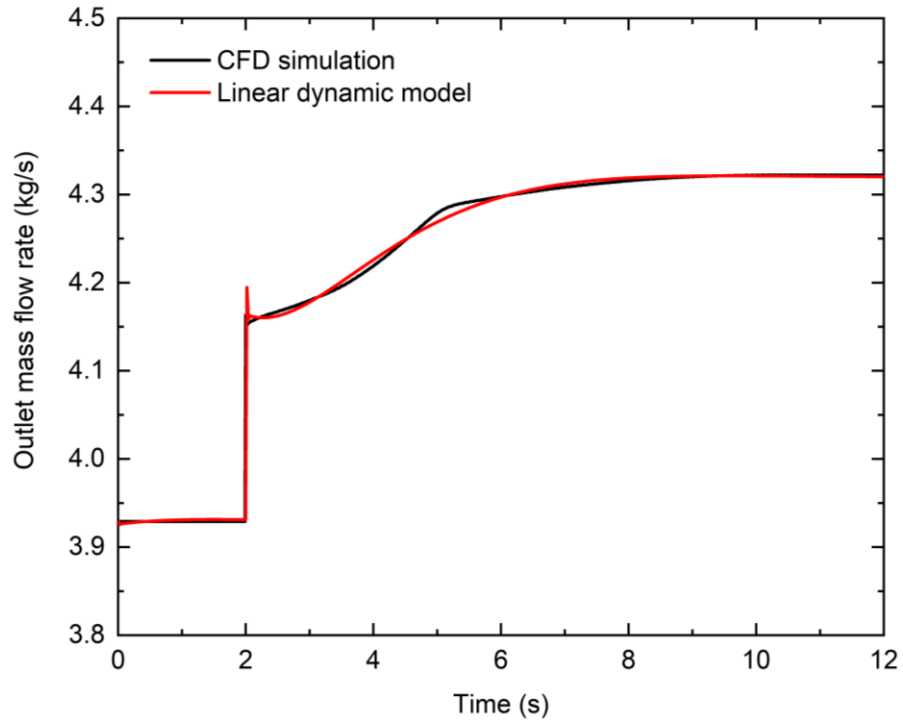
$$G_{r31}(s) = \frac{20.46s^4 + 281.9s^3 + 448.8s^2 + 909.5s + 211.8}{s^5 + 1.76s^4 + 5.969s^3 + 6.427s^2 + 4.194s + 1.101} \quad (6.13)$$

$$G_{r32}(s) = \frac{-3.388s^8 - 10.24s^7 - 162.5s^6 - 404.6s^5 - 1601s^4 - 2369s^3 - 977s^2 - 640.5s + 53.52}{s^9 + 1.862s^8 + 55.11s^7 + 80.76s^6 + 674s^5 + 588.6s^4 + 1118s^3 + 670.3s^2 + 389.8s + 9.111} \quad (6.14)$$

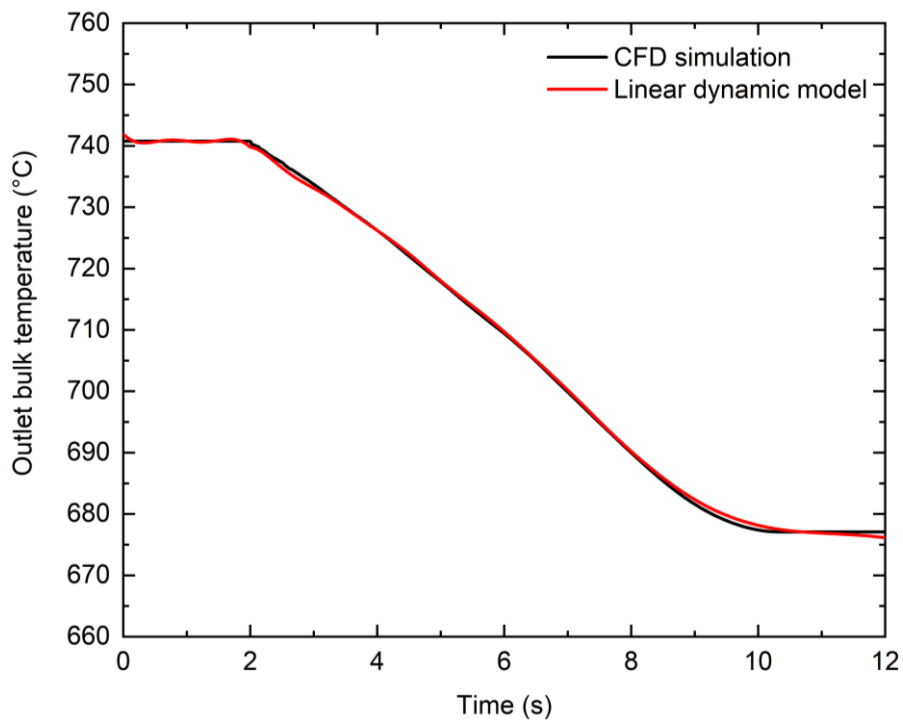
$$G_{r33}(s) = \frac{10^{-4}(73.78s + 7.294)}{s^6 + 4.655s^5 + 15.79s^4 + 20.64s^3 + 14.44s^2 + 7.749s + 0.7372} \quad (6.15)$$

6.3.3. Validation of transfer functions

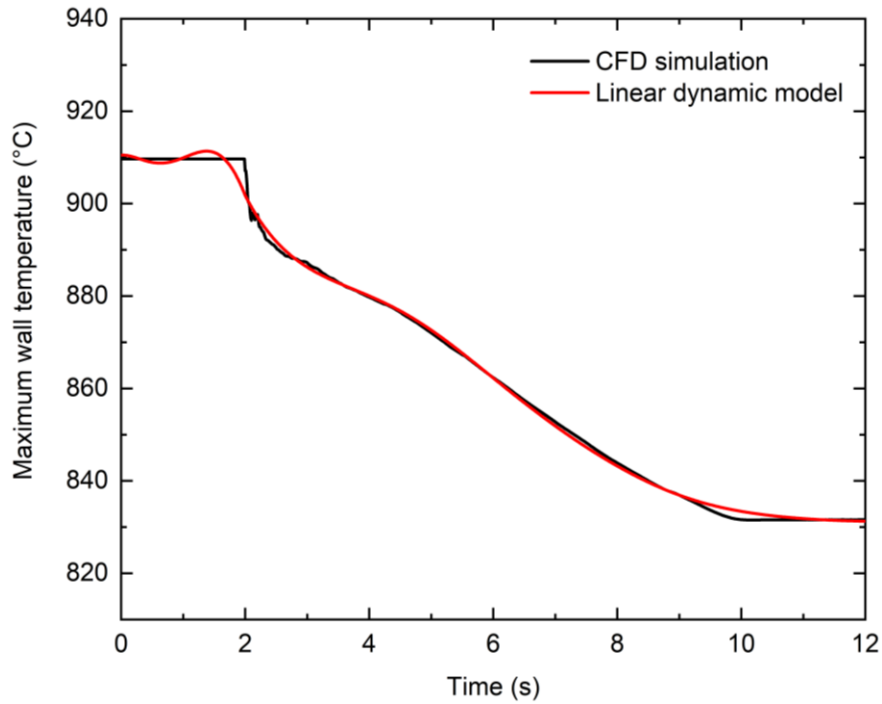
The above transfer functions derived from CFD simulations need to be evaluated whether they can characterize the dynamic behaviors of the nonlinear system around the design points. The dynamic responses generated by the linear dynamic model and results from transient CFD simulations are compared when inputs are subjected to step perturbations. Figs. 6.4 - 6.6 exhibit the comparisons at the conditions of step perturbations of inlet mass flow rate, inlet temperature, and heat flux, respectively.



(a) Outlet mass flow rate

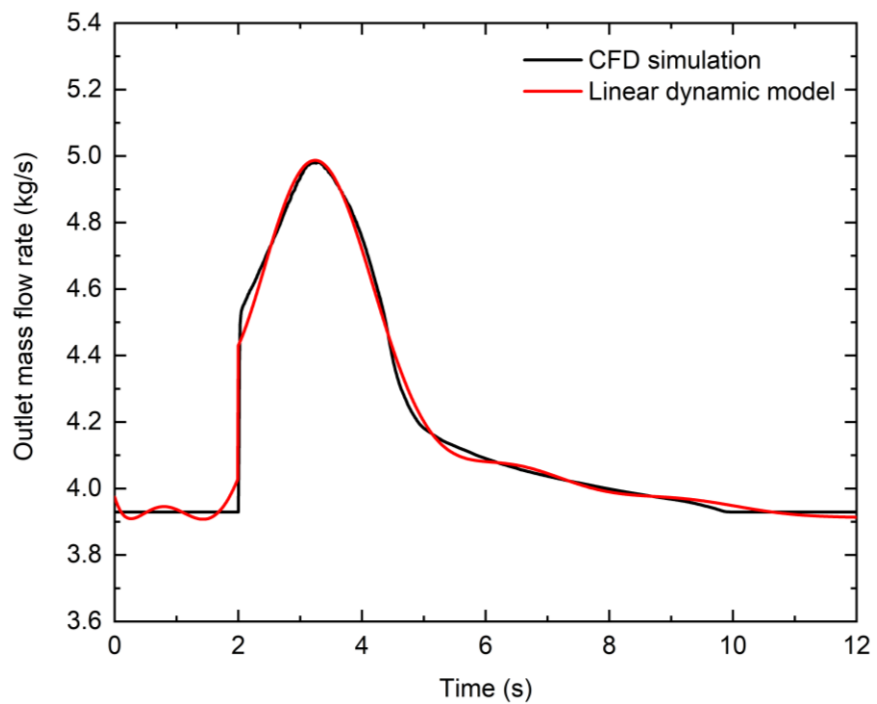


(b) Outlet bulk temperature

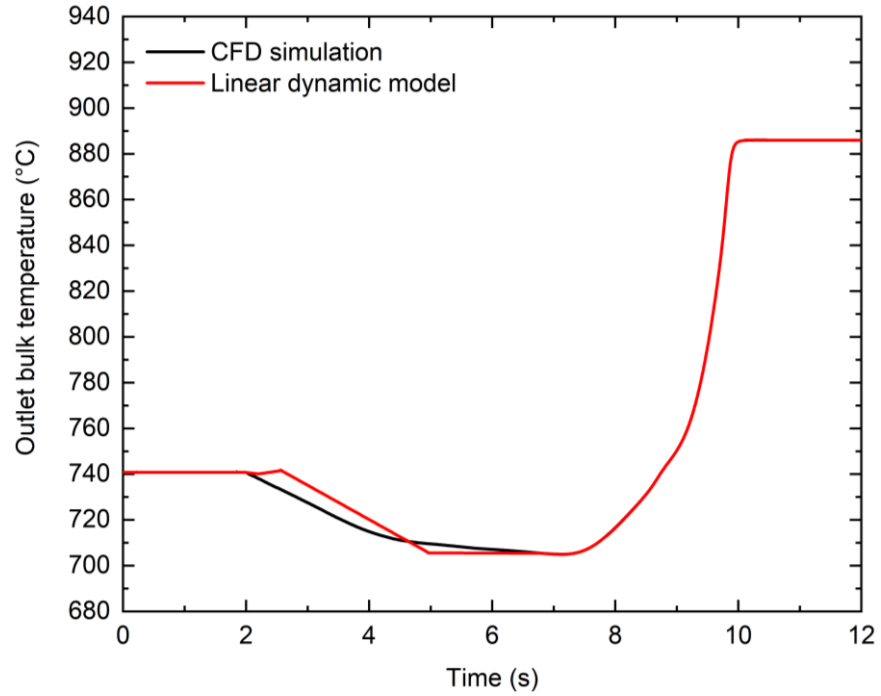


(c) Maximum wall temperature

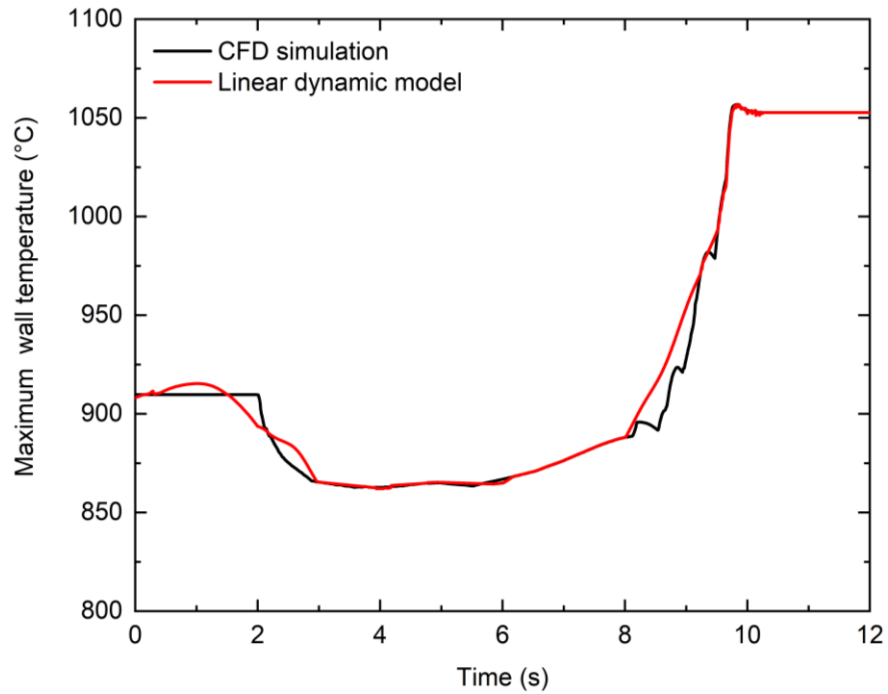
Figure 6.4: Comparison of responses obtained by CFD simulations and linear dynamic model with a perturbation in the inlet mass flow rate



(a) Outlet mass flow rate

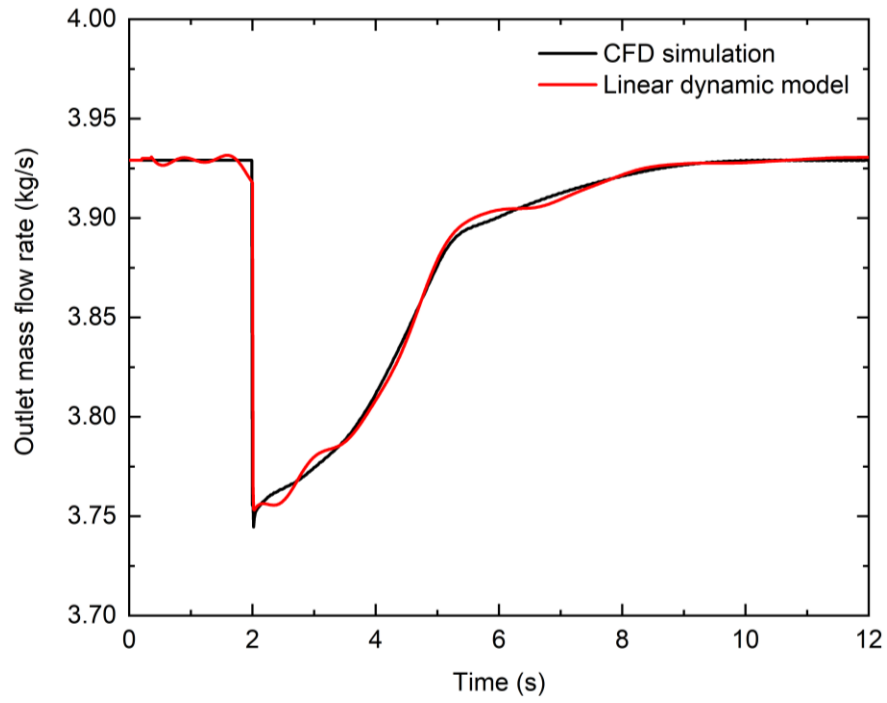


(b) Outlet bulk temperature

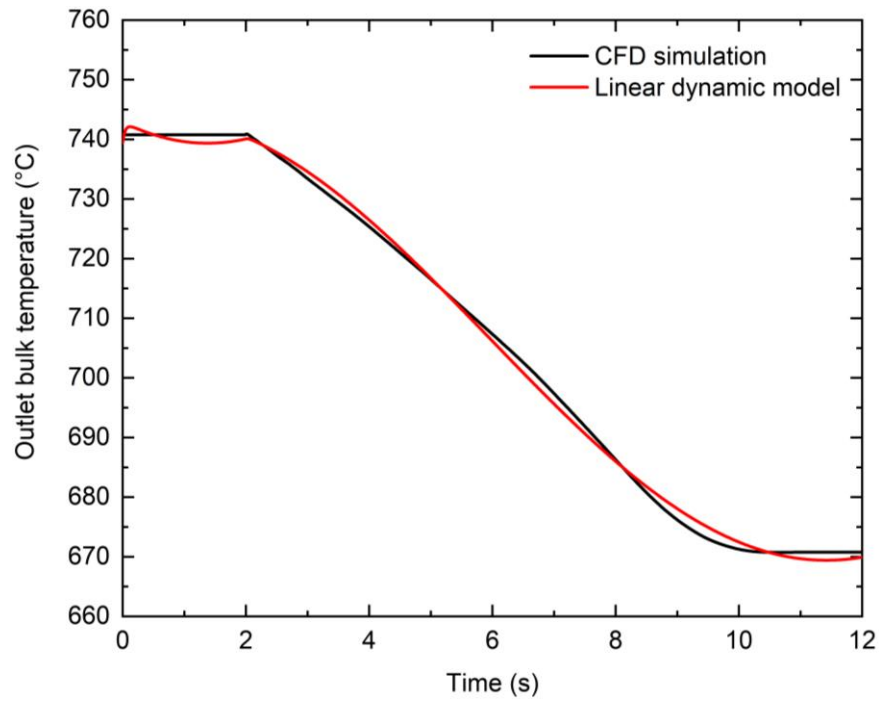


(c) Maximum wall temperature

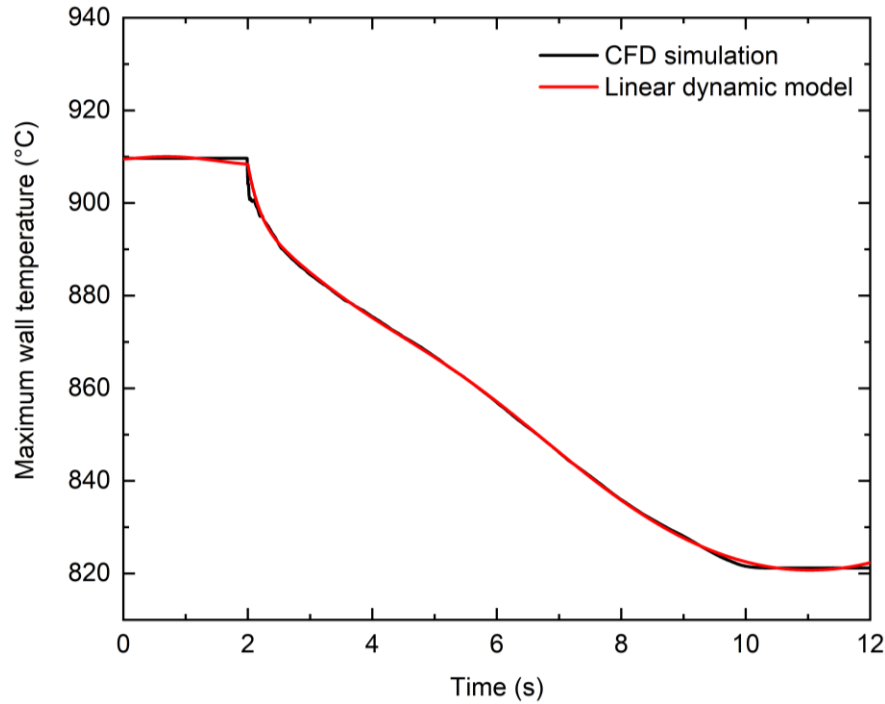
Figure 6.5: Comparison of responses obtained by CFD simulations and linear dynamic model with a perturbation in the inlet temperature



(a) Outlet mass flow rate



(b) Outlet bulk temperature



(c) Maximum wall temperature

Figure 6.6: Comparison of responses obtained by CFD simulations and linear dynamic model with a perturbation in the heat flux introduced

6.4. Design of the feedback control system

The objective of the feedback control system is to regulate outputs back to the design point in time when the fuel bundle is subjected to perturbations. As shown above, the fuel bundle has multiple inputs and outputs. When the perturbation is added to one input, all outputs will change. Therefore, the interaction degree of inputs and outputs at the steady state is investigated in this study, so that the most relevant input and output can be identified. The relative gain array (RGA) is commonly used to evaluate the cross-coupling between inputs and outputs of a system at the steady state condition [19, 20]. The RGA is the normalized form of the steady state gain matrix of a system, which describes the influence of an input on an output with respect to that on the rest outputs. The steady state gain matrix K_r of the fuel bundle is obtained from $G_{r(s)}$ as:

$$K_r = \begin{bmatrix} 0.9996 & 0.01 & 4.96 \times 10^{-6} \\ 160.23 & 2.22 & 8.54 \times 10^{-4} \\ 192.29 & 5.87 & 9.89 \times 10^{-4} \end{bmatrix} \quad (6.16)$$

Accordingly, the RGA of the system at the design point can be obtained as follows:

$$RGA_r = \begin{bmatrix} 1.37 & 0.00 & -0.37 \\ 0.00 & 0.98 & 0.02 \\ -0.37 & 0.02 & 1.35 \end{bmatrix} \quad (6.17)$$

Normally the relative gains of the respective input and output near 1 should be paired and negative relative gains should not be paired [20]. Therefore, the fuel bundle can be seen as a diagonally dominant system at the design point. The interaction between the respective input and output can be determined as: the outlet mass flow rate mainly depends on the inlet mass flow rate, the outlet temperature is determined primarily by the inlet temperature, and the maximum cladding temperature is affected most by the heat flux on the fuel rod. Consequently, the fuel bundle can be regarded as a multiple single-input-single-output (SISO) system. In the feedback control system, one PID controller is used for each most relevant input and output pair to regulate the corresponding output back to the design point. Therefore, three controllers are needed for this three-input and three-output system. To satisfy the purpose of regulating deviations to zero when the system is subjected to perturbations, PI/PID type controllers are selected. The general transfer function from of a PID controller could be expressed as [21]:

$$C_{(s)} = K_p + K_I/s + K_D s \quad (6.18)$$

where K_p , K_I , and K_D are the proportional, integral, and derivative gains. These gains are adjusted to satisfy the following design specifications: the overshoot is less than 15%, the rise time and settling time are both below 10 s. Table 6.3 shows these gains for the three controllers.

Table 6.3 Specifications of controllers

Controllers	K_p	K_I	K_D	Rising time (s)	Settling time (s)	Overshoot (%)
PI_1	0.7413	116.8418		0.0265	0.0763	5.16

PI_2	0.045	0.0902		9.06	6.23	10.2
PID_3	6.0910e+3	5.4748e+4	67.63598	0.221	2.26	14.2

6.5. Evaluation of the performance of the feedback control system

The block diagram of the feedback control system for the fuel bundle is presented in Fig. 6.7. Since the control system is constructed according to linear dynamic models, it is essential to evaluate the performance of the feedback control system at nonlinear conditions.

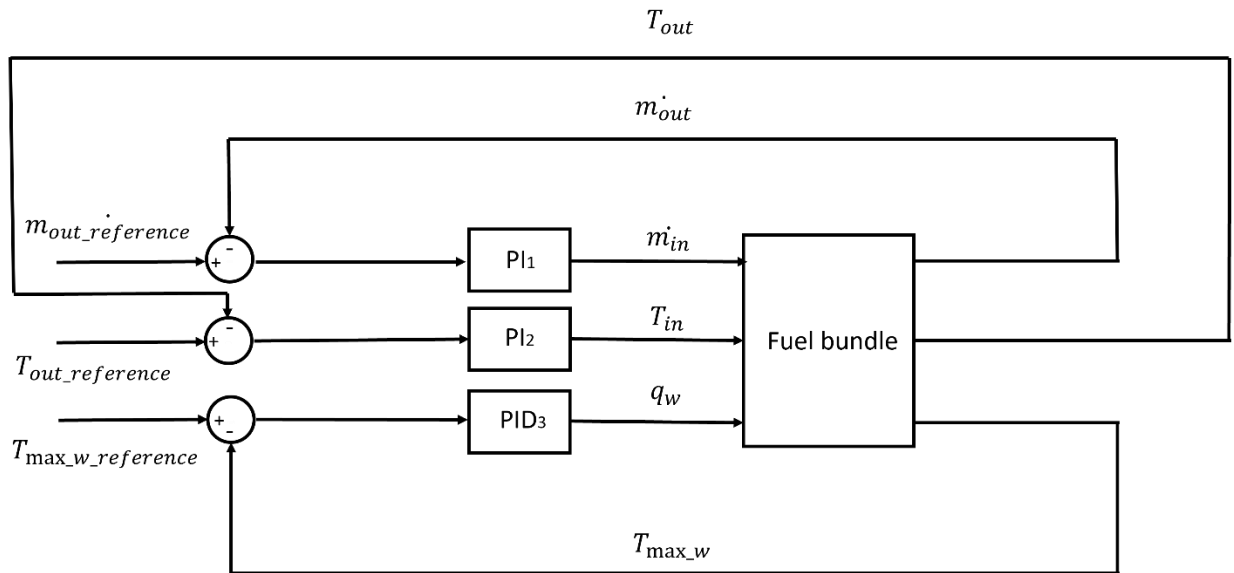


Figure 6.7: Block representation of the feedback control system

The performance evaluation is carried out through incorporating the feedback control system into the nonlinear transient CFD simulations. Controllers in the system are activated after the perturbation of the input has been held for 12 s. Then, the PID controllers are activated to regulate the system. This is carried out through embedding the designed control system into the transient CFD simulations through user-defined functions, which is given in the flowchart shown in Fig. 6.8. The deviations of the output results of the transient CFD

simulations from the design point values at each time step are taken as the input variables for the controllers and the outputs of the controllers are the inputs for the CFD simulations in the following time step. Therefore, the controllers and the transient CFD simulations form a closed loop. The time step size for transient CFD simulations and the sampling time interval of the control system are both 0.01 s. Figs. 6.9 - 6.11 show the responses of outputs from nonlinear CFD simulations when the system is subjected to the perturbation of the three inputs, respectively. It can be seen that the feedback control system can regulate outputs to design point in time at around 8 s.

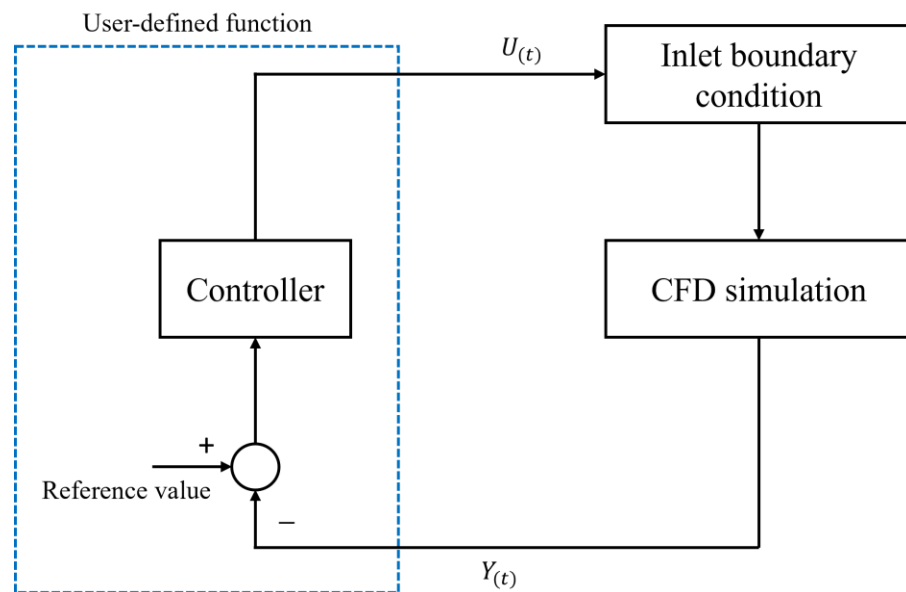
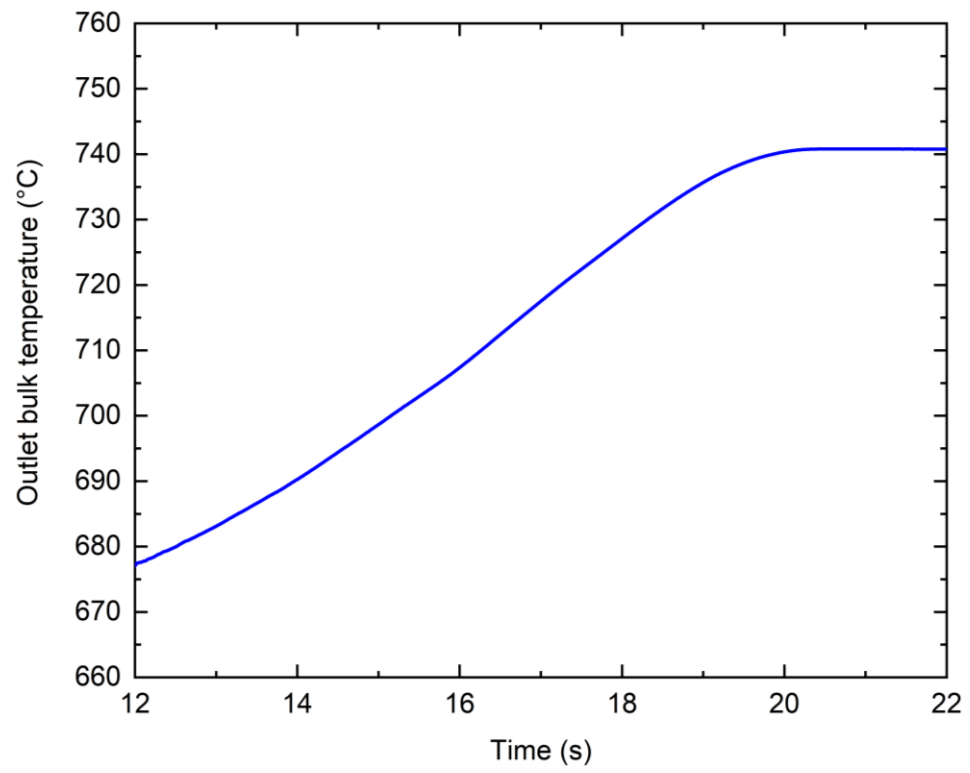
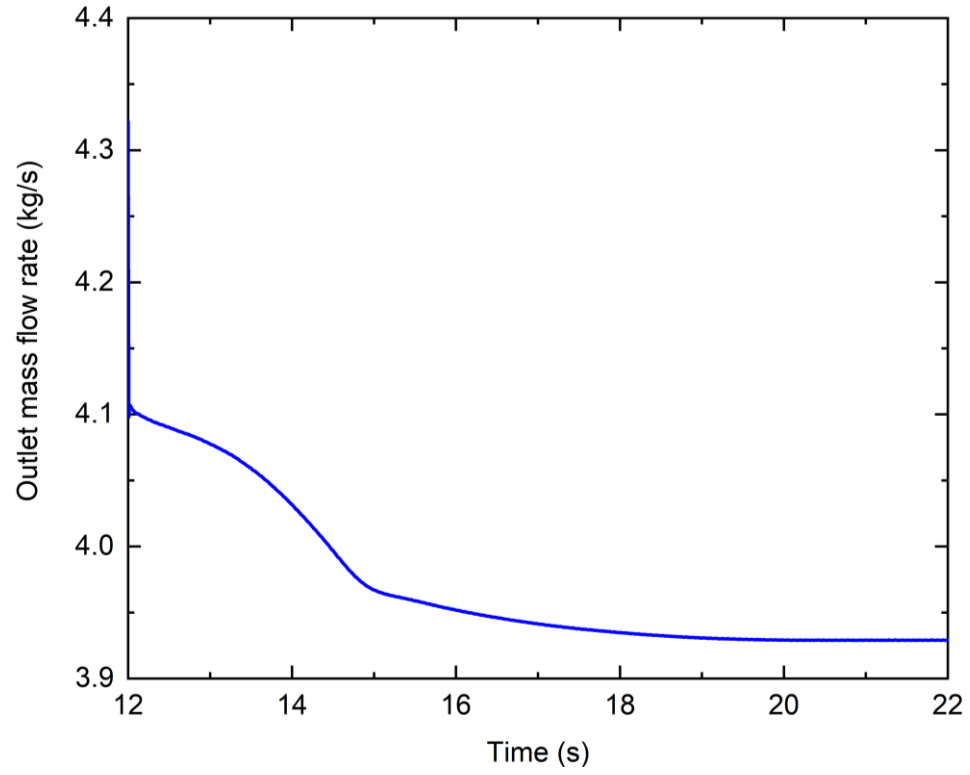


Figure 6.8: Flowchart of embedding controllers in the CFD simulations



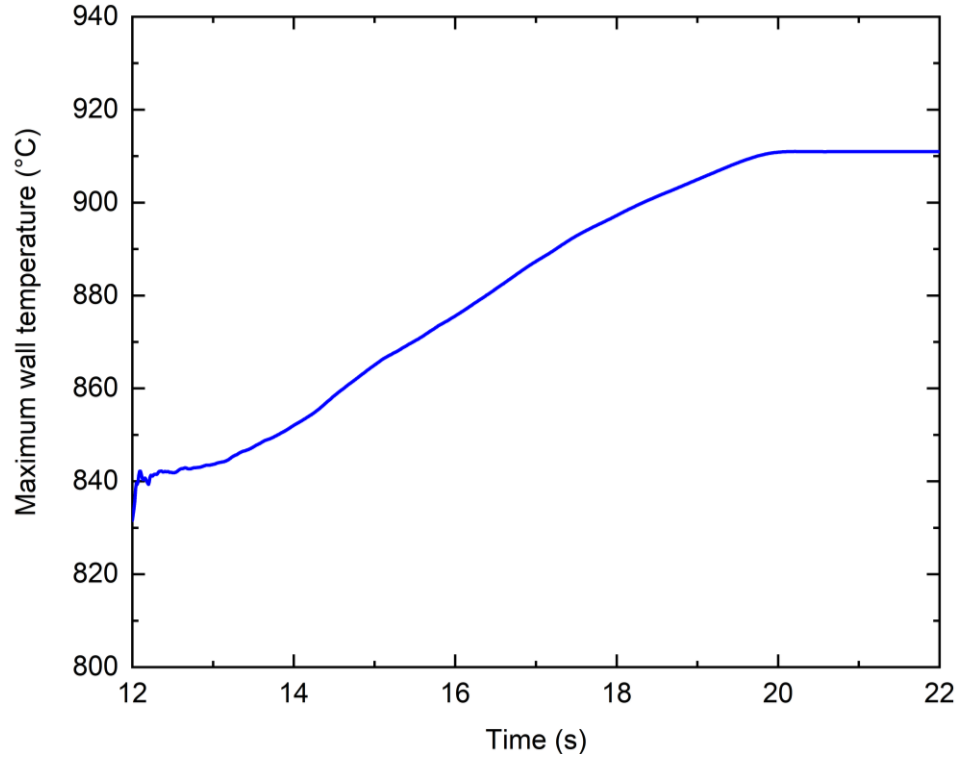
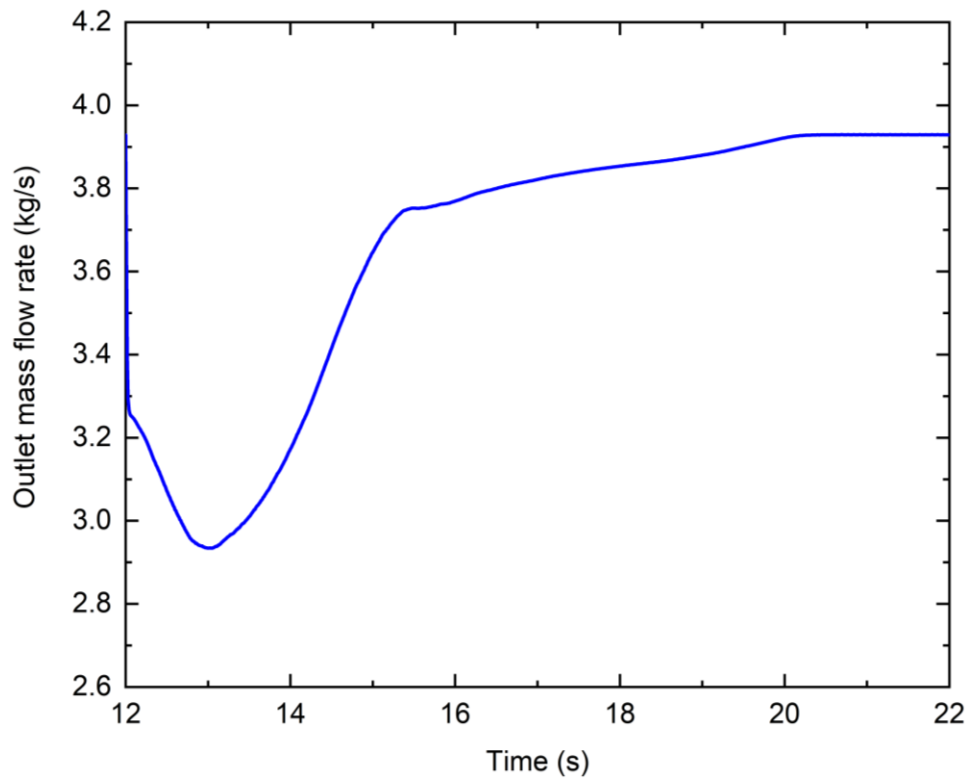


Figure 6.9: Output responses by CFD simulations when the system is subjected to the perturbation in the inlet mass flow rate



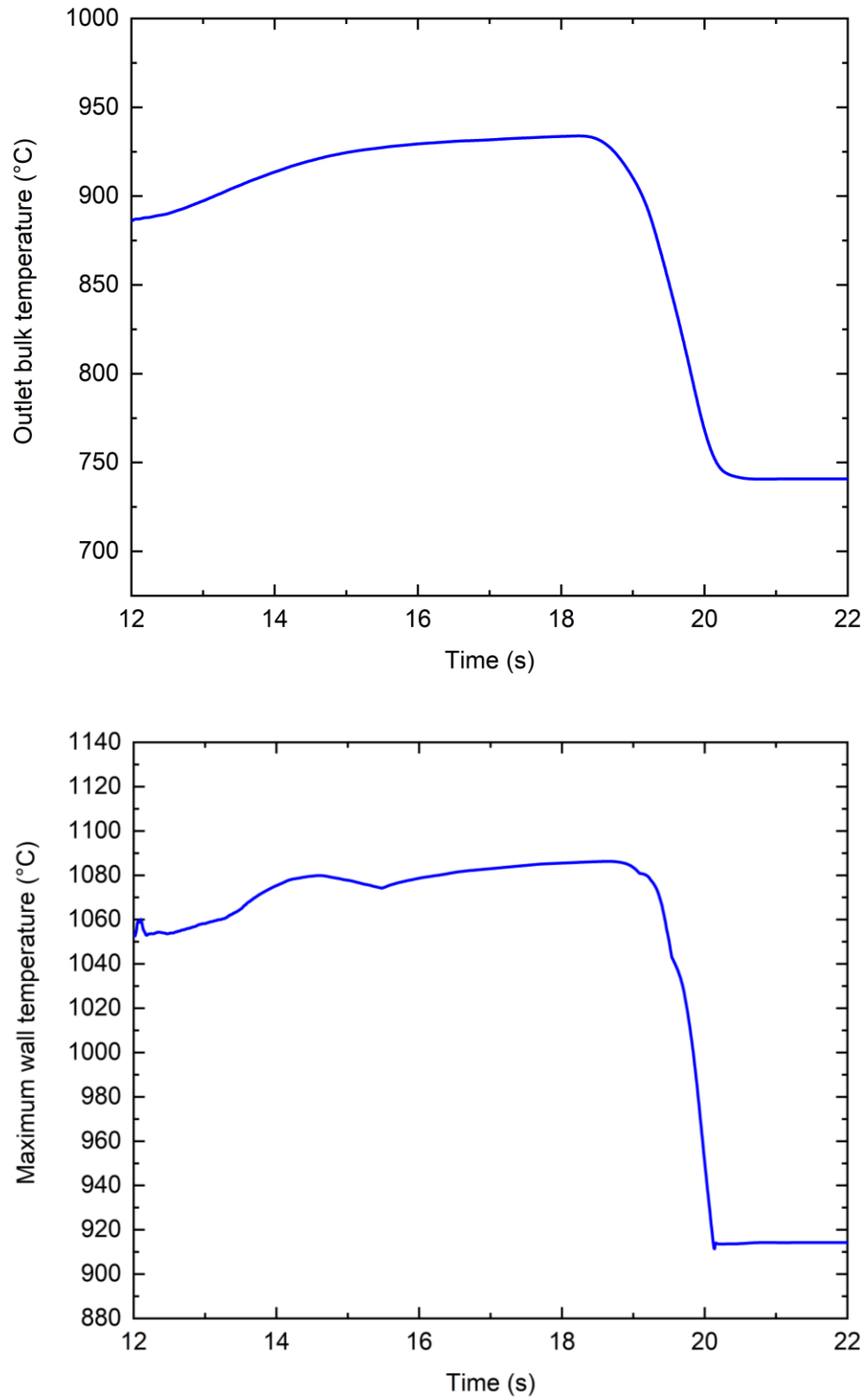
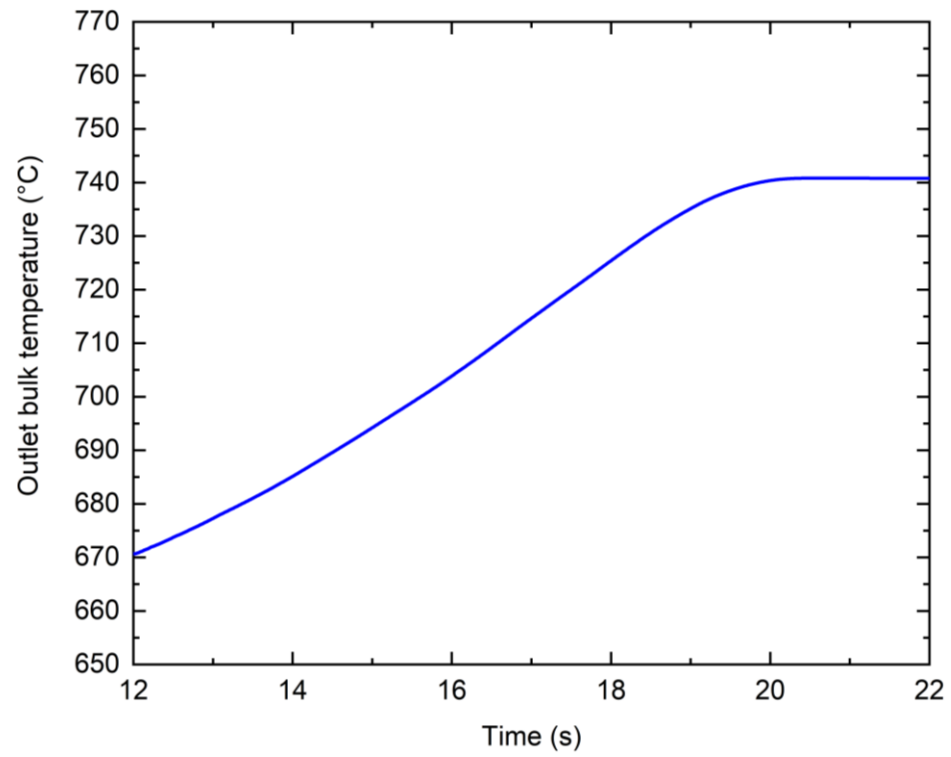
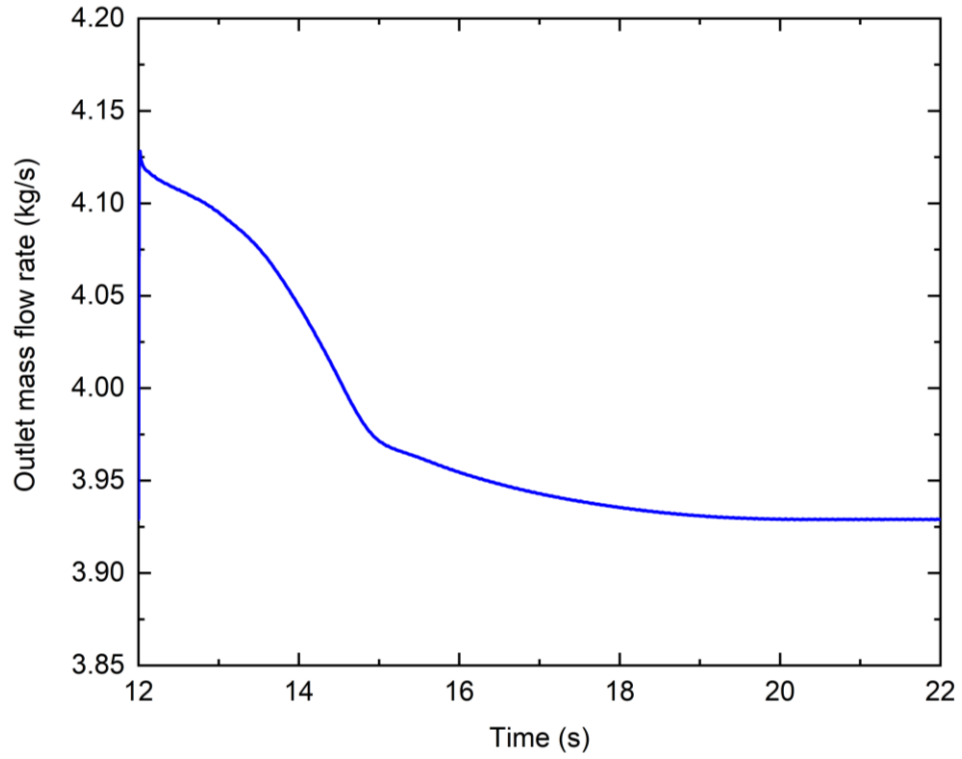


Figure 6.10: Output responses by CFD simulations when the system is subjected to the perturbation in the inlet temperature



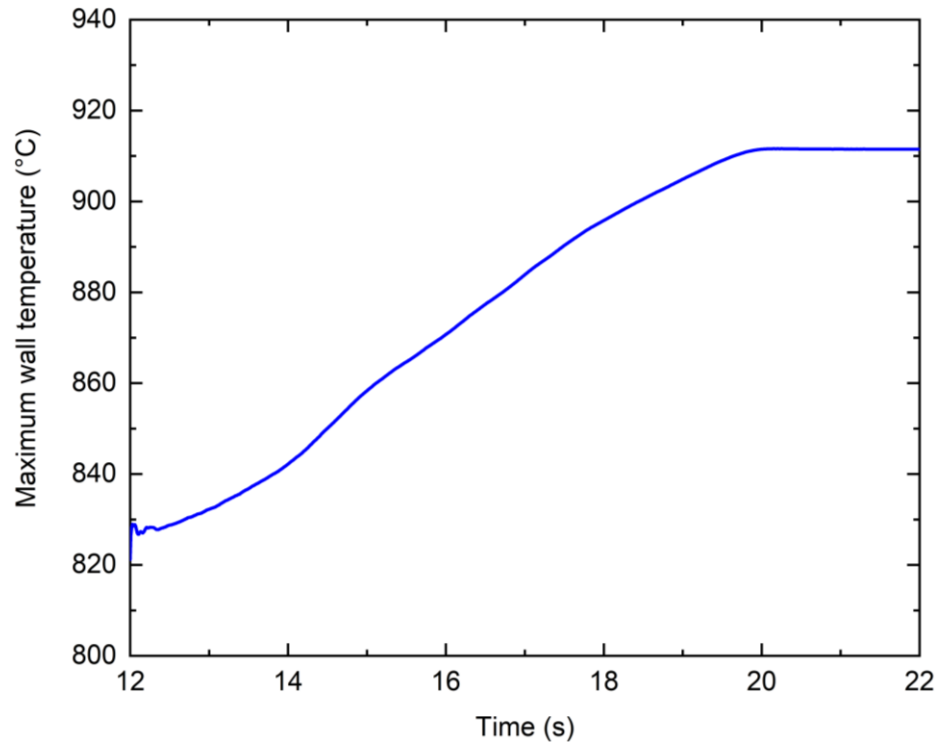


Figure 6.11: Output responses by CFD simulations when the system is subjected to the perturbation in the heat flux on the fuel rod

6.6. Conclusion

The knowledge of the dynamic behaviors of the fluid flow and heat transfer in the reactor is essential for safe operation. In this study, the feedback control system for the reactor is developed. The dynamic relationship between inputs and outputs of the reactor were obtained from transient CFD simulations, and then the results from the linear dynamic models are validated through the comparison of the results from nonlinear transient CFD simulations. Based on the linear dynamic models, three PID controllers are synthesized in the feedback control system to regulate the inputs for the SCWR so that the deviation of the SCWR outputs from the designed values could be minimized accordingly. In addition, the performance of the feedback control system was evaluated. The results showed that the control system can regulate the reactor to the design point in time when it is subjected to disturbances.

References

- [1] I. L. Pioro, Ed., *Handbook of Generation IV Nuclear Reactors*, 1st ed. Duxford, UK: Elsevier—Woodhead Publishing, 2016.
- [2] T. Nakatsuka, Y. Oka, and S. Koshizuka, “Control of a Fast Reactor Cooled by Supercritical Light Water,” *Nucl. Technol.*, vol. 121, no. 1, pp. 81–92, Jan. 1998.
- [3] Y. ISHIWATARI, Y. OKA, and S. KOSHIZUKA, “Control of a High Temperature Supercritical Pressure Light Water Cooled and Moderated Reactor with Water Rods,” *J. Nucl. Sci. Technol.*, vol. 40, no. 5, pp. 298–306, May 2003.
- [4] P. Sun, J. Jiang, and J. Shan, “Construction of dynamic model of CANDU-SCWR using moving boundary method,” *Nucl. Eng. Des.*, vol. 241, no. 5, pp. 1701–1714, May 2011.
- [5] P. Sun and J. Jiang, “Construction and Analysis of a Dynamic Model for a Canadian Direct-Cycle SCWR for Control System Studies,” *Nucl. Technol.*, vol. 180, no. 3, pp. 399–421, Dec. 2012.
- [6] P. Sun, J. Jiang, and K. Wang, “Decoupling Control of Canadian Supercritical Water-Cooled Reactors,” *Nucl. Technol.*, vol. 185, no. 3, pp. 239–258, 2014.
- [7] P. Sun, B. Wang, J. Zhang, and G. Su, “Control of Canadian once-through direct cycle supercritical water-cooled reactors,” *Ann. Nucl. Energy*, vol. 81, pp. 6–17, Jul. 2015.
- [8] P. Sun and J. Zhang, “Control strategy study for once-through direct cycle Canadian SCWRs,” *Prog. Nucl. Energy*, vol. 98, pp. 202–212, Jul. 2017.
- [9] R. V. Maitri, C. Zhang, and J. Jiang, “Computational fluid dynamic assisted control system design methodology using system identification technique for CANDU supercritical water cooled reactor (SCWR),” *Appl. Therm. Eng.*, vol. 118, pp. 17–22, 2017.

- [10] H. Han, C. Zhang, and J. Jiang, “Dynamic models and control system design for heated channels in a Canadian SCWR,” *Ann. Nucl. Energy*, vol. 151, p. 107973, Feb. 2021.
- [11] Q. Jiang, C. Zhang, and J. Jiang, “A CFD assisted control system design with applications to NO_x control in a FGR furnace,” *Combust. Theory Model.*, vol. 11, no. 3, pp. 469–481, 2007.
- [12] Q. Meng, Y. Wang, X. Yan, and Z. Li, “CFD assisted modeling for control system design: A case study,” *Simul. Model. Pract. Theory*, vol. 17, no. 4, pp. 730–742, 2009.
- [13] R. Zhang, C. Zhang, and J. Jiang, “A new approach to design a control system for a FGR furnace using the combination of the CFD and linear system identification techniques,” *Combust. Theory Model.*, vol. 15, no. 2, pp. 183–204, 2011.
- [14] M. Yetisir, H. Hamilton, R. Xu, M. Gaudet, D. Rhodes, M. King, K. Andrew, and B. Benson, “Fuel Assembly Concept of the Canadian Supercritical Water-Cooled Reactor,” *J. Nucl. Eng. Radiat. Sci.*, vol. 4, no. 1, pp. 1–7, Jan. 2018.
- [15] A. N. Domínguez, N. Onder, Y. Rao, and L. Leung, “EVOLUTION OF THE CANADIAN SCWR FUEL-ASSEMBLY CONCEPT AND ASSESSMENT OF THE 64 ELEMENT ASSEMBLY FOR THERMALHYDRAULIC PERFORMANCE,” *CNL Nucl. Rev.*, pp. 1–18, Jun. 2016.
- [16] ANSYS, “Ansys Fluent Theory Guide,” 2013.
- [17] H. Han and C. Zhang, “A Modified Turbulent Model for the Supercritical Water Flows in the Vertical Upward Channels,” *J. Supercrit. Fluids*, vol. 187, p. 105632, Aug. 2022.
- [18] L. Ljung, “System Identification Toolbox: User’s Guide, R2022a.”
- [19] E. Bristol, “On a new measure of interaction for multivariable process control,” *IEEE Trans. Automat. Contr.*, vol. 11, no. 1, pp. 133–134, Jan. 1966.

- [20] S. Skogestad and I. Postlethwaite, *Multivariable feedback control : analysis and design* , 2nd ed. Chichester, England ; John Wiley, 2005.
- [21] N. S. Nise, *Control systems engineering* , 5th ed. Hoboken, NJ: Wiley, 2008.

7. Construction of the Dynamic Model and Control System for the Canadian SCWR Power Plant

Nomenclature

Symbols

A_{CV}	Percentage of the control valve opening, %
G	Transfer function
G_{11}	Transfer function from the outlet plenum temperature to the feedwater flow rate
G_{12}	Transfer function from the outlet plenum temperature to the heat flux
G_{13}	Transfer function from the outlet plenum temperature to the control valve opening
G_{21}	Transfer function from the maximum wall temperature to the feedwater flow rate
G_{22}	Transfer function from the maximum wall temperature to the heat flux
G_{23}	Transfer function from the maximum wall temperature to control valve opening
G_{31}	Transfer function from the main steam pressure to the feedwater flow rate
G_{32}	Transfer function from the main steam pressure to the heat flux

G_{33}	Transfer function from the main steam pressure to the control valve opening
K_D	Derivative gain
K_I	Integral gain
K_P	Proportional gain
M	Mass flow rate, kg/s
P	Pressure, Pa
q	Heat flux, W/m ²
s	Complex variable in Laplace transform
T	Temperature, °C

Subscripts

c	Condenser
CV	Control valve
FP	Feedwater Pump
MSL	Main Steam Line
OP	Outlet Plenum
in	Inlet
R	Reactor
T	Turbine
W	Wall
max	Maximum

Acronyms

CANDU	Canada Deuterium Uranium
CFD	Computational Fluid Dynamics
LWR	Light Water-Cooled Reactor
RGA	Relative Gain Array
SCFPP	Supercritical Fossil-Fueled Power Plant
SCFR	Supercritical Water-Cooled Fast Reactor
SCWR	Supercritical Water-Cooled Reactor
SISO	Single-Input-Single-Output

7.1.Introduction

The interest in the nuclear power plant has increased in recent years due to the increasing power demand and adverse effects of climate change caused by fossil fuels. The supercritical water-cooled nuclear reactor (SCWR) was one of the six concepts which were proposed as the Generation IV reactors [1]. Following the maturation of technologies in the existing light water-cooled reactors (LWRs) and supercritical fossil-fueled power plants (SCFPPs), the SCWRs are under development in the past decade. The Canadian SCWR is a heavy water-moderated and supercritical light water-cooled reactor. To achieve a higher power conversion efficiency (>45%), it operates at 25 MPa. The fuel bundle in the reactor includes a two-ring 64-element fuel rods [2].

In the SCWR power plant, the supercritical water is heated in the reactor and sent to the turbine directly. The heat balance between the reactor and the turbine is regulated by the pressure of the main steam since the temperature of the main steam needs to be kept constant in the normal operation. If the reactor power is a little bit too high the steam pressure will rise. In the nuclear power plant, mainly two plant control strategies are used: the reactor-following-turbine and the turbine-following-reactor operations [3]. In the reactor-following-turbine operation mode, the pressure of the main steam is controlled by the reactor while the turbine control valve regulates the electric power. In this operation mode, the reactor needs to respond rapidly to load changes. When the changes are sharp, the fluctuating flow rate of the steam may lead to the considerable variations of temperatures in the reactor, such as the temperature of the cladding surface around the fuel rods, which will affect the safety of the reactor. In the turbine-following-reactor mode, the pressure of the main steam is controlled by the turbine control valve and the electric power is controlled by the reactor power. The function of the turbine control valve is to adjust the steam flow rate into the turbine. When the control valve opening is increased, the main steam flow rate increases, and then the pressure and the temperature of the main steam will decrease. Although the response to load changes in this operation mode is slower than the former mode, the reactor power plant can run relatively stably. Therefore, this operation mode is used in this work.

A few studies on the control system design for SCWR power plants have been conducted [4–10]. The turbine-following-reactor operation mode was used in the previous studies by Nakatsuka et al. [3, 4] for the control system designs for the supercritical water-cooled fast reactor (SCFR) and the supercritical high temperature thermal reactor power plants. Sun [5] constructed a linear dynamic model for the Canada Deuterium Uranium (CANDU) SCWR system. Based on the linear dynamic model, the dynamic characteristics of the control system and the coupling analysis between different inputs and outputs of the system were presented. Sun et al. then attempted to use different control methods, such as the use of feedback controllers, feedforward controllers [6, 7], the hybrid feedback and feedforward control strategy [8] to improve the performance of the control system. In addition, a linear parameter-varying strategy was also proposed by Sun et al. [9] to obtain satisfactory performance of the control system at different operating conditions. In the above studies, the model of the reactor is simplified as a one-dimensional thermal system. However, the fluid flow and heat transfer in the power plant system are three-dimensional. Therefore, the reactor model should be improved further based on three-dimensional flow and heat transfer characteristics of the thermal system. Maitri et al. [10] and Han et al. [11] proposed the two-dimensional and three-dimensional models for the CANDU supercritical water-cooled reactor, respectively. Based on the 64-element SCWR [2], Han and Zhang [12] also proposed a linear dynamic model of the reactor which was constructed based on the full scale three-dimensional computational fluid dynamics (CFD) simulations of the supercritical water flow and heat transfer in the rod channels.

In this study, the linear dynamic model of the 64-element Canadian SCWR power plant is first constructed. Based on the linear dynamic model, the dynamic responses of the outputs of system when it is subjected to variations of the inputs are evaluated. Then, the feedback controllers are designed for the control system and the evaluation of the performance of the designed control system is carried out.

7.2. Configuration of the Canadian SCWR power plant

Fig. 7.1 exhibits the diagram of the simplified Canadian SCWR power plant and Table 7.1 shows the operating condition at the design point. The supercritical coolant goes into the fuel assembly in the reactor core. In the fuel assembly, the supercritical water flows downward through a central flow tube and then reversely upward through the fuel elements in the fuel bundle. After the water absorbs the heat generated by nuclear fission in fuel rods, it flows into the turbine through the outlet header. After the turbine, the working fluid flows into the condenser. Then, the feedwater from the condenser is pumped back to the reactor, as shown in Fig. 7.1. In order to operate the reactor at a relatively stable mode, the control strategy used in this study is the turbine-following-reactor operation. The main steam from the nuclear reactor drives the turbine, and the control valve of the turbine is used to adjust the main steam flow rate going into the turbine and keep the pressure of the main steam as the design point.

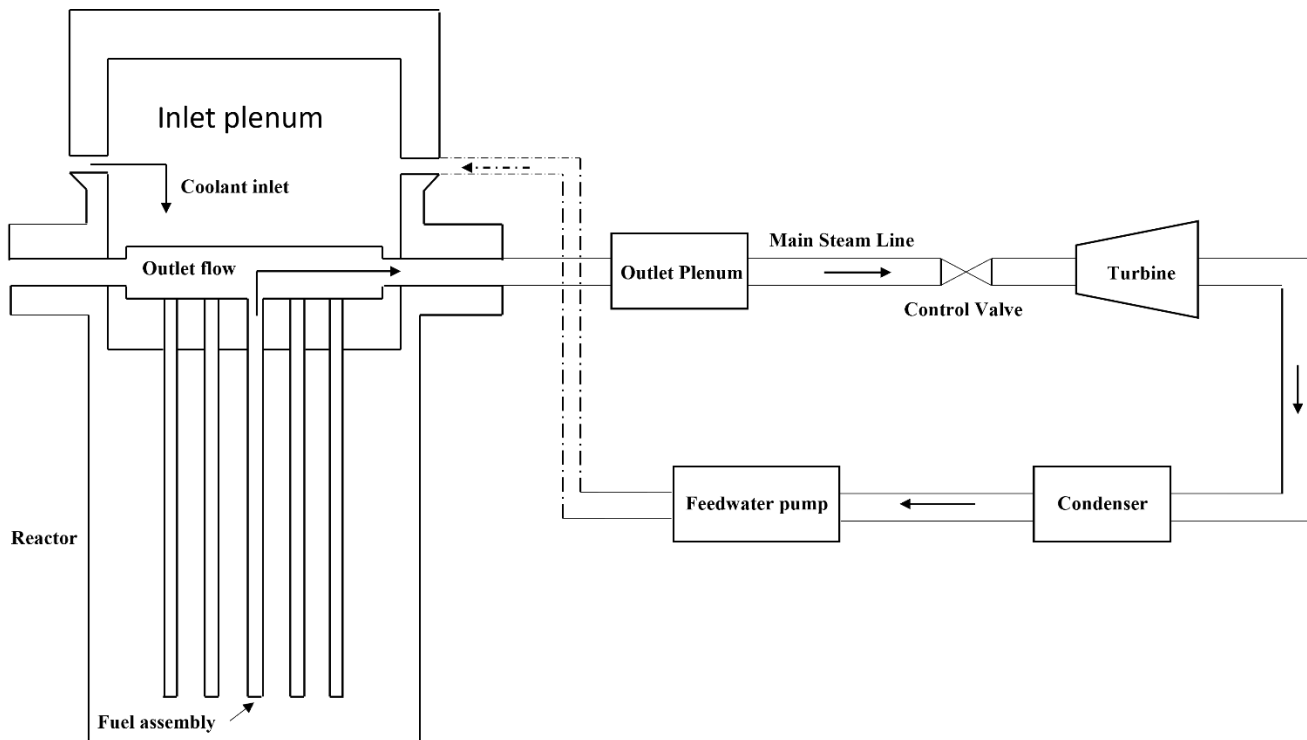


Figure 7.1: Diagram of the Canadian SCWR power plant

Table 7.1 Specifications of the Canadian SCWR

Thermal power	2540 MW
Flow rate	1320 kg/s
Number of channels	336
Inlet temperature	350°C
Operating pressure	25 MPa
Heated length	5 m

7.3. Construction of the dynamic model for the Canadian SCWR power plant

In order to construct the dynamic model for the SCWR power plant, the dynamic models are needed for all components in the SCWR power plant.

7.3.1. Linear dynamic models for each component

7.3.1.1. Feedwater pump

The transfer function of the dynamic model of the feedwater pump can be expressed as [5]:

$$G_{FP,P(s)} = \frac{\delta M_{FP,P(s)}}{\delta P_C(s)} = -39.6 \quad (7.19)$$

where $M_{FP,P}$ is the change of mass flow rate of the feedwater contributed by the pressure of condenser P_C .

7.3.1.2. Reactor

The transfer function of the reactor model is from the previous work [12]:

$$G_R(s) = \begin{bmatrix} \frac{\delta M_R(s)}{\delta M_{FP(s)}} & \frac{\delta M_R(s)}{\delta T_{in(s)}} & \frac{\delta M_R(s)}{\delta q(s)} \\ \frac{\delta T_R(s)}{\delta M_{FP(s)}} & \frac{\delta T_R(s)}{\delta T_{in(s)}} & \frac{\delta T_R(s)}{\delta q(s)} \\ \frac{\delta T_{W_max}(s)}{\delta M_{FP(s)}} & \frac{\delta T_{W_max}(s)}{\delta T_{in(s)}} & \frac{\delta T_{W_max}(s)}{\delta q(s)} \end{bmatrix} \quad (7.20)$$

$$\frac{\delta M_{R(s)}}{\delta M_{FP(s)}} = \frac{42.95s^2 + 52.54s + 44.28}{s^3 + 68.48s^2 + 96.16s + 44.29} \quad (7.21)$$

$$\frac{\delta M_{R(s)}}{\delta T_{in(s)}} = \frac{0.01139s^5 + 0.02959s^4 + 0.1029s^3 + 0.1088s^2 + 0.1427s + 0.03218}{s^5 + 2.707s^4 + 8.535s^3 + 10.62s^2 + 10.94s + 3.182} \quad (7.22)$$

$$\frac{\delta M_{R(s)}}{\delta q(s)} = \frac{0.0004862s^8 + 0.002397s^7 + 0.03164s^6 + 0.1042s^5 + 0.5411s^4 + 1.088s^3 + 2.705s^2 + 2.906s + 1.057}{s^9 + 262.7s^8 + 1501s^7 + 1.655 \times 10^4 s^6 + 5.982 \times 10^4 s^5 + 2.491 \times 10^5 s^4 + 4.864 \times 10^5 s^3 + 8.496 \times 10^5 s^2 + 7.166 \times 10^5 s + 2.13 \times 10^5} \quad (7.23)$$

$$\frac{\delta T_{R(s)}}{\delta M_{FP(s)}} = \frac{-35.43s^6 - 50.78s^5 - 797.6s^4 - 170s^3 - 1537s^2 + 5183s + 3600}{s^7 + 4.627s^6 + 30.51s^5 + 92.96s^4 + 175.4s^3 + 202.8s^2 + 53.42s + 22.47} \quad (7.24)$$

$$\frac{\delta T_{R(s)}}{\delta T_{in(s)}} = \frac{166.2s^{15} + 6078s^{14} + 1.071 \times 10^4 s^{13} + 3.949 \times 10^5 s^{12} + 1.82 \times 10^5 s^{11} + 7.999 \times 10^6 s^{10} + 9.215 \times 10^5 s^9 + 6.96 \times 10^7 s^8 - 1.624 \times 10^6 s^7 + 2.763 \times 10^8 s^6 - 2.191 \times 10^7 s^5 + 4.669 \times 10^8 s^4 - 4.11 \times 10^7 s^3 + 2.655 \times 10^8 s^2 - 1.392 \times 10^7 s + 2.132 \times 10^7}{s^{19} + 13.11s^{18} + 179.1s^{17} + 1429s^{16} + 1.043 \times 10^4 s^{15} + 5.761 \times 10^4 s^{14} + 2.716 \times 10^5 s^{13} + 1.101 \times 10^6 s^{12} + 3.575 \times 10^6 s^{11} + 1.11 \times 10^7 s^{10} + 2.46 \times 10^7 s^9 + 6.09 \times 10^7 s^8 + 8.591 \times 10^7 s^7 + 1.767 \times 10^8 s^6 + 1.376 \times 10^8 s^5 + 2.429 \times 10^8 s^4 + 7.938 \times 10^7 s^3 + 1.215 \times 10^8 s^2 + 6.714 \times 10^6 s + 9.625 \times 10^6} \quad (7.25)$$

$$\frac{\delta T_{R(s)}}{\delta q(s)} = \frac{10^{-4}(2.576 s^3 + 6.862s^2 + 4.012s + 2.553)}{s^4 + 2.373s^3 + 2.146s^2 + 1.093s + 0.299} \quad (7.26)$$

$$\frac{\delta T_{W_max(s)}}{\delta M_{FP(s)}} = \frac{20.46s^4 + 281.9s^3 + 448.8s^2 + 909.5s + 211.8}{s^5 + 1.76s^4 + 5.969s^3 + 6.427s^2 + 4.194s + 1.101} \quad (7.27)$$

$$\frac{\delta T_{W_max(s)}}{\delta T_{in(s)}} = \frac{-3.388s^8 - 10.24s^7 - 162.5s^6 - 404.6s^5 - 1601s^4 - 2369s^3 - 977s^2 - 640.5s + 53.52}{s^9 + 1.862s^8 + 55.11s^7 + 80.76s^6 + 674s^5 + 588.6s^4 + 1118s^3 + 670.3s^2 + 389.8s + 9.111} \quad (7.28)$$

$$\frac{\delta T_{W_max(s)}}{\delta q(s)} = \frac{10^{-4} (73.78s + 7.294)}{s^6 + 4.655s^5 + 15.79s^4 + 20.64s^3 + 14.44s^2 + 7.749s + 0.7372} \quad (7.29)$$

7.3.1.3. Outlet plenum

The outlet plenum in this study consists of the outlet feeders and outlet header. 336 fuel channels are assembled in the reactor. Therefore, 336 outlet feeders connect the reactor to one outlet header. The transfer function of the outlet plenum is given as [5]:

$$G_{OP(s)} = \begin{bmatrix} \frac{\delta T_{OP(s)}}{\delta T_{R(s)}} & \frac{\delta T_{OP(s)}}{\delta M_{R(s)}} \\ \frac{\delta M_{OP(s)}}{\delta T_{R(s)}} & \frac{\delta M_{OP(s)}}{\delta M_{R(s)}} \end{bmatrix} = \begin{bmatrix} \frac{3.2292}{(s+0.69)(s+4.68)} & 0 \\ \frac{1.14s^2 + 0.7866s + 0.034866}{(s+0.69)(s+4.68)} & 336 \end{bmatrix} \quad (7.30)$$

where T_{OP} and M_{OP} are outlet temperature and outlet mass flow rate of the outlet plenum respectively.

7.3.1.4. Main steam line

The main steam line connects the reactor and the turbine, therefore, the variations of the temperature and the mass flow rate of the outlet plenum in the reactor will affect the temperature and the pressure of the main steam line. The transfer function of the main steam line between the reactor and turbine is shown as [5]:

$$G_{MSL(s)} = \begin{bmatrix} \frac{\delta T_{MSL(s)}}{\delta T_{OP(s)}} & \frac{\delta T_{MSL(s)}}{\delta M_{OP(s)}} & \frac{\delta T_{MSL(s)}}{\delta M_{MSL(s)}} \\ \frac{\delta P_{MSL(s)}}{\delta T_{OP(s)}} & \frac{\delta P_{MSL(s)}}{\delta M_{OP(s)}} & \frac{\delta P_{MSL(s)}}{\delta M_{MSL(s)}} \end{bmatrix} = \begin{bmatrix} \frac{0.7}{s+0.7} & 0 & 0 \\ \frac{3 \times 10^{-2}}{s+0.7} & \frac{1.31 \times 10^{-2}}{s} & -\frac{1.31 \times 10^{-2}}{s} \end{bmatrix} \quad (7.31)$$

where T_{MSL} and P_{MSL} are temperature and pressure of the main steam respectively.

7.3.1.5. Turbine control valve

When the heat in the reactor is a bit too high, the pressure of the main steam will go up. In the turbine-following-reactor control strategy, the opening of the control valve needs to be larger to increase the main steam flow rate, so that the pressure of main steam can be regulated back to the design point. The transfer function of the control valve is described as [5]:

$$G_{CV(s)} = \begin{bmatrix} \frac{\delta M_{MSL(s)}}{\delta A_{CV(s)}} & \frac{\delta M_{MSL(s)}}{\delta T_{MSL(s)}} & \frac{\delta M_{MSL(s)}}{\delta P_{MSL(s)}} \end{bmatrix} = \begin{cases} [2640 & -0.37 & 26.74] & A_{CV} \leq 50\% \\ [792 & -0.37 & 26.74] & A_{CV} > 50\% \end{cases} \quad (7.32)$$

where A_{CV} is the percentage of the control valve opening and M_{MSL} is the mass flow rate of the main steam, respectively.

7.3.1.6. Turbine and condenser

In this study, we assume the pressure in the condenser is constant. The transfer functions of the turbine and condenser are given as [14]:

$$G_T(s) = \left[\frac{\delta P_T(s)}{\delta P_{MSL}(s)} \right] = [2.68 \times 10^{-4}] \quad (7.33)$$

$$G_C(s) = \left[\frac{\delta P_C(s)}{\delta P_T(s)} \right] = [1] \quad (7.34)$$

where P_T and P_C are pressures of the turbine and the condenser, respectively.

7.3.2. Linear dynamic model for the SCWR power plant

The block diagram of the linear dynamic model for the Canadian SCWR power plant is shown in Fig. 7.2. The inputs of the dynamic model are the feedwater flow rate, heat flux on the fuel rod, and the opening percentage of the control valve. The outputs of the dynamic model are the outlet temperature of the outlet plenum, the maximum wall temperature of the fuel rods, and the pressure of the main steam.

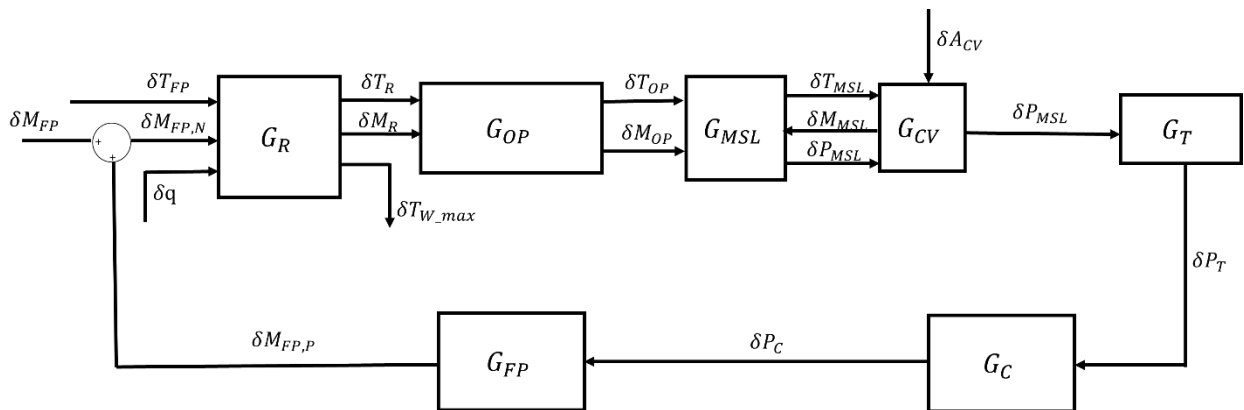


Figure 7.2: Block diagram of the linear dynamic model for the Canadian SCWR power plant

The relationship between inputs and outputs of the Canadian SCWR power plant is:

$$\begin{bmatrix} \delta T_{OP} \\ \delta T_{W_max} \\ P_{MSL} \end{bmatrix} = \begin{bmatrix} G_{11} & G_{12} & G_{13} \\ G_{21} & G_{22} & G_{23} \\ G_{31} & G_{32} & G_{33} \end{bmatrix} \begin{bmatrix} \delta M_{FP} \\ \delta q \\ \delta A_{CV} \end{bmatrix} \quad (7.35)$$

where the transfer functions of the linear dynamic model are presented in the following:

$$G_{11} = \frac{-35.43s^6 - 50.78s^5 - 797.6s^4 - 170s^3 - 1537s^2 + 5183s + 3600}{s^7 + 4.627s^6 + 30.51s^5 + 92.96s^4 + 175.4s^3 + 202.8s^2 + 53.42s + 22.47} \quad (7.36)$$

$$G_{12} = \frac{10^{-4}(8.318s^3 + 22.16s^2 + 12.96s + 8.244)}{s^6 + 7.743s^5 + 18.12s^4 + 20.28s^3 + 13.1s^2 + 5.135s + 0.9655} \quad (7.37)$$

$$G_{13} = 0 \quad (7.38)$$

$$G_{21} = \frac{20.46s^4 + 281.9s^3 + 448.8s^2 + 909.5s + 211.8}{s^5 + 1.76s^4 + 5.969s^3 + 6.427s^2 + 4.194s + 1.101} \quad (7.39)$$

$$G_{22} = \frac{7.378 \times 10^{-3}s + 7.294 \times 10^{-4}}{s^6 + 4.655s^5 + 15.79s^4 + 20.64s^3 + 14.44s^2 + 7.749s + 0.7372} \quad (7.40)$$

$$G_{23} = 0 \quad (7.41)$$

$$G_{31} = \frac{0.9309s^2 + 1.139s + 0.9595}{s^3 + 68.48s^2 + 96.16s + 44.29} \quad (7.42)$$

$$G_{32} = 0 \quad (7.43)$$

$$G_{33} = \frac{-34.45s^{13} - 742s^{12} - 6111s^{11} - 2.432 \times 10^4s^{10} - 4.924 \times 10^4s^9 - 5.107 \times 10^4s^8 - 2.815 \times 10^4s^7 - 8546s^6 - 1530s^5 - 163.8s^4 - 10.05s^3 - 0.3163s^2 - 3.854 \times 10^{-3}s - 2.145 \times 10^{-6}}{s^{14} + 22.22s^{13} + 194.4s^{12} + 856.7s^{11} + 2043s^{10} + 2711s^9 + 2068s^8 + 974.2s^7 + 276s^6 + 48.01s^5 + 5.096s^4 + 0.3125s^3 + 9.872 \times 10^{-3}s^2 + 1.21 \times 10^{-4}s + 6.755 \times 10^{-8}} \quad (7.44)$$

7.4. Evaluation of the dynamic model for Canadian SCWR power plant

7.4.1. Dynamic characteristics of the open-loop system

In order to capture the dynamic behaviors of the system when it is subjected to disturbances, the output responses are obtained when a $\pm 5\%$ step perturbation is added at each input and other two inputs hold at the design point values. Figs. 7.3 - 7.5 present the changes of the three outputs of the system due to the disturbances of the inputs, respectively.

7.4.1.1. Step increase in the feedwater flow rate

The heat flux and the control valve opening are kept unchanged when a 5% step decrease is added in the feedwater flow rate. From Figs. 7.3 - 7.5, it can be seen that due to the increase in the feedwater flow rate, the temperature of the outlet plenum and the maximum wall temperature decrease. At the steady state, the decrease magnitudes are 26.4°C (3.6%) and 31.6 °C (3.4%), respectively, while the main steam pressure increases by 0.36 MPa (1.44%).

7.4.1.2. Step decrease in the heat flux

A 5% step decrease in the heat flux on the fuel rod is introduced. At the same time, the feedwater flow rate and the control valve opening remain at the design values. Figs. 7.3 - 7.5 show that the step decrease of the heat flux results in an 18.8 °C drop in the temperature of the outlet plenum and a 43.6°C drop in the maximum wall temperature at the steady state, but almost has no impact on the main steam pressure.

7.4.1.3. Step decrease in the control valve opening

The control valve opening reduces by 5% when the feedwater flow rate and the heat flux remain unchanged. It is shown that the main steam pressure rises by 0.8 MPa at the steady state due to the step decrease in the control valve opening. In addition, the temperature of the outlet plenum and the maximum wall temperature are not affected by the change of the control valve opening.

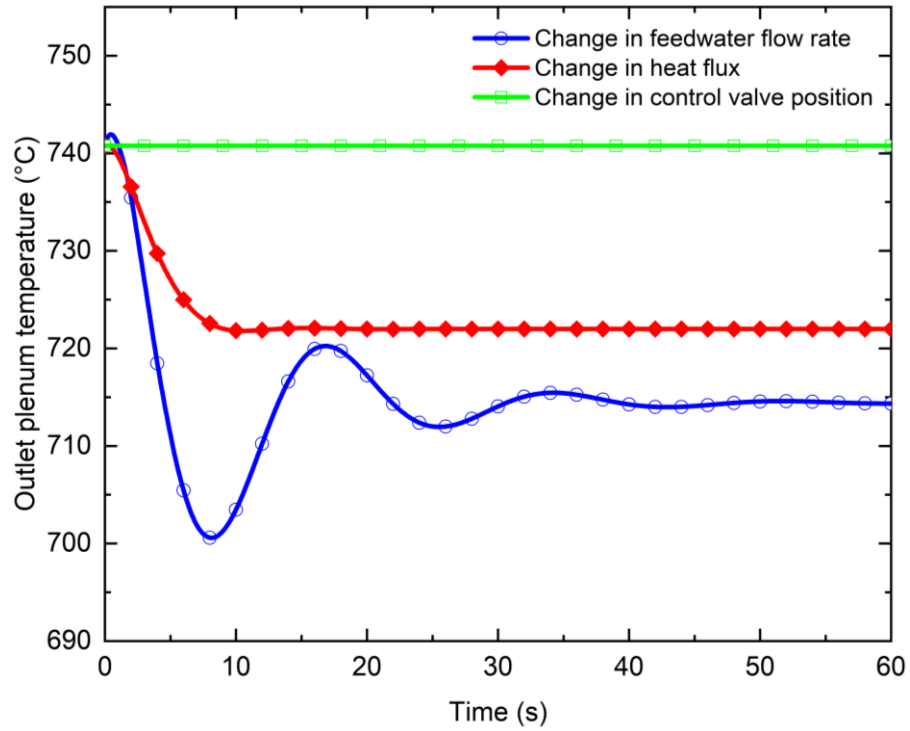


Figure 7.3: Responses of the temperature of the outlet plenum to step variations of different inputs

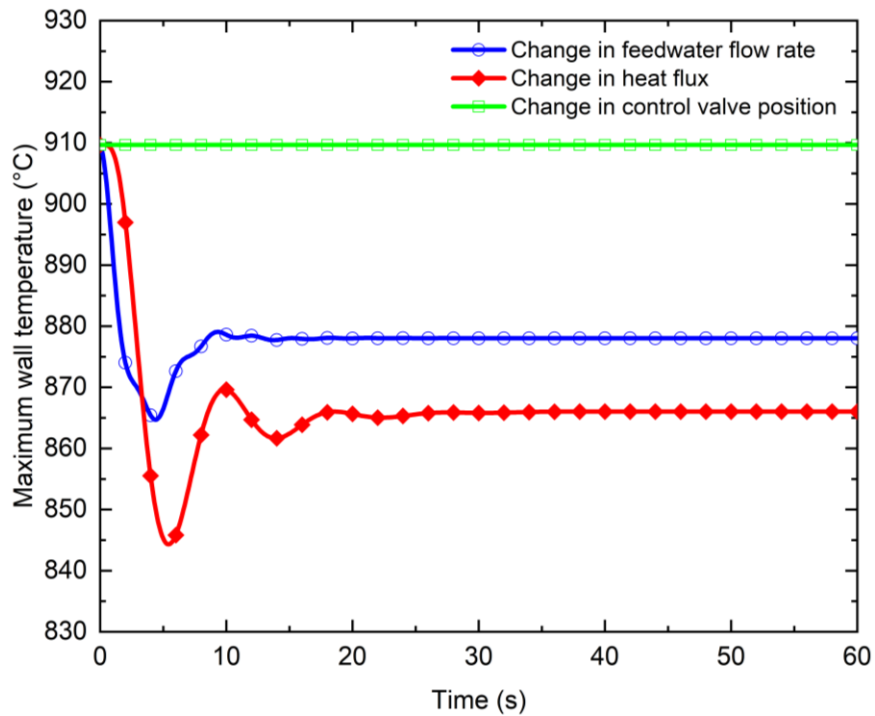


Figure 7.4: Responses of the maximum wall temperature of fuel rods to step variations of

different inputs

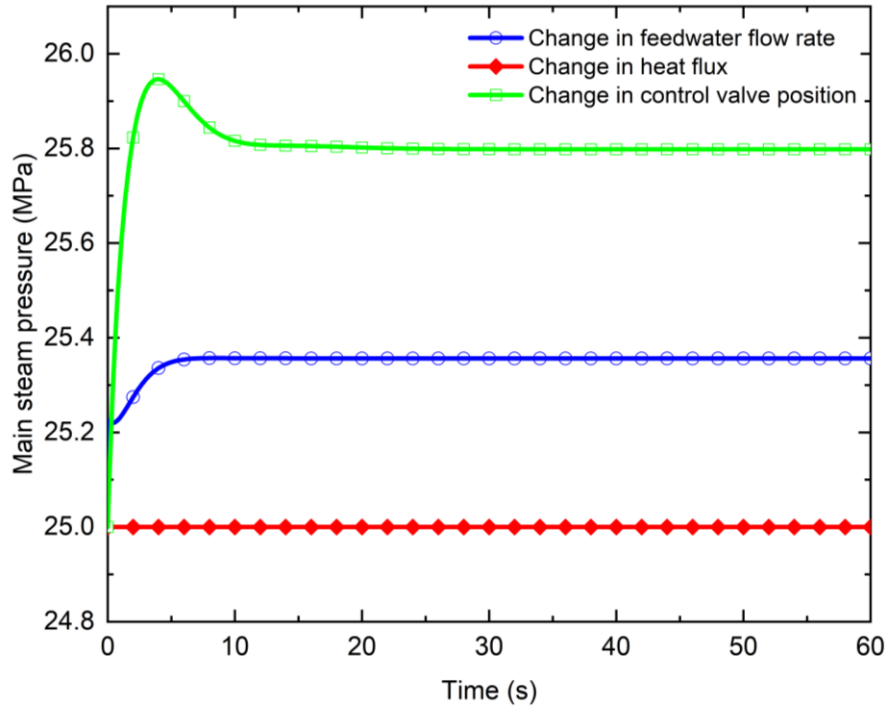


Figure 7.5: Responses of the pressure of the main steam line to step variations of different inputs

7.4.2. Cross-couple of inputs and outputs

The coupling degree between different inputs and outputs of the Canadian SCWR power plant at the steady state is determined so that the most relevant input and output can be paired before the design of controllers. The relative gain array (RGA) is commonly used to evaluate the cross-coupling between inputs and outputs of a system at the steady state condition [15, 16]. The RGA is used for evaluating the influence of an input on an output with respect to that on the rest outputs. The steady state gain matrix K of the entire SCWR system is calculated as:

$$K = \begin{bmatrix} 160.23 & 9 \times 10^{-4} & 0 \\ 192.29 & 10^{-3} & 0 \\ 0.02 & 0 & -31.75 \end{bmatrix} \quad (7.45)$$

Based on K , RGA of the system is calculated as:

$$\text{RGA} = \begin{bmatrix} 1.49 & -0.49 & 0 \\ -0.49 & 1.49 & 0 \\ 0 & 0 & 1 \end{bmatrix} \quad (7.46)$$

It is obvious that the diagonal inputs and outputs are dominantly paired. The system can be regarded as diagonally dominant and a multiple single-input-single-output (SISO) system at the design operating condition. Therefore, the outlet temperature of the outlet plenum is controlled by the mass flow rate of the feedwater, the maximum cladding temperature is regulated by the heat flux on the fuel rod, and the pressure of the main steam is adjusted by the opening percentage of the control valve.

7.5. Design and performance evaluation of the feedback control system

7.5.1. Design of the feedback control system

In the feedback control system, the controllers are used for regulating the deviations of the corresponding outputs to zero or as small as possible when the system is subjected to disturbances. Therefore, three controllers are needed for this three-input and three-output system. The general transfer function for a PID controller is expressed as [17]:

$$C_{(s)} = K_P + K_I/s + K_D s \quad (7.47)$$

where K_P , K_I , and K_D are the proportional, integral, and derivative gains, respectively. The parameters of the controllers are tuned to meet the control requirements for the system [3, 6]: (1) the overshoot is less than 15%, (2) the rise time is less than 20s, and (3) the settling time is below 50 s. Table 7.2 shows the parameters for the controllers used in the feedback control system.

Table 7.2 Parameters and specifications of controllers

Controllers	K_P	K_I	K_D	Rising time (s)	Settling time (s)	Overshoot (%)
PID_1	0.0026	7.8608e-4	0.0022	17.5	43.7	0

I_2		150.0763		4.91	26.3	0
PI_3	-0.0599	-0.088		0.736	2.72	5.88

7.5.2. Performance evaluation of the control system

In order to evaluate the performance of the designed feedback control system, the deviations of the outputs from the design point due to the 5% step perturbations on the inputs are evaluated, and the controllers are activated to regulate the outputs of the system back to the design point. $t = 0$ is the time when the controllers are activated. The responses of the outlet plenum temperature, the maximum wall temperature, the main steam pressure after the controllers activated are shown in Figs. 7.6 - 7.8, respectively.

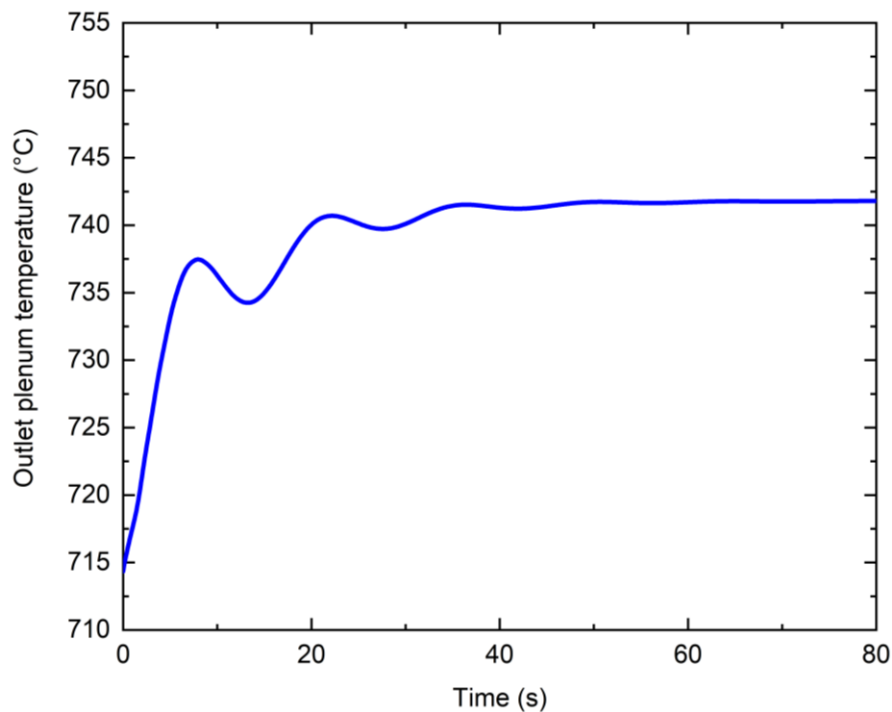


Figure 7.6: Response of the temperature of the outlet plenum using the feedback control after the step perturbation introduced

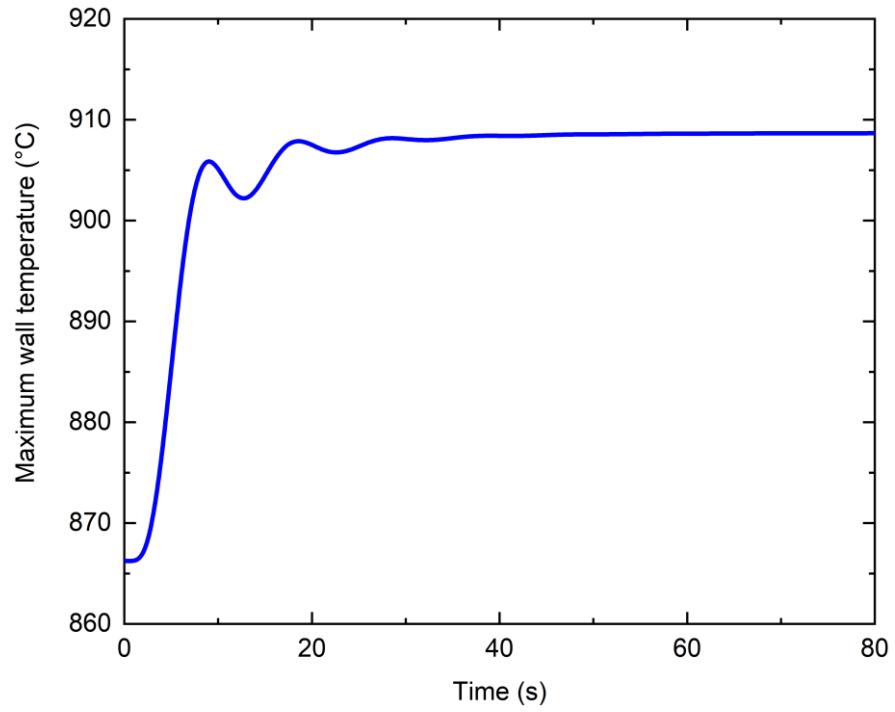


Figure 7.7: Response of the maximum wall temperature of fuel rods using the feedback control after the step perturbation introduce

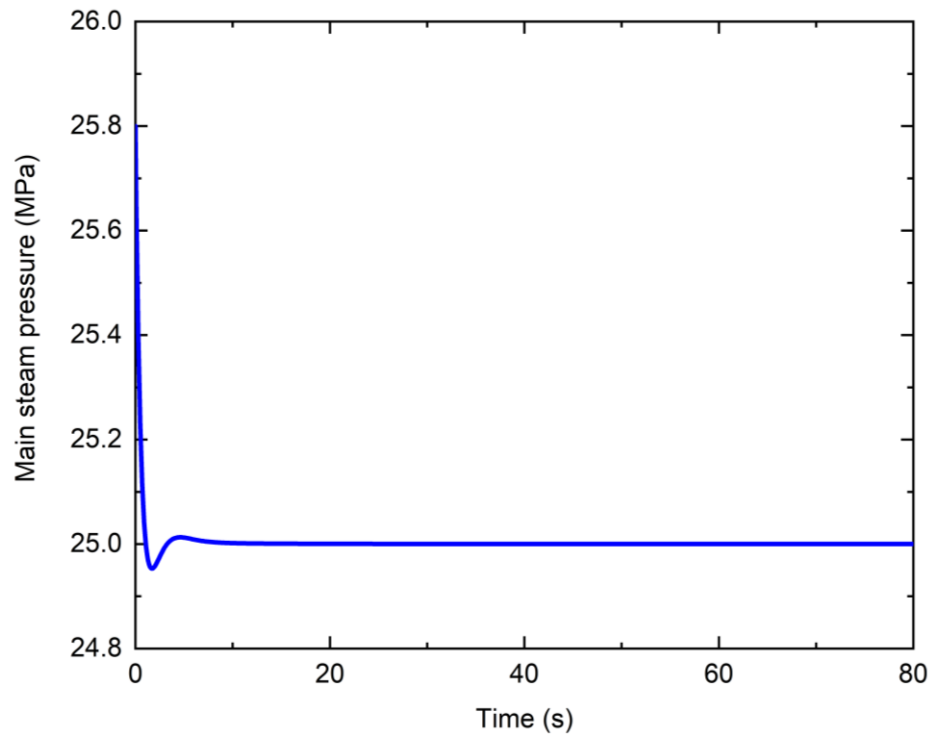


Figure 7.8: Response of the pressure of the main steam using the feedback control after the step perturbation introduced

It can be seen that the outlet plenum temperature and the maximum wall temperature increase and settle at the original design values in 50s using the feedback control system, as shown in Figs. 7.6 and 7.7, respectively. The response of the control system to a 0.8 MPa step increase in the main steam pressure is presented in Fig. 7.8. It shows that the main steam pressure can rapidly go back to the design value. In general, the feedback control system can return the system back to the design point in around 50s. Therefore, the designed feedback control system can effectively regulate and return the power plant back to the design point when there are perturbations.

7.6. Conclusion

The construction of the linear dynamic model and feedback control system for the Canadian SCWR power plant, which focus on the thermodynamic aspect, are developed in this study. Based on the linear dynamic model, the dynamic responses of outputs of the system are investigated when the perturbations of input variables are introduced. Three controllers are designed in the feedback control system to reduce the deviations of the outputs to zero. The performance of the feedback control system is also evaluated. The results show that the designed control system can regulate the system to the designed operating condition satisfactorily.

References

- [1] GIF, “R&D Outlook for Generation IV Nuclear Energy Systems: 2018 Update,” 2018.
- [2] M. Yetisir, H. Hamilton, R. Xu, M. Gaudet, D. Rhodes, M. King, K. Andrew, and B. Benson, “Fuel Assembly Concept of the Canadian Supercritical Water-Cooled Reactor,” *J. Nucl. Eng. Radiat. Sci.*, vol. 4, no. 1, pp. 1–7, Jan. 2018.
- [3] T. Nakatsuka, Y. Oka, and S. Koshizuka, “Control of a Fast Reactor Cooled by Supercritical Light Water,” *Nucl. Technol.*, vol. 121, no. 1, pp. 81–92, Jan. 1998.
- [4] Y. ISHIWATARI, Y. OKA, and S. KOSHIZUKA, “Control of a High Temperature Supercritical Pressure Light Water Cooled and Moderated Reactor with Water Rods,” *J. Nucl. Sci. Technol.*, vol. 40, no. 5, pp. 298–306, May 2003.
- [5] P. Sun and J. Jiang, “Construction and Analysis of a Dynamic Model for a Canadian Direct-Cycle SCWR for Control System Studies,” *Nucl. Technol.*, vol. 180, no. 3, pp. 399–421, 2012.
- [6] P. Sun, B. Wang, J. Zhang, and G. Su, “Control of Canadian once-through direct cycle supercritical water-cooled reactors,” *Ann. Nucl. Energy*, vol. 81, pp. 6–17, Jul. 2015.
- [7] P. Sun and J. Zhang, “Control strategy study for once-through direct cycle Canadian SCWRs,” *Prog. Nucl. Energy*, vol. 98, pp. 202–212, Jul. 2017.
- [8] P. Sun, J. Feng, X. Yuan, L. Zhao, and F. Liu, “Robust Control of Once-Through Canadian Supercritical Water-Cooled Reactors,” *Nucl. Technol.*, vol. 199, no. 1, pp. 35–46, 2017.
- [9] P. Sun, J. Zhang, and G. Su, “Linear parameter-varying modeling and control of the steam temperature in a Canadian SCWR,” *Nucl. Eng. Des.*, vol. 313, pp. 225–235, Mar. 2017.
- [10] R. V. Maitri, C. Zhang, and J. Jiang, “Computational fluid dynamic assisted control system design methodology using system identification technique for CANDU

- supercritical water cooled reactor (SCWR),” *Appl. Therm. Eng.*, vol. 118, pp. 17–22, 2017.
- [11] H. Han, C. Zhang, and J. Jiang, “Dynamic models and control system design for heated channels in a Canadian SCWR,” *Ann. Nucl. Energy*, vol. 151, p. 107973, Feb. 2021.
- [12] H. Han and C. Zhang, “Construction of a feedback control system based on CFD simulations for the 64-element Canadian SCWR,” submitted to *Prog. Nucl. Energy*.
- [13] P. Sun, “Dynamic Model Construction and Control System Design for Canadian Supercritical Water-cooled Reactors,” Phd Thesis, Western University, 2012.
- [14] B. Cui, “3keymaster SCWR Simulator Graph,” 2016.
- [15] E. Bristol, “On a new measure of interaction for multivariable process control,” *IEEE Trans. Automat. Contr.*, vol. 11, no. 1, pp. 133–134, Jan. 1966.
- [16] S. Skogestad and I. Postlethwaite, *Multivariable feedback control: analysis and design*, 2nd ed. Chichester, England ; John Wiley, 2005.
- [17] N. S. Nise, *Control systems engineering*, 5th ed. Hoboken, NJ: Wiley, 2008.

8. Summary

8.1. Summary and contributions

In this work, a variable turbulent model for the fluid flow and heat transfer in the supercritical water flow channels were developed. Then, the model was applied in investigating the fluid flow and heat transfer of the supercritical water in the 64-element rod bundle at the design point and under different operating conditions. In addition to the numerical investigations, the linear dynamic model of the reactor was obtained through transient CFD simulations and the control systems for the reactor and the entire SCWR power plant were constructed.

In Chapter 3, a modified turbulent model for the supercritical fluid flows in the vertical upward channels was proposed. This work involved extensive studies of evaluations of the existing turbulent models in both tube and rod bundles under various operating conditions. Special attention was given to the development of a new variable model, which includes the variations of turbulent Prandtl number with the thermophysical properties and operating parameters. The application of the modified turbulent model for the simulation of the supercritical fluid flows results in a great improvement in the prediction of the wall temperatures, especially for the condition in channels with multiple fuel rods.

In Chapter 4, the full-scale three-dimensional flow and heat transfer of supercritical water in the 64-element rod bundle was studied using the modified turbulent model developed in Chapter 3 by computational fluid dynamics (CFD) simulations. Some interesting aspects of the flow and heat transfer phenomenon were observed. First, the possibility of the existence of the gap vortices in the flow subchannels was confirmed. Higher streamwise velocities and normal Reynolds stresses always exist at the center subchannel regions. Second, although the bulk temperature of the fluid and the wall temperatures of the fuel rods generally increase along the axial flow direction, it was found that the circumferential wall temperature distribution around the fuel rod surface is extremely non-uniform and

there are large differences of the maximum cladding surface temperatures between different fuel rods.

In Chapter 5, the parametric effects was investigated for the flow and heat transfer of supercritical water in the 64-element Canadian SCWR fuel bundle. The effects of operating pressure, inlet temperature, heat flux, and mass flux on the heat transfer of upward supercritical water flow in the 64-element fuel bundle were studied numerically. Since the buoyancy effect contributes to the heat transfer deterioration, the criteria of the onset of buoyancy effects on heat transfer for supercritical water in circular tubes were also used to evaluate the buoyancy effects on the heat transfer deterioration of supercritical water flow in the fuel bundle under different operating conditions. It was shown that the wall temperatures generally increase as the increase in the inlet temperature, heat flux, or the decrease in the mass flux. In addition, it was also found that the buoyancy-affected zones mainly exist at the entrance region around the pseudocritical temperature due to the sharp decrease of density. The buoyancy-affected zone is reduced with the increase in the inlet temperature and heat flux, and it can be ignored when the mass flux is more than a certain value because the pseudocritical region becomes narrowed at a higher mass flux.

In Chapter 6, a design of the feedback control system for the 64-element SCWR was presented. First, before the construction of the feedback control system, the dynamic relationships between inputs and outputs of the reactor were obtained through transient computational fluid dynamics (CFD) simulations. The linear dynamic model of the reactor was obtained using system identification techniques and validated with nonlinear full-scale CFD simulations. Second, the performance of the feedback control system was evaluated. It was shown that the designed feedback control system can regulate the reactor back to the design point in time when the system is subjected to disturbances.

In Chapter 7, based on the linear dynamic model for each component in the Canadian SCWR power plant, a linear dynamic model for the entire SCWR power plant was

developed, which includes the reactor, feedwater pump, outlet plenum, main steam line, turbine, and condenser. The dynamic characteristics of the system and the steady-state interaction between different inputs and outputs of the system were analyzed. Finally, the control system for the SCWR power plant was constructed and the performance of the control system is satisfactory.

8.2.Recommendations for future work

Some suggestions for the future work based on the studies completed in this work are presented as follows:

1. Experimental validation and calibration of the modified turbulent model

In this work, the experimental results used for the validation of the modified model are limited. When more experimental data for supercritical flows in different types of rod bundles under different operating conditions are available, the turbulent model can be further improved.

2. Propose the onset criteria for DHT in supercritical water rod bundles based on experimental results

So far, only the onset criteria of DHT for supercritical water in tubes have been investigated. With extensive experimental data in the future for rod bundles, correlations of criterion could be obtained to describe the onset of DHT phenomenon for supercritical water in rod bundles.

3. Couple neutronics into the CFD simulations and control system for the reactor

With the assumption of the uniform heat flux on the heat flux, the maximum cladding surface temperatures predicted by the CFD simulations in this work might be higher than the actual values. Therefore, the neutronics will be coupled into the CFD simulations in the future study. In addition, the linear dynamic model and control system in this work are conducted without considering the feedback effects of the coolant density and fuel

temperatures on the reactor power. Therefore, multi-physics that couples neutronics and thermal hydraulics of reactors will be used in the control system designs.

4. Validation of the linear dynamic model of the SCWR power plant

The linear dynamic model for the Canadian SCWR power plant constructed in this work has not been verified by the experimental results from the SCWR power plant since the experiments are not available now. Therefore, it needs to be validated by the experimental data once they are available.

Curriculum Vitae

Name: Huirui Han

Post-secondary Western University

Education and London, Ontario, Canada

Degrees: 2018-2022 Ph.D.

Western University

London, Ontario, Canada

2016-2018 M.E.Sc.

North China Electric Power University

Beijing, China

2011.09-2015.06 B.Eng

Related Work Teaching Assistant

Experience: Western University

2016-2017, 2018-2022

Journal Publications:

H. Han, C. Zhang, J. Jiang, “ Dynamic models and control system design for heated channels in a Canadian SCWR,” *Annals of Nuclear Energy*, vol. 151, p. 107973, Feb. 2021.

H. Han, C. Zhang, “ A Modified Turbulent Model for the Supercritical Water Flows in the Vertical Upward Channels,” *The Journal of Supercritical Fluids*, vol. 187, p. 105632, Aug. 2022.

H. Han and C. Zhang, “Numerical investigations of the effect of operation conditions on the heat transfer of the supercritical water in the Canadian SCWR fuel bundle,” *The Journal of Supercritical Fluids*, vol. 191, p. 105760, Dec. 2022.

Book Chapters:

R. Maitri, H. Han, C. Zhang, and J. Jiang, “Numerical Investigation of the Deteriorated Heat Transfer Phenomenon for Supercritical Water Flows in Vertical Circular Tubes,” in *Complementary Resources for Tomorrow*, A. Vassel-Be-Hagh and D. S.-K. Ting, Eds. Cham: Springer International Publishing, 2020, pp. 235–248.

Conference Articles and Abstracts:

(Abstract, Presented) H. Han and C. Zhang, “Numerical analysis of heat transfer of supercritical water in multiple rod channels,” 13th International Symposium on Supercritical Fluids, Montreal, Quebec, Canada, May 15-18, 2022.

(Abstract, Presented) H. Han and C. Zhang, “Numerical simulation of the supercritical water flow in the Canadian SCWR fuel bundle,” Proceedings of the Canadian Society for Mechanical Engineering International Congress, Charlottetown, PE, Canada, June 27-30, 2021.

(Article, Presented) H. Han and C. Zhang, “Numerical investigation of the thermodynamics behaviors in the central downward circular tube of the 64-element Canadian SCWR fuel bundle,” Joint Congress of the Canadian Society for Mechanical Engineering and CFD Society of Canada, London, Ontario, Canada, June 2-5, 2019.

(Article, Presented) H. Han and C. Zhang, “Numerical simulation of fluid flow and heat transfer of the supercritical water in different fuel rod channels,” Proceedings of the Canadian Society for Mechanical Engineering International Congress, Toronto, Ontario, Canada, May 27-30, 2018.

(Article, Presented) H. Han and C. Zhang, “Numerical simulation of fluid flow and heat transfer of the supercritical water in different fuel rod channels,” 25th Annual Conference of the CFD Society of Canada, Windsor, Ontario, Canada, May 27-30, 2017.